The role of GPR56 and collagen III in islet functions

Olaniru, Oladapo Edward

Awarding institution:
King's College London

THE ROLE OF GPR56 AND COLLAGEN III IN ISLET FUNCTIONS

A thesis submitted by

Oladapo Edward Olaniru

For the award of Doctor of Philosophy from

King's College London

Diabetes Research Group

Division of Diabetes and Nutritional Sciences

Faculty of Life Sciences & Medicine

King's College London

In loving memory of my Dad.

You are so loved and missed.

Acknowledgement

First, I would like to thank my supervisors Professor Shanta Persaud and Professor Peter Jones for their support and guidance throughout this PhD programme. Shanta was incredibly helpful; she made sure I had a bigger picture of my work, wrote compelling references for my scholarship/grants applications, provided timely feedback on my project and thesis, introduced me to a collaborator and so on. It was indeed an honour to have worked with you. Thanks to Peter for making the Diabetes Research Group a stimulating sanctuary – I've always wondered how you managed to make such a large group a lovely and supportive environment to work in.

To all the past and present members of the Diabetes Research Group, I say thank you. Special thank you to Ahmed Arzouni for his friendship and support. Thank you to Jai Gondi, Thomas Hill, Klaudia Toczyska, Sian Simpson, Elizabeth Evans, Patricia Fonseca Pedro, Elisabeth Thubron, Patricio Atanes, Amazon Austin, Zara Franklin, Zoheb Hassan, Ross Hawkes, Robert Drynda, Bo Liu, Mustafa Dogan, Anastasia Tsakmaki, Inmaculada Maldonado, Chloe Rackham, Attilio Pingitore and Stefan Amisten. Thanks to Aileen King, James Bowe and Amazon Austin for teaching me the technically demanding islet isolation in my first year- I never knew I would ever be proficient in this! I'm grateful to Professor Xianhua Piao for hosting me in her lab at Harvard Medical School. Stefanie Giera and Rong Luo at HMS were incredibly generous with their time in showing me how to make quality images with Adobe Photoshop/Illustrator, ImageJ software and in discussing GPR56 in general.

I thank Commonwealth Scholarship Commission for providing funding for my studies. I'm grateful to EFSD for awarding me with Albert Renold Fellowships on two occasions. I also thank the Department of Physiology for awarding me with a KCL Peter Baker Travelling Fellowship to Boston and thanks to the Society of Endocrinology for an early career grant. I thank University of Jos for granting me study leave. Many thanks to Professor John Aguiyi of University of Jos for his support and for inspiring me with his enthusiasm for science.

My heartfelt thanks go to my sweetheart, Bolaji Olaniru, for always being there, for motivating me when I was acting lazy or telling me to take a break when I should. We've been through this together and here's to the future and everything in it. To my cute chubby Sam, thank you for

distracting me with hide and seek when I needed a break from thesis writing. I'm also grateful to my parents and siblings for their encouragement and support. Thank you to the Oyewoles, the Ajiboyes, the Igbekeles, the Bamigbolas, the Adedirans and the Olaniru family. Finally, I'm grateful to God for the gift of life.

[This page is intentionally left blank]

Abstract

G-protein coupled receptors (GPCRs) are surface membrane receptors that convey a diverse array of signals and control many physiological processes within cells. Several human disorders are as a result of mutations in these receptors and they are the targets of more than 40% of all drugs in modern medicine. This thesis is focused on GPR56, a member of the adhesion class of GPCRs that is the most abundantly expressed GPCR mRNA in human islets. GPR56 is also highly enriched in endocrine progenitors in the developing pancreas. Its function in islets, however, remains elusive. Previous studies have indicated that extracellular matrix collagen III is the ligand of GPR56 in the developing brain, where GPR56-collagen III interaction is important for maintaining pial basement membrane integrity and in the normal development of cerebral cortex. The aim of this project was to investigate the importance of GPR56 in islet functions.

GPR56 mRNA was detected by RT-PCR in MIN6 β-cells and in mouse and human islets, while mRNA encoding collagen III was detected in islets but not in MIN6 β-cells. Islet GPR56 expression was confirmed by detection of a 70kDa immunoreactive protein and immunohistochemistry revealed that it was strongly expressed by ductal and β-cells and faintly by exocrine acini cells. In the developing mouse pancreas, GPR56 was expressed by $PDX1^+$, $NGN3^+$ and $SOX9^+$ endocrine progenitor cells. GPR56 was strongly expressed at the early days of pancreas development and became downregulated as the cells differentiated. It was then upregulated at the stage of β-cell replication between E18 and P9. Immunostaining revealed that collagen III was present in islet capillaries but not in endocrine cells. Acute exposure of islets to 100nM collagen III increased insulin output in a GPR56-dependent manner. In addition, pre-exposure of islets to collagen III for 48 h exhibited enhanced insulin secretion at stimulatory glucose concentration, without affecting insulin content.

The role of GPR56 in regulating islet mass and β-cell proliferation was determined using GPR56 knockout (KO) mice. Deletion of GPR56 did not affect mouse body weight. There was a trend of mild glucose intolerance in adult KO mice fed on normal diet compared with the WT mice, but there was no difference in islet insulin content. Quantification of islet size and proliferating β-cells in fixed, immunostained pancreas samples revealed that islets from adult, postnatal day 56

mice (P56) KO mice were smaller than WT islets and this was more pronounced in P9 mice, as a consequence of decreased β-cell proliferation as indicated by BrdU incorporation. Moreover, the number of β-cells actively replicating in the cell cycle, as determined by Ki67 staining, was greater in the WT islets compared to KO islets at P9, leading to less β-cells but higher numbers of α-cells in KO islets. However, there were no differences in islet capillary density or percentage islet nerve area. In addition, transient transfection of MIN6 β-cells, a mouse insulinoma cell line with functional similarity to mouse islets, with 1.2mg of GPR56 plasmids resulted in a 20 fold increase in GPR56 expression and this was associated with increased β-cell proliferation and reduced apoptosis.

In summary, the data presented in this thesis have demonstrated that GPR56 is expressed by mouse and human islets and collagen III is localised to islet blood vessels, suggesting that GPR56 may be regulated in a paracrine manner by local interaction with its activating ligand. In addition, GPR56 is differentially expressed during mouse islet development, where it is required at key stages of proliferation and differentiation of endocrine cells. However, GPR56 is not required for islet innervation and vascularisation of the developing endocrine pancreas. Evidence is also provided for the role for GPR56 in islet mass regulation, as a consequence of increased β-cell proliferation and decreased apoptosis.

Abbreviations

Abbreviation	Definition
$[Ca^{2+}]i$	intracellular calcium
°C	degrees centigrade
Ab	antibody
AC	adenylyl cyclase
Ach	acetylcholine
ADP	adenosine diphosphate
Ag	antigen
AGE	advanced glycation end products
ANOVA	analysis of variance
ATP	adenosine triphosphate
BFPP	bilateral frontoparietal polymicrogyria
BM	basement membrane
bp	base pair
BrdU	5-bromo-2'-deoxyuridine
BSA	bovine serum albumin
Ca^{2+}	calcium ion
cAMP	cyclic adenosine 3,5-monophosphate
cDNA	complementary DNA
CNS	central nervous system
CO_2	carbon dioxide
Col I	collagen I
Col III	collagen III
Col IV	collagen IV
cpm	counts per minute
DAG	diacylglycerol
DI H_2O	deionised water
DMEM	Dulbecco's modified eagle's medium
DMSO	dimethylsulphoxide
DNA	deoxyribonucleic acid

dNTPs	deoxynucleoside triphosphates
DPP-4	dipeptidyl peptidase-4
DTT	dithiothreitol
E	embryonic
ECL	enhanced chemiluminescence
ECM	extracellular matrix
EDTA	ethylenediaminetetraacetic acid
ELISA	enzyme-linked immunosorbent assay
ER	endoplasmic reticulum
FBS	fetal bovine serum
Fura-2 AM	fura-2 acetoxymethyl derivative
GDP	guanosine bisphosphate
GFAP	glial fibrillary acidic protein
GLP-1	glucagon-like peptide-1
GLUT-2	glucose transporter-2
GLUT-4	glucose transporter-2
GPCR	G-protein coupled receptor
GPR56	G-protein coupled receptor 56
$GPR56^{C}$	G-protein coupled receptor 56 C-terminal
$GPR56^{N}$	G-protein coupled receptor 56 N-terminal
GSIS	glucose stimulated insulin secretion
H	hour
HbA1c	glycated haemoglobin A1c
HCl	hydrochloric acid
Hobbit	homolog of blimp-1 in T cells
IFN-γ	interferon gamma
IL-1β	interleukin-1 beta
INS1	rat insulinoma β-cell line
IP3	inositol 1,4,5,-trisphosphate
IP3R	inositol 1,4,5-trisphosphate receptor
IPGTT	intraperitoneal glucose tolerance test

IRS	insulin receptor substrate
K^+	potassium ion
K_{ATP}	ATP-sensitive potassium channel
kDa	kilodalton
Kir6.2	inward rectifier K+ channel
KO	knockout
LADA	latent autoimmune diabetes of adulthood
MAPK	mitogen-activated protein kinase
MEM	minimum essential medium
MIN6	mouse insulinoma β-cell line
ml	millilitre
mM	millimolar
MODY	maturity-onset diabetes of the young
MOPS	3[N-morpholino]propanesulphonic acid
MPCs	multipotent progenitor cells
mRNA	messenger RNA
Mwt	molecular weight
NaOH	Sodium hydroxide
NFAT	nuclear factor of activated T-cells
ng	nanogram
NGN3	neurogenin-3
nM	nanonmolar
OGTT	oral glucose tolerance test
P	postnatal
p	probability
PAGE	polyacrylamide gel electrophoresis
PBND	PCR buffer with non-ionic detergent
PBS	phosphate-buffered saline
PCR	polymerase chain reaction
PDX1	pancreatic and duodenal homeobox 1
PEG	polyethylene glycol

PGC-1α4	peroxisome proliferator-activated gamma co-activator 1-alpha 4
PI	phosphatidylinositol
PI3K	phosphatidylinositol-3-kinase
PIP_2	phosphatidylinositol 4,5-bisphosphate
PIP_3	phosphatidylinositol-3, 4,5-trisphosphate
PKA	protein kinase A
PKB	protein kinase B
PKC	protein kinase C
PLC	phospholipase C
PP	pancreatic polypeptide
PPARγ	peroxisome proliferator-activated receptor-γ
pSc	peri-islet Schwann cell
PVDF	polyvinylidene fluoride
qPCR	quantitative polymerase chain reaction
RBD	Rho binding domain
RIA	radioimmunoassay
RNA	ribonucleic acid
RRP	readily releasable pool
RT	reverse transcription
RT-PCR	real time polymerase chain reaction
SDS	sodium dodecylsulphate
SEM	standard error of mean
SGLT-2	sodium-glucose transport protein 2
siRNA	small interfering RNA
SOX9	SRY-Box 9
SPARC	secreted protein acidic and rich in cysteine
SRE	serum response element
SUR1	ATP-sensitive sulphonylurea receptor
T1D	type 1 diabetes
T2D	type 2 diabetes mellitus
TCA	tricarboxylic acid

TG2	transglutaminase 2
TM	transmembrane domain
TNF-α	tumour necrosis factor alpha
Tris	tris(hydroxymethyl)aminomethane
tRNA	transfer RNA
TZD	thiazolidinedione
UV	ultraviolet
v/v	volume in volume
VEGF	vascular endothelial growth factor
VGCC	voltage-gated Ca2+ channel
w/v	weight in volume
WHO	World Health Organization
α	alpha
β	beta
γ	gamma

Table of Contents

Table of Figures

Chapter 1

Table of Tables

Chapter 1

Chapter 1 Introduction

1.1 Diabetes mellitus

Diabetes was first recognised by the ancient Egyptians around 1500 BC as a rare disorder where those affected urinate excessively and suffer from weight loss. The Greek physician Aretaeus was said to use the term 'diabetes', meaning 'flowing through' to imply that the patients were drained of fluid, while 'mellitus' was added by Thomas Willis to indicate that the urine of the sufferers had a sweet taste. Attraction of ants to urine was a way for identifying victims with the 'honey urine' by the ancient Indian physicians (MacCracken et al., 1997; Polonsky, 2012).

From a rare disease in the Middle Ages, diabetes is now a global epidemic, with 415 million people currently living with the disease, and this is predicted to rise beyond 642 million by 2040, indicating that one person in ten will have diabetes if the current trend is allowed to continue (International Diabetes Federation, 2015). The main drivers of increased diabetes prevalence are over-nutrition coupled with sedentary lifestyle, as a result of urbanisation and increasing global transition to western lifestyles (Narayan et al., 2010). Low and middle-income countries are the worst hit, with majority of people suffering from diabetes younger than 60, in their most productive years. Globally, diabetes places immense economic burden on healthcare systems, with an estimated annual global expenditure ranging between $612 billion to $1099 billion (da Rocha Fernandes et al., 2016).

Diabetes mellitus is a disorder of glucose homeostasis. According to the American Diabetes Association benchmarks, adopted by the World Health Organisation, diabetes is diagnosed if plasma glucose is ≥ 7mM after a fasting period of at least 8 h or if it is ≥11.1mM two hours after oral ingestion of 75g equivalent of glucose. Glycated haemoglobin (HbA1c) of ≥6.5% is also indicative of diabetes (Figure 1-1) (American Diabetes Association, 2011). Individuals who do not meet these thresholds but have high plasma glucose are referred to as prediabetics. Such individuals are said to have impaired fasting glucose and impaired glucose tolerance, described

as fasting glucose levels of between 5.6 and 6.9mM and glucose levels of 7.8 – 11mM two hours after consuming a sugar-rich drink respectively (American Diabetes Association, 2014).

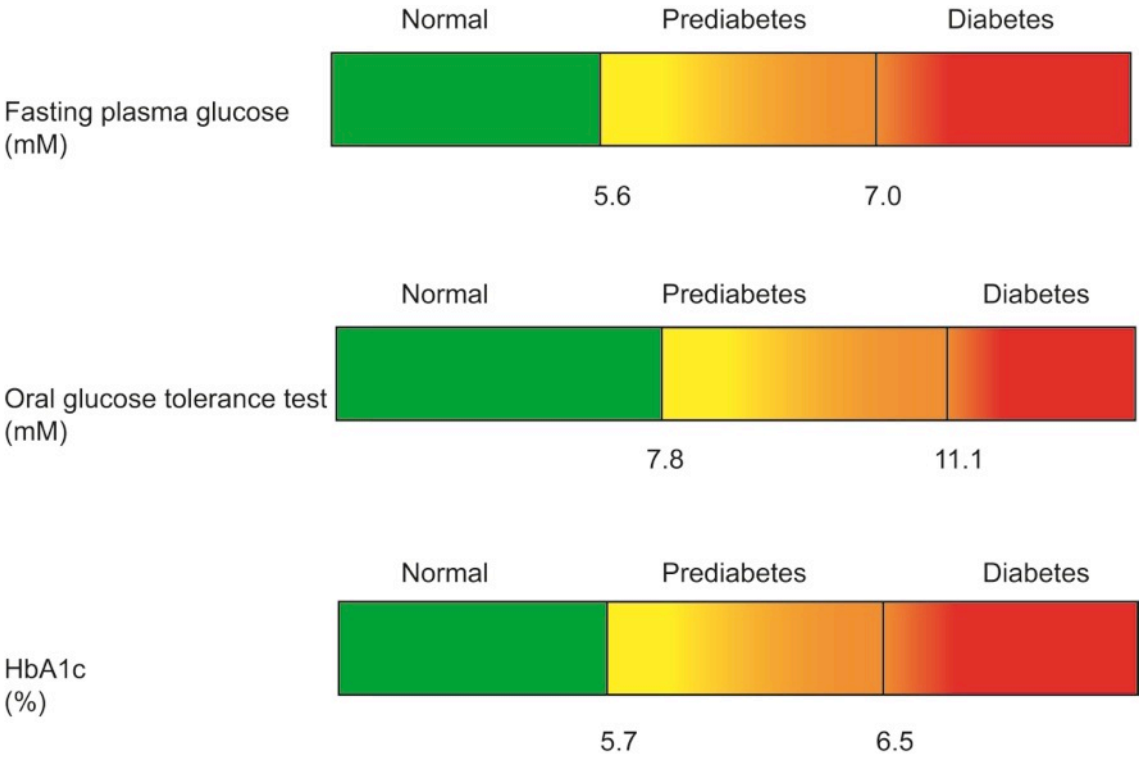

Figure 1-1 Diagnostic criteria for prediabetes and diabetes using fasting plasma glucose, oral glucose tolerance test or HbA1c.

1.1.1 Classification

Traditionally, diabetes is classified into two main types: type 1 and type 2. Type 1 diabetes (T1D) is primarily due to autoimmune destruction of pancreatic β-cells, leading to severe insulin deficiency and total dependence on exogenous insulin administration. It accounts for about 5 - 10% of diabetes cases and affects mostly young people. At the time of diagnosis, up to 80% of β-cells have been destroyed by infiltrating macrophages and $CD8^+$ T cells (Notkins et al., 2001). Environmental factors may also drive the pathogenesis of T1D, as its incidence changes with seasons, with higher incidence observed in autumn and winter and lower in summer (Moltchanova et al., 2009). Type 2 diabetes (T2D), on the other hand, arises from insulin resistance and reduction in pancreatic β-cell mass that culminate in reduced insulin secretion. It is the commonest form of diabetes affecting about 90-95% of all diabetes patients. Unlike T1D

where there is complete lack of endogenous insulin, in T2D, β-cells are still able to produce insulin but the target tissues such as skeletal muscles and adipose have become less sensitive to insulin. β-cells therefore compensate for increased resistance by producing more insulin. With increasing insulin resistance coupled with β-cells dysfunction, β-cells begin to fail, producing insufficient insulin, which eventually leads to a rise in circulating blood glucose.

The classification of diabetes into type 1 and 2 is oversimplified, as other diabetes subtypes have been identified. When diabetes is first identified during pregnancy, it is called gestational diabetes and it is temporary in most cases. Although T1D is primarily diagnosed in children and adolescents, it has been proposed that up to 15% of T2D cases seen in adults, may in actuality, be T1D. A new class of diabetes to cater for this adult group, known as Latent Autoimmune Disease of Adults (LADA), has been suggested (Leslie et al., 2008). LADA, also referred to as slowly progressing insulin-dependent diabetes or type 1.5 diabetes, describes a subset of patients with features of T2D in addition with underlying autoimmunity (Leslie et al., 2016). However, lack of firm diagnostic criteria for LADA and genetic similarity with T1D has diminished enthusiasm for this 'new' class of diabetes. LADA is now regarded as a variant of T1D rather than a disease of its own (Rolandsson and Palmer, 2010). Another less common diabetes subtype is maturity onset diabetes of the young (MODY), which is also known as monogenic diabetes. It accounts for about 1-2% of all diabetes cases and is commonly diagnosed in children. It presents clinically like T2D and it is not dependent on insulin therapy. At least 13 genes including hepatocyte nuclear factor (HNF) and glucokinase have been implicated in its onset, each having its own clinical presentation and management (Bishay and Greenfield, 2016).

T1D and T2D are complex disorders with social, environmental, genetic and behavioural factors contributing to disease onset (Tuomi et al., 2014). Unlike monogenic and neonatal diabetes that are single gene disorders, T1D and T2D are polygenic disorders, with several genes playing a role in disease development. In T1D, alleles at the human leucocyte antigen locus account for about 50% of all hereditary cases while such predominant genetic susceptibility locus has not been identified in T2D (Polonsky, 2012). Genome wide association studies have identified hundreds of genetic variants that increase susceptibility to T2D. On aggregate, these variants

only account for 10% of the hereditability of T2D but can increase the risk of an individual developing T2D by up to 15% (Fuchsberger et al., 2016).

1.1.2 Effects of chronic hyperglycaemia in diabetes

Persistently elevated blood glucose, referred to as hyperglycaemia, is a common feature of all forms of diabetes, which causes microvascular and macrovascular complications observed in long standing diabetes. The risk of developing complications is influenced by genetic factors and the duration of hyperglycaemia. Increased insulin resistance, insulin deficiency and decreased insulin secretion mainly drive hyperglycaemia. As a result of insulin deficiency, catabolism is activated leading to increased hepatic gluconeogenesis. Moreover, increased circulating free fatty acids are also present in T2D and their inhibition of glucose uptake into muscles further contribute to elevated blood glucose.

The long-term effect of diabetes on nerves, kidney and eyes causes neuropathy, nephropathy and retinopathy respectively, and they are termed microvascular complications. Cardiovascular and peripheral vascular diseases arising from the effect of chronic hyperglycaemia on heart and macrovasculature are classified as macrovascular complications. The complex cascades leading to cellular damage in prolonged hyperglycaemia are not fully understood, but generation of reactive oxygen species, activation of the polyol pathway and formation of advanced glycation end products (AGE) have all been implicated (Negre-Salvayre et al., 2009). During hyperglycaemia, intracellular glucose levels of tissues such as neurons, retina and glomerulus that do not require insulin for glucose uptake are raised, eventually leading to increased oxidative phosphorylation and production of free radicals. The amount of highly reactive radicals generated is considerably higher than what cellular anti-oxidants can handle, thereby damaging mitochondrial membrane and DNA. In addition, the polyol pathway is activated as a result of elevated intracellular glucose. Thus, aldose reductase reduces glucose to sorbitol, which accumulates within the cell because of its inability to diffuse out of cell membranes. By its osmotic effect, sorbitol depletes levels of intracellular myoinositol, a precursor of membrane phospholipids, hence causing cellular damage.

Another mechanism of cellular damage in uncontrolled diabetes is the formation of AGE. AGEs are formed from non-enzymatic, irreversible attachment of circulating reducing sugars such as glucose and fructose to functional and structural proteins including albumin, globulin and collagen (Singh et al., 2014). Lipids and nucleotides are also susceptible to glycation. Glycation disrupts the normal function of molecules and interferes with receptor recognition. The attachment of reducing sugars to collagen causes arterial stiffness, diminished myocardial compliance and increased propensity for bone fracture (Saito et al., 2006). Accumulation of AGEs intracellularly causes generation of destructive radicals and receptor-mediated increase in apoptosis and inflammation (Persaud and Jones, 2003).

1.1.3 Treatment of diabetes mellitus

There are presently no cures for T1D or T2D. The main goal of treatment is to maintain blood glucose level within a range that will prevent or slow down the development of complications while preventing severe hypoglycaemic episodes. The mainstay therapy for people suffering from T1D is administration of exogenous insulin. To cater for daily fluctuations in plasma glucose or for post-prandial glucose correction, different insulin formulations have been developed, which are long-acting and short-acting insulin. Long-acting insulin, such as glargine and degludec, are meant to provide basal insulin throughout the day while short-acting insulin, such as lispro and aspart, are used when rapid reduction in plasma glucose level is required. Glargine and degludec are administered once daily and they both reduce the risk of nocturnal hypoglycaemia (Owens et al., 2014). Short-acting analogues have rapid onset of action and are usually given 15 min before meals. They achieve peak plasma concentration about 1 h after subcutaneous injection and can last for 4 to 6 h (Sanlioglu et al., 2013).

The first step in the management of T2D is to set a glycaemic target that is appropriate for each individual patient, which is dependent on the availability of home-support systems, age, ability to self-care and other psychosocial factors. The current guideline sets a target of achieving HbA1c level of less than 6.5% (Handelsman et al., 2011). Lifestyle changes such as weight loss, calorie restriction and exercise, are recommended for improving glycaemic control. Patients are encouraged to eat balanced diet, food rich in fibre, legumes, whole grains, and less than 7% saturated fat, combined with moderate intensity exercise of 30min daily for at least 5 days a

week (American Diabetes Association, 2011). Weight loss is an effective strategy for reducing incidence of T2D in individuals at high risk of developing diabetes (Feldman et al., 2017). However, maintaining weight loss is difficult as weight is normally gained back as a result of increased appetite and feeding. Dietary starches that are resistant to enzymatic digestion in the colon and hence available for fermentation by colonic bacteria producing short chain fatty acids, have been shown to reduce food intake and they may therefore be useful in long term weight maintenance (Nilsson et al., 2008; Guess et al., 2015). In addition to maintaining weight loss, fermentable carbohydrates have been shown to reduce ectopic fat in prediabetes and they mediate their beneficial effects by activating free fatty acid receptor 2 (FFAR2) to potentiate anorexic signalling in the gut (Guess et al., 2015; Brooks et al., 2017). Importantly, research efforts are underway to increase the resistant starch content of commonly consumed food so that the beneficial effects of fermentable carbohydrate on glucose homeostasis and weight loss can be felt at a population level (Petropoulou et al., 2016).

For individuals with uncontrolled diabetes from lifestyle modifications, pharmacological intervention is the next line of action. It is a popular option for treatment of T2D, with many agents available commercially. Metformin is a commonly prescribed drug and it reduces hepatic gluconeogenesis by activating AMP-activated protein kinase. It is well tolerated, does not cause weight gain and rarely elicits hypoglycaemia, although it may cause gastrointestinal discomfort at a higher dose. Sulphonylureas, such as glibenclamide and glipizide, bypass metabolic coupling to stimulate insulin release by closing β-cell K_{ATP} channels, leading to membrane depolarisation. They may however, cause weight gain and induce hypoglycaemia (Shimizu et al., 2012). Thiazolidinediones, on the other hand, provide glycaemic control by activating peroxisome proliferator-activated receptor γ with concomitant reduction in peripheral insulin resistance and inhibition of glucose production by the liver (DeFronzo, 2009). Sodium-glucose co-transporter 2 (SGLT2) inhibitors were recently approved for treatment of T2D. The kidney usually reabsorbs 120 – 140g glucose daily, via SGLT2 transporter proteins located in the proximal tubules. However, under conditions of hyperglycaemia the blood glucose may exceed the maximal renal reabsorption capacity of about 450g/day, and so the excess is excreted in urine. SGLT2 inhibitors increase renal glucose excretion by blocking the SGLT2 transporters and thus lowering the threshold for glucose reabsorption (Vallon and Thomson, 2016). The

resulting glucosuria does not cause hypoglycaemia, as the drugs become ineffective once the blood glucose reaches the minimum renal reabsorption capacity of approximately 80g per day. SGLT2 inhibitors also increase glucose uptake by the muscle, reduce systolic blood pressure, decrease hepatic gluconeogenesis and increase insulin sensitivity (Monami et al., 2014). Other available medications such as GLP-1 analogues and dipeptidyl peptidase IV (DPP-4) inhibitors including some advantages and disadvantages associated with their use are summarised in Table 1-1.

Table 1-1: Pharmacological interventions for the management of T2D (Ismail-Beigi, 2012).

Class	**Examples**	**Advantages**	**Disadvantages**
Biguanides	Metformin	Decreased cardiovascular events, rare occurrence of hypoglycaemia, improved lipid profile, they have been in clinical use for decades	GIT discomfort,
Sulfonylureas	Glibenclamide, glipizide, glimepiride	Extensively used in the clinics	Weight gain, hypoglycaemia
Thiazolidinediones	Pioglitazone	Hypoglycaemia rarely occurred, longer lasting effects than metformin or glibenclamide, improved lipid profiles, pioglitazone is beneficial for coronary atherosclerosis, they have been in clinical use for decades	Expensive, weight gain, heart failure, oedema, increased risk of bone fracture
DPP-4 inhibitors	Linagliptin, sazagliptin, sitagliptin	Hypoglycaemia is rare	Costly, risk of pancreatitis, angioedema, less efficacy compared with GLP-1 mimetics
Alpha-glucosidase inhibitors	Acarbose, voglibose	Decreased postprandial glucose, rare occurrence of hypoglycaemia	Flatulence, GIT discomfort
GLP-1 receptor agonists	Exenatide, liraglutide,	Weight loss, rare hypoglycaemia,	Nausea and vomiting, unknown long term safety
Sodium glucose co-transporter 2 (SGLT2) inhibitors	Empagliflozin, dapagliflozin,	Low risk of hypoglycaemia	Vaginal yeast infections, urinary tract infections

1.2 Islets of Langerhans

Physiologically, the pancreas can be divided into exocrine and endocrine pancreas. The exocrine pancreas is the largest part of the pancreas. It is made up of acini cells arranged in small lobes. The exocrine pancreas secretes digestive enzymes such as proteases, lipase and amylase into the gut for breaking down protein, carbohydrate and lipid, while the endocrine compartment is made up of 2-3% of the total pancreatic volume. The endocrine pancreas is also known as the islets of Langerhans, and secretes mainly insulin, glucagon, somatostatin and pancreatic polypeptide. The islets of Langerhans are clusters of cells that are scattered throughout the pancreas (Figure 1-2 A) and were first described in 1869 by the German anatomy student Paul Langerhans. Islets are largely spherical in shape, with an average diameter of 100 - 200μm in mammals, irrespective of species, while pancreas size is dependent on species, increasing with body size (Jones and Persaud, 2010). Although islets have similar sizes, a healthy human pancreas contain up to a million islets while mouse pancreas has approximately 1000 islets (Bonnevie-Nielsen et al., 1983). However, only about 150 to 250 islets are recovered following collagenase digestion of mouse pancreas.

1.2.1 Islet cell types and morphology

Islets are comprised of five different cell types each producing a unique hormone. They are the insulin secreting β-cells, glucagon-secreting α-cells, somatostatin-secreting δ-cells, pancreatic polypeptide expressing cells and ghrelin expressing ε-cells. Human islets have proportionally fewer β-cells and more α-cells compared to mouse islets. Mouse islets consist of approximately 60–80% β-cells, 15–20% α-cells, <10% δ-cells, <5% PP cells and about 1% ghrelin cells while human islets contain about 50% β-cells, 40% α-cells, <10% δ-cells and few PP-cells (Cabrera et al., 2006; Steiner et al., 2010). Interspecies differences in the arrangement of the different islet cell types have been observed. In mice, islets are typically composed of densely packed β-cells located in the inner core, surrounded by a mantle of α-cells (Figure 1-2 B), while in human islets, β-cells are intermingled with other islet cells (Figure 1-3) (Kim et al., 2009).

Islets are richly supplied with blood vessels, accounting for approximately 15% of the total pancreatic blood supply despite its mass being only 2-3% of total pancreatic volume. Human

and mouse islets differ in many features including their vascular architecture. Human islets have fewer capillary density and less tortuous capillary networks compared to mouse islets (Brissova et al., 2015). Unlike mouse islets with single basement membrane (BM), the blood vessels of human islets have duplex BM consisting of an outer parenchyma BM and an inner capillary BM (Virtanen et al., 2008). The implication of the double BM in human islets is speculated to provide extra protection against autoimmune insulitis, since rapid and massive lymphocyte infiltration was observed in islets of NOD mice compared with human islets at early stage of T1D (Otonkoski et al., 2008).

Islets are also richly innervated, supplied by both sympathetic and parasympathetic nerve fibres containing the neurotransmitters norepinephrine and acetylcholine respectively. The sympathetic signal inhibits insulin and stimulates glucagon release to increase glucose supply in conditions of stress and anxiety. Sympathetic innervation is also necessary for pancreatic cytoarchitecture during islet development and functional maturation in mice (Borden et al., 2013). Differences in innervation between human and mouse islets have been identified. In human islets, sympathetic fibres preferentially innervate vascular smooth muscles rather than endocrine cells thereby providing an indirect effect on islet functions (Rodriguez-Diaz et al., 2011a). Generally, human islets are scarcely innervated with very few parasympathetic nerves in contrast with mouse islets with densely packed fibres. In human islets, α-cells secrete acetylcholine which exerts a paracrine effect on neighbouring β-cells and prime them for increased insulin secretion (Rodriguez-Diaz et al., 2011b).

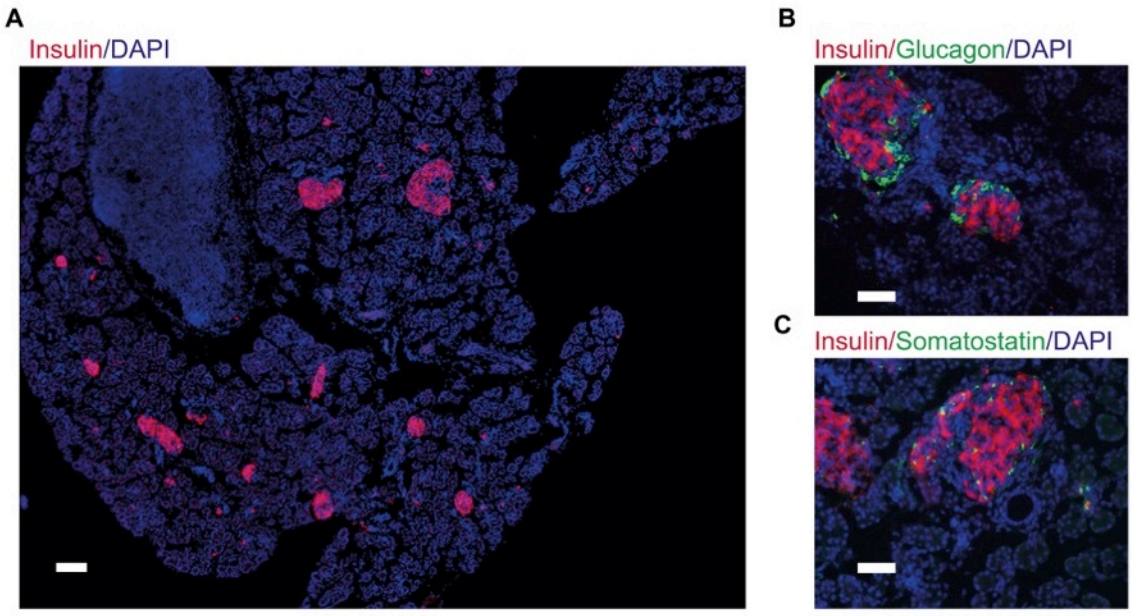

Figure 1-2: Anatomy of pancreas and islets of Langerhans from postnatal day 9 mice. A) The figure shows islets, identified by insulin immunostaining, scattered throughout pancreas as islands of cell clusters. Islets consist of about 2-3% of the total pancreatic volume. Scale bar = 100μm. B) Image of typical mouse islets showing β-cell core surrounded by a thin layer of α-cells, identified by glucagon immunostaining. Scale bar = 50μm. C). Somatostatin-producing δ-cells (green immunofluorescence) are scattered among other islet cells. Scale bar = 50μm.

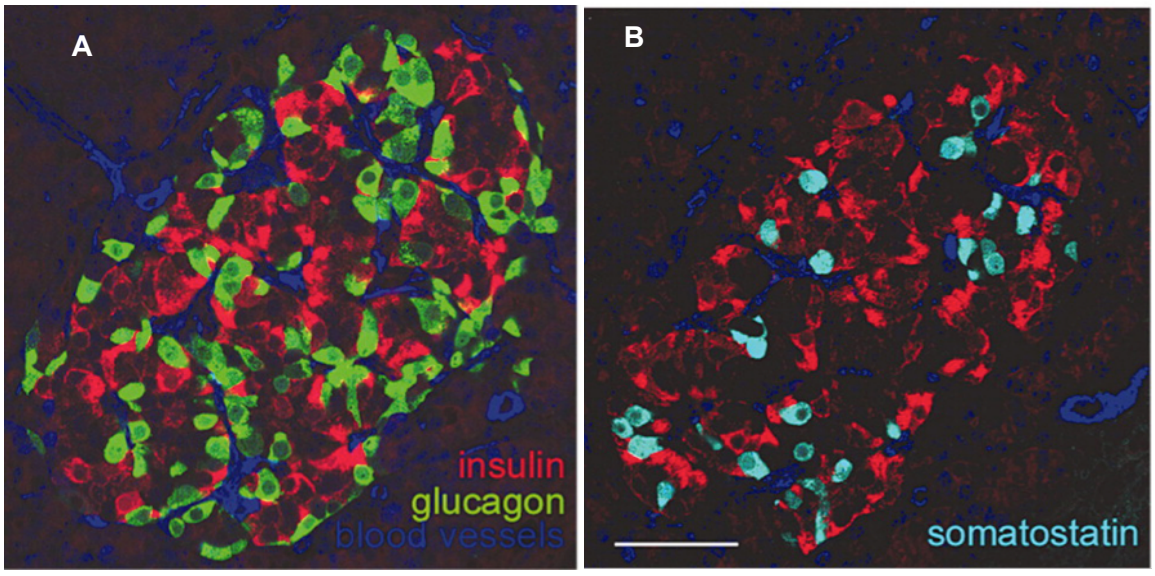

Figure 1-3: Human islets. A) Image shows the distribution of β-cells (red) and α-cells (green) in human islets indicating that their arrangement is less defined compared to mouse islets. Compared to mouse

islets, human islets contain proportionally fewer β-cells and a higher number of α-cells. B) Somatostatin-containing δ-cells are also scattered among other islet cells. Scale bar = 50μm. Images obtained from (Cabrera et al., 2006).

1.2.2 Intra-islet hormone communication

The spatial arrangement and interaction of islet cells in rodents and humans have functional implications in their ability to rapidly and efficiently respond to changes in blood glucose as a single entity rather than individually. Thus, insulin secretion from intact islets upon glucose challenge is synchronous and several-fold higher than from isolated β-cells (Do and Thorn, 2015). Islet cell types have co-ordinated mechanisms for maintaining glucose homeostasis via gap junctions, cell-cell contacts or through paracrine/autocrine signalling. Islet cells are functionally attached via gap junctions. Electron micrographs show that gap junctions such as connexin-36, tight junctions and E-cadherin are found along the membrane area where a β-cell meets another β-cell, allowing electrical activities and invariably intracellular calcium oscillation to spread from one cell to the other (Dahl et al., 1996). In addition, cell-cell contact suppresses insulin secretion at low glucose by regulating trafficking of insulin granules to the cell membrane and exocytosis (Benninger et al., 2011).

Moreover, islet cells can exert a functional influence on themselves or on neighbouring cells through the hormone that they secrete, by autocrine and paracrine signalling. For instance, glucagon is secreted from the α-cells at glucose concentrations of less than 3mM, and is inhibited by hyperglycaemia, when insulin secretion is stimulated. Insulin therefore inhibits glucagon secretion while glucagon stimulates insulin secretion. On the other hand, δ-cells regulate the secretory function of α- and β-cells by secreting somatostatin, which is a powerful inhibitor of glucagon and insulin secretion. Somatostatin receptors 2 and 5, Gi/o coupled GPCRs, are expressed on mouse and human α- and β-cells and their activation by somatostatin inhibits glucagon and insulin release (Gromada et al., 2001; Braun, 2014). The paracrine effect of islet hormones demonstrated in in vitro studies was, however, difficult to prove in vivo, as it had been noted that the amount of endogenous glucagon and somatostatin secreted into the venous effluent were too high to produce any local physiological effect (Kawai et al., 1982; Do

and Thorn, 2015). Other molecules secreted by the endocrine cells such as cations, neurotransmitters and nucleotides also contribute to the intra-islet paracrine interactions.

1.2.3 Islet-extracellular matrix interactions

Islets are also regulated by components of extracellular matrix (ECM), which are present in three islet areas: the peri-islet basement membrane (BM), interstitial BM and vascular BM (Korpos et al., 2013). The peri-islet BM and interstitial BM form the peri-islet capsule that encases each islet. The distribution of the various components of ECM in islets has been a subject of debate. However, recent data have shown that the peri-islet BM is mainly composed of collagen IV, laminin, nidogen and heparan sulfate proteoglycans (Korpos et al., 2013), while the interstitial BM is composed mainly of collagen I and III. The vascular BM is made up of laminin and collagen III. Collagen III, which is a ligand for GPR56 in the brain, is expressed by blood vessels and is found in the lobar, lobular and acinar septa of human and rat pancreas. It is not present in between individual endocrine cells but it is found in the ECM surrounding human islets (Deijnen et al., 1994). The traditional function of collagens was to provide mechanical support to tissues but recent studies have provided insights into their crucial roles in matrix-receptor signalling. Before the discovery of the integrin family, cells were thought to be attached to collagens by cell-specific ‘glues’ known as nectins including osteonectin and chondronectin. Osteonectin which is now referred to as Secreted Protein Acidic and Rich in Cysteine (SPARC) is expressed in islets by fibroblast and endothelial cells and it inhibits β-cell proliferation and survival (Ryall et al., 2014).

The peri-islet capsule provides a protective role against inflammatory assault. For example, in the NOD mouse model of T1D, the ECM component at the site of leucocyte infiltration at the peri-islet capsule is completely destroyed (Irving-Rodgers et al., 2008), which highlights the importance of the ECM component in T1D onset.

1.3 Glucose homeostasis

The islets of Langerhans play an important role in ensuring that plasma glucose levels are maintained within a narrow range of about 3 to 5mM in healthy individuals, despite glucose fluctuations that arise from intermittent eating and fasting. Although the regulation of glucose homeostasis is complex and involves many organs including the liver, skeletal muscle, fat, and the brain, insulin is the primary hormone responsible for bringing down elevated postprandial glucose, through glucose uptake by insulin sensitive tissues and glucose storage. Insulin is generated in humans from enzymatic cleavage of proinsulin, a 9kDa peptide containing two chains of insulin (A chain: 21 amino acids and B chain: 30 amino acids) joined by a C-peptide (Liu et al., 2014). Mature insulin is stored in secretory vesicles together with C-peptides and other biologically active compounds. Following nutrient absorption from the gastrointestinal tract, β-cells sense increase in circulating glucose, and insulin granules are released by exocytosis into the interstitial space, where they are transported via the blood stream to target tissues. Insulin binds to insulin receptors (IR) on target tissues. IR, being a tyrosine kinase autophosphorylates downstream insulin receptor substrate protein leading to translocation of glucose transporter 4 (GLUT4) to the cell surface of skeletal muscles and adipocytes (Ottensmeyer et al., 2000). The increased number of GLUT4 on the plasma membrane facilitates glucose uptake via an energy-independent process. Insulin secretion is then switched off by β-cells once the circulating nutrients are depleted while glucagon may be turned on to prevent hypoglycaemia. Glucagon binds to the Gs coupled glucagon receptor to generate cAMP, which activates protein kinase A (PKA). The eventual result is increased plasma glucose due to increased gluconeogenesis and glycogenolysis and decreased glycogen synthesis.

1.3.1 Regulation of insulin secretion

Insulin secretion is regulated by both nutrients e.g. glucose, amino acids and non-nutrients e.g. neurotransmitters, Glucose is a powerful regulator of insulin secretion from the β-cells. Unlike myocytes and adipocytes that utilises GLUT4 for glucose uptake, β-cells take up glucose via GLUT2 in rodents and GLUT1, 2 and 3 in humans (Mueckler and Thorens, 2013). GLUT2 is a high capacity, low-affinity glucose transporter, implying that it is functional only during periods of elevated blood glucose, allowing for large and rapid glucose influx into the β-cells. Once inside

the β-cells, glucose is phosphorylated by glucokinase to glucose-6-phosphate in the glycolytic pathway. Glucokinase ensures that insulin release is proportional to circulating extracellular glucose that is within the range of 5 and 15mM (Guo et al., 2012). Pyruvate, the end product of the glycolytic pathway, is converted to ATP in the mitochondria through the tricarboxylic acid cycle. This increases ATP/ADP ratio within the cell where ATP binds to the ATP-sensitive K^+ channel to close it (Ashcroft et al., 1984). In euglycaemia, inwardly rectifying potassium current maintains a resting membrane potential through potassium efflux; therefore, closure of the K^+ channel prevents K^+ efflux thereby causing membrane depolarisation. Depolarisation of β-cell membrane recruits Ca^{2+} intracellularly via the L-type voltage-gated calcium channel (VGCC) (Henquin, 2000). Increase in cytosolic calcium causes the 'readily releasable pool' of insulin granules to be docked to the plasma membrane for exocytosis leading to insulin secretion. This whole process is referred to as K_{ATP} channel dependent pathway or triggering pathway of insulin secretion and it accounts for the initial spike of insulin release seen in glucose stimulated insulin secretion perifusion experiments (Straub and Sharp, 2002). The initial spike, brought about by release of insulin granules from the immediately releasable pool is known as first phase insulin secretion.

As insulin release follows a biphasic pattern, the initial spike is immediately followed by a sharp decline in insulin release before it picks up slowly until a plateau is reached. This slowly releasing phase of insulin secretion is known as the second phase and a K_{ATP} channel independent pathway controls it (Gembal et al., 1992). The amplifying pathway or K_{ATP} channel independent pathway increases the efficacy of intracellular calcium to increase insulin secretion. It requires glucose metabolism and is dependent on the triggering pathway. Although the mechanism of the amplifying pathway is not fully understood, apart from adenine nucleotides, activation of major second messengers such as PKA, PKC, PI3K, ATP and acyl CoA are not involved in its regulation of insulin secretion (Sato and Henquin, 2014). It has been suggested that targeting this pathway may be beneficial, as the process involved in the amplifying pathway are impaired in T2D (Henquin, 2000).

Additional pathways involved in augmenting insulin secretion from β-cells are through the action of non-nutrients on receptors situated on their extracellular surface. Many of the non-nutrients signal by activating G-protein coupled receptors.

1.4 G-protein coupled receptors

G-protein coupled receptors (GPCRs) are the largest class of surface membrane receptors that convey a diverse array of signals and control many physiological processes. GPCRs have wide tissue distribution and more than 300 of them are expressed by human islets (Amisten et al., 2013). They share several similarities, such as possession of a single polypeptide with an extracellular N-terminus. Linked to this is a seven transmembrane domain (TM1 – TM7), with three extracellular and three intracellular loops, and an intracellular C-terminus (Gether, 2000). GPCRs are sometimes interchangeably referred to as '7TM receptors'; however, there are receptors with seven transmembranes that do not signal via G-proteins. GPCRs are generally expressed at low levels with only 0.01% to 0.001% of the Expressed Sequence Tags corresponding to GPCRs (Fredriksson and Schiöth, 2005). They constitute less than 2% of the human genome despite their large numbers of about 800 (Banères et al., 2011). More than half of the GPCRs have sensory functions and they are referred to as odorant or sensory GPCRs. Odorant GPCRs are expressed on specific cell types where they respond to external stimuli such as light, taste, odour and pheromones. On the other hand, non-odorant GPCRs are widely expressed in different tissue types and they respond to diverse endogenous agonists that regulate various biological processes (Mombaerts, 2004; Gao and Chess, 1999).

The first attempt to classify GPCRs made use of sequence similarities to group them into six classes. They were named by alphabets, as Class A (rhodopsin-like), Class B (secretin receptor family), Class C (metabotropic glutamate), Class D (fungal receptor), Class E (cyclic AMP receptor) and Class F (frizzled receptor). Of these, only classes A, B, C and F are found in vertebrates (Kolakowski, 1994). However, because of their abundance, this classification could not take into account the subtle differences between the GPCRs within the same group and an alternative system was developed to relate GPCRs structures to their functions and ligand preference. Based on structural similarity, the GPCR superfamily is sub-divided into five

classes: **G**lutamate, **R**hodopsin, **A**dhesion, **F**rizzled/taste and **S**ecretin, referred to as GRAFS classification (Fredriksson et al., 2003).

GPCRs exert their effects mainly via heterotrimetric G-proteins containing α, β and γ subunits. Activation of GPCR releases GTP-bound Gα from the complex. There are four main types of Gα: $G\alpha_i$, $G\alpha_s$, $G\alpha_{q/11}$ and $G\alpha_{12/13}$ (Simon et al., 1991; Strathmann and Simon, 1991). The coupling preference of the GPCRs to any of these Gα subtypes determines their effect on insulin secretion. Generally, GPCRs that signal via Gαs or Gαq tend to increase insulin secretion while signalling via Gαi inhibits it (Ahrén, 2009). The effect of $G\alpha_{12/13}$ on insulin secretion is not yet known. Recruitment of $G\alpha_s$ stimulates adenylyl cyclase leading to increased cyclic AMP. Coupling to $G\alpha_i$ inhibits adenylyl cyclase but stimulates mitogen-activated protein kinase (MAPK). $G\alpha_{q/11}$ signalling activates phospholipase C (PLC) that breaks down PIP_2 into diacylglycerol and inositol triphosphate. These second messengers increase intracellular calcium levels by releasing calcium from the internal stores and also stimulate protein kinase C (PKC). In addition, $G\alpha_{q/11}$ increases phosphoinositol-3-kinase and Akt signalling. Activation of $G\alpha_{12/13}$ leads to increase in Rho signalling and remodelling of actin cytoskeleton (Suzuki et al., 2009). On the other hand, GPCRs can bind to non-G proteins such as β-arrestins to mediate distinct biological processes. β-arrestins bind to C-terminal domains of GPCRs that have been phosphorylated by a group of kinases called GPCR kinases, and causes them to be internalised and recycled or degraded (Oh and Olefsky, 2016).

1.4.1 GPCRs as novel targets for T2D therapy

GPCRs play important roles in modern medicine, as they are the targets of about 50% of all prescription drugs in clinical use (Cook, 2010). GPCRs are involved in growth, differentiation, secretion, maturation and survival of islet cells (Ahrén, 2009), therefore certain GPCRs have emerged as potential targets for treating islet dysfunction and T2D. The most well studied islet GPCR target is glucagon-like peptide 1 (GLP-1) receptor. GLP-1 is released by enteroendocrine cells upon nutrient stimulation into the blood stream, where it is largely degraded by dipeptidyl peptidase 4 (DPP-4) before it reaches the pancreas. GLP-1 has three main effects on islet functions. First, it increases insulin secretion via Gs and cAMP recruitment by binding to GLP-1R on β-cells. The glucose-lowering effect of GLP-1 has also been linked to its ability to

substantially inhibit glucagon secretion. Secondly, since a small fraction of the released GLP-1 reaches the pancreas, it has been suggested that endogenous GLP-1 may modulate islet function indirectly through the CNS by acting on enteroendocrine neurons. GLP-1 also improves islet function by inhibiting β-cell apoptosis and promoting β-cell proliferation (Preitner et al., 2004; Xu et al., 1999; Doyle and Egan, 2007; Tourrel et al., 2001). Synthetic ligands of GLP-1R are available commercially as injectables for T2D and they include exenatide and liraglutide (Table 1-1). A strategy to increase the amount of GLP-1 that reaches the pancreas such as by inhibiting DPP-4 has also been developed (Oh and Olefsky, 2016). Other GPCRs that have received considerable attention for diabetes therapy include GPR40/FFAR1, GPR119, GPR120/FFAR4 and TGR5. In some cases, molecules targeting these GPCRs have either been discontinued due to lack of efficacy or currently undergoing clinical trials (Table 1-2).

Table 1-2: Summary of GPCRs that have received considerable attention in diabetes therapy and the status of their ligands in clinical trials (Hodge et al., 2013; Reimann and Gribble, 2016; Oh and Olefsky, 2016).

Receptor	**Ligands**	**Effect of GPCR activation**	**Clinical trials**
GPR40	Natural: long chain non-esterified fatty acids Synthetic: TAK-875, AMG-837, JTT-851, P11187	Increased GLP-1, increased insulin, improved glucose tolerance	None in clinical trials
GPR119	Natural: oleoylethanolamide, monooleoyglycerol Synthetic: MBX-2982, GSK1292263, PSN-821	Increased GLP-1, increased insulin and, increased β-cell survival	MBX-2982: Discontinued due to lack of efficacy GSK1292263: discontinued due to lack of efficacy PSN-821: Phase II
GPR120	Natural: long chain non-esterified fatty acids Synthetic: GW9508, TUG-891, Compound A	Increased GLP-1, decreased somatostatin, reduced inflammation	None in clinical trials
TGR5	Natural: bile acids Synthetic: SB756050	Increased GLP-1, increased energy expenditure	SB756050: Discontinued due to lack of efficacy

1.4.2 Adhesion GPCRs

The adhesion GPCR family is made up of 33 members with nine distinct subclasses (Table 1-3). In addition to the canonical seven transmembrane segments common to other GPCRs, adhesion GPCRs have extended N-terminal and undergo self-cleavage during maturation at the GPCR proteolytic site (GPS) within the GPCR autoproteolysis-inducing (GAIN) domain. The GAIN domain is a unique evolutionarily conserved structure of adhesion GPCR that is required for self-cleavage (Prömel et al., 2013). The N and C terminals re-associate upon maturation and remain non-covalently attached. The GPS is found immediately upstream of the first transmembrane loop and is rich in cysteine residues alternating with tryptophan in a C-W-W-C-C conserved sequence (Araç et al., 2012). The N-terminal of adhesion GPCRs contains mucin-like motifs, which is suggested to help them in cell adhesion and cell-matrix interactions. Adhesion GPCRs are widely expressed in tissues such as the reproductive tract, neurons, stomach, lungs and various tumour cells, where they play varying roles in angiogenesis, cell adhesion, immune recognition and neuronal migration (Simundza and Cowin, 2013).

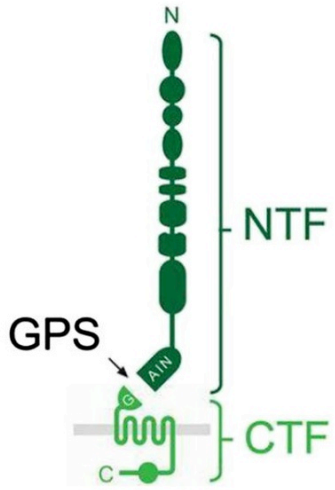

Figure 1-4: Adhesion GPCR architecture. Adhesion GPCRs have unusually long N-terminal fragment (NTF) containing several adhesive motifs and it is joined non-covalently to the C-terminal fragment (CTF) at the GPCR proteolytic site (GPS) within the GAIN domain (Hamann et al., 2015).

1.4.3 Mode of signalling of adhesion GPCRs

As mentioned earlier, N-terminal fragment of most mature adhesion GPCRs attaches non-covalently with the membrane bound C-terminal fragment at the GPS, and the cleavage of this has been suggested to modulate receptor activity. The GPS is a highly conserved cysteine-rich sequence, found immediately upstream the first transmembrane strand. Increased activities were observed in studies involving GPR56, CD97 and BAI1 mutants where the N-terminal domains have been removed (Paavola et al., 2011; Ward et al., 2011; Stephenson et al., 2013). Based on this observation, two modes of signalling have been proposed for adhesion GPCRs: i) the extracellular domain acts as an inverse agonist of constitutive signalling, and its removal, whether by ligand binding or mechanical detachment, is necessary for receptor activation, and ii) a part of the extracellular domain buried in the GAIN segment acts as a tethered agonist, which is exposed to the 7TM upon ligand binding. The second scenario seems more likely, as it has been demonstrated in a number of adhesion GPCRs including GPR56, GPR126, GPR133, GPR64 and GPR114 (Wilde et al., 2016; Stoveken et al., 2015; Liebscher et al., 2014; Demberg et al., 2015; Kishore et al., 2016; Stoveken et al., 2017).

1.4.4 Role of adhesion GPCRs in metabolic functions

Many of the adhesion GPCRs are expressed in pancreas or islets but at low levels, except latrophilin 1, ELTD1 and GPR56 that are strongly expressed (

Table 1-3). More than two-thirds of adhesion GPCRs are still orphans with no known endogenous ligands. Studies using knockout mouse models are beginning to shed light on the biological effect of adhesion GPCRs on endocrine and metabolic functions. For instance, adipose tissue specific deletion of GPR116 produced mice that were glucose intolerant and insulin resistant (Nie et al., 2012). PDX1 specific deletion of the adhesion GPCR Celsr2/3 produced mice that were glucose intolerant. However, the insulin secretory capacity of their β-cells was not affected. In addition to impaired glucose tolerance, loss of Celsr2/3 produced mice with severe pancreatic β-cell differentiation deficiency (Cortijo et al., 2012) while single nucleotide polymorphisms in Celsr2 have been correlated with reduced low-density lipoprotein levels in humans (Kathiresan et al., 2008).

Table 1-3: Expression profile of adhesion GPCRs in human pancreas (protein) and islets (protein or mRNA). Protein information for most of the GPCRs were from immunohistochemistry data from the human protein atlas project (Uhlen et al., 2015). RNA expression were from qPCR and RNA-Seq data (Amisten et al., 2013; Uhlen et al., 2015). Yes (+++): strongly expressed, Yes(++): moderately expressed, Yes(+): slightly expressed, No: not detected or unavailable data, (-): unknown or not yet investigated.

Adhesion GPCR / **Subgroup**		**Expression in human?**		**Ligands**	**Phenotype in KO mice**
		Pancreas	**Islets**		
I	ADGRL1 (LPHN1)	Yes	Yes (+++)	α-latrotoxin	-
	ADGRL2 (LPHN2)	No	Yes (+)	α-latrotoxin	-
	ADGRL3 (LPHN3)	Yes	No	Fibronectin leucine rich transmembrane protein 3	-
	ADGRL4 (ELTD1)	No	Yes (++)	-	-
II	ADGRE1 (EMR1)	No	No	-	-
	ADGRE2 (EMR2)	No	Yes (+)	-	-
	ADGRE3 (EMR3)	No	No	-	-
	ADGRE4 (EMR4)	No	No	-	-
	ADGRE5 (CD97)	No	Yes (+)	-	-
III	ADGRA1 (GPR123)	No	Yes (+)	-	-
	ADGRA2 (GPR124)	No	Yes (+)	Glycosaminoglycans	-
	ADGRA3 (GPR125)	Yes	Yes (+)	-	-
IV	ADGRC1 (CELSR1)	No	Yes (+)	-	-
	ADGRC2 (CELSR2)	No	Yes (+)	-	-
	ADGRC3 (CELSR3)	No	Yes (+)	-	Impaired β-cell differentiation
V	ADGRD1 (GPR133)	Yes	Yes (+)	-	-
	ADGRD2 (GPR144)	No	No	-	-
VI	ADGRF1 (GPR110)	Yes	No	-	-
	ADGRF2 (GPR111)	No	No	-	-
	ADGRF3 (GPR113)	No	Yes (+)	-	-
	ADGRF4 (GPR115)	No	Yes (+)	-	-
	ADGRF5 (GPR116)	No	Yes (+)	-	Hyperlipidaemia, impaired glucose tolerance and insulin resistance, decreased adipocyte size

VII	ADGRB1 (BAI1)	No	No	Phosphatidylserine	-
	ADGRB2 (BAI2)	No	Yes (+)	-	-
	ADGRB3 (BAI3)	No	Yes (+)	-	-
VIII	ADGRG1 (GPR56)	Yes	Yes (+++)	Collagen III, TG2, heparin, progastrin	-
	ADGRG2 (GPR64)	No	No	-	-
	ADGRG3 (GPR97)	No	Yes (+)	Beclometazone dipropionate	-
	ADGRG4 (GPR112)	No	Yes (+)	-	-
	ADGRG5 (GPR114)	No	Yes (+)	-	-
	ADGRG6 (GPR126)	No	Yes (+)	Collagen IV	-
	ADGRG7 (GPR128)	No	No	-	-
IX	ADGRV1 (VLGPR1)	Yes	No	-	-

1.4.5 GPR56

GPR56, previously known as Cyt28, is a member of the adhesion class of GPCRs. It was recently renamed adhesion G-protein coupled receptor G1 (ADGRG1) when the nomenclature of the entire class of adhesion GPCRs was revised in 2015 (Hamann et al., 2015). GPR56 is located on chromosome 8 in mouse and chromosome 16 in human, suggesting a similar evolutionary origin involving gene duplication.

GPR56 consists of 13 exons, with 693 amino acids in human and 697 in mouse. It undergoes alternative splicing to yield four isoforms namely $GPR56_{687}$, $GPR56_{692}$, $GPR56_{523}$ and $GPR56_{518}$ (Kim et al., 2010). Consistent with other adhesion GPCRs, GPR56 has an usually long N-terminal ($GPR56^{N}$) segment consisting of 393 amino acids, which is further divided into four segments. The first 26 amino acids is a signal peptide, followed by the ligand binding site (27 – 160 aa), the STP region (108 – 177 aa), which is rich in serine, threonine and proline and the GPS. GPR56 agonist, collagen III, acts by binding to the ligand binding domain while another GPR56 binding partner, transglutaminase 2, binds to the STP segment. Deletion of the region between amino acids 97 and 143 on GPR56 completely abolished collagen III binding property (Li et al., 2008). $GPR56^{N}$ is heavily glycosylated with 7 glycosylation sites, which is important in trafficking GPR56 to the cell surface. Mutations in $GPR56^{N}$, which either prevent cell surface

expression or alters glycosylation pattern are linked to a rare human disease called bilateral frontoparietal polymicrogyra (BFPP) (Jin et al., 2007).

1.4.5.1 Tissue distribution of GPR56

GPR56 has a wide tissue distribution. It is expressed in thyroid gland, brain, pancreas, testis, lungs, placenta, muscle, kidney, liver, adipose and heart (Iguchi et al., 2008; White et al., 2014; Bjarnadóttir et al., 2004; Amisten et al., 2015; J. B. Regard et al., 2008). Because of its abundant expression in leukocytes and stem cells, GPR56 has been postulated to be a marker for cytotoxic T cells, haematopoietic and neural stem cells (Terskikh et al., 2001; Della Chiesa et al., 2010; Peng et al., 2011). GPR56 is expressed in the CNS where it plays a role in neural cells migration and cortical development (Singer et al., 2013). The hippocampus and the hypothalamus are particularly known for their high GPR56 mRNA expression (Liu et al., 1999). With this varied tissue expression ranging from brain cells to peripheral tissues, GPR56 may play a more general/basic cell function. However, it may play an important role in tissues where it is highly expressed, since it is well established that receptors that are abundantly expressed in a particular tissue play significant role in the functions of that tissue (Regard et al., 2008). GPR56 is the most abundant GPCR in human islets (Amisten et al., 2013). If the high mRNA expression of GPR56 identified in human islets translates to abundant protein level, GPR56 may therefore serve as a key modulator of islet functions.

1.4.5.2 Physiological functions of GPR56

GPR56 was the first adhesion GPCR to be linked to a human disease known as BFPP. BFPP is an inherited human brain disorder involving improper lamination of the cerebral cortex, and arises as a result of loss of function germline mutation in GPR56. The four missense mutations which all occur at the N-terminal are R38W, Y88C, C91S and C346S. Patients with BFPP suffer from moderate to severe mental retardation, seizures, poor eye muscle co-ordination and cerebral hypoplasia (Piao et al., 2004; Parrini et al., 2009; Luo, Yang, et al., 2011). Studies in neuronal development in mice have indicated that GPR56 is critical for the proper formation of the cerebellum, as it allows the developing neurons to adhere to the ECM of pial basement membrane. Failure of this process leads to neuronal overmigration and ectopia. Moreover, loss of GPR56 leads to hypomyelination of the CNS as a result of defective development of

oligodendrocyte precursor cells (Luo et al., 2011; Li et al., 2008). Outside the CNS, GPR56 plays structural functions in seminiferous tubule development where its absence during embryogenesis leads to male infertility (Chen et al., 2010). GPR56 is highly expressed in $NGN3^+$ endocrine progenitors in the developing pancreas (Gu et al., 2004), but its function in islet development is not yet known. The function of GPR56 in the brain is well established and it may provide clues about its role in islets. Although islets and the brain do not arise from the same developmental origin, they share several similarities such as the presence of similar evolutionary conserved elements, overlap of several metabolic pathways and gene expression. It is likely that GPR56 may play similar role in development, proliferation and migration in islets.

1.4.5.3 Agonist and binding partners of GPR56

It was postulated that adhesion GPCRs will have multiple interacting ligands due to their usually long N-terminal segment with adhesive motifs, and their broad expression in many tissues. Indeed, four binding partners have been identified for GPR56 and they include collagen III, transglutaminase 2, heparin, and progastrin. A synthetic peptide TYFAVLM/P7, that selectively activates GPR56 based on the stachel sequence present in its GAIN domain, has also been reported (Stoveken et al., 2015).

Collagen III

Collagen III was the first GPR56 agonist to be discovered. It binds to GPR56 to regulate cortical brain development. Collagen III activates GPR56 with an EC_{50} of 84nM (Luo et al., 2011). Collagen III, a fibril forming substance, is a major structural component of the ECM of many tissues. In the pancreas, it is found in islets vasculature and also in the lobar, lobular and acinar septa (Deijnen et al., 1994). An antibody directed against the N-terminal of GPR56 was also found to have similar agonistic effect as collagen III. The $GPR56^N$ antibody produced GPR56-dependent SRE/NFkB and RhoA signalling (Iguchi et al., 2008)

Transglutaminase 2

Transglutaminase 2 (TG2) was identified as a putative binding partner of GPR56 by in situ receptor affinity probe. It binds to the STP region of $GPR56^N$ but it is unclear whether it acts as a traditional agonist as no downstream signalling is known. The interaction between TG2 and

GPR56 is thought to play a part in suppressing melanoma tumour growth and metastasis (Xu et al., 2006). TG2, also known as tissue transglutaminase or high molecular weight GTP binding protein, is a ubiquitous protein with three distinct biological functions. First, it is a Ca^{2+} dependent transamidase serving as a cross-linking protein forming amide bonds between glutamine and lysine. Secondly, it functions as an intracellular G protein for many GPCRs, activating phospholipase C and, lastly, as an adaptor protein facilitating interactions between ECM and integrins to promote cell adhesion (Lorand and Graham, 2003).

Report on the roles of TG2 on glucose homeostasis is conflicting. The transamidase activity of TG2 was suggested to modulate insulin exocytosis from isolated islets while inhibitors of TG2 decreased glucose stimulated insulin secretion in a dose-dependent manner (Bungay et al., 1986). Islets isolated from TG2 null mice were less sensitive to glucose and they secrete less insulin compared to wild type. In these mice, blood glucose concentration was considerably high after OGTT compared to wild type mice (Bernassola et al., 2002). In humans, TG2 was identified as a candidate gene for early onset diabetes. Missense mutations in TG2 gene were found in some Italian families with maturity onset diabetes of the young (Porzio et al., 2007). On the other hand, Iismaa and colleagues found no difference in the glucose stimulated insulin secretion in homozygous TG2 null mice compared to the wild type (Iismaa et al., 2013). Overexpression of the TG2 gene also showed no effect on glucose homeostasis. The animals used in the Bernassola study were cross-bred from different strains which the Iismaa group claimed would ordinarily make them develop insulin resistance. They argued that inhibitors of TG2, such as monodancylcadaverine used in previous experiments, would obviously decrease glucose-stimulated insulin secretion because those inhibitors prevent insulin exocytosis. On examining the pedigrees of the Italian families with missense mutations in TG2 encoding genes, they ruled out that the mutation is not fully penetrant and concluded that there is no association between tranglutaminase 2 and glucose homeostasis.

Heparin

Heparin is another high molecular weight binding partner of GPR56. It interacts with GPR56 between amino acids 26 to 35 and 190 to 200, which partially overlaps with collagen III and TG2 binding sites respectively. The functional consequence of GPR56-heparin interaction includes

promotion of cell adhesion and migration. However, activation of downstream signalling molecules was not detected (Chiang et al., 2016).

Progastrin

It was recently shown that progastrin, a cleaved form of preprogastrin produced by the G-cells of the small intestine, binds GPR56 to promote proliferation and reduced apoptosis of colonic epithelial cells (Jin et al., 2017). Gastrin is typically expressed in developing pancreas and it becomes turned off in adult islets (Larsson et al., 1976). Gastrin expression is switched on in adult islets exposed to severe hyperglycaemia, in rodents and humans with T2D, but disappears when glucose level is restored to normal, indicating that it could be a marker for reversible dedifferentiating β-cells (Dahan et al., 2016). Gastrin increases islet mass by stimulating β-cell neogenesis from transdifferentiated (from acinar to ductal cells) exocrine tissue (Rooman et al., 2002).

1.4.5.4 Signalling pathways of GPR56

Collagen III binds to GPR56 to activate RhoA through Gα12/13 protein in the developing brain. However, in β-cells, activation of GPR56 by collagen III has been shown to inhibit RhoA (Dunér et al., 2016), indicating that collagen III – GPR56 activation may have differential effects on RhoA signalling based on cell type. Rho protein family belongs to the Ras superfamily and include small GTPases such as Rho, Rac and Cdc42. They are involved in the formation of actin cytoskeleton, maintaining cell polarity and migration. In skeletal muscles, GPR56 couples to Gα12/13 to activate mammalian target of rapamycin (mTOR). In addition, GPR56 associates with Gq11, which is stabilized by the scaffolding proteins CD9 and CD81 (Little et al., 2004). The function of this interaction on GPR56 signalling is not yet known, but it is likely to couple to PKC. Full length GPR56 inhibits VEGF by suppressing PKCα while truncation of STP region of GPR56 or overexpression of $GPR56^{C}$ activates VEGF and PKCα, which in turn leads to increased angiogenesis in melanoma cells (Yang et al., 2011). Overexpression of GPR56 induces the transcriptional activities of NFAT, NF-κB, TCF and E2F response elements while at the same time suppressing expression of c-myc and p53, suggesting that GPR56 may be involved in cell adhesion, proliferation and apoptosis (Iguchi et al., 2008; Kim et al., 2010; Shashidhar et al., 2005).

1.5 Aims

The overall aim of this thesis is to identify the expression and function of GPR56 and collagen III in islets of Langerhans. Specifically, the objectives are to:

- ✓ Determine the mRNA and protein expression of GPR56, its agonist, collagen III, and its binding partners, CD81 and latrophilin 1 in islets.
- ✓ Investigate the role of GPR56 in islet development
- ✓ Investigate the effect of GPR56 on β-cell adhesion and pseudoislet formation.
- ✓ Investigate the effect of GPR56 on β-cell proliferation and apoptosis using gain-of-function studies. The effect of GPR56 deletion on β-cell proliferation and islet mass will also be investigated using GPR56 KO mice
- ✓ Characterise the islet architecture, islet vascularisation/innervation and glucose handling properties of GPR56 KO mice
- ✓ Study the acute and chronic effect on collagen III on insulin secretion and determine whether it exerts its effect via GPR56
- ✓ Determine the downstream signalling of GPR56 in islets.

Chapter 2

Chapter 2 Materials and Methods

2.1 MIN6 β-cell culture

Cell culture is a common technique for the growth and maintenance of cells outside their normal environment. For cells to grow and replicate, they must be provided with the necessary nutrients to which they were exposed to *in vivo*. Culture media, therefore, are usually extracellular salt solutions to which appropriate nutrients for cell growth have been added. Such nutrients include amino acids, vitamins, inorganic salts, and glucose. Serum and antibiotics are also added to culture media. Serum provides grow factors and acts as a pH buffer while antibiotics prevent bacterial contamination.

Pancreatic β-cell lines offer excellent alternatives to primary islets in the study of β-cell function. Although primary islets are the obvious gold standard model for clinically relevant studies on islet functions, they are not readily available and are laborious to isolate. Isolating human islets, for example, is labour-intensive, and expensive in terms of the facilities required for maintaining Good Manufacturing Practices. Human islets are also in short supply as they are prioritised for transplantation. Cell lines that share the necessary similarities with islets, such as the ability to secrete insulin upon glucose challenge, have therefore been developed. Such cell lines with close functional resemblance to primary β-cells include INS1 and MIN6 β-cells (Skelin et al., 2010; Persaud, 1999).

The MIN6 β-cell line used in this thesis was established from pancreatic tumour material derived from a transgenic mouse in which the insulin promoter drove SV-40 antigen expression and uncontrolled β-cell proliferation. MIN6 β-cells express Glut-2 and glucokinase, which are the primary determinants of functional β-cells for glucose entry and phosphorylation. However, despite their close functional resemblance to primary β-cells, cell lines also have their limitations. MIN6 β-cells for instance, showed decreased insulin secretory responses to glucose

at high passage, usually above 55 (Hauge-Evans et al., 1999), so it is important to use these cells within a defined passage range to maximise the usefulness of the data obtained.

2.1.1 Maintaining and sub-culturing MIN6 β-cells

MIN6 β-cells were maintained in culture at 37^0C in Dulbecco Modified Eagle's Medium (DMEM) containing 10% fetal bovine serum (FBS), 2mM L-glutamine and 100U/ml penicillin/0.1mg/ml streptomycin. Passages from 24 to 45 were used for the experiments described in this thesis. Phenol red was present in the DMEM: it acted as a pH indicator and changes in colour from orange to yellow when there was a build-up of acidic metabolites indicated that the cells were overgrown or that the medium had not been changed regularly.

MIN6 β-cells were grown as monolayers in an aseptic environment and medium was changed every 3-4 days to replenish nutrients. Once the cells were about 70-80% confluent, they were sub-cultured by trypsinisation. Briefly, MIN6 β-cells were exposed to a solution of trypsin/EDTA (0.1%/0.02%) for about 2 min in an incubator at 37^0C. As MIN6 β-cells are adherent cells, they become detached from tissue culture flask in the presence of trypsin/EDTA. Trypsin digests the anchorage sites between cells and the flask while EDTA, being a chelating agent, binds to Ca^{2+} and makes it unavailable for calcium-dependent adhesion. Trypsin/EDTA is sufficient to lift cells from the flask, but in order to aid complete detachment of cells and to prevent excessive exposure of cells to trypsin, which can cause over-digestion, the flask was given a firm tap against the palm. Serum-containing DMEM was then added to stop trypsin's action. After centrifugation at 1000rpm for 2 min, the MIN6 β-cell pellet was re-suspended in fresh DMEM and cells were sub-cultured in a T75 or T125 flask containing 15ml or 25ml media respectively.

2.1.2 Cryopreservation and thawing of MIN6 β-cells

MIN6 β-cells can be preserved for future use by freezing them in a cryoprotectant at -196^0C. At this temperature, all biological and biochemical activities that can cause cell death are arrested and cells can be stored long term without affecting viability and function. Once MIN6 β-cells had reached a confluency of about 70 to 80%, they were trypsinised and re-suspended in 10ml of DMEM as described in section 2.1.1. After centrifugation, cells were re-suspended in freezing medium made up of 10% ($^V/_V$) sterile DMSO in full DMEM to give 1 x10^6 viable cells / ml and

transferred into Nunc® cryovials. DMSO was used as a cryoprotectant, to prevent cell damage, which can occur from ice crystal formation at freezing temperatures. The cryovials were then transferred into a cryogenic freezing container called 'Mr Frosty' and placed in a -80^{0}C freezer overnight before being transferred into liquid nitrogen (-196^{0}C) for longer storage. Mr Frosty has an outer compartment, which was filled with 100% iso-propranol that allows a uniform cooling rate of -1^{0}C/min. This is important for cell preservation as it controls the rate and size of ice crystal formation.

To reconstitute cells from frozen storage, cryovials were retrieved from liquid nitrogen and quickly placed into a 37^{0}C water bath with gentle agitation to facilitate thawing. Once thawed, the cryovial contents were immediately transferred into sterile 15ml Eppendorf tubes followed by the addition of 10ml full DMEM and centrifuged at 1000rpm for 5 min. The supernatant was aspirated and cells were re-suspended in fresh growth medium before being transferred into a 25cm^3 tissue culture flask (T25). Cells were allowed to adhere overnight and medium was replaced to remove any non-adherent cells or residual DMSO. The cells were then cultured in an incubator (95% air/ 5% CO_2) at 37^{0}C.

2.1.3 Cell counting and viability

MIN6 β-cell suspensions were mixed with 0.2% trypan blue in equal volumes and allowed to stand for 5 min, to enable compromised cells take up the dye. Trypan blue is a low molecular weight dye which allows viable cells to be distinguished from non-viable ones: viable cells with intact plasma membranes will not take up dye and they stain bright under a light microscope. However, dead cells appear dark blue as the dye is able to access the cell interior via the compromised plasma membrane. The haemocytometer chamber was created by placing a moistened cover slip over the slide and pressing firmly until Newton rings were observed. 10µl of the MIN6 β-cell-Trypan blue mixture was added to the chamber by capillary action. Using the 10X objective of a phase-contrast inverted microscope, cells in the four 0.1mm^3 corner squares (Figure 2-1) were counted and an average cell density was calculated. The total number of cells/ml was estimated using the formula below, while taking into account dilution with Trypan blue:

Total cell number/ml = Average cell number of the four corner squares x 10^4 x 2 (dilution factor)

10^4 is the conversion factor to convert 10^{-4}ml to 1 ml. 10^{-4}ml is the volume of one large corner square which was obtained by multiplying the area of the square with the depth created by the cover slip.

Therefore the volume of a corner square = 1mm^2 x 0.1mm = 0.1cm x 0.1cm x 0.01cm

= 10^{-4} mm^3 or 10^{-4} ml

To estimate cell viability, the number of viable cells was expressed as a percentage of the total number of viable and non-viable cells.

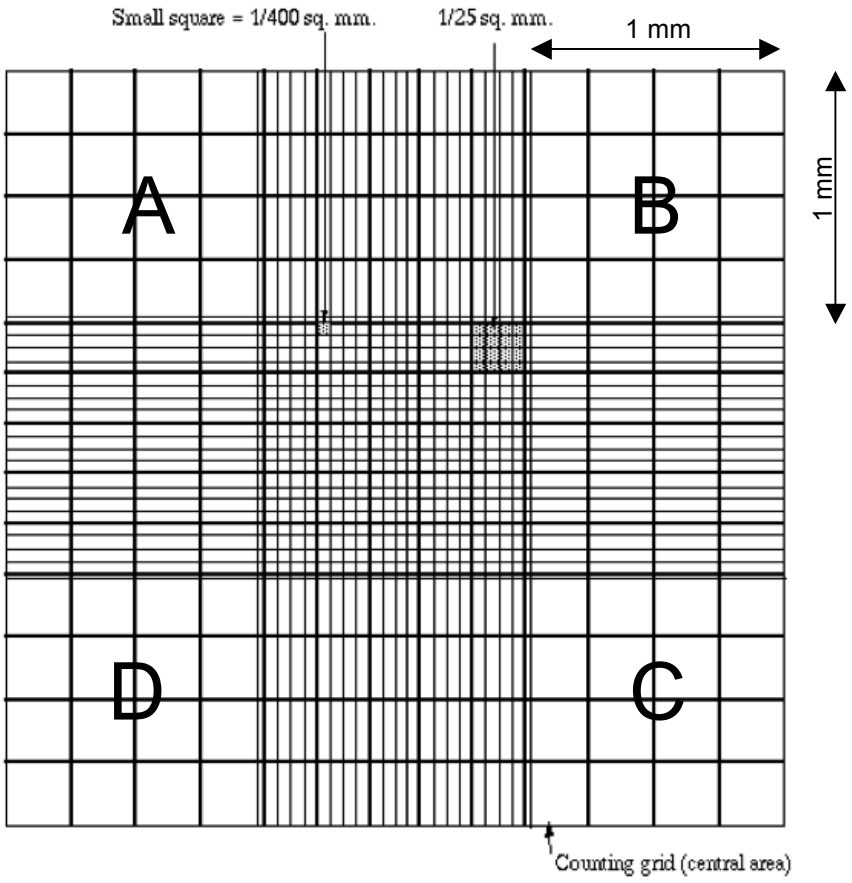

Figure 2-1: Haemocytometer grids showing the four corner squares used for cell counting. Cells in A, B, C & D were counted and an average was calculated. Each corner grid is 1mm by 1mm and the cover slip creates a depth of 0.1mm, giving a volume of 0.1mm^3. (Image taken from www.nexcelom.com)

2.2 Islet isolation and maintenance

2.2.1 Isolation and culture of mouse islets

Islets were isolated from ICR and C57BL/6 mice (≥25g) aged 6 – 8 weeks. Mice were humanely killed by cervical dislocation before incisions were made to expose the abdominal cavity. 2 – 3 ml collagenase solution (1mg/ml collagenase in Minimal Essential Medium) was injected via the bile duct into the pancreas after clamping the ampulla of vater, which is the point at which the bile duct empties into the small intestine (Figure 2-2). The distended pancreas was carefully dissected out and placed in a water bath at 37^0C for 10 min to aid the digestion of the exocrine tissue surrounding the islets. Digestion was stopped by adding 25ml of MEM supplemented with 10% FBS and the digest was centrifuged three times at 1400 rpm for 1.15 min each. The supernatant was discarded and pancreas pellets were re-suspended in DMEM, vortexed and passed through a sieve that prevents non-digested fat and exocrine tissues >425µm from passing through. Islets were purified by histopaque gradient centrifugation at 3510rpm. Histopaque is a polysucrose solution with a density of 1.077g/ml. Islets at the interface of MEM and histopaque were retrieved, washed three times in MEM at 1500rpm before being handpicked and sterile-washed in RPMI (supplemented with 10% FBS, 2mM L-glutamine and 100U/ml penicillin/0.1mg/ml streptomycin). Islets were maintained in culture at 37^0C (95%air/5%O_2) prior to use.

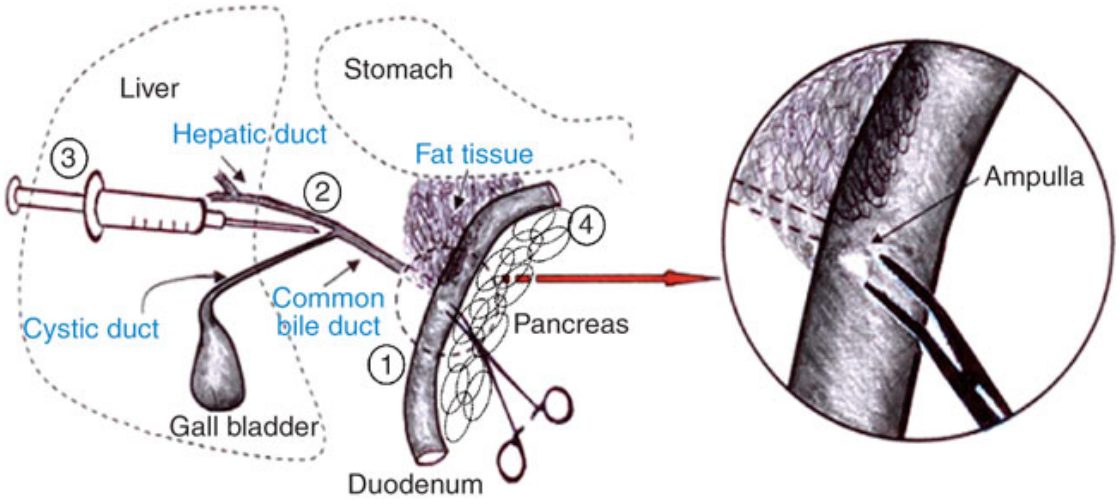

Figure 2-2: Steps involved in islet isolation. 1) The ampulla of vater was first located and clamped with a bulldog clamp. As shown in the insert, it is the point at which the common bile duct empties into the small

intestine. 2) A needle was inserted into the bile duct at the junction where hepatic and cystic ducts meet. 3) Collagenase solution was injected until the pancreas was distended and, 4) the collagenase-containing pancreas was retrieved by dissecting it away from the duodenum, stomach and spleen. Image taken from Li et al., 2009.

2.2.2 Isolation and culture of human islets

Human islets were provided by the Islet Isolation/Transplantation Unit of King's College Hospital. They were isolated from healthy, non-diabetic, heart-beating cadaveric donors. Appropriate ethical approval was obtained from the Ethics Committee of King's College London and consent for research use was obtained from the relatives of donors. Islets were isolated by Liberase digestion of the exocrine pancreas and isolated islets were maintained in CMRL medium for 24 – 48h at 37^0C (95% air/ 5% CO_2) prior to use.

2.3 Gene expression

Polymerase Chain Reaction (PCR) is a common technique used for detecting and quantifying gene expression. This was made possible by the invention of novel thermal cyclers that enable reproducible, cycle-by-cycle detection and quantification of accumulating PCR products. The success of this technique, however, relies on two earlier steps, which are the isolation of high quality RNA or DNA and, in the case of RNA, its conversion into complementary DNA (cDNA).

2.3.1 Total RNA extraction

Total RNA was extracted from MIN6 β-cells, mouse and human islets using the Qiagen RNeasy column kits. Isolated islets and MIN6 β-cell pellets were either stored at -80°C in RNA*later*® solution prior to use or immediately lysed in 500µl of RLT buffer containing 2-mercaptoethanol ($1\%^{V}/_{V}$). RLT buffer contains a high concentration of guanidine isothiocyanate (GITC), which denatures cellular proteins, including RNAses. MIN6 β-cells and islets have high concentrations of RNAses, and 2-mercaptoethanol ($1\%\ ^{V}/_{V}$) was added to enhance the inactivation of these enzymes.

For mouse and human islets, up to 700µl of lysate was homogenised by being passed through a QIAshredder column with centrifugation for 2min at 12000 rpm. MIN6 β-cells, on the other

hand, were pipetted up and down several times, which is sufficient to disrupt and homogenise the cells. Homogenisation is necessary as it reduces lysate viscosity and allows efficient binding of extracts to the RNA column. Equal volumes of 70% ethanol were added to the lysates, which were mixed thoroughly by pipetting and then transferred to RNeasy spin columns. The columns were centrifuged at 12,000rpm for 30 sec, flow-through was discarded and the columns were washed with 350µl of Buffer RW1. This buffer contains guanidine salt and ethanol, which enables the removal of carbohydrate, fat and protein from the RNA column.

On-column DNase digestion was carried out by adding 80µl of DNase incubation mix, prepared by mixing 10µl of DNase 1 stock solution with 70µl buffer RDD. Each column was washed with Buffer RW1 and total RNA was eluted with 30µl of nuclease-free water. Total RNA concentration and purity, as measured by the 260/280 and 260/230 ratios, was determined using a Nanodrop spectrophotometer. Nucleic acids absorb maximally at 260nm, proteins at 280nm and guanidine HCL, EDTA and phenolate ions (from TRIzol reagent) will absorb phenolate ions at approximately 230nm: comparing absorbance at these wavelengths provides an indication of the presence of contaminants. Ideally, a 260/280 ratio greater than or equal to 2.0 is considered pure for RNA. A considerably lower ratio may indicate the presence of protein or other contaminants that strongly absorb near 280nm. When column-based RNA kits are used, carryover of GITC can lower the 260/230 ratio, which does not necessarily signify poor quality RNA. RNA was stored at -80^{0}C prior to cDNA conversion.

2.3.2 cDNA synthesis

RNAs were converted to cDNAs by reverse transcription using the High Capacity cDNA Reverse Transcription Kit. The kit uses random primers for initiating the first strand synthesis ensuring that cDNAs are made from all RNAs present in the sample, including mRNA and tRNA. A 2X reverse transcription master mix (Table 2-1) was mixed with an equal volume of total RNA, retrieved as described in section 2.3.1, and kept on ice until ready to load into a thermal cycler. Reverse transcription was carried out using the conditions shown in Table 2-2. Samples were stored at -20^{0}C prior to use.

Table 2-1: Preparation of 2X reverse transcription (RT) master mix for a 20µl reaction. For each reaction, 10µl of the master mix was pipetted into an Eppendorf tube and mixed with 10µl of RNA.

Components	**Amount (µl) per reaction**	Final concentration
10x Reverse Transcription buffer	**2.0**	**1x**
25x dNTP mix (100mM)	0.8	4mM
10x RT random primers	2.0	1x
Multiscribe reverse transcriptase (50 U/**µl**	1.0	2.5 U/µl
Nuclease-free water	4.2	-

Table 2-2: Thermal cycling conditions for cDNA synthesis using the high capacity cDNA reverse transcription kit.

	Step 1	**Step 2**	**Step 3**	**Step 4**
Temperature(^{0}C)	25	37	85	4
Time (min)	10	120	5	∞

2.3.3 Primer design and validations

Primers (Table 2-3) were designed using the Primer3 tool at http://biotools.umassmed.edu/bioapps/primer3_www.cgi, followed by primer blast (http://www.ncbi.nlm.nih.gov/tools/primer-blast/) to ensure that the primers are specific to their target DNA sequences. The MFold tool (http://unafold.rna.albany.edu/?q=mfold) was used to check that the primers do not contain significant secondary structure within the amplicon and primer regions, and a positive delta G value, which represents the free energies of all possible structures, was indicative of this. Primers were also designed to have similar annealing temperatures such that multiple real-time PCR could be performed at the same time with the same PCR programme. In most cases, intron-flanking primers were designed such that one primer was on one exon while the other was on a different one, separated by introns. With this method, genomic contamination can easily be detected as the presence of a short intron will produce a longer PCR product while amplification will not occur if the intron is of thousands of bases long. For some experiments, quantitative PCR was performed using QuantiTech primers specific for GPR56 and COL3A1.

Table 2-3: List of primers used for PCR or qPCR including their forward (F) and reverse (R) sequences, and their amplicon lengths. Primers were designed to give short products of ~90-230bp as amplification of such short products occurs with very high efficiency.

	Primer sequence 5' -3'	**Product length (bp)**
Human COL4A1	F- CCGTGGGACCTGCAATTACT R- ACGGCGTAGGCTTCTTGAAC	89
Human COL3A1	F- GACCCTAACCAAGGATGCAA R- GGAAGTTCAGGATTGCCGTA	200
Mouse COL3A1	F- GTCCACGAGGTGACAAAGGT R- GATGCCCACTTGTTCCATCT	204
Mouse GPR126	F- CTGGGAATCTCCACACGGTA R- CCACATCCGCACACTGAGA	144
Mouse CD81	F- CATGATCCACAGACCACCAG R- AGGCAAACAGGATCACAAGG	202
Human CD81	F-AGATCGCCAAGGATGTGAAG R- GGTTGCTGATGATGTTGCTG	201
Mouse GPR56	F- TTGCAGCAGCTTAGCAGGTA R-GATCCTCTAGACCGGCTGTG	199
Human GPR56	F- ATCCTGCTTCTGCAACCACT R- TAGTCCCGAGGTTTCCTCCT	198
Mouse Lphn1	F- CAACGGTGTGGTGAAAGTTG R- AGATGACAGGGTCCATGAGG	200
Human Lphn1	F- GTCCCCTACAAAGTGGAGCA R- CCACGAGGCATACTCAGTCA-3	195
Mouse β-actin	F- AGCCATGTACGTAGCCATCC R- TCTCAGCTGTGGTGGTGAAG	227
Human β-actin	F- CGTGCGTGACATTAAGGAGA R- CAGGCAGCTCGTAGCTCTTC	107

2.3.4 Polymerase chain reaction (PCR)

A large quantity of DNA is required in order to investigate the expression of a specific gene and this can be readily achieved by using the polymerase chain reaction (PCR) in which many thousands of copies of DNA can be produced from a single strand DNA. The process mimics the natural DNA replication that occurs within cells. It involves rapid sequential changes in temperature to allow primers to bind to specific sequences on template DNA (annealing), followed by elongation by a heat-stable DNA polymerase using deoxynucleotides and the dissociation of the newly formed products when the temperature is raised so that another cycle can begin. The combination of reverse transcription and polymerase chain reaction (RT-PCR) are powerful tools for identifying low abundance RNAs in samples.

A PCR master mix was prepared (Table 2-4) and 17μl was pipetted into nuclease-free 0.2ml PCR tubes. 1μl of cDNAs from MIN6 β-cells, mouse or human tissue, together with 1μl of forward and reverse primers of the gene of interest, were added. cDNAs were not added to tubes containing distilled water or non-reverse-transcribed RNA and they served as negative controls to exclude possible contamination from genomic DNA. The cycling conditions were set as follows: initial denaturation at 94^0C for 2 min, denaturation at 94^0C for 40 sec, annealing at 60^0C for 40 sec and extension at 74^0C for 1 min, repeated 32 times, followed by a final extension at 74^0C for 10 min. The PCR products and a DNA size ladder were separated on 1.5% agarose gels at 100V for 30min and DNA was visualised under UV light. The sizes of the PCR products were extrapolated from the DNA ladder.

Table 2-4: Components of the PCR master mix used for cDNA amplification.

Components	**Amount (µl) per reaction**	Final concentration
Molecular grade water	10.0	-
5x Green Go Taq flexi buffer	4.0	-
PCR nucleotide mix (40mM)	0.8	1.6mM
Forward primer (100**µM)**	1.0	5µM
Reverse primer (100**µM)**	1.0	5µM
$MgCl_2$ (25mM)	2.0	2.5mM
Go Taq DNA polymerase (**5 U/µl)**	0.2	0.05 U/µl

2.3.5 Quantitative PCR

Real time PCR was performed on a LightCycler 480 96-well plate thermal cycler using the SYBR green-based method. cDNAs were diluted 1:5 with nuclease-free water and mixed with SYBR green master mix (Table 2-5). Primers were either designed in-house (Table 2-3) or Qiagen Quantitect validated primers were used. Primer efficiency was determined by absolute quantification using reference standards and primers with efficiency of greater than 98% were used in the experiments described in this thesis. Housekeeping gene normalisation with GAPDH was first carried out to determine the concentration of cDNA to be used for the quantification step. This entailed a pre-incubation at 95^0C for 5 min, cycling for 40 cycles: 95^0C for 10 sec, 60^0C at single mode acquisition for 30 sec, then a melt step was performed at 65-97^0C. The dilution factor required to generate a GAPDH Ct (cycle threshold) value of 18 for each cDNA was calculated. The Ct value is the number of cycles required for the fluorescent signal to exceed background noise. Quantifications were performed by qPCR by screening each pair of desired primers against the various cDNAs, with pre-incubation at 95^0C for 5 min, cycling for 40 cycles: 95^0C for 10 sec, 60^0C at single mode acquisition for 30 sec and finally a melting analysis at 65-97^0C. Amplified PCR product specificity was determined for each run by melting curve analysis and by end-point agarose gel electrophoresis and expression of target gene transcripts were normalised against the reference gene GAPDH (Pfaffl, 2001).

Table 2-5: SYBR green master mix for qPCR.

Components	**Amount (µl) per reaction**
SYBR MasterMix	5
cDNA	1
Nuclease-fee water	1
Primers	2
Total	10

2.4 Over-expression of GPR56 in MIN6 β-cells

2.4.1 GPR56 plasmid DNA and bacterial transformation

Full coding sequence of mouse GPR56 DNA cloned into pCMV-Sport 6 vector (Figure 2-3) was a gift from Dr Xianhua Piao of Children's Hospital and Harvard Medical School, Boston. 50ng of GPR56 DNA was gently mixed with 50µl of *E. coli* competent cells and placed on ice for 10 min. Transformation, which is the process by which cells take up recombinant vector, was carried out by the heat shock method. The DNA / *E. coli* mixture was placed in a 42^0C water bath for 45 sec and immediately placed on ice for 2 min. 900µl of ice-cold SOC medium was added and the cells were allowed to grow at 37^0C for 1 h on a shaking incubator. This step allows the bacteria to generate protein for the antibiotic resistance gene encoded on the plasmid backbone such that they will be able to survive in the presence of antibiotic in subsequent steps. LB agar plates containing ampicillin were prepared (Table 2-6) and allowed to solidify. 50µl of the transformation mixture was plated on the agar plates and incubated at 37^0C overnight. Only cells that picked up plasmid DNA with ampicillin resistance gene will be able to form colonies (Figure 2-4).

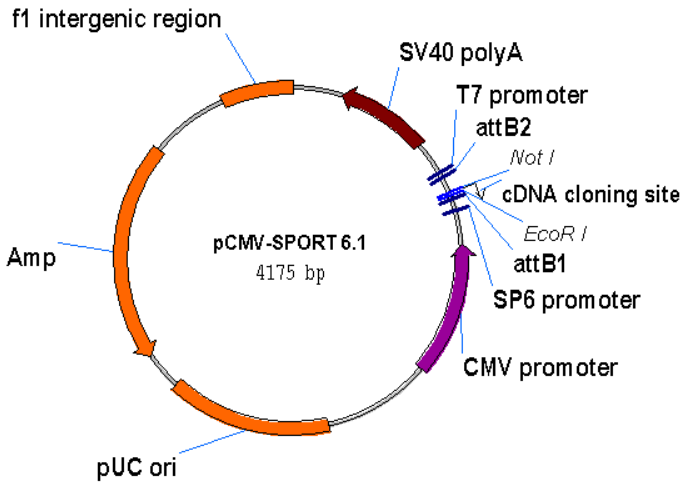

Figure 2-3: pCMV-sport 6 vector showing multiple cloning sites where GPR56 DNA was inserted. The plasmid contains ampicillin resistant gene which allows selection of bacterial transformants.

Table 2-6: Preparation of LB agar plates incorporating ampicillin antibiotics. LB agar powder was dissolved in distilled water and autoclaved. It was allowed to cool down to about 50^0C when ampicillin was added and mixed thoroughly. The solution was aliquoted to five 10cm petri dishes and allowed to solidify.

Reagents	**Amount**	Final concentration/plate
LB agar (3.7%)	3.7g	0.74g
Distilled water	100ml	20ml
Ampicillin (100mg/ml)	100µl	20µg

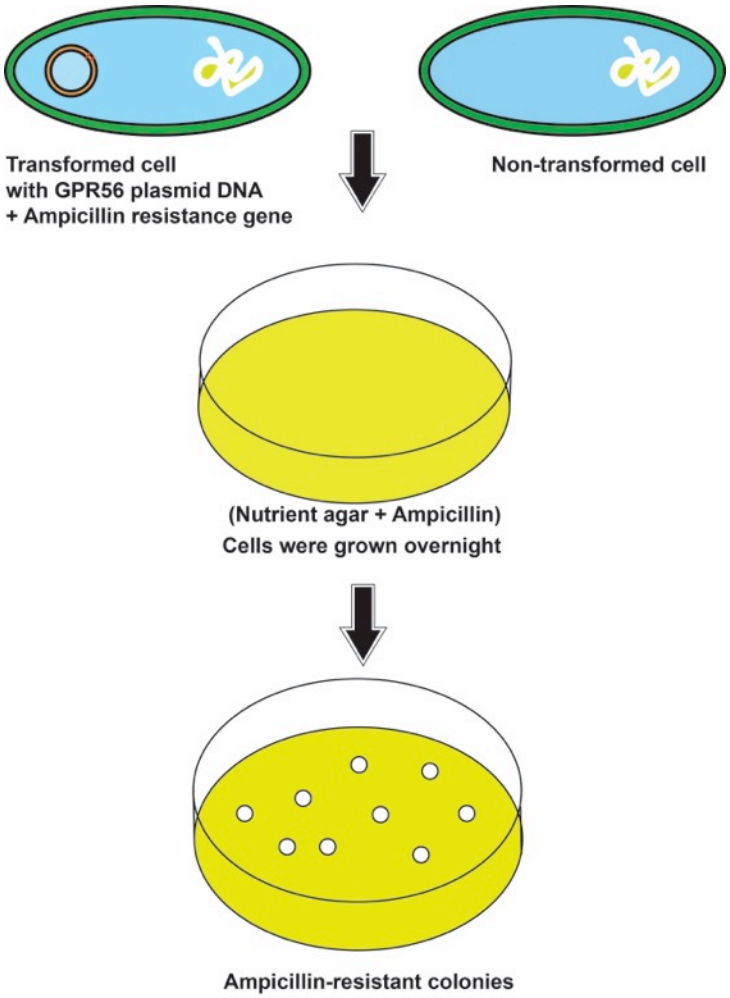

Figure 2-4: Selecting bacteria with GPR56 plasmid DNA. Bacteria that picked up GPR56 plasmid DNA will be resistant to ampicillin because of their ampicillin resistance gene. They will therefore form colonies on nutrient agar containing ampicillin while non-transformed cells will die.

2.4.2 Growth of bacterial culture and plasmid DNA purification

A flask containing 3ml LB culture medium (Table 2-7) was inoculated with a single bacteria colony from the agar plate and incubated for 16 h at 37^0C with vigorous shaking. It is not recommended to grow the cells for more than 16 h. This is because the cells enter stationary phase and cell lysis will begin to occur which will lower plasmid yield. Using a QuickLyse tube, bacterial cells were pelleted from culture by centrifuging at 13,000 rpm for 1 min at room temperature and supernatant was discarded. Plasmid DNA purification was carried out using the QuickLyse miniprep kit. The identity of the eluted DNA was confirmed by sequencing.

Table 2-7: Preparation of LB culture medium. LB broth was dissolved in distilled water and autoclaved. It was allowed to cool down to room temperature and ampicillin was added.

Reagents	**Amount**
LB broth	2.5g
Distilled water	100ml
Ampicillin (100mg/ml)	100 µl

2.4.3 Transient overexpression of GPR56 in MIN6 β-cells

MIN6 β-cells grown to about 80% confluent were lysed with trypsin/EDTA and seeded onto 6 well-plate at a density of 3 x 10^5 cells per well. After overnight culture, MIN6 β-cells were transfected with 0, 12ng or 1200ng GPR56 plasmid DNA with lipofectamine 2000. Lipofectamine and Opti-MEM were mixed at 1:15 before been incubated with various concentrations of GPR56 plasmid DNA (Table 2-8) for 5 min. 150µl of the transfection mix was added to each well and incubated either overnight or for 3 days, and the degree of transfection was determined by qPCR as described in section 2.3.5. The effect of overexpressing GPR56 in MIN6 β-cells on insulin secretion, β-cell proliferation or apoptosis was carried out as described in sections 2.6.2, 2.7.4 and 2.7.2 respectively.

Table 2-8: Transfection procedure for GPR56 plasmid DNA. Mix 1 and 2 were incubated at room temperature for 5 min. The tubes were bulked up with pcDNA vector to ensure that each reaction mix has equal concentration of vector. 150µl of each reaction mix (0% = 0ng, 1% =12ng and 100% =1200ng PGR56 plasmid DNA) were added to the wells containing MIN6 β-cells.

	Volumes (µL) for 0% plasmid	**Volumes (µL) for 1% plasmid**	**Volumes (µL) for 100% plasmid**
Mix 1			
Opti-Mem	150	150	150
Lipofectamine-2000	10	10	10
Mix 2			
OptiMem (make up to 150 µL)	147.79	147.52	120.0
pCMV-Sport mGPR56 A (dil 1/10) (82.94 ng/µl)	0	0.30	30.0
pcDNA3 (1133.3 ng/µl)	2.21 (100%)	2.18 (99%)	0
Combined volume	310	310	310

2.5 Protein expression

2.5.1 Protein extraction

Cell lysis and protein solubilisation was carried out with RIPA (Radio-Immunoprecipitation Assay) buffer. RIPA buffer is available commercially and is formulated to enable efficient cell lysis without altering the biological activity of the protein or causing protein degradation. The composition of RIPA buffer is shown in Table 2-9. To further preserve protein integrity, protease and phosphatase inhibitors are normally added to RIPA buffer before use.

MIN6 β-cells were grown as monolayers until they were about 70 - 80% confluent. Lysis buffer was prepared by adding one tablet each of PhosStop phosphatase inhibitor and protease inhibitor cocktail to 10ml chilled RIPA buffer. Media was carefully aspirated from MIN6 β-cells and 500µl of lysis buffer was added. The flask was further incubated on ice for 5 min before the cells were scrapped and lysate was transferred into pre-chilled 1.5ml tubes. With isolated islets, approximately 300 islets were incubated in 100µl RIPA lysis buffer for 30 min on ice and sonicated briefly for 20 sec. Lysates of islets and MIN6 β-cells were centrifuged at 10,000rpm

for 10 min at 4^0C. The supernatant was carefully removed and either stored in 4% sample buffer at -20^0C or protein concentration was determined by the bicinchoninic acid method.

Table 2-9: Components of RIPA lysis buffer. One tablet each of complete protease inhibitor and PhosStop phosphatase inhibitor was added to 10 ml of RIPA buffer.

Reagents	**Final concentration (pH 8.0)**
NaCl	150mM
Tris	50mM
IGEPAL® CA-630	1%
Sodium deoxycholate	0.5%
Sodium dodecyl sulphate	0.1%

2.5.2 Protein quantification

Quantification of protein concentration in cell lysates was carried out by the bicinchoninic acid (BCA) method. This is a two-step assay based on the reduction of cupric ion to cuprous ion, when copper is chelated by protein in an alkaline environment to form a light blue complex, a reaction known as the biuret reaction. In the second step, bicinchoninic acid reacts with the reduced cuprous ion to form an intense purple colour. The BCA/cuprous ion complex is soluble, with a strong absorbance at 560nm that increases linearly with concentration, allowing an increasing concentration of protein to be determined. The advantage of the BCA protein assay is that it is highly sensitive and selective to cuprous ion. Unlike the Coomassie-based methods, the universal peptide backbone contributes to colour formation in the BCA assay thereby minimising the effect of compositional differences of various proteins.

A serial dilution of bovine serum albumin (from 2mg to 0mg/ml) in lysis buffer was made and this served as the standard. Samples, diluted to 1:10 and 1:100, were added as well as the standards in triplicates to a 96-well plate. 200µl of BCA working solution (solutions A and B in 50:1) was added to each well and mixed briefly on a plate shaker while avoiding air bubbles. The plate was incubated at 37^0C for 30min and absorbance was read on a Chameleon plate

reader at 595nm – this wavelength was the closest available filter to 560nm. Figure 2-5 shows a typical standard curve generated by plotting absorbance against concentration. The concentration of samples was estimated from the standard curve.

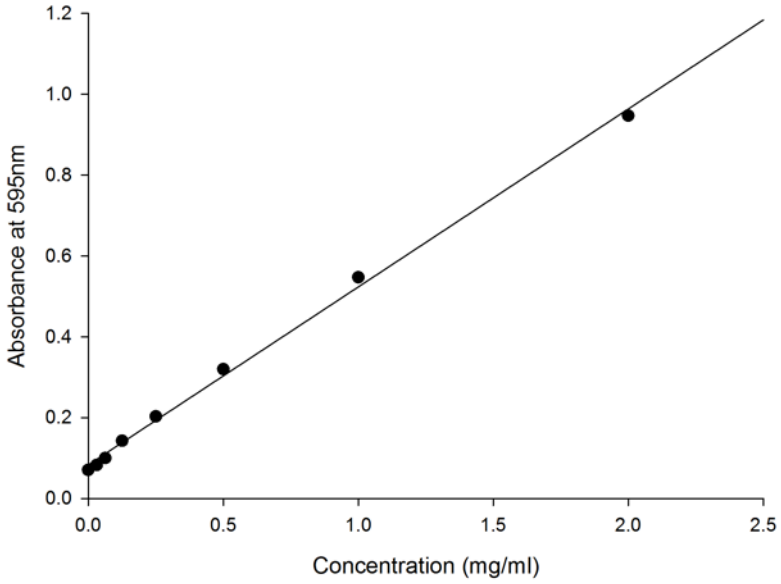

Figure 2-5: A typical BCA assay standard curve for determining protein concentration. The average absorbance of standards measured in triplicate at 595nm is plotted against concentration. Protein concentration of samples is extrapolated from the curve based on their absorbance.

2.5.3 Sodium Dodecyl Sulphate Polyacrylamide Gel Electrophoresis (SDS-PAGE)

Gel electrophoresis is an important technique for separating proteins based on their mass. When electric field is applied to charged particles in solution, they migrate to electrodes of opposite charge. Their rate of movement is determined by several factors including the ionic strength of the solution, pH, charge, size and nature of the separating matrix. The supporting matrix could be a semi-solid gel made from agar or polyacrylamide. The mass of the protein to be separated determines the percentage concentration of polyacrylamide to use – larger protein will separate faster in low percent polyacrylamide and vice versa (Table 2-10). In SDS-PAGE, sodium dodecyl sulphate, a strong detergent, is used to treat the samples to ensure a uniform charge to mass ratio, such that separation is based on size alone.

Pre-cast NUPAGE® 12% gel was used to separate proteins of about 10 to 80kDa. In circumstances where different protein sizes were to be separated, 7.5% or 14% gels were freshly prepared (Table 2-11). Protein lysates from MIN6 β-cells, mouse or human islets were boiled in 1.5% SDS loading dye for 5 min before they were loaded on to gels along with 3.6 - 260kDa pre-stained molecular weight marker. The gel was placed in a mini-cell electrophoresis chamber filled with 1X MOPs running buffer (Table 2-12) and run at 150V for 1 – 2 h or until the dye front has reached the bottom of the gel.

Table 2-10: Protein separation range based on percent concentration of polyacrylamide gel.

Acrylamide concentration (%)	**Protein separation range (kDa)**
5	60-210
7.5	35-95
10	15-70
15	4-45

Table 2-11: Preparation of 7.5% and 14% polyacrylamide gels. The lower resolving gel was first made by mixing 4X resolving buffer, distilled water, 30% acrylamide, ammonium persulphate (APS), and TEMED and immediately poured between glass plates. The gel was overlaid with water and allowed to polymerise for 30 min. Water was removed and the resolving gel was overlaid with 4% stacking gel while a well former (comb) was gently placed in position and the gel was allowed to set.

Reagent	**4%**	**7.5%**	**14%**
Distilled water	6.1ml	19.4ml	10.7ml
4X ProtoGel® Resolving Buffer (1.5M Tris-HCl, 0.4% SDS, pH 8.8)	.....	10.0ml	10.0ml
ProtoGel® Stacking Buffer (0.5M Tris HCl, 0.4% SDS, pH 6.8)	2.5ml	.....	.....
30% Acrylamide	1.3ml	10.0	18.7
10% APS	0.1	0.2	0.2
TEMED	25µl	50µl	50µl
Total volume (for 4 gels)	10.25	39.65	39.65

Table 2-12: Preparation of 20X MOPS running buffer. The reagents were initially dissolved in 400ml distilled water and the volume was made up to 500ml with distilled water. 1x MOPS running buffer was used for gel electrophoresis.

Reagent	**Amount (g) in 500ml**	Final concentration
MOPS	104.6	1M
Tris Base	66.6	1M
SDS	10	69.3mM
EDTA	3	20mM

2.5.4 Western Blotting

Western blotting, also known as immunoblotting, is used to identify specific protein from tissue lysate after the proteins have been separated by size using gel electrophoresis. The protein is first transferred from the gel unto a solid matrix with high protein binding affinity such as nitrocellulose or polyvinylidene fluoride (PDVF) membrane. Nitrocellulose is commonly used as it was the first to be discovered and it has excellent binding and retention properties. However, it is of less mechanical strength and unlike PDVF, it is not suitable for re-probing or for further processing such as sequencing.

Following electrophoresis, a sandwich of gel, blotting membrane, filter papers and filter pads was made (Figure 2-6) and placed in a cassette. The cassette was then immersed in transfer buffer (Table 2-13) and allowed to run for 2 h at 90V. Protein transfer was confirmed by staining with Ponceau S, a reversible red stain that identifies the presence of protein on membrane. After few washes in PBS to remove the dye, the membrane was incubated in blocking buffer (5% w/v milk in TBST) for 1 h to reduce non-specific staining. The membrane was transferred to 5ml blocking buffer containing appropriate amount of primary antibody and incubated overnight at 4^0C. The membrane was washed three times in TBST after which it was incubated for 1 h in blocking buffer containing secondary antibody conjugated to horse-radish peroxide. After washing off excess antibody thrice in TBST, immunoreactive protein was identified by chemiluminescent detection using ECL reagents (Amersham). Light emission produced by the ECL substrate was captured on a photographic film and the molecular weight of the targeted protein was determined by comparing it to a full-range rainbow molecular weight marker.

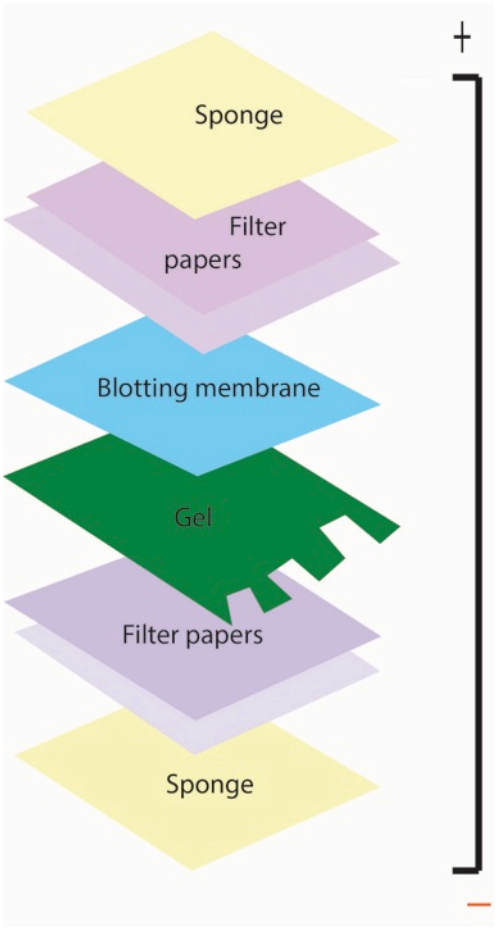

Figure 2-6: Assembly of western blot sandwich. The sandwich was made such that proteins can migrate from the gel to the membrane (from negative to positive electrode) when current is applied. Proteins are negatively charged and they will move towards the positive electrode.

Table 2-13: Preparation of 1x transfer buffer.

Reagent	**Amount (ml)**
Distilled water	849
20X NuPAGE Transfer buffer	50
Anti-oxidant	1
Methanol	100

2.5.5 Immunohistochemistry

Immunohistochemistry (IHC) is a method for identifying the expression and localisation of an antigen of interest in tissue sections using antibody directed against the antigen. IHC was used in this thesis to provide information on the expression of GPR56, collagen III and collagen IV in developing or adult pancreas as well as their colocalisation with insulin, glucagon, somatostatin, CD31 or TUJ1. Freshly retrieved mouse pancreases were fixed in 4% paraformaldehyde either overnight or for 3-5 h depending on tissue thickness, to arrest biological degradation by forming chemical bridges between proteins. Other aldehyde fixatives that could be used include formalin, 10% Neutral Buffered Formalin and glutaraldehyde. However, 4% paraformaldehyde is a better choice as it yields low background during immunostaining. After fixation, the pancreas was transferred into 70% ethanol and stored at 4^0C or processed immediately for paraffin embedding. The pre-embedding processes involve the complete removal of water from the cellular spaces of the tissues by passing them through a series of graded ethanol, xylene and then paraffin. The tissues were then embedded in paraffin wax and cut to 5μm thick with a microtome before being mounted on superfrost slides.

Pancreases retrieved from embryos and postnatal mice were fixed in 4% paraformaldehyde and cryoprotected in 30% sucrose overnight at 4^0C or for few hours until the tissue sank. This occurs when water has been displaced from the cellular space and the tissue reaches a negative buoyancy. After the pancreas was frozen in OCT medium using absolute ethanol and dry ice, they were either stored at -80^0C until ready for sectioning or cut to 12μm thick using a cryostat at -20^0C. The sections were mounted onto superfrost slides and stored at -80^0C until use.

2.5.5.1 Tissue de-waxing and antigen retrieval

Paraffin preserves tissue morphology and allows thin sections to be made but it must be removed before immunostaining to allow antibodies to have complete access to the antigen of interest. Paraffin-embedded sections were de-waxed by heating at 56^0C for 30 sec and washed twice in xylene for 5 min each. Sections were then rehydrated in a series of ethanol washes involving 5min each in 100%, 95% and 70% ethanol, and subsequently in water.

As mentioned in earlier, paraformaldehyde fixation causes protein cross-linking which induces conformational changes that mask antigenic sites and make them unrecognisable by antibody. It is therefore necessary to restore antigenicity before adding primary antibodies. Antigen retrieval was carried out by heat-induced epitope retrieval method. Slides were boiled in 10mM citric acid solution pH 6.0 (Table 2-14) in a pressure cooker for 15 – 20 min until a hissing sound was heard, and heating was continued for a further 2 min 30 sec. The slides were then washed in PBS. In experiments involving BrdU staining, additional antigen retrieval steps were carried out. In this case, sections were incubated with 2N HCl for 10 min at 37^0C and later neutralised by incubating sections in 0.1M borate pH8.5 for 10 min.

Table 2-14: Preparation of 1M citric acid stock solution. The stock solution was made by dissolving citric acid in distilled water and stored at room temperature. Citric acid working solution was prepared by diluting 8ml 1M Citric acid stock in 800ml distilled water and pH was adjusted to 6.0 with 5M NaOH.

Reagent	**Amount**	Final concentration
Citric acid	105g	1M
Distilled water	500ml	-

2.5.5.2 Detection method

Fluorescent detection method was used for most of the immunostaining described in this thesis. Prior to adding primary antibodies of interest (Table 2-15), sections were blocked with 1% BSA and 10% normal goat serum in PBS containing 0.1% triton-X-100 for 1h at room temperature in a humidifying chamber. To keep the solution on the sections, wax pen was used to carefully draw circles around sections. After the blocking step, primary antibody of interest at the appropriate dilution was added and slides were incubated overnight at 4^0C in a humidifying chamber. For sections used as negative control, blocking buffer alone was added, without any primary antibody. After three washes in PBS, fluorophore-conjugated secondary antibody (Table 2-16) targeting the species in which the primary antibody was raised was added to the sections and incubated for 1h at room temperature in the dark. All onward steps were performed in the dark to prevent photo bleaching as secondary antibodies are sensitive to light. Slides were rinsed thrice in PBS and nuclei were counted-stained with DAPI (1:500) for 10min

at room temperature, then washed in PBS and mounted with Fluoromount® aqueous mounting medium. Images were visualised with Nikon Eclipse Ti inverted microscope or with Nikon Eclipse TE 2000-U.

For protocols involving 3,3'-diaminobenzidine (DAB) detection system, endogenous peroxidases were blocked by incubating sections in 3% hydrogen peroxide for 15min, after the antigen retrieval steps. Primary antibody was then added and subsequently, biotinylated secondary antibody or a universal biotinylated link antibody was added to the tissue section for 30 min. Sections were washed briefly with PBS containing 0.25% (v/v) Triton-X-100 before being incubated with HRP-conjugated streptavidin for 30 min, followed by the addition of DAB. The development of a dark brown precipitate at the antigenic sites when DAB was added was monitored under a light microscope and the reaction was stopped by washing sections in PBS-T when adequate labelling has been reached.

2.5.5.3 Quantification of β-cell mass

Staining for insulin identified β-cells in mouse and human pancreas sections. β-cell mass was then measured using the area quantification tool of the NIS Elements 3.0 software on Nikon Eclipse TE-2000 microscope or with ImageJ.

2.5.5.4 Antibodies

The following primary antibodies were used for immunostaining:

Table 2-15: A list of primary antibodies used for immunohistochemistry including their working concentrations, manufacturers and catalogue numbers.

Primary antibody	**Dilution**	**Manufacturer/Catalogue number**
Rabbit polyclonal anti-GPR56	1:50	Abcam ab194881
Mouse monoclonal anti-GPR56	1:25	Millipore MABN310
Rabbit monoclonal anti-GPR56^{C}	1:250	Piao's lab (199)
Rat monoclonal anti-BrdU	1:100	Bio-Rad OBT0030S
Guinea pig polyclonal anti-insulin	1:200	Dako A0564
Mouse monoclonal anti-glucagon	1:50	Sigma G2654
Rat monoclonal anti-somatostatin	1:25	Abcam ab30788
Rabbit polyclonal anti-collagen III	1:50	Abcam ab7778
Rabbit polyclonal anti-collagen IV	1:100	Abcam ab6586
Rabbit anti-neurogenin3	1:25	Abcam ab38548
Rabbit polyclonal anti-Ki67	1:100	Abcam ab66155
Mouse monoclonal anti-Ki67	1:100	BD Biosciences 550609
Rat monoclonal anti-CD31	1:100	BD Biosciences 553370
Rabbit monoclonal anti-TUJ1	1:1000	Covance MRB-435P
Rabbit polyclonal anti-collagen III	1:1000	Life Span Biosciences LS-B693

Secondary antibodies

Table 2-16: A list of secondary antibodies used for IHC at the indicated dilutions. The antibodies were made up in blocking buffer containing 1% BSA and 10% goat serum in PBS with 0.1% Triton-X-100 prior to use.

Secondary antibody	**Dilution**	**Manufacturer/Catalogue number**
Alexa-fluor 488 goat anti-mouse IgG	1:1000	Invitrogen A11029
Alexa-fluor 594 donkey anti-guinea pig IgG	1:100	Jackson immunolab 706-585-148
Alexa-fluor 488 goat anti-rat IgG	1:1000	Invitrogen A11006
Alexa-fluor 594 donkey anti-rat IgG	1:100	Jackson immunolab 712-585-150
Alexa-fluor 488 anti-rabbit IgG	1:100	Jackson immunolab 711-545-152
Alexa-fluor 546 anti-guinea pig IgG (highly cross-adsorbed)	1:1000	Invitrogen A11074
Alexa-fluor 555 goat anti-rabbit IgG	1:1000	Invitrogen A21428
Alexa fluor 488 goat anti-rabbit IgG	**1:1000**	**Invitrogen A11070**

2.6 Measurements of insulin secretion

2.6.1 Quantification of insulin content

Quantification of islets insulin content was done by the acid ethanol method. 10 islets were incubated at 4^0C overnight in 250µl of acidified ethanol (prepared by mixing absolute ethanol, deionised water and concentrated HCL in 52:17:1 ratio respectively), after which they were sonicated on ice for 20 sec. The solution was centrifuged at 2000rpm for 1min and supernatant was diluted with borate buffer to 1:2500. Insulin content was determined by radioimmunoassay as described in section 2.6.4.

2.6.2 Static insulin secretion

The acute effect of collagen III on insulin secretion from islets was determined in static secretion experiments. Mouse and human islets were cultured overnight in RPMI containing 10% NCS, 2mM L-glutamine and 100U/ml penicillin/0.1mg/ml streptomycin at 37^0C in an atmosphere of 95% air / 5% O_2. Islets were pre-incubated for 1 h in a physiological buffer (Gey & Gey, 1936) supplemented with 2mM glucose (Tables 2-17 and 2-18). Three islets (small, medium and large) per replicate were transferred to 0.5ml Eppendorf tubes then exposed to 300µl of the physiological buffer containing either 2mM or 20mM glucose in the presence or absence of collagen III for another 1 h at 37^0C. Islets exposed to the muscarinic agonist carbachol (500µM) served as positive control. Islets were centrifuged at 2000rpm for 1 min at 4^0C and 100µl of supernatant was diluted 1:5 with borate buffer and stored at -20°C prior to insulin radioimmunoassay.

In similar experiments to assess the effects on insulin secretion of chronic exposure of islets to collagen III and IV, islets were cultured on dishes coated with 100nM collagen III or IV for 48 h. To coat dishes with collagen, 100nM collagen III or IV was spread on petri dishes and incubated at 37^0C for 5 h. Any remaining liquid was carefully removed and the petri dishes were kept at 4^0C in a sealed and sterile environment prior to use. After 48 h incubation, islets were retrieved and exposed to either 2mM or 20mM glucose for 1 h, after the initial pre-incubation in 2mM glucose. Insulin secretion was determined by radioimmunoassay.

Table 2-17: Composition of stock physiological salt solution. The reagents were completely dissolved in 1.5L distilled water after which the volume was made up to 2L and stored at 4^0C.

Reagents	**Amount (g/2L)**	**Final concentration [mM] when diluted**
Sodium chloride	26.00	111.00
Potassium chloride	1.48	5.00
Sodium hydrogen carbonate	9.08	27.00
Magnesium chloride hexahydrate	0.84	1.00
Potassium dihydrogen orthophosphate	0.12	0.22
Magnesium sulphate heptahydrate	0.28	0.28

Table 2-18: Preparation of physiological salt solution for experimental use. The pH of the solution was adjusted to 7.4 with 5% CO_2/95% air before use.

Reagents	Amount	Final concentration
2x stock solution	250ml	1x
Distilled water	250ml	-
Glucose	0.18g	2mM
Calcium chloride (1M)	1ml	2mM
Bovine serum albumin	0.25g	0.05%

2.6.3 Dynamic insulin secretion

To determine the dynamic insulin secretory profile of islets to acute exposure to collagens III and IV, mouse and human islets were perifused with physiological buffer containing the agents of interest in a perifusion system (Figure 2-7). This system consists of 8-16 chambers maintained at 37^0C in a temperature-controlled environment. Each chamber was lined with 1µm pore size nylon membrane to make sure that islets cannot pass through. Groups of 40 mouse islets or 150 human islets were transferred to chambers using a micropipette and islets were pre-perifused for 1h with physiological buffer containing 2mM glucose at a flow rate of 0.5ml/min. The perifusate was discarded during this period after which the islets were exposed to agents of interest at specific time intervals. Perifusates were collected every 2min and insulin released from the islets was quantified by radioimmunoassay.

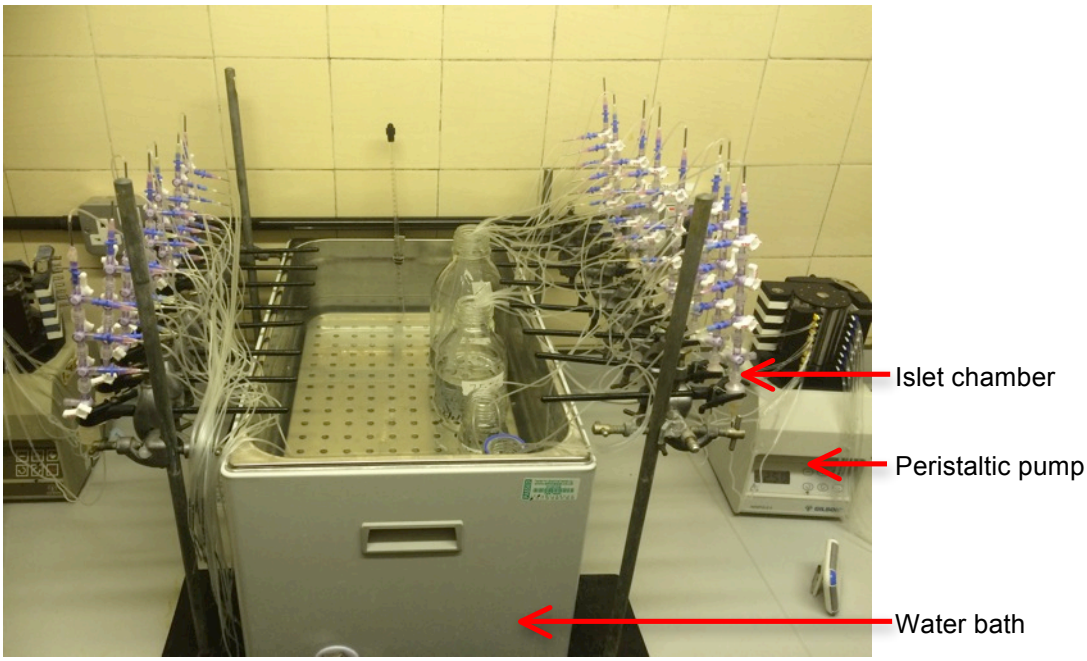

Figure 2-7: The perifusion system. The perifusion system consists of a water bath to maintain buffer temperature at 37°C, islet chambers, pvc tubes and valves, and a peristaltic pump for delivering the buffers to the islets. The system was made air-free after loading the islets into the chambers. Islets were perifused with agents of interest and perifusates was collected every 2min for quantification of released insulin by radioimmunoassay.

2.6.4 Radioimmunoassay

Radioimmunoassay is a very sensitive method for quantifying the concentration of an antigen of interest in a biochemical assay by making use of radioisotopic labelling. This assay is based on the principles of antibody (AB) and antigen (AG) interaction, in the presence of a radiolabelled form of the antigen (AG*), which is the tracer. AG, the substance to be measured, and its corresponding AG* compete for the limited binding sites on the AB such that at equilibrium, the following equation applies:

$$AB + AG + AG^* \longleftrightarrow AB{:}\,AG + AB{:}\,AG^* + AG + AG^*$$

Thus, based on the law of mass action, keeping the concentration of antibody (AB) and tracer (AG*) constant while increasing the concentration of antigen (AG), the equilibrium will be shifted to favour an increase in AB: AG and decrease AB: AG*. On the other hand, by decreasing AG,

AB: AG will decrease with a resultant increase in AB: AG* since more AB sites are available for AG* to bind. The amount of AB: AG* present at any given time can then be measured using a suitable radiometric detector.

To measure insulin concentrations in experimental samples, a 10ng/ml insulin stock was diluted serially in triplicate with borate buffer (Table 2-19) to give a range of concentrations over which the assay is sensitive (10ng/ml to 0.04ng/ml). Samples were diluted with borate buffer and assayed in duplicates. The radioactive tracer was I^{125}-insulin, and it was diluted with borate buffer to give an approximate count of 10,000cpm per tube while the antibody used was bovine anti-insulin, diluted 1/10. Reference tubes were also set up in triplicate to measure non-specific binding, maximum binding of the antibody as well as total γ emission of the tracer. Antibody and tracer were added to tubes containing experimental samples and standards (Table 2-20) and all tubes were left to equilibrate at 4^0C for 48 – 72h. Following the period of equilibration, 1ml precipitant (Table 2-21) was added to each tube except those measuring total γ emission, to precipitate the antigen-antibody complexes. The tubes were centrifuged at 3000rpm at 4^0C for 15min and the supernatant was aspirated. The radioactivity of the pellet was determined by a Packard Cobra II γ counter in counts per min per ml (cpm/ml). Plotting cpm/ml against log concentration generated a standard curve from which the concentration of insulin in the samples was determined.

Table 2-19: Preparation of borate buffer. The reagents were dissolved in 1.8L distilled water and the pH was adjusted to 8.0 with conc. HCl before the volume was made up with dH_2O to 2L. BSA (100% w/v) was then added and allowed to dissolve before the buffer was stored at 4^0C.

Reagents	**Amount (g/2L)**	Final concentration (mM)
Boric acid	16.5	133.0
NaOH	5.4	10.0
EDTA	7.4	67.5

Table 2-20: Preparation of standards, reference tubes and samples for the insulin radioimmunoassay.

	Buffer (µl)	**Antibody (µl)**	**Tracer (µl)**	**Standard (µl)**	**Sample (µl)**
Non-specific binding (NSB)	200		100		
Maximum binding (MB)	100	100	100		
Total radioactivity (T)			100		
Standards		100	100	100	
Samples		100	100		100

Table 2-21: Preparation of the precipitant. The γ-globulin was dissolved in PBS before 30% PEG was added with continuous mixing, giving a concentration of 15% PEG in the precipitant. Tween-20 was added to the mixture to prevent γ-globulin from sticking to the tubes. The 30% PEG stock solution was prepared by dissolving 600g polyethylene glycol in distilled water and made up to 2L.

Reagents	**Amount (1L)**	Final concentration
30% PEG	500ml	15%
γ-globulin	1000mg	1%
PBS	500ml	-

2.7 Cell adhesion, apoptosis and proliferation

2.7.1 Colorimetric cell adhesion assay

To determine the effects of collagens I, III, IV and fibronectin on the adhesion properties of MIN6 β-cells, a colorimetric cell adhesion assay was used. 96-well plates were coated with 100nM each of collagen I, III, IV or fibronectin, or with 0.5% BSA and non-specific binding sites were blocked for 45 min with 0.5% BSA at 37^0C. BSA sticks to the part of the wells not covered by collagens. MIN6 β-cells were maintained overnight in serum-free DMEM and retrieved by trypsinisation (section 2.1.1). Groups of 30,000 cells were seeded into the coated plates and left to adhere at 37^0C for 90 min. Non-adherent cells were washed off with serum-free DMEM containing 0.1% BSA and the remaining adherent cells were fixed with 4% paraformaldehyde, and stained with crystal violet (5mg/ml in 2% ethanol). After five washes with distilled water, plates were allowed to air dry then adherent cells were lysed in 2% SDS for 30 min. The adherent cell density was determined by measuring absorbance at 595nm with a Chameleon plate reader.

2.7.2 Caspase-Glo 3/7 apoptosis assay

Apoptosis, a programmed cell death, is mediated by a set of proteases known as caspases. The initial cell death signal is induced by initiator caspases 8 and 10 and the ensuing cell death is carried out by effector caspases 3 and 7. The caspase-Glo 3/7 Assay kit recognises the activation of caspases 3 and 7 within cells, and cleavage of a tetrapeptide sequence within a substrate following caspase 3/7 activation results in light emissions that can be detected using a plate luminometer. The intensity of light emitted is proportional to the amount of activated caspase 3/7 present within the sample.

Groups of 20,000 MIN6 β-cells or 3-5 islets per well were cultured in media containing 2% FBS in the presence or absence of 100nM collagen III for 48 h, with a subsequent 20h incubation in the presence or absence of a cytokine cocktail (1U/μl TNF-α, 0.05U/μl IL-1β and 1U/μl IFN-γ). A working solution of the reagent was made by mixing caspase 3/7-Glo buffer with caspase 3/7-Glo substrate and 25μl of the reconstituted reagent was added to each well (also containing 25μl). Plates were incubated at room temperature for 1 h and luminescence intensity, a measure of caspase 3/7 activities, was measured by a Veritas luminometer at 450nm.

2.7.3 BrdU ELISA

Proliferation of β-cells *in vitro* was determined by BrdU incorporation using a colorimetric BrdU ELISA kit. 20,000 native MIN6 β-cells or MIN6 β-cells transfected with GPR56 plasmids as described in section 2.4.3 were seeded onto 96-well plate and incubated overnight at 37^0C in DMEM supplemented with 10% FBS. The cells were then serum-starved for 24 - 48h and labelled with 100μM BrdU labelling solution for 4h at 37^0C. Non-transfected cells grown in the presence of serum served as positive control. The cells were fixed and denatured for 30 min with a 200μl/well FixDenat solution after which the wells were dried by blotting. Anti-BrdU antibody was added to each well which bind to the BrdU incorporated into newly synthesised DNA. The wells were washed three times with PBS and 25μl of substrate solution was added. The well plate was placed on a shaker until sufficient colour developed, which took about 5 to 10 min. Reaction was stopped by adding Stop solution (Sulphuric acid) and absorbance was read at 450nm on a microplate reader.

2.8 Measurement and manipulation of second messenger generation

2.8.1 Single cell calcium microfluorimetry

The effect of collagen III and other agents of interest on intracellular calcium recruitment was carried out by single cell calcium microfluorimetry. This technique allows real time measurement of the changes in cytosolic calcium concentration within cells. Calcium signalling is a central factor in insulin secretion and data obtained from measuring changes in cytosolic calcium could provide information on β-cell health. To measure calcium, cells are incubated with fluorescent dyes such as Fura-2AM that causes a shift in excitation wavelength from 380nm to 340nm when the dye is bound to calcium. This therefore allows intensity measurement of Ca^{2+}-free and Ca^{2+}-bound form of the dye to be made. By expressing the level of $[Ca^{2+}]i$ as a ratio of these excitation wavelengths, changes in intensity as a result of factors unrelated to intracellular calcium such as dye leakage and changes in cell thickness is minimised.

MIN6 β-cells (1.5 $X10^5$ cells) were seeded on acid-ethanol washed coverslip initially for 1 h for the cells to attach in serum free DMEM. Incubation buffer was changed to DMEM containing 10% FBS and cells were incubated for 24 h. For experiments involving mouse or human islets,

about 100 – 200 islets were partially dispersed (Figure 2-8) in 200µl accutase for 5min at 37^0C and mixed intermittently every 2 min before being seeded on acid-washed coverslip as described for MIN6 β-cells. The cells were then loaded with 5µM Fura2-AM for 30 min at 37^0C before being transferred to a temperature-controlled chamber maintained at 37^0C and perifused with physiological buffer supplemented with 2mM glucose. A shutter system was used to expose the cells alternatively to 340nm and 380nm while emission at 510nm was captured using an inverted epi-fluorescent microscope (Zeiss Axiovert 135). Cells of interest were selected and data was collected every 3 sec by OptoFluor imaging software.

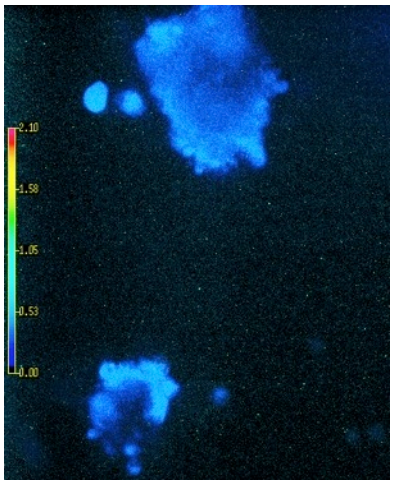

Figure 2-8: Partially dispersed human islets. Human islets were incubated for 5min in accutase at 37^0C before being loaded with Fura-2AM for 30min. Dispersed cells were viewed under 20x objective of a fluorescent microscope.

2.8.2 GTP-Rho pull down assay

Native MIN6 β-cells or MIN6 β-cells transfected with GPR56 plasmid was serum-starved for 36 h, after which the cells were stimulated with 100nM collagen III or 20mM glucose for 5, 10 and 15min, and lysed in 300µl of lysis buffer. Isolated islets cultured overnight were incubated in the presence or absence of 100nM collagen III for 10 min and lysed in lysis buffer. After centrifuging for 10min at 12,000rpm, protein concentration was determined. Protein concentration was normalised and an aliquot was used as input loading control while the remaining supernatant was incubated with 25µg GST-RBD beads for 2h at 4^0C. The resin was washed twice with lysis buffer at 2600rpm for 30sec and boiled in Laemmli sample buffer. Input loading control and the resin were separated by SDS-PAGE and bound-RhoA was detected by immunoblotting.

2.9 In vivo studies

2.9.1 GPR56 knockout mouse model

All *in vivo* studies involving GPR56 knockout (KO) mice were carried out at Children's Hospital and Harvard Medical School, Boston, USA, and conformed to the guidelines of the Animal Use and Care Committee of Boston Children's Hospital. GPR56 KO mice on a mixed 129/BL6/FvB/Balb/c background were obtained from Genetech/Lexicon. The targeting strategy involves the replacement of exons 2 and 3 by LacZ/Neo, which leads to the deletion of the start ATG codon and causes a frame-shift. The TG2/GPR56 double KO mice used in this thesis were generated and maintained by Dr Paio's lab and were different from the one mentioned in Chapter 1.

2.9.2 Confirmation of gene knockout

2.9.2.1 Genotyping

To determine the genotypes of the transgenic mice, about 2mm of their tail tips were cut into 200µl of PBND (PCR buffer with non-ionic detergent) buffer (Table 2-22) containing 10µl (100µg/ml) proteinase K and digested overnight at 55^0C. The tubes were further heated for 10 min at 95^0C to inactivate proteinase K before being centrifuged at 12,000 rpm for 10 min. A master mix was prepared (Table 2-23) and Betaine/DMSO was added due to the high GC content in the promoter region. PCR was carried out with the following primers: DNA 085-14, 5'-

AAA GTA GCT AAG ATG CTC TCC-3'; Neo 3A, 5'-GCA GCG CAT CGC CTT CTA TC-3'; and 91-111, 5'-GA CTT CCG CTT CTG TGG CCA G-3'. A touch-down PCR cycling protocol was used, where annealing occurred at 65^0C for the first 10 cycles and gradually decreases by 1^0C/cycle to 55^0C. The next 30 cycles annealed at 55^0C.. PCR products were separated on 1.5% ultrapure agarose gel at 200V for 1h.

Table 2-22: Preparation of PBND buffer. The reagents were dissolved in 450ml deionised water and volume was adjusted to 500ml with deionised water, and autoclaved. It was aliquoted and stored at -20. Gelatin will not dissolve until after autoclaving.

Reagents	**Amount**	**Final concentration**
1M Tris-HCL stock, pH 8.3	5ml	10mM
KCl	1.87g	50mM
$MgCl_2.6H_2O$	0.255g	2.5mM
IGEPAL	2.25ml	0.45% v/v
Tween 20	2.25ml	0.45% v/v
Gelatin	0.05g	0.1mg/ml

Table 2-23: PCR master mix for 20 genotyping reactions

Reagents	**Volume (µl)**
Sterile double distilled water	248.5
10x PCR buffer (15mM $MgCl_2$)	50
100mM dNTPs	2
$MgCl_2$	34
Betaine (Sigma B0300)	130
DMSO	6.5
200µM primer DNA085-14	1
200µM primer Neo3A	1
200µM primer 91-111	1.5
5U/µl Taq polymerase	4

2.9.2.2 Immunohistochemistry staining

The GPR56 KO mice described in this thesis were whole body knockout model. Immunohistochemistry was therefore performed on pancreatic sections to determine whether GPR56 protein in β-cells was also deleted. Wax-embedded pancreas sections from wild type (WT) and KO mice were processed as described in section 2.5.5 and stained for the c-terminal domain of GPR56. Staining for insulin revealed β-cells. The GPR56 C-terminal antibody (199) was developed and validated previously in Professor Piao's lab (Luo et al., 2011, 2014).

2.9.3 Glucose tolerance tests

Intraperitoneal glucose tolerance test (IPGTT) was carried out on adult mice from 8 to 12 week old. Mice were fasted overnight for a maximum of 16 h by removing food but allowed free access to water. Basal glucose level was measured with Accu-Chek glucose meter and strips prior to intraperitoneal administration of 30% glucose at 2g/kg. Blood was obtained by pinpricks to the tails of the animals using 27G needle. Plasma glucose concentrations were later measured at 15, 30, 60, 90 and 120 min.

2.9.4 BrdU delivery

Age-matched adult GPR56 WT and KO mice were given BrdU (50mg/kg) intra-peritoneally (IP) daily for 5 days while P9 mice were given 50mg/kg BrdU IP for 24 h prior to pancreas retrieval. The pancreases were fixed in 4% paraformaldehyde and processed either for paraffin embedding or fixed-frozen.

2.10 Statistical analyses

In all cases, normality of data distribution was evaluated using D'Agostino or Shapiro-Wilk tests. Normally distributed data were analysed using a two-tailed Student's t-test or ANOVA, as appropriate. Repeated measurements in the same animal at different time points were determined by two-way repeated measurement ANOVA with appropriate post hoc tests. However, non-Gaussian data were analysed by Mann-Whitney U test. Statistical analyses were performed using GraphPad Prism 7. Data are presented as mean ± SEM and $p<0.05$ was considered significant. Immunohistochemistry images in Chapters 3, 4 and 5 were scored blindly before quantification.

Chapter 3

Chapter 3 Characterisation of GPR56 expression in developing and adult pancreas

3.1 Introduction

The adhesion G-protein coupled receptor family is the second largest class of GPCRs in the mouse and human genome (Bjarnadóttir et al., 2004). These receptors are generally thought to be involved in cell adhesion and cell-matrix interaction because of the presence of several adhesive motifs on their N-terminals. Adhesion GPCRs are expressed in both central and peripheral tissues including the brain, reproductive tracts and lungs, where they play varying roles including cortical development (Li et al., 2008; Piao et al., 2004), cell migration (Iguchi et al., 2008) and immunity (Nijmeijer et al., 2016).

GPR56 is a member of the adhesion GPCR family that has received considerable attention in the last decade, because it was the first adhesion GPCR to be associated with a human disease, known as bilateral frontoparietal polymicrogyria (BFPP). BFPP is a rare human brain disorder caused by germline mutations in GPR56, which presents as cognitive and motor dysfunctions manifesting in cerebral hypoplasia, seizures and mental retardation (Parrini et al., 2009).. It arises as a result of improper neuronal migration during cortical development, suggesting that GPR56 is essential for cell migration (Fujii et al., 2013; Luo, Yang, et al., 2011).

Similar to other adhesion GPCRs, GPR56 is ubiquitously expressed. Its expression has been reported in the brain, testis, thyroid, placenta, small intestine and stomach (Liu et al., 1999). GPR56 expression has also been detected in metabolically active tissues such as skeletal muscle, adipose, and liver (Amisten et al., 2015; Iguchi et al., 2008) and it is the most abundantly expressed GPCR mRNA in human islets (Amisten et al., 2013). GPR56 was found to be high at the protein level in pancreas and kidney, with medium expression reported in brain, liver and spleen (Huang et al., 2008). The broad expression of GPR56 in both central and peripheral tissues suggests that it may play a more general but fundamental role.

It is thought that the unusually long N-terminal domain of GPR56 allows it to bind to many partners, including collagen III, transglutaminase 2 (TG2) and CD81. Collagen III is a ligand for GPR56 in the developing brain, where it couples to $G_{\alpha 12/13}$ and RhoA signalling (Iguchi et al., 2008; Luo, Jeong, et al., 2011). TG2 interacts with GPR56 to suppress melanoma growth and metastasis (Xu et al., 2006), but it is unclear whether TG2 is a traditional agonist as no downstream signalling has been identified. In addition, the tetraspanin protein CD81 acts as a scaffolding protein to stabilise the association of GPR56 with G_q (Tritarelli et al., 2004). The functional significance of this interaction is also not known.

As stated above, GPR56 is a developmental gene. It is critical for the proper formation of the rostral cerebellum as it allows the developing neurons to adhere to the extracellular matrix of the pial basement membrane (Koirala et al., 2009). The failure of this process leads to neuronal overmigration and ectopia. In addition, loss of GPR56 leads to hypomyelination of the CNS as a result of defective development of oligodendrocyte precursor cells (Giera et al., 2015). Outside the CNS, GPR56 plays structural functions in seminiferous tubule development in mice where its absence during embryogenesis leads to male infertility (Chen et al., 2010). In the developing pancreas, GPR56 mRNA is robustly expressed in NGN3+ endocrine progenitors (Gu et al., 2004), but its function in islet development is not yet known.

GPCRs that are highly expressed in a given tissue are known to play important physiological role in those tissues. For example, opsins that are important for light detection are highly expressed in the eye, while the glucagon-like peptide 1 receptor, a major therapeutic target for treating diabetes, is abundantly expressed in islets (Regard et al., 2008). It is therefore likely that GPR56 may play an important role in islet function, if the abundant mRNA level already reported in islets translates to high protein expression. This chapter describes the expression of GPR56 and its binding partners in mouse and human islets, as well as their cellular localisation. The expression of GPR56 in endocrine progenitors and in different stages of islet development was also examined.

3.2 Aims

- Determine whether GPR56 is expressed in the developing pancreas and whether it colocalises with markers of pancreatic progenitors.
- Quantify the expression of GPR56 at different stages of islet development
- Determine whether deletion of GPR56 has any effect on proliferation and differentiation of endocrine progenitors.
- Determine the expression of GPR56 and its binding partners in adult mouse and human islets, as well as their cellular localisation.

3.3 Methods

3.3.1 PCR

Total RNAs from MIN6 β-cells, mouse islets, human islets, mouse and human exocrine cells were extracted and reversed-transcribed to cDNAs as described in Section 2.3.2. The mRNA expression of GPR56 and its binding partners was investigated by RT-PCR, using specific forward and reverse primers designed to amplify the targets of interest (Table 2.3). The amplified products were separated on 1.5% agarose gels containing 0.5μg/μl ethidium bromide and DNA bands were visualised under UV light.

3.3.2 Western blotting

Protein was extracted from mouse brain and MIN6 β-cell samples with RIPA buffer (Section 2.5.1) and protein concentrations were determined by the BCA method. Following protein separation by SDS-PAGE, fractionated proteins were transferred to a blotting membrane and probed with a commercially available monoclonal antibody directed against GPR56. The membrane was further incubated with the corresponding secondary antibody and immunoreactive protein was identified by the enhanced chemiluminescent method (Section 2.5.4).

3.3.3 Fluorescent immunohistochemistry

Freshly retrieved mouse pancreases were fixed in 4% paraformaldehyde overnight before being cryoprotected and frozen, or transferred into 70% ethanol and paraffin embedded. Fixed frozen or wax-embedded mouse pancreases and archived human pancreas blocks were cut to 10μm or 5μm sections respectively and IHC was carried out as described in Section 2.5.5. Pancreas sections were incubated overnight with antibodies directed against GPR56, collagen III, collagen IV, insulin, glucagon, somatostatin, NGN3, SOX9 or CD31. After incubating with fluorophore-conjugated secondary antibodies (Table 2-16) targeting the species in which the primary antibody was raised, images were visualised with a Nikon TE 2000 fluorescence microscope.

3.4 Results

3.4.1 Expression of GPR56 mRNA by MIN6 β-cells, mouse islets, human islets and exocrine cells

RT-PCR revealed that mouse and human endocrine and exocrine cells express GPR56 mRNA (Figure 3-1). The amplicons obtained correspond to the predicted sizes of the nucleotide sequence generated using the chosen primer pairs (199bp for mouse GPR56 and 198bp for human). As expected, no amplification was seen when MIN6 β-cell RNA, mouse islet RNA or distilled water were used instead of cDNAs, indicating that the amplified DNA bands were not due to genomic DNA contamination. The expression of GPR56 mRNA was stronger in mouse islets than in mouse exocrine cells while the expression level in human islets was comparable to that in human exocrine cells (Figure 3-1). However, it is not possible to quantify relative expression levels by the standard RT-PCR method shown here.

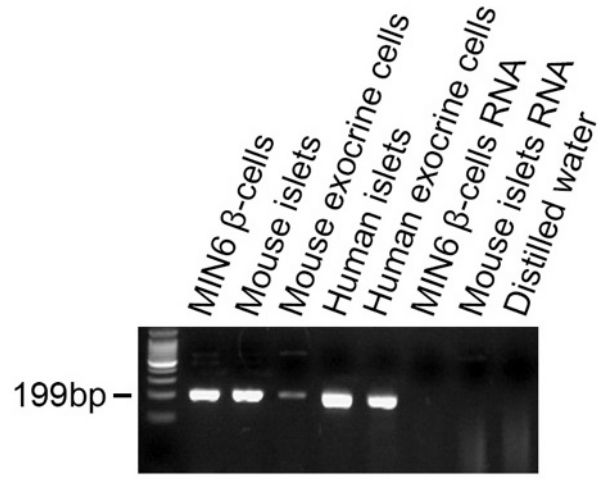

Figure 3-1 Detection of GPR56 mRNA in mouse and human pancreatic cells. cDNAs from the indicated tissues were amplified by reverse-transcriptase PCR. Amplified products were run on a 1.5% agarose gel containing ethidium bromide and DNA bands were visualised under UV light. GPR56 is expressed in MIN6 cells, mouse and human islets, and in exocrine cells. A molecular size marker and RNAs from MIN6 cells and mouse islets, and distilled water containing mouse and human primers but no cDNA, were run on the same gel. Amplicons correspond to the predicted size of the nucleotide sequence generated using the chosen primer pairs.

3.4.2 GPR56 protein expression

Having detected GPR56 mRNA in β-cells, it was investigated whether GPR56 message is translated to protein. As protein is the primary determinant of cell phenotype and the mRNA level of a gene is not necessarily directly correlated to its protein level (Lundberg et al. 2010), western blotting was used to identify the expression of GPR56 protein in whole brain and MIN6 β-cell lysate. Cell lysates were subjected to SDS-PAGE and the separated proteins were blotted on to PDVF membrane, before being immunoprobed with an antibody directed against the N-terminal domain of GPR56. It is known that GPR56 can exist either as a full length protein or in a cleaved form, as during processing, the N-terminal segment of GPR56 is cleaved at the GPS motif (Xu et al., 2006). Consistent with a previous report (Iguchi et al., 2008), GPR56 was mainly expressed as the full length 70kDa protein in adult mouse brain, with lower expression of the 65kDa cleaved form (Figure 3-2A, left side). In MIN6 β-cells, GPR56 was expressed at 70kDa, in a full-length form, and its cleaved form was not detected. (Figure 3-2A, right side).

This could mean that the cleaved form of GPR56 is not expressed by β-cells or that MIN6 β-cells had lower GPR56 protein expression than in brain.

The expression of GPR56 protein in human pancreas was investigated by fluorescence immunohistochemistry, Using the same antibody that had been used in the western blotting experiments, archived blocks of human pancreas were cut to 5μm thick and identification of GPR56 expression was carried out as described in Section 2.5.5. As shown in Figure 3-2B, GPR56 was strongly expressed in human islet cells, with apparently faint expression in the exocrine cells. However, consecutive sections that were subjected to the same immunostaining procedure but without GPR56 antibody also indicated background staining in the exocrine pancreas, indicating that this was non-specific staining (Figure 3-2B, right). The restriction of GPR56 expression to endocrine cells of the human pancreas is not consistent with detection of GPR56 mRNA in human acinar cells, suggesting that there may have been some endocrine cell contamination of the human exocrine cell samples used in Figure 3-1.

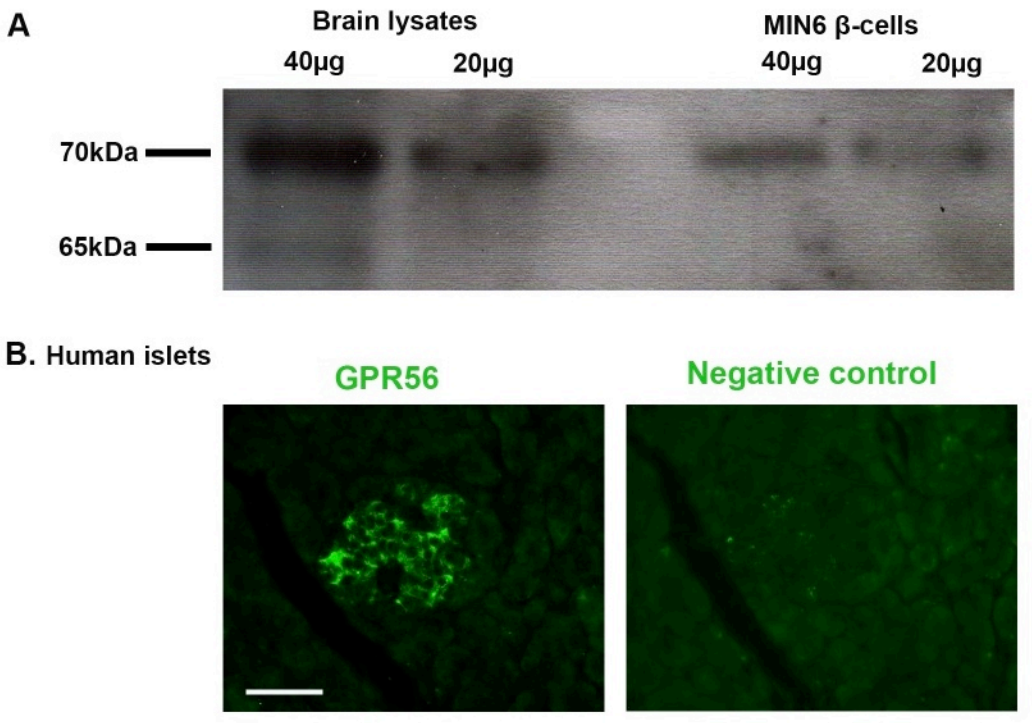

Figure 3-2 Protein expression of GPR56 in whole mouse brain, MIN6 β-cells and human islets. A) Whole brain and MIN6 β-cell lysates were separated by SDS-PAGE and subjected to western blotting. Immunoreactive bands for GPR56 were seen at 70kDa in whole brain and MIN6 β-cell lysates. A second band appeared faintly at 65kDa in whole brain lysate. B) GPR56 expression was detected by immunohistochemistry in wax-embedded human pancreas sections. As expected, no immunoreactivity was observed in the negative control sections where GPR56 antibody was omitted. Scale bar = 50µm.

3.4.3 Localised expression of GPR56 in mouse and human islets

A careful analysis of the cellular localisation and expression pattern of a protein may provide useful clues pertaining to its functions in vivo. Previous studies that reported the protein expression of GPR56 in the pancreas have used methods such as western or northern blotting that cannot distinguish expression within the exocrine or endocrine parts of the pancreas or between individual endocrine cells (Huang et al., 2008; Liu et al., 1999; Shashidhar et al., 2005). This may be due to non-availability of an appropriate antibody for immunostaining at the time of study or the fact that the primary aim of these papers was not islet focused.

To confirm the cellular localisation of GPR56 in mouse and human islets, double immunostaining of GPR56 with insulin, glucagon or somatostatin was carried out on sections

from adult mouse and human pancreases. Immunostaining of mouse pancreas sections showed that GPR56 is expressed strongly by islets compared to the surrounding exocrine cells (Figure 3-3B, E & H). On the other hand, GPR56 expression was not detected in α and δ-cells (Figure 3-3C &I).

It was observed from BLAST multiple alignment tests that mouse and human GPR56 share 81% sequence homology, suggesting that the GPR56 localisation pattern in human pancreas may be similar to that of mouse. To test this, immunohistological staining was carried out on serial sections of wax-embedded human pancreas with antibodies specific to GPR56, insulin, glucagon or somatostatin. As observed previously (Figure 3-2B) GPR56 was strongly expressed in human islets, but unlike in mouse pancreas, there was little or no staining in the surrounding exocrine acinar cells (Figure 3-4). Comparable to mouse islets, it could be seen that GPR56 is expressed by human β-cells but it is absent in glucagon producing α-cells and somatostatin secreting δ-cells. In mouse and human islets, there was >95% co-expression of GPR56 and insulin in β-cells (Figure 3-5), suggesting that GPR56 may have β-cell specific functions in both mouse and man.

Consistent with the literature, the pattern of expression of endocrine cells in mouse islets is different to that of human. Thus, unlike in mouse islets where β-cells are present in the core of the islets surrounded by a mantle of α-cells (Figure 3-3A), in human islets α-cells are scattered among other endocrine cells (Figure 3-4A).

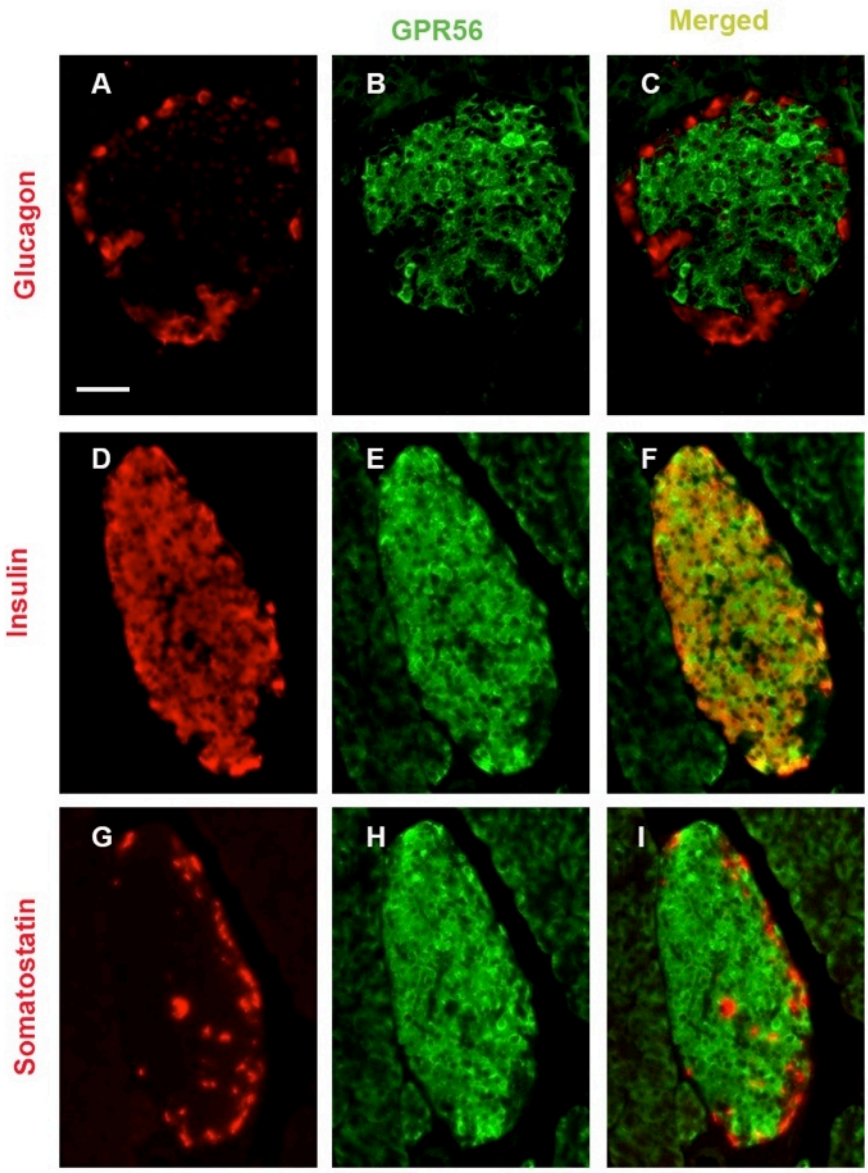

Figure 3-3 GPR56 is expressed by mouse β-cells. 5μm sections of paraffin embedded mouse pancreas were immunoprobed with GPR56 antibody and tagged with a fluorescent secondary antibody (B, E & H). Subsequently, sections were incubated with glucagon, insulin or somatostatin antibodies and tagged with corresponding secondary antibodies respectively (A, D & G). Images were merged (C, F & I) and co-localisation is indicated in yellow. Images are representative of seven different sections. Scale bar =50μm.

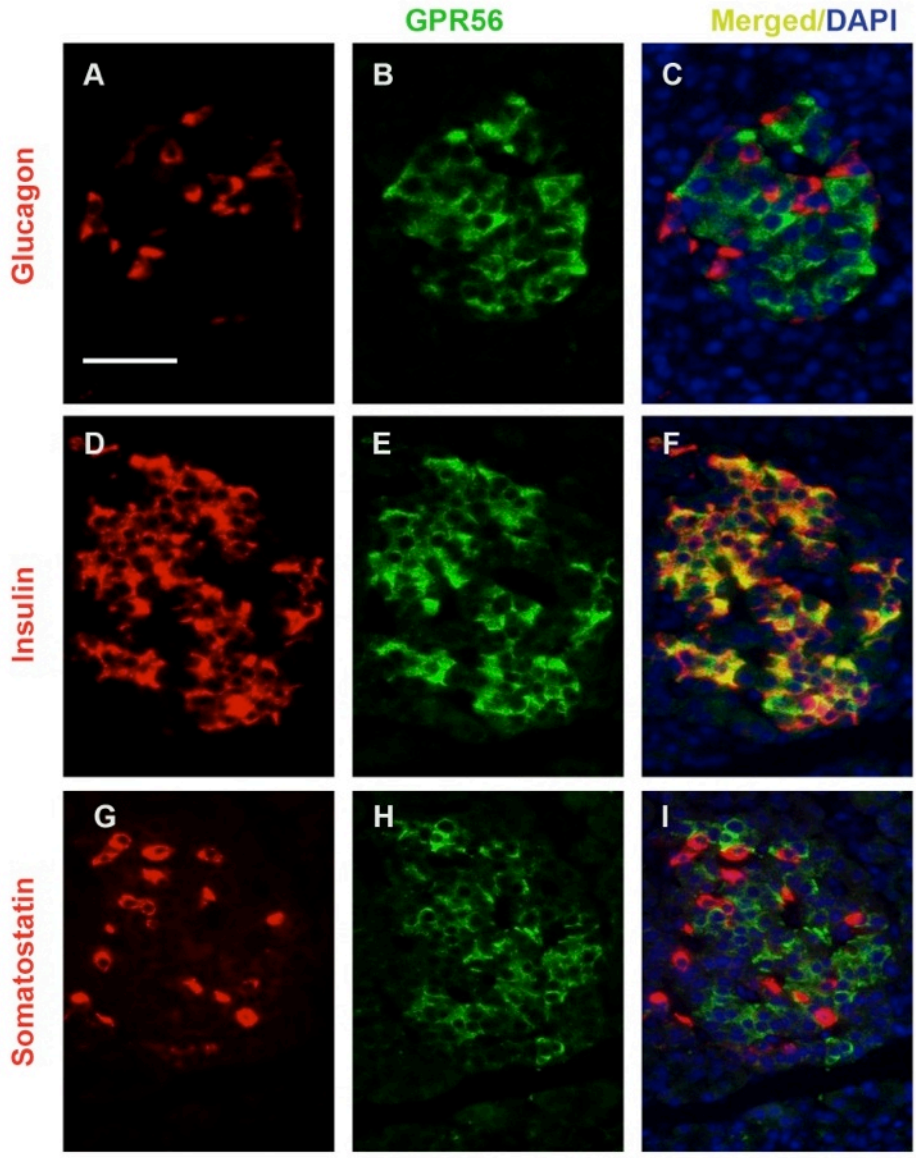

Figure 3-4 GPR56 is expressed by human β-cells. 5μm sections of paraffin embedded human pancreas were immunoprobed with GPR56 antibody and tagged with a fluorescent secondary antibody (B, E & H). Subsequently, sections were incubated with glucagon, insulin or somatostatin antibodies and tagged with corresponding secondary antibodies respectively (A, D & G). Images were merged (C, F & I) and co-localisation is indicated in yellow. Images are representative of five different sections. Scale bar = 50μm.

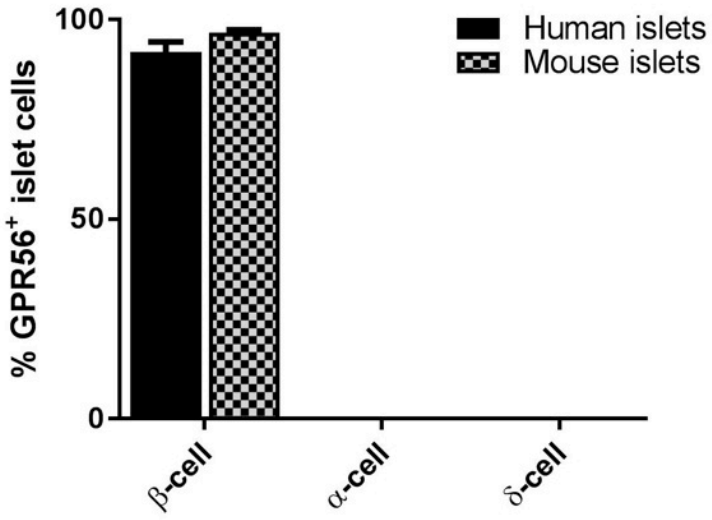

Figure 3-5 Percentage of islet endocrine cells expressing GPR56 in mouse and human pancreas sections. $GPR56^+$ islet cells in mouse and human islets were counted with ImageJ software. The number of individual islet cells expressing GPR56 is represented as a percentage of the total number of islet cells. Data are represented as mean + S.E.M, n = 5 sections.

3.4.4 Expression of GPR56 in islet development

It has been proposed that GPR56 may be involved in islet development because its mRNA transcript was highly expressed in endocrine progenitor cells (Gu et al., 2004). To identify expression of GPR56 during mouse islet development, immunohistological staining was performed on sagittal sections of mouse embryos and pancreases that were retrieved at E11 and E13-E16 respectively. The midgut was used to locate the position of the pancreatic primordium in E11 embryonic sections since the dorsal and ventral buds of the pancreas are evaginations of the midgut (Figure 3-6A & B). GPR56 protein was detected in the pancreas at the earliest available stage of development: at E11, when the dorsal and ventral buds are yet to fuse, it was present in both buds (Figure 3-7C). In addition, its expression was also evident in the pancreas at E13 and E16 (Figure 3-7D & E).

Shortly after the fusion of the lateral and dorsal buds, the primitive pancreas undergoes significant structural changes that are marked by budding at the edges of the pancreas, also known as the tip region, and rearrangement of the cells at the inner or trunk region to form the mature organ structure. The cells at the tip region later form the exocrine pancreas while those

at the trunk region predominantly give rise to endocrine and ductal lineages (Shih et al., 2013). As shown in Figure 3-6D, GPR56 was detected at the tip region (marked by rosette-like buds) and the trunk region at E13, with similar expression levels in both regions. At E16, when the islet structure is morphologically distinguishable from the exocrine cells, GPR56 expression was noticeably greater in islets compared to the surrounding cells (Figure 3-6E).

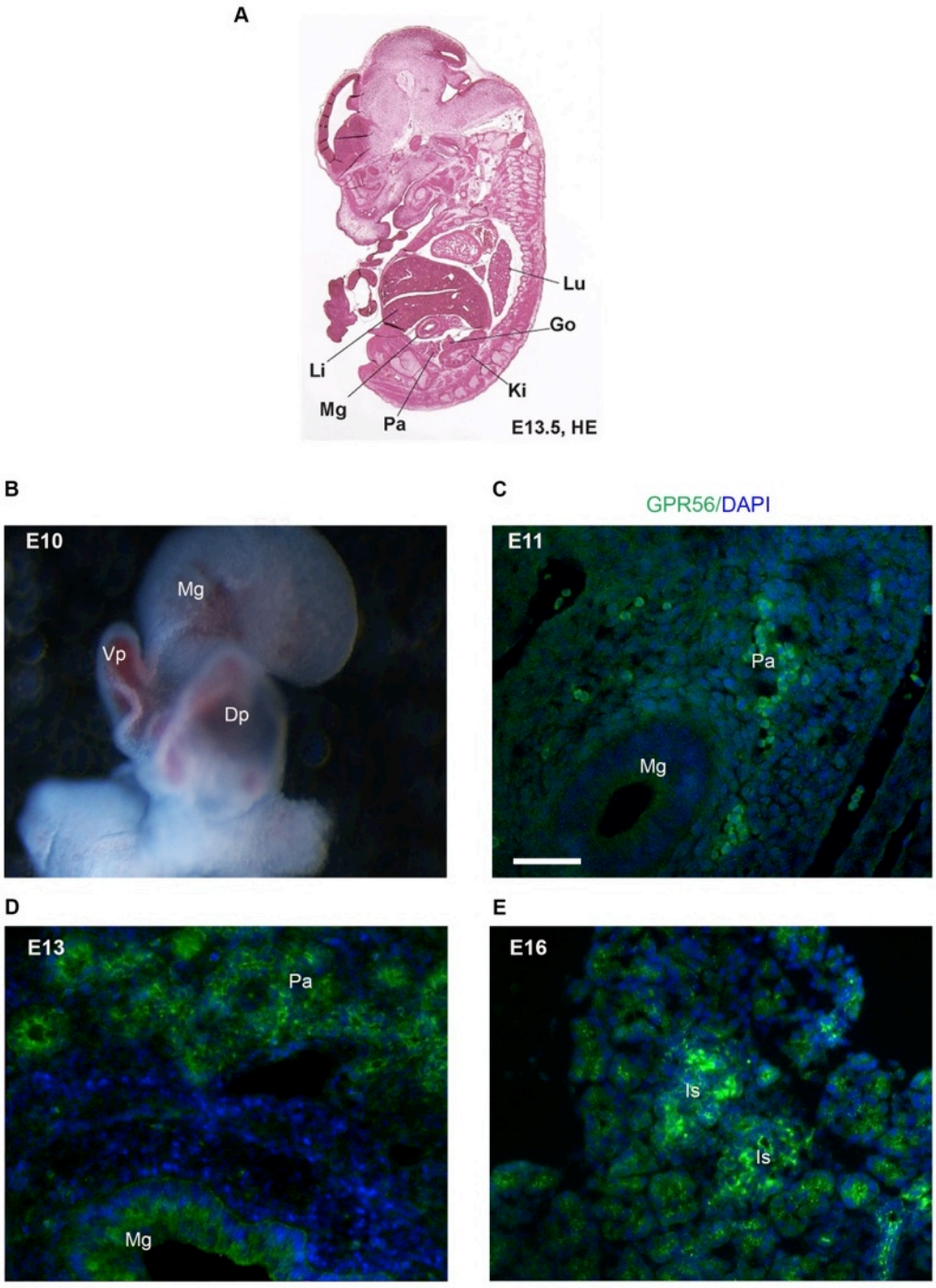

Figure 3-6 Expression of GPR56 in embryonic mouse pancreas. A) Image shows the lateral view of a mouse embryo at E13.5 stained with haematoxylin. Image was taken from (Saisawat et al., 2014). B) The midgut region of a mouse embryo at E10 was microsurgically dissected. Image shows the dorsal and ventral pancreas as outgrowths of the midgut, which are yet to fuse at this stage C) Wax-embedded E11 mouse embryo was sectioned sagittally and immunoprobed for GPR56. GPR56 is expressed in both the ventral and dorsal buds of the pancreatic primordium. D) A sagittal section of a mouse embryo at E13 showing expression of GPR56 in the pancreas. E) The image shows expression of GPR56 in E16

pancreas. Li = liver, Mg =mid gut, Pa = pancreas, Vp= ventral pancreas, Dp = dorsal pancreas, Ki = kidney, Go = gonad, Lu = lung, Is = islet, Scale bar = 100μm for C, D & E only.

As GPR56 expression was restricted to the β-cells in adult mouse and human islets (Figure 3-3 - Figure 3-5), it was investigated whether this restriction started during islet development in the embryo or acquired after birth by carrying out double immunostaining of GPR56 and insulin in mouse embryonic pancreas sections at E18. At this stage of development GPR56 was expressed by β-cells and it colocalised with insulin (Figure 3-7C), consistent with what was observed in adult mouse and human islets. However, not all GPR56-expressing cells were positive for insulin (Figure 3-7B) and some insulin^{+} β-cells were negative for GPR56 (Figure 3-7A & B).

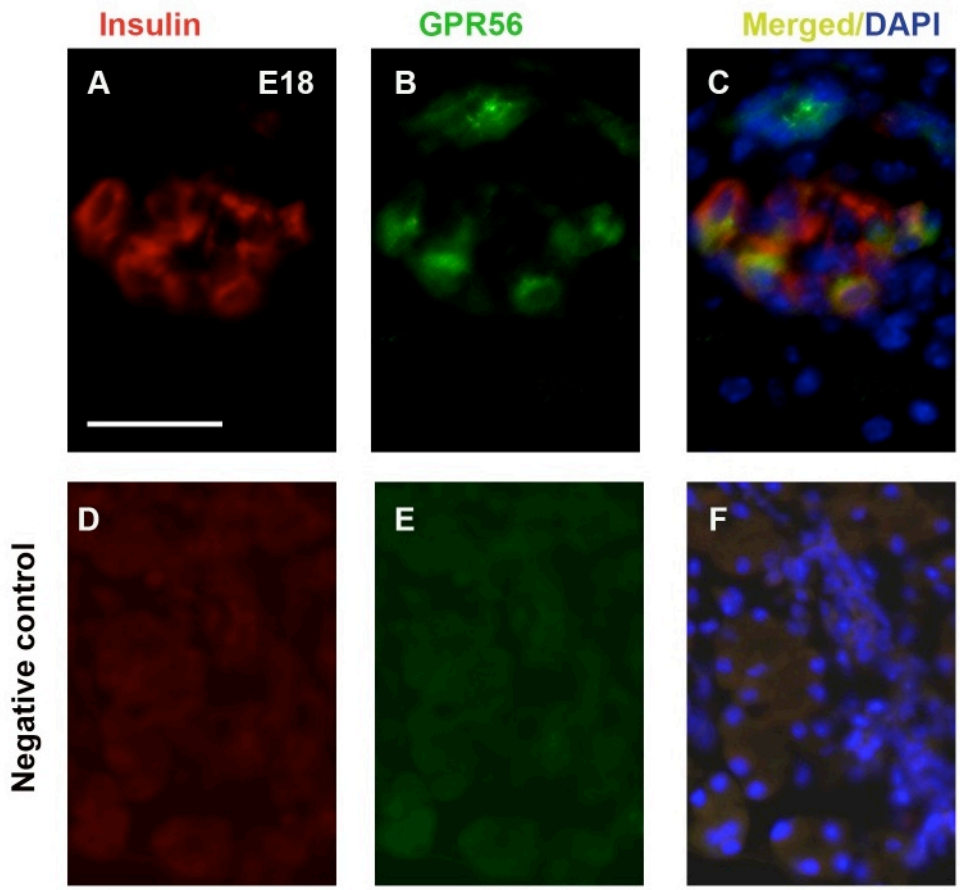

Figure 3-7 GPR56 colocalises with insulin in developing islets at E18. Antigens were retrieved for 12 min and double IHC was performed on 10µm sections of E18 mouse pancreas for (A) insulin and (B) GPR56. C) GPR56 and insulin immunostaining were merged and colocalisation is indicated in yellow. GPR56 is expressed by some β-cells. Not all GPR56^{+} cells are positive for insulin and vice versa. (D-F) Images show non-detection of (D) insulin and (E) GPR56 when primary antibodies were omitted in the immunostaining procedure. Scale bar = 100µm.

To confirm the specificity of GPR56 and insulin antibodies, the immunostaining procedure was repeated with PBS replacing the primary antibodies, followed by incubation with the appropriate secondary antibodies. Using the same exposure time, no immunopositive signals were seen in the absence of the primary antibodies (Figure 3-7D-F), indicating that the signals in A & B are positive for insulin and GPR56 respectively.

Double IHC was also carried out on E18 mouse pancreas sections using antibodies for GPR56 and glucagon or somatostatin. Glucagon expressing α-cells were detected at E18, with no colocalisation with GPR56 (Figure 3-8D, E&F). As shown in Figure 3-8G, somatostatin positive δ-cells were expressed in embryonic mouse pancreas at E18. Similar to adult islets, no colocalisation between $GPR56^+$ cells and $somatostatin^+$ cells was observed (Figure 3-8I). Since GPR56 is only expressed by β-cells in embryonic islets (Figure 3-8C), the $GPR56^+$ cells that do not co-localise with insulin are either progenitor cells that are yet to differentiate to β-cells or ductal cells.

As shown earlier, GPR56 mRNA was detected in exocrine cells of adult mouse pancreas (Figure 3-1). Following a similar line of investigation, it was therefore determined whether GPR56 is expressed by developing mouse acinar cells. Pancreases were dissected from embryonic day 18 (E18) and 9-day-old mice (P9) and fixed-frozen. 10μm sections were immunoprobed for GPR56 and amylase, which is a marker for acinar cells. Consistent with the mRNA expression in adult mouse pancreas, GPR56 was faintly expressed in exocrine cells compared with endocrine and ductal cells where amylase was not present (Figure 3-9). At E18 and P9, GPR56 was faintly colocalised with amylase while at P9, it was strongly expressed by islets and ductal cells.

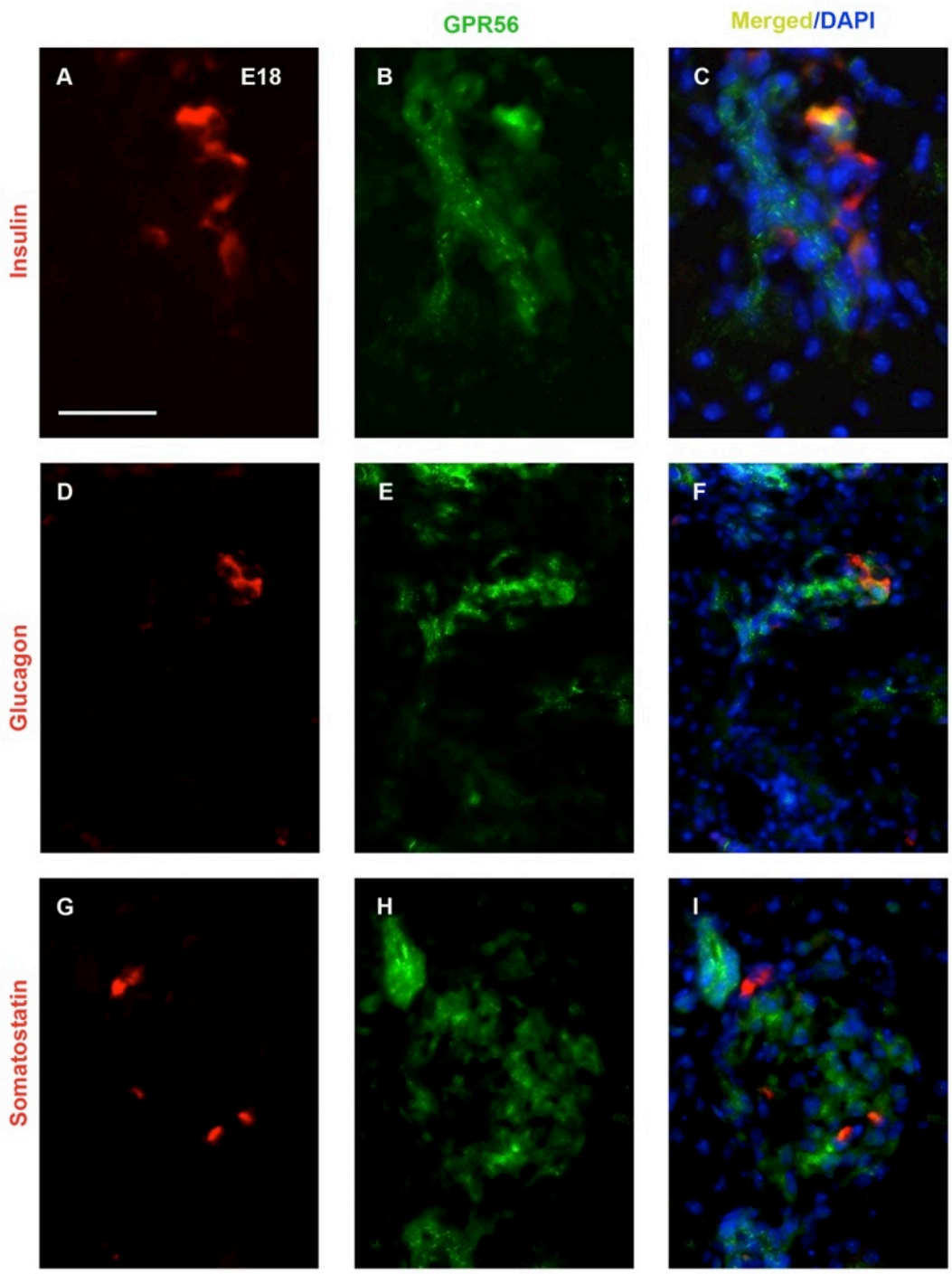

Figure 3-8 GPR56 is not expressed by embryonic α-cells or δ-cells. Double immunostaining of GPR56 (green) with insulin, glucagon or somatostatin (red) was performed on E18 fixed-frozen mouse pancreas sections. GPR56 is co-expressed by some insulin positive β-cells (A – C). GPR56 was not detected in α- or δ-cells (D – F; G-I).Scale bar = 100μm.

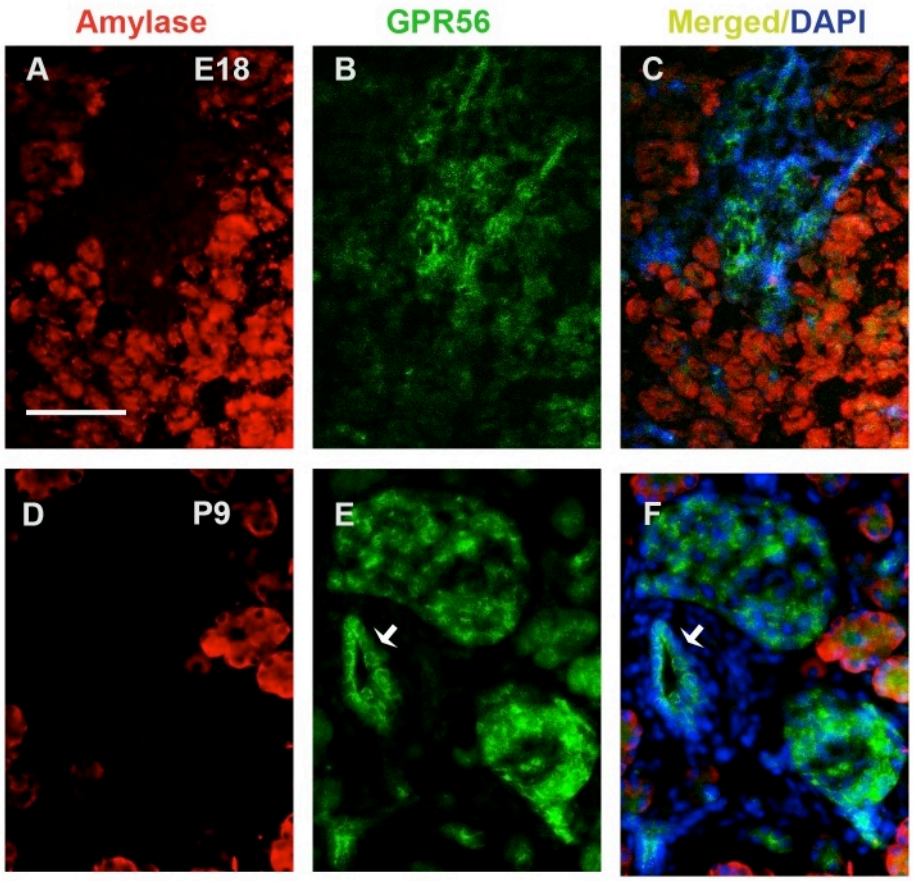

Figure 3-9 GPR56 is expressed at low levels by the exocrine acinar cells in embryonic and post-natal mouse pancreas. Fixed-frozen mouse pancreas sections were immunoprobed for amylase and GPR56 at E18 and P9.. GPR56 faintly colocalised with amylase at E18 (A-C) and in early postnatal pancreas (D-F). At P9, GPR56 expression was detected in ductal (arrows in E&F) and endocrine cells (D–F). Scale bar = 50μm.

3.4.5 Expression of GPR56 at different stages of mouse islet development

E15 was the earliest time point at which it was possible to quantify expression of GPR56 in islet development, due to limited availability of tissues. GPR56 was abundantly expressed in both the exocrine and endocrine pancreas at E15 and it colocalised with insulin (Figure 3-10B&C). There was a gradual decline in the expression of GPR56 in exocrine cells as the mice mature from E15 to P9 (Figure 3-10B, E, H&K), while its expression in the islets was maintained. Overall, quantification of GPR56 expression by ImageJ analysis indicated that there was a decrease in GPR56 expression in the whole pancreas at E16 and this decrease was maintained till E18 (Figure 3-10M). Thereafter, GPR56 expression began to increase and at P9 it had reached the level it was at in the E15 pancreas specimens.

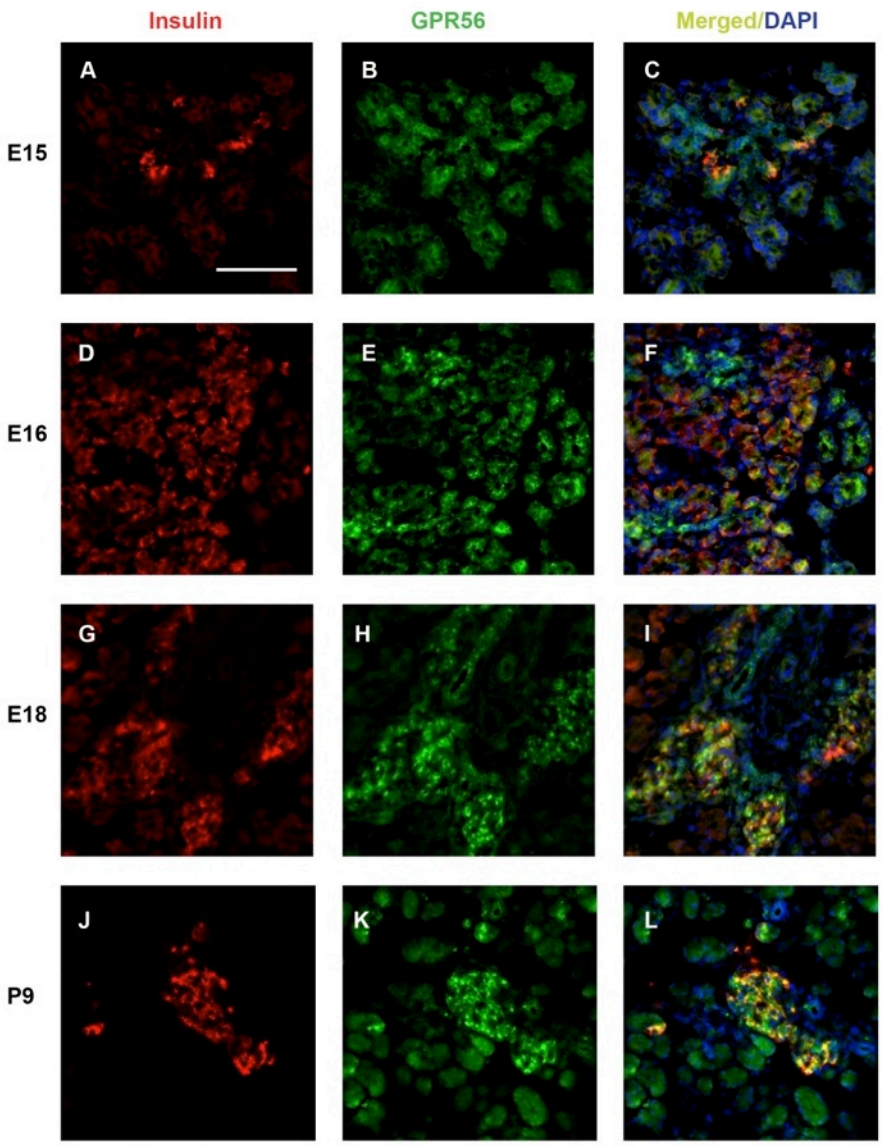

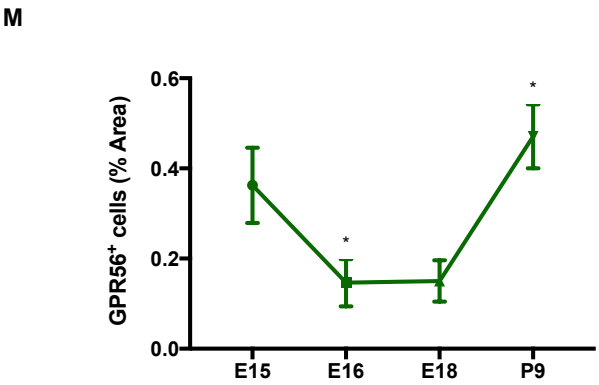

Figure 3-10 Expression pattern of GPR56 in developing mouse pancreas. Fixed-frozen mouse pancreas sections were immunoprobed for GPR56 and insulin, and the expression levels of the two proteins were quantified by ImageJ. A-L) Representative images showing the expression of GPR56 and insulin at E15 to P9, with colocalisation indicated in yellow. Scale bar = 100μm. M) The graph shows the percentage area of

GPR56^{+} cells in the pancreas at different developmental stages. *$p<0.05$, n=10 sections, Kruskal-Wallis test with Dunn's posthoc test.

3.4.6 Expression of GPR56 by endocrine progenitor cells

Endocrine progenitors are positive for neurogenin 3 (NGN3), a transcription factor expressed exclusively by pancreatic cells that will later form the islets. They differentiate terminally to form α-, β-, δ- and pancreatic polypeptide (PP) cells. To confirm that endocrine progenitor cells express GPR56, NGN3 expression was first assessed by IHC in fixed frozen or wax embedded pancreas sections from E18 mice. Figure 3-11 and Figure 3-12 show that, in mouse pancreas the subcellular localisation of NGN3 is both cytoplasmic and nuclear, consistent with what was observed in the hippocampus (Simon-Areces et al., 2010).

NGN3 expression is tightly controlled during islet development, maintaining a balance between endocrine cell proliferation and differentiation. NGN3 is downregulated during differentiation. It was shown by lineage tracing that each endocrine cell transiently expresses NGN3 for up to 48 h, after which the expression is switched off and the cells become terminally differentiated (Gu et al., 2002). Figure 3-11B and Figure 3-12B, E & H show that NGN3 is highly expressed in some cells in the developing pancreas, while it is weakly expressed in others. Dual staining with an insulin antibody indicates that NGN3 is expressed in some β-cells, while other insulin-expressing cells are negative for NGN3 (Figure 3-11C). This suggests that the cells are in transition of their progenitor status being turned off. NGN3 expression is biphasic in mouse pancreas development with early NGN3-expressing progenitors appearing with primary transition of islet development and they become reactivated again just prior to secondary transition. The first wave of cells expressing NGN3 give rise mostly to α-cells while the later NGN3-expressing precursors give rise to all endocrine cell types (Villasenor et al., 2008; Johansson et al., 2007). Glucagon$^+$ α-cells are the first to be expressed in islet development at E9.5 and Figure 3-12F show that NGN3 expression in most of the glucagon$^+$ α-cells has been completely turned off, since they were negative for NGN3 at E18.5 when majority of α-cells had been formed (Johansson et al., 2007). This is also true for δ-cells, as none of the somatostatin immunoreactivity colocalise with NGN3 in any cells (Figure 3-12H&I).

To confirm the specificity of the NGN3 antibody that was used for IHC, wax-embedded mouse pancreas sections were subjected to the same IHC procedures in the absence of the NGN3 antibody. As expected, immunopositive signals were absent (Figure 3-12H&I) indicating that the

primary antibody was specific to NGN3 and that the signals seen in Figure 3-12B, E&H were not due to background fluorescence from the secondary antibody.

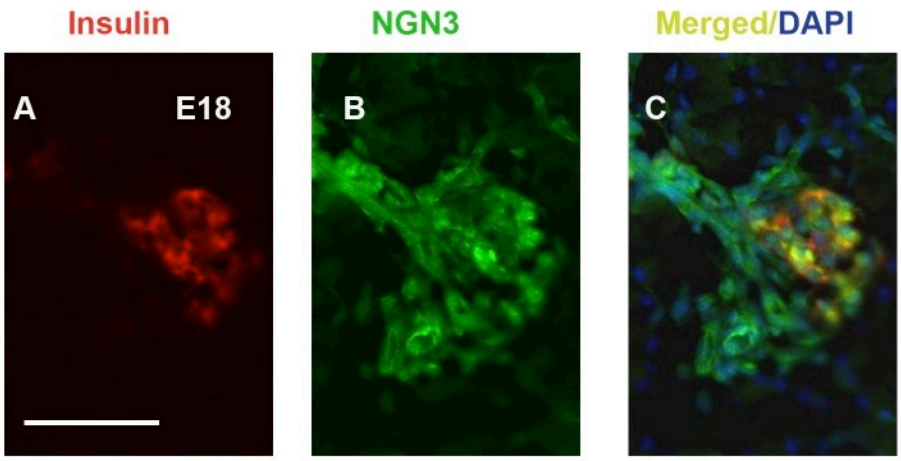

Figure 3-11 Expression of insulin and NGN3^{+} endocrine progenitors in the pancreas at E18. Frozen pancreas sections were incubated with insulin and NGN3 antibodies. A) Insulin positive β-cells are already in clusters at E18, resembling the adult islet structure. B) Image shows that NGN3^{+} cells are restricted to an islet-like cluster at E18 (although there appears to be some NGN3^{+} duct cells), with no expression at the surrounding exocrine acinar cells. Subcellular localisation of NGN3 is both nuclear and cytoplasmic. C) Image shows colocalisation of insulin with NGN3^{+} cells in yellow and NGN3+ progenitor cells that are yet to differentiate. Scale bar = 100μm.

Having established the expression pattern of NGN3 in the embryonic mouse pancreas, it was next determined whether NGN3 positive cells express GPR56. Double IHC staining for NGN3 and GPR56 was performed on mouse pancreas sections at E13 and E16. At E13, most of the NGN3 positive cells co-express GPR56 (Figure 3-13), while at E16 most of the GPR56 positive cells no longer colocalise with NGN3 (Figure 3-15 A-C). As shown in Figure 3-14, GPR56 was expressed in cells that were positive for pancreatic and duodenal homeobox 1, a transcription factor that is important for pancreas development and functional maturity of β-cells (Romer and Sussel, 2015). In addition, as SOX9 is important in determining endocrine and ductal cell lineage fate, the expression of GPR56 was investigated in SOX9^{+} cells. It can be seen from Figure 3-15D-F that SOX9 was expressed in the pancreas at E16 and it colocalised with GPR56.

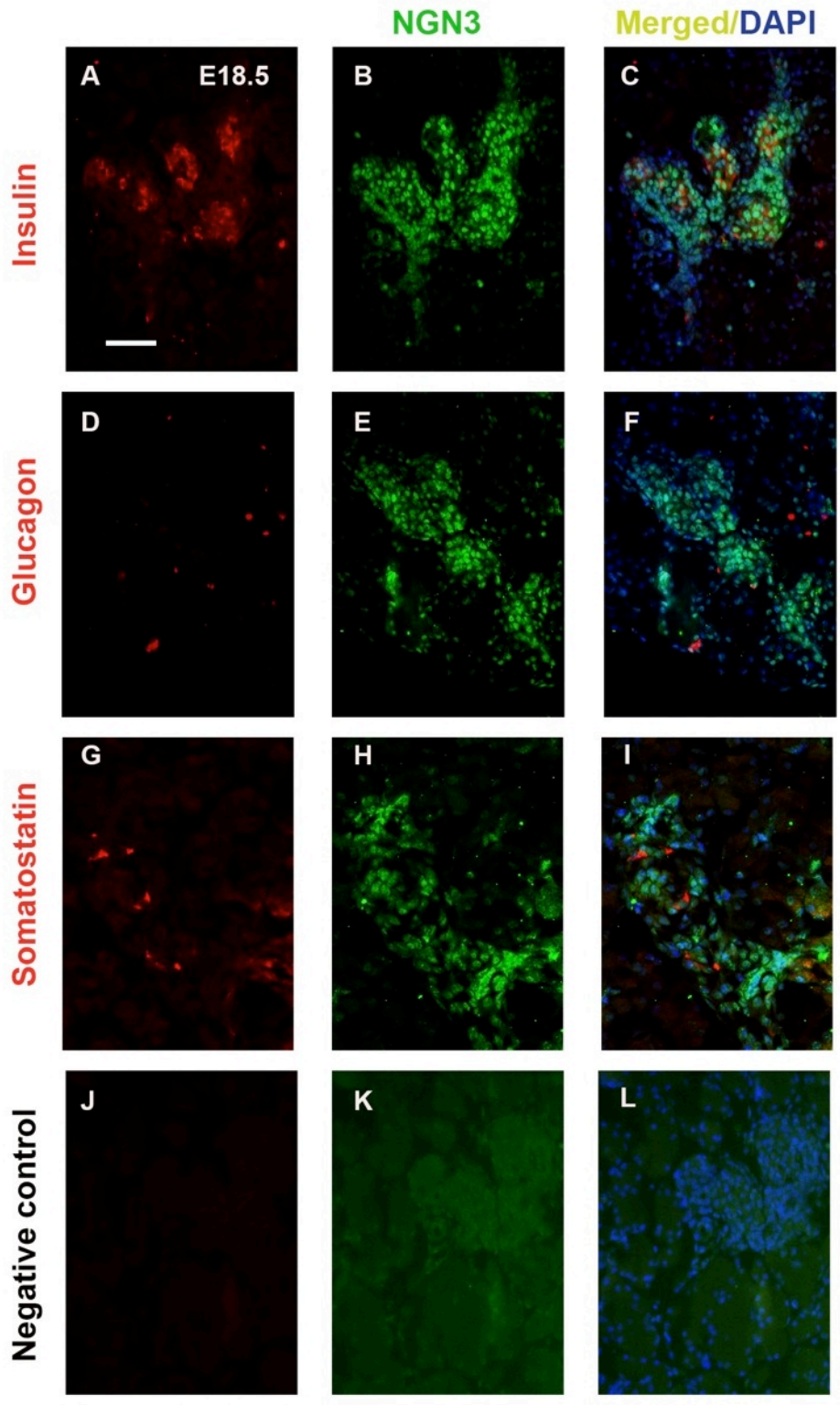

Figure 3-12 Expression of NGN3 in developing islet endocrine cells. Paraffin embedded mouse pancreas sections were immunoprobed for insulin, glucagon, somatostatin and NGN3. A-C) Images show the expression of insulin and its colocalisatioin with NGN3. D-F) show glucagon+ cells, the majority of which do not express NGN3 (F). G-I) show somatostatin positive cells that do not colocalise with NGN3. J-L) are negative control images where primary antibodies were omitted in the IHC procedures. Scale bar = 50μm.

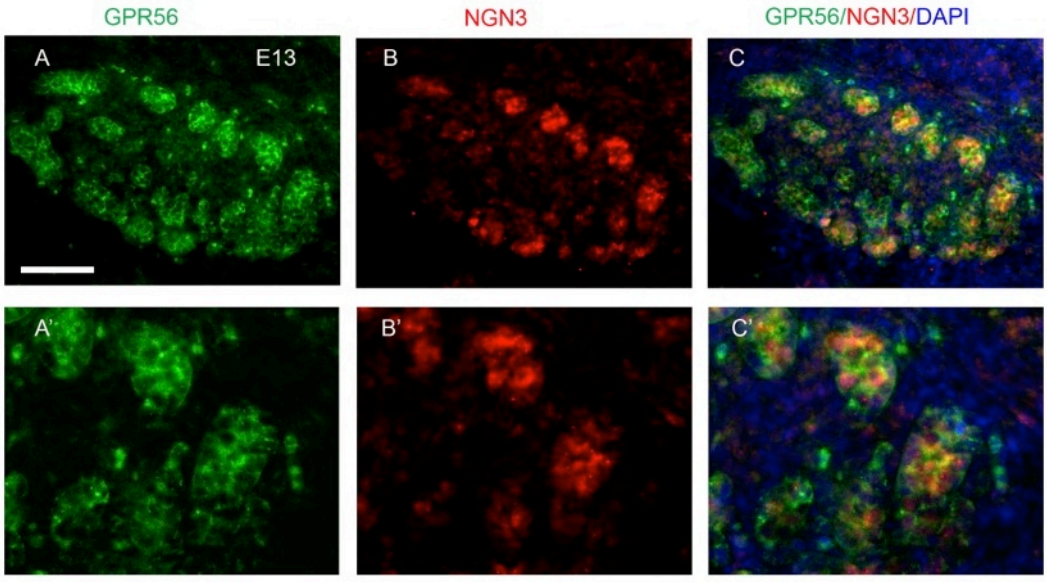

Figure 3-13 Expression of GPR56 by NGN3^{+} progenitors at E13. Frozen mouse embryo was sectioned sagittally and immunoprobed for GPR56 and NGN3. A) Image shows the expression of GPR56 and B) NGN3 with C) colocalisation indicated in yellow. A' – C' are magnified images of A – C respectively. Scale bar = 100μm

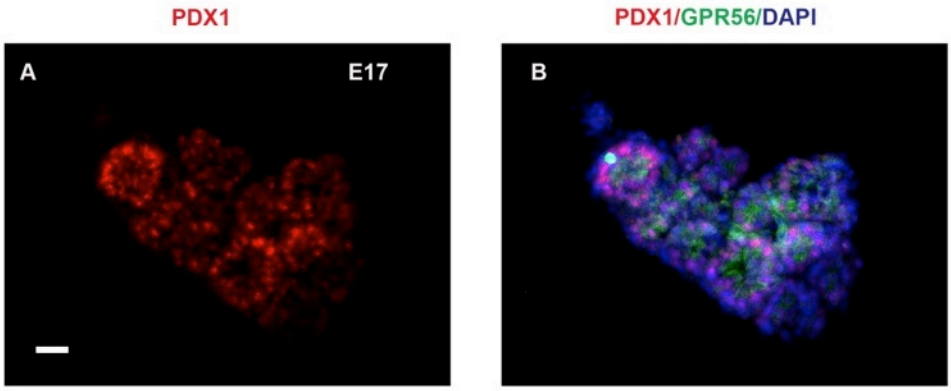

Figure 3-14 Expression of GPR56 by PDX1^{+} pancreatic cells. Frozen mouse pancreas sections at E17 were immunoprobed for PDX1 and GPR56. A) Image shows the expression of PDX1 and B) colocalisation of PDX1^{+} cells with GPR56. Scale bar = 20μm.

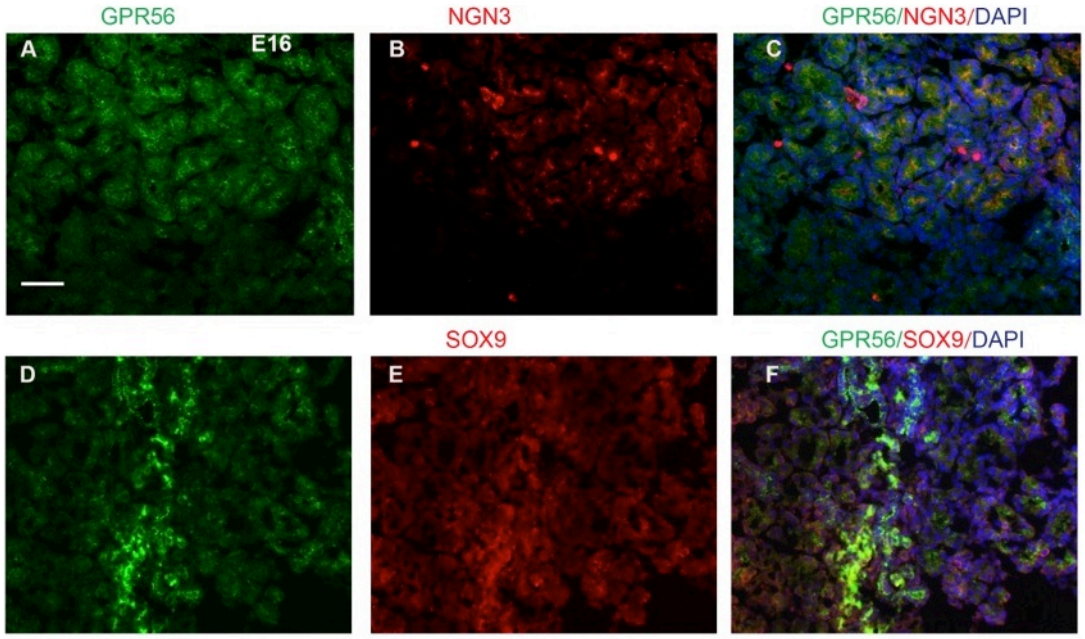

Figure 3-15 Expression of GPR56 in NGN3^{+} and SOX9^{+} progenitors at E16. Double IHC for GPR56 and NGN3 or GPR56 and SOX9 was carried out on 10μm sections of E16 mouse pancreas. A) GPR56 was expressed in mouse pancreas at E16. B) NGN3 was also detected. C) Image shows limited colocalisation of GPR56 and NGN3 in yellow. D-F Images show the expression of SOX9 in developing islet and ductal cells and its colocalisation with GPR56. Scale bar =100μm.

3.4.7 Effect of GPR56 deletion on differentiation of endocrine progenitors

The effect of GPR56 on differentiation of endocrine progenitors was investigated by staining for NGN3 in embryonic pancreases retrieved from GPR56 WT and GPR56 KO mice. Prior to pancreas retrieval, pregnant dams were injected IP with BrdU, to label replicating cells. Immunostaining for NGN3 and BrdU was carried out and the number of $NGN3^+$cells/mm^2 and $BrdU^+$ cells/mm^2 were quantified by ImageJ (Figure 3-16A-D). At E16, there was an increased number of $NGN3^+$ progenitors in GPR56 KO pancreas ($NGN3^+$ cells/mm^2; WT: 3,012 ± 211, KO: 3,880 ± 266, n=6-11 replicates, p=0.05), suggesting reduced differentiation (Figure 3-16E). However, there was no change in proliferation of progenitor cells at E16 ($BrdU^+$ cells/mm^2; WT: 475.8 ± 44.6, KO: 448.2 ± 18.2, n=6-11 replicates, p>0.2) (Figure 3-16F).

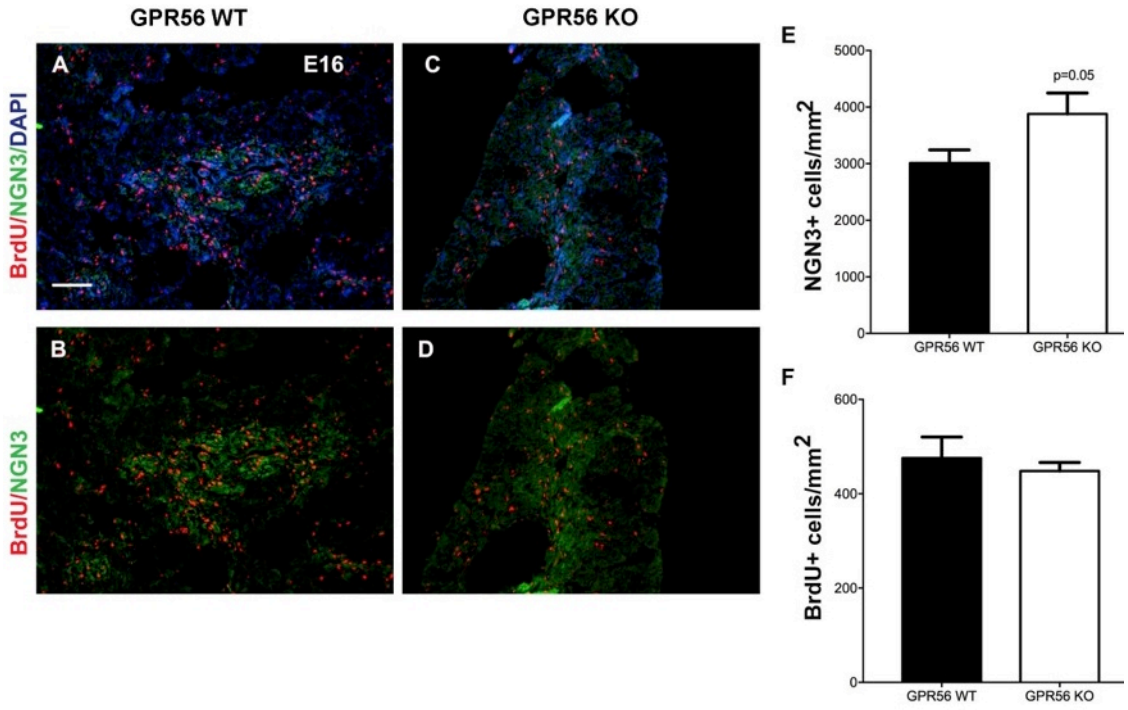

Figure 3-16 Effect of GPR56 deletion on differentiation and proliferation of endocrine progenitors at E16. Pregnant dams were given BrdU IP and pancreases were retrieved 2 h later and fixed frozen. 5µm sections were immunostained for NGN3 and BrdU in A-B) GPR56 WT pancreases and C-D) GPR56 KO pancreases. Scale bar = 100µm. E) There was a trend towards increased $NGN3^+$ cells in GPR56 KO pancreas, p=0.05, Student's t-test, n= 6 sections (KO) and 11 sections (WT). F) There was no difference in $BrdU^+$ cells at E16, p>0.2, Student's t-test, n= 6 sections (KO) and 11 sections (WT). Data are presented as Mean + SEM.

3.4.8 Detection of the GPR56 agonist, collagen III, in mouse and human islets

Collagen III is a ligand for GPR56 in the developing brain (Luo et al., 2011). To find out whether it is also expressed in the pancreas, fluorescence IHC was carried out on adult mouse and human pancreas sections. Collagen III staining was seen around the lobar and acinar septa of the pancreas, at the peri-islet basement membrane and within islets, in both mouse and human pancreas (Figure 3-17 A, B, E & F). Collagen III did not colocalise with insulin^{+} β-cells (Figure 3-17B &F). Immunostaining was also carried out for collagen IV to determine whether it has a similar pattern of expression as collagen III, since collagen IV has been reported to be present primarily in the basement membrane (Korpos et al., 2013) Collagen III and IV have similar staining pattern in human islets (Figure 3-17 E, & G), but in mouse pancreas there was marked intra-islet staining of collagen IV, perhaps reflecting its presence in the vascular network ECM. Overall, the IHC staining indicated that collagens III and IV are both found within and surrounding each islet, and also in the exocrine pancreas.

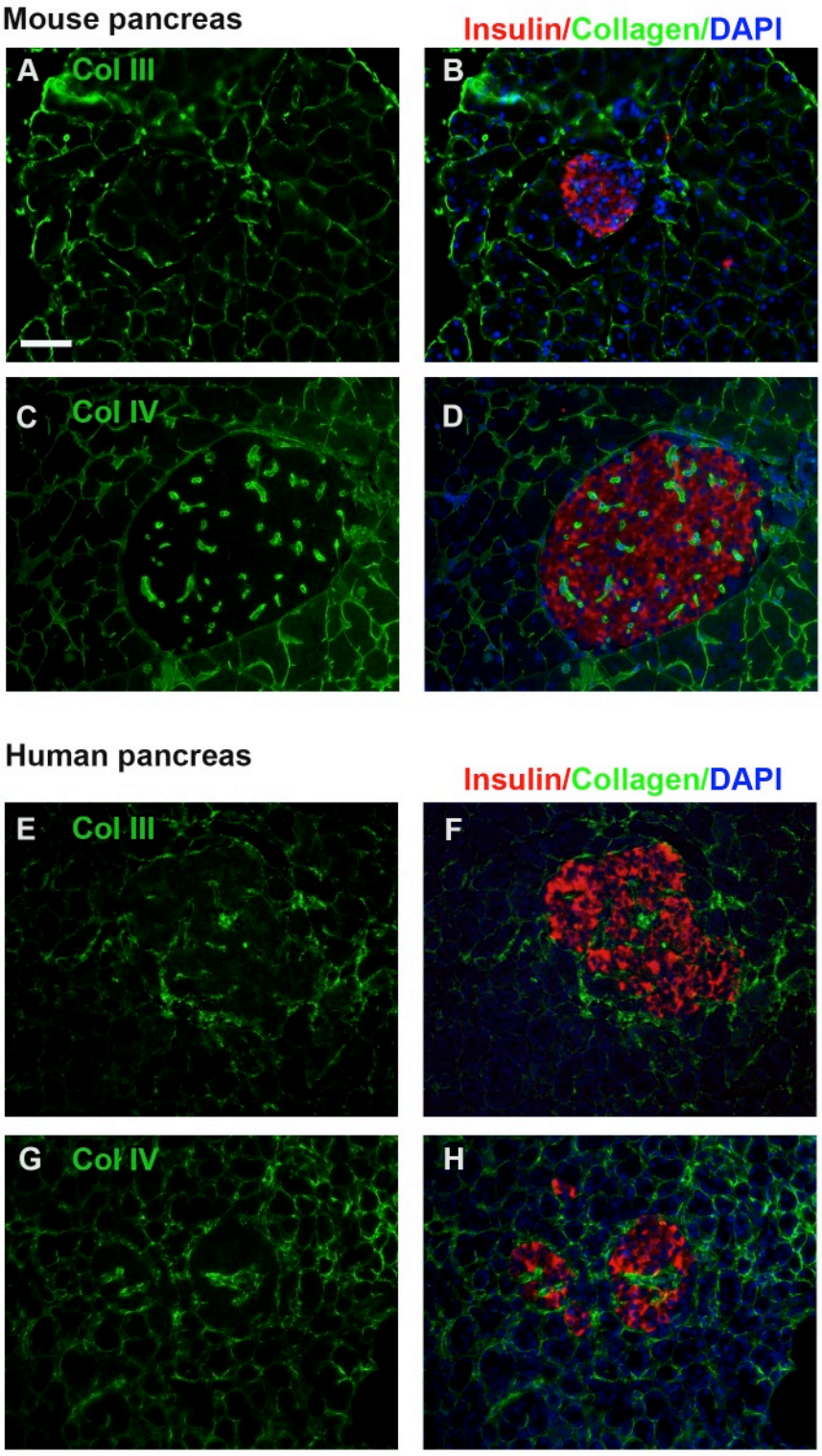

Figure 3-17 Detection of collagen III and IV in mouse and human pancreas. Upper panel: Wax-embedded sections of mouse pancreas showing expression of collagen III (A) and IV (C) and their non-colocalisation with insulin (B&D). Each image is representative of seven replicates. Lower panel: Wax-embedded sections of human pancreas showing expression of collagen III (E) and IV (G) and their non-colocalisation with insulin (F&H). Each image is representative of four replicates. Scale bar = 50μm.

3.4.9 Collagen III is expressed by islet vascular endothelial cells

In order to confirm that β-cells do not synthesise collagen III, RT-PCR was performed on cDNAs obtained from MIN6 β-cells, mouse and human islets, and exocrine cells. As shown in Figure 3-18A, collagen III mRNA was not detected in MIN6 β cells, but it was amplified in cDNAs extracted from mouse and human islets, and pancreatic exocrine cells. It was confirmed that high quality MIN6 cell cDNA had been used in the PCR amplification since the expected 229bp product was generated when β-actin primers were used instead of collagen III primers. As expected, no products were obtained when MIN6 β-cell RNA or distilled water were used with collagen III primers instead of cDNA, indicating that the bands were not due to genomic DNA contamination. Given that collagen III is present in the blood vessels of human and rat pancreas (Deijnen et al., 1994), it is likely that the collagen III mRNA detected in the islets was due to its localisation to the vascular basement membrane. To confirm this, immunohistological staining of collagen III and CD31, a marker of vascular endothelial cells, was carried out on mouse pancreas sections. CD31 was detected in islets and blood vessels, and it colocalised with collagen III (Figure 3-18B, dotted circle), indicating that collagen III is produced by the vascular endothelial cells rather than the β-cells.

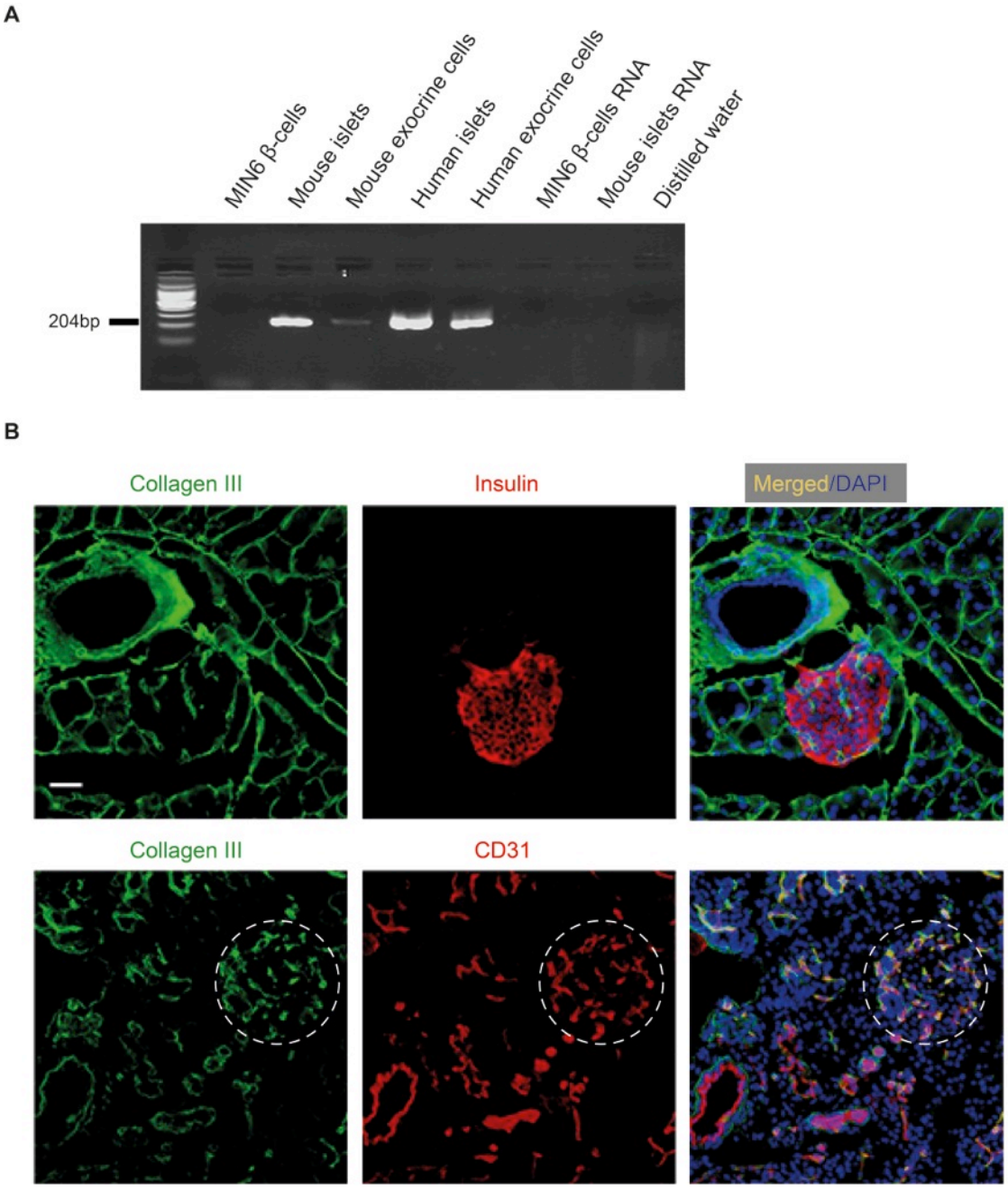

Figure 3-18 Collagen III is expressed by pancreatic vascular endothelial cells. A) Products of RT-PCR amplification using mouse and human col3a1 primers with cDNAs obtained from MIN6 β-cells, mouse and human islets and exocrine cells. Amplicons correspond to the predicted sizes of the nucleotide sequence generated using the chosen mouse and human primer pairs. No amplification was observed when cDNAs were replaced with RNA or distilled water. B) Images show the expression of collagen III and its colocalisation with CD31. Collagen III was detected in islets but it did not colocalise with insulin^{+} β-cells. Collagen III colocalised with CD31^{+} endothelial cells present within mouse islet (dotted circle). Scale bar = 50μm.

3.4.10 Expression of other binding partners of GPR56 in islets

The ability of the 1000+ GPCRs in the human genome to signal specifically through a limited number of heterotrimeric G-proteins has been shown to be mediated via scaffolding proteins such as the tetraspanins (Pierce et al., 2002). Tetraspanins are able to couple GPCRs to mediators of downstream signalling such as Gαq. For instance, GPR56 forms a stable complex with Gαq through CD81, a cell surface tetraspanin. Immunodepletion of CD81 from this complex led to complete dissociation of Gαq/11 from GPR56, suggesting that CD81 is important in stabilising the GPR56- Gαq/11 complex (Little et al., 2004). In islets, it is possible that CD81 must be expressed on the cell surface for GPR56 to couple to Gαq/11. The expression of CD81 mRNA was therefore investigated in mouse and human islets by RT-PCR using primers specific for CD81. The expression of CD81 mRNA was seen in MIN6 β-cells, mouse islets, mouse exocrine cells and human islets, but it was not expressed by human exocrine cells (Figure 3-19). Distilled water used for diluting the cDNAs served as a negative control. The amplification of the mouse and human β-actin amplicons (227bp and 107bp respectively) in the cDNA samples indicates their viability.

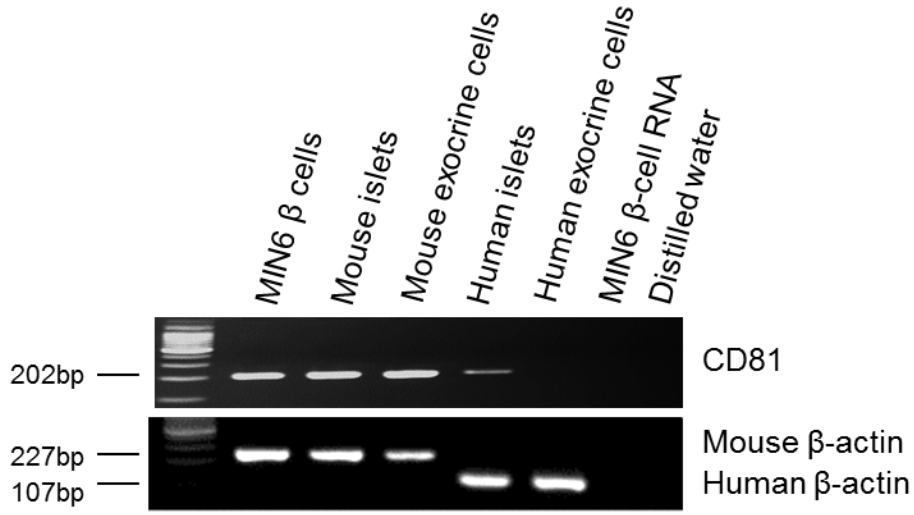

Figure 3-19 Expression of CD81 mRNA in mouse and human islets. CD81 mRNA was detected in MIN6 β-cells, mouse islets, and mouse exocrine cells. It was not detected in human exocrine cells but was faintly expressed in human islets. Amplicons correspond to the predicted sizes of the nucleotide sequence generated using the chosen primer pairs. Amplification of β-actin was used as a loading control.

As a 'split-personality receptor', the N-terminal fragment of GPR56 can couple with the C-terminal component of another adhesion GPCR, and vice versa, to form a functionally active complex. This has been demonstrated for GPR56 and latrophilin 1 in the brain (Silva et al., 2009), so the expression of latrophilin 1 in mouse and human islets was therefore investigated. RNAs from MIN6 cells, mouse and human islets were reverse transcribed to cDNAs and the expression of latrophilin 1 was investigated by standard PCR. Latrophilin 1 mRNA was detected in all the tissues investigated, with strong expression in MIN6 β-cells, mouse and human islets compared with the exocrine cells (Figure 3-20). No amplification was seen when distilled water was used instead of cDNA. Amplification of β-actin in the cDNAs indicates their viability.

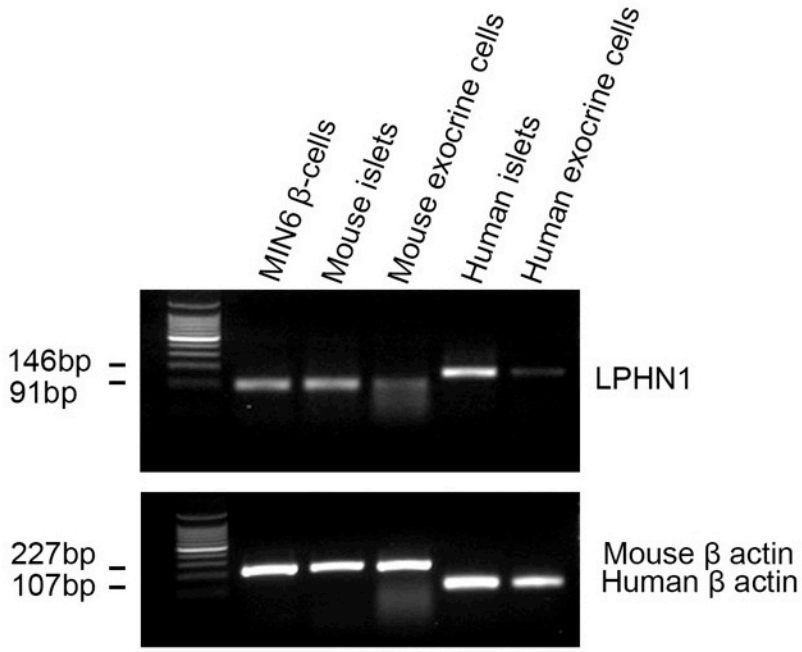

Figure 3-20 Expression of latrophilin1 mRNA in mouse and human islets. Images show products of RT-PCR amplification using primers for latrophilin 1 and mouse and human β-actin primers. Amplicons correspond to the predicted sizes of the nucleotide sequences generated using the chosen primer pairs. Latrophilin1 mRNA was expressed in MIN6 β-cells, mouse and human islets and faintly in the exocrine cells. β-actin was used as a loading control.

3.5 Discussion

In mouse, pancreas development starts as early as E9 and occurs in two phases. The first phase, which is also known as primary transition, takes place between E9 and E12.5. During this phase, the majority of the cells are multipotent progenitor cells (MPCs). As the nascent pancreas enlarges and buds, the MPCs, marked by their expression of transcription factors such as PDX1, Ptf1a and SOX9, undergo extensive proliferation. Towards the end of the primary transition, the first wave of differentiation begins, with the majority of the differentiated cells being glucagon-expressing α-cells. After E12.5, substantial differentiation occurs, giving rise to all the endocrine cell types, with β-cells appearing first, followed by δ-cells and then PP cells (Herrera et al, 1999). This is known as phase II or secondary transition (Jensen et al., 2000).

Whereas several studies have reported the role of GPR56 in brain development (Bae et al., 2014; Iguchi et al., 2008; Piao et al., 2004; Li et al., 2008), nothing is known about the expression and function of GPR56 in developing and adult pancreas. The data presented in this chapter demonstrate that GPR56 is expressed in adult and embryonic pancreas, and it is colocalised with differentiating $NGN3^+$ cells, $SOX9^+$ cells, acini, ductal cells and mature β-cells. Consistent with a previous report that GPR56 maintains progenitors in a proliferative state (Giera et al., 2015), the images presented here show that GPR56 is strongly expressed at E11 during MPC proliferation and it became downregulated during the differentiation stage, before E18. In addition, at the early stage of pancreas development, GPR56 was strongly expressed in cells that will later form islets and exocrine cells but became progressively downregulated in acinar cells as the pancreas develops. However, genetic lineage tracing would be required to show that the GPR56 expressing cells actually turned into islets or acinar cells. Since GPR56 is expressed before the appearance of β-cells, it is possible that the $GPR56^+$/$insulin^-$ sup-population are progenitor cells, while the $GPR56^-$/$insulin^+$ sup-population are cells in which GPR56 has been turned off after terminal differentiation to β-cells. After the cells have acquired β-cell identity, GPR56 expression is then turned back on. Once the mature islet structure has been formed at E18, GPR56 expression was upregulated in islets compared to the surrounding exocrine cells and this pattern was maintained postnatally.

It is not yet clear what specifies the timing of GPR56 expression in the developing pancreas. However, the human GPR56 locus has 17 transcriptional start sites. In muscle cells and haematopoietic stem cells these sites are targets for transcription factors such as peroxisome proliferator-activated receptor gamma co-activator 1-alpha 4 (PGC-1α4) and heptad complex respectively (White et al., 2014; Solaimani Kartalaei et al., 2015). Although the instructive signals that initiate the expression of GPR56 in the developing pancreas are not known, transcription factors are likely to be involved, as Hobit, a homolog of blimp-1 in T cells, induces GPR56 expression in cytotoxic lymphocytes (Saito et al., 2013). This is further supported by the expression of GPR56 in $NGN3^{+}$ cells in the pancreas, since NGN3 is a transcription factor necessary for the specification of endocrine cells. However, further experiment is required to determine whether NGN3 modulates the expression of GPR56 or not.

The pancreas is largely made up of exocrine cells that secrete digestive enzymes into pancreatic ducts, with a minority of endocrine cells, comprising mainly α-, β-, and δ-cells, which secrete glucagon, insulin and somatostatin respectively. Genetic tracing has revealed that exocrine and endocrine cells have the same origin and arise from multipotent progenitor cells (Gu et al., 2002). What governs the choice of progenitor cells to either become endocrine or exocrine is not completely understood, but transcription factors belonging to the basic-helix-loop family such as Ptf1a and Nkx6.1 have been implicated (Dong et al., 2008). Ptf1a is expressed in both exocrine and endocrine precursor cells. Downregulation of Ptf1a favours the conversion of pancreatic progenitors to an endocrine fate and vice versa (Dong et al., 2008). Given that GPR56 is strongly expressed in MPCs, and during lineage decision, cells with stronger expression follow the endocrine and ductal routes. In contrast, since it is downregulated in those cells that become acinar cells, GPR56 may be a novel contributor to the cell fate mechanism. Figure 3-21 shows a schematic that incorporates the data generated in this chapter to demonstrate the possible role for GPR56 in pancreas development.

Mouse embryos at developmental stages before E11 were not available for the studies described here, so the earliest time point that was investigated was E11. GPR56 was detected in the pancreas at this early stage of development. It was strongly expressed by all the cells in the pancreatic primordium, suggesting that it is expressed in pancreatic progenitors. The

function of GPR56 at this stage would be to keep the undifferentiated cells in a proliferative state, thereby maintaining a pool of progenitor cells. This is further supported by its coexpression with SOX9, a crucial transcription factor necessary for promoting proliferation and survival of progenitor cells and whose absence in mice leads to pancreatic hypoplasia (Seymour et al., 2007). During cell fate decision, most of the MPCs at the trunk region that later differentiate to form endocrine and ductal cells (Romer and Sussel, 2015) retained stronger GPR56 expression while those at the tip region, which later form the exocrine acini, showed progressive downregulation of GPR56 expression.

As the mouse matures, islet cells migrate from the epithelium to form clusters and they do not resemble adult islet structure until E18.5 (Bader et al., 2016; Villasenor et al., 2008). Figure 3-22 shows a schematic of GPR56 expression at different stages of pancreas development in the mouse, based on the data generated in this chapter. During the period of differentiation and migration, GPR56 expression is reduced implying that GPR56 inhibits endocrine cell differentiation and migration. The increased number of $NGN3^{+}$ cells in E16 pancreases from GPR56 KO mice further supports this, suggesting that in the absence of GPR56 there is reduced differentiation of these progenitor cells into β-cells. This inhibitory role is consistent with its function in preventing the differentiation of oligodendrocyte precursor cells in the brain (Giera et al., 2015). In the developing forebrain, GPR56 inhibits the migration of neural progenitor cells (Iguchi et al., 2008) and any defects in this process leads to cortical malformation (Li et al., 2008). GPR56 may therefore play a role in allowing islet cells to migrate to form the three dimensional architecture as its expression is repressed during this process. Further work in which GPR56 is specifically deleted in β-cell, will be required to confirm this regulatory role of GPR56 in islet development.

After the islets have formed, GPR56 expression was upregulated, coinciding with the phase where β-cells proliferate to increase islet mass. GPR56 was expressed exclusively by the β-cells in islets, so it may be involved in regulating β-cell proliferation and islet mass. In addition, the expression of GPR56 postnatally in ductal cells is particularly intriguing, as ductal epithelium has long been speculated to be a reservoir for pancreatic progenitor cells, which may be activated to replenish lost β-cells in T2D (Sharma et al, 1999). Although adult β-cells have

diminished capacity to replicate, there are mounting evidences to support the existence of progenitor cells in ductal epithelium that can transdifferentiate to β-cells. Following pancreatic injury or ligation, insulin$^+$ cells were identified in ductal tissues, indicating that β-cells may be formed from pre-existing ductal cells (Bonner-Weir et al., 2010). In human pancreas, insulin$^+$ and glucagon$^+$ cells have been reported in pancreatic ducts (Carpino et al., 2016) while obesity and T2D were found to increase ductal cell proliferation and the number of insulin$^+$ cells in ductal epithelium (Butler et al., 2010). However, β-cell neogenesis from the pancreatic duct is a subject of on-going debate as other groups have failed to identify other sources of new β-cells apart from replication of pre-existing β-cells (Teta et al., 2007; Dor et al., 2004).

Although a lot is known about transcription factors regulating islet differentiation and development, the signals that activate these processes are not clearly understood. It is thought that extracellular matrix components provide cues for cells to migrate during organ development (Langenhan et al., 2016) and they regulate branching morphogenesis during pancreas development (Shih et al., 2016). The detection of collagen III, a component of the basement membrane and the agonist of GPR56, and other GPR56 binding partners within the islet environment suggest that GPR56 may be activated in a paracrine manner to regulate pancreas development and islet functions. Whether this is true or not will be investigated in the following chapters.

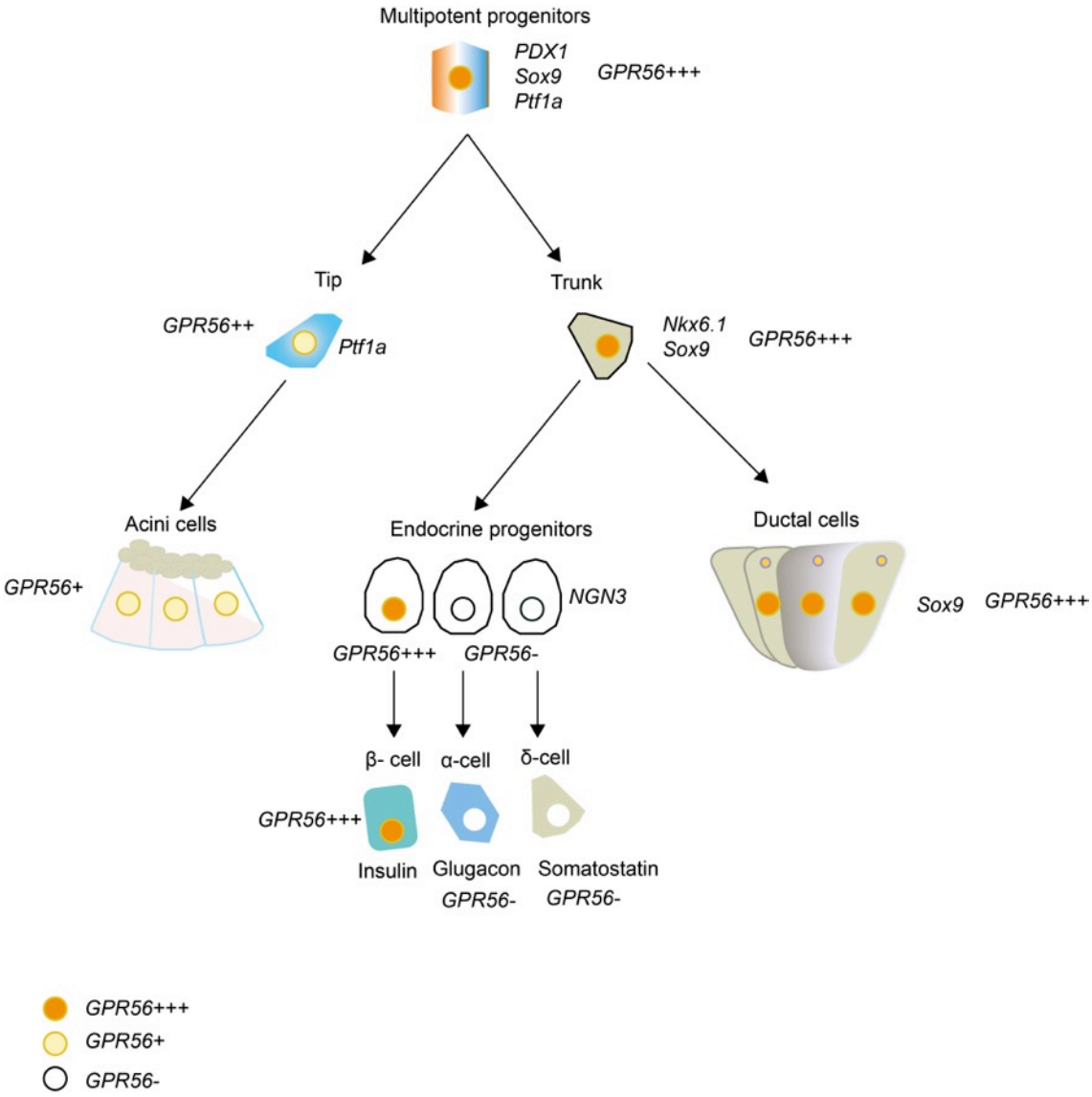

Figure 3-21 A schematic showing the expression of GPR56 in pancreas development during lineage decisions. Between E9 and E12.5, transcription factors such as Pdx1, Sox9 and Ptf1a mark pancreas identity and they maintain the expansion of multipotent progenitor cells (MPC). During this period, GPR56 is strongly expressed. As the MPCs decide their fate, GPR56 is strongly expressed by those progenitors at the trunk region that later form ductal and endocrine cells while it is progressively downregulated in the progenitors present in the tip region, that form the acini cells. As $NGN3^{+}$ endocrine progenitors are unipotent cells, the progenitors that are strongly positive for GPR56 differentiate to form β-cells, while $NGN3^{+}$ cells that are negative for GPR56 form the α and δ-cells. GPR56+++ = strongly positive for GPR56, GPR56+ = GPR56 expression is downregulated, GPR56- = GPR56 is not expressed.

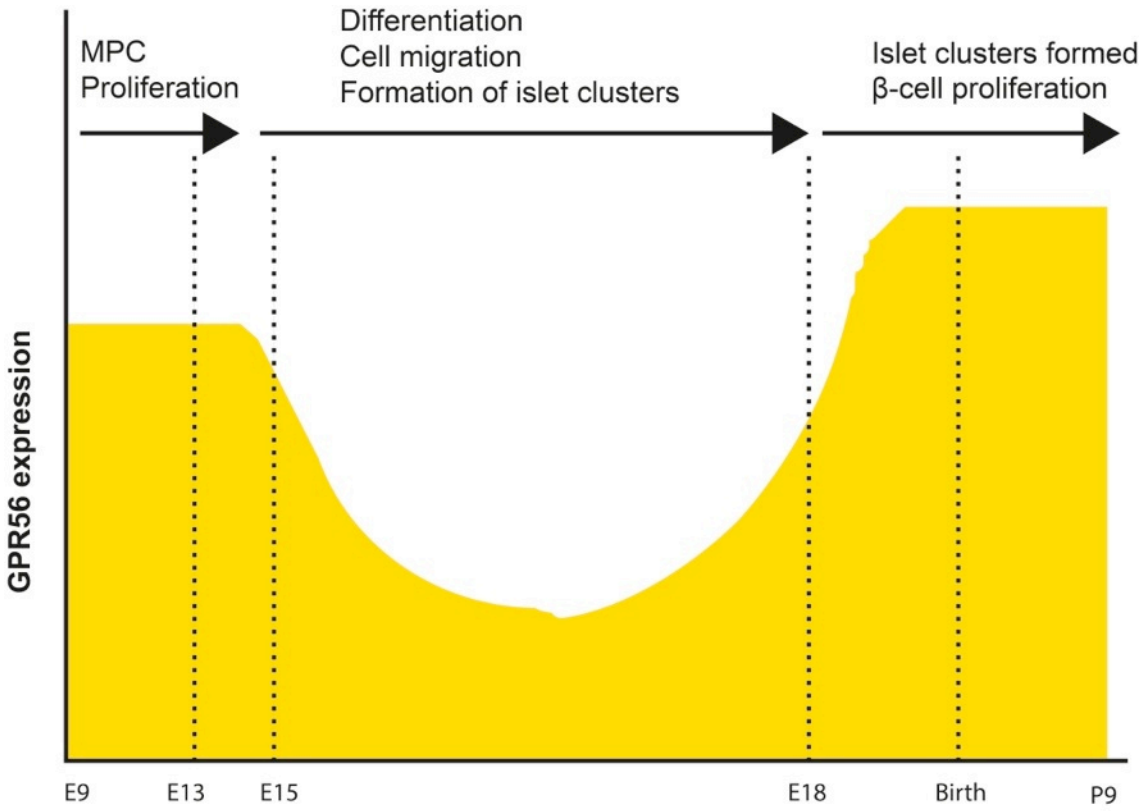

Figure 3-22 Expression pattern of GPR56 at different stages of pancreas development. This schematic is based on the immunohistochemical staining of embryonic mouse pancreas depicted in Figures 3-6-3-14. During the phase that marks the extensive proliferation of multipotent progenitor cells (MPCs) before E15, GPR56 is strongly expressed, while it is downregulated as the cells differentiate and migrate to form islet clusters. After the islet clusters are formed, GPR56 expression is upregulated, coinciding with the phase where β-cell proliferation occurs. The shaded area represents GPR56 expression.

Chapter 4

Chapter 4 The in vivo functions of GPR56 in glucose homeostasis, islet vascularisation and innervation

4.1 Introduction

Glucose homeostasis is a tightly controlled process in which blood glucose concentration is maintained within a normal range of 4-7mM. This is mainly achieved by feedback communication between islets and insulin-sensitive tissues. Following nutrient ingestion, β-cells are stimulated to release insulin, which facilitates glucose uptake into skeletal muscles and adipocytes and inhibits gluconeogenesis by the liver (Kahn et al., 2014). Information from the liver, skeletal muscles and fat on the other hand, either positively or negatively regulates the amount of insulin released from the β-cells, depending on blood glucose concentration. Thus, if insulin resistance is present, as is the case in obesity, insulin output is increased to maintain normal glucose levels. The critical role played by the β-cells in the pathophysiology of diabetes is underscored by the observation that insulin resistance alone is not sufficient to cause T2D due to β-cell compensatory mechanisms of increased insulin secretion and increased β-cell mass (Ahrén, 2009). Failure of the β-cells to respond appropriately to increased insulin demand will mean that glucose concentration will continue to increase and this will culminate in uncontrolled hyperglycaemia and T2D.

With the increasing rise in the incidence of T2D and the failure of the current therapies to prevent the progressive decline in β-cell function, several new treatment approaches are being developed. The aim of these novel therapies is to reduce hyperglycaemia and thus minimise the long-term microvascular and macrovascular complications. G-protein coupled receptors (GPCRs) are known to bind with high affinity to small molecules and are therefore attractive targets for drug development, and one of the recently implemented clinical therapies activates GLP-1R (Doyle and Egan, 2007). In addition, molecules targeting GPR40 and GPR119 are presently in clinical trials (Burant, 2013; Ritter et al., 2016). Interestingly, human islets express over 200 non-odorant GPCRs (Amisten et al., 2013), the majority of whose functions are yet to

be established, indicating that an increased understanding of these receptors may lead to the discovery of new treatments for diabetes.

The GPCR under investigation in this thesis, GPR56, may be involved in metabolic processes, as it is highly expressed in the hypothalamus and cerebral cortex (Piao et al., 2004; Haitina et al., 2008) – regions of the brain involved in regulating energy homeostasis and eating behaviour. It has been identified that outside the CNS, GPR56 expression was highest in mouse pancreas (Haitina et al., 2008), which fits with observations that this is the most abundant GPCR in islets (Amisten et al., 2013). Islets and hypothalamus are tightly connected by the neuro-entero-islet axis and there is evidence for direct involvement of hypothalamic neurons in modulating glucose-stimulated insulin secretion (GSIS) (Parton et al., 2007; Osundiji et al., 2012). GPR56 is exclusively expressed by the β-cells of mouse and human islets, as described in Chapter 3. It is coupled to the Gq subunit (Little et al., 2004), a protein that activates phospholipase C-mediated hydrolysis of phosphatidyl inositol bisphosphate (PIP_2) and increased insulin secretion (Jones and Persaud, 2010). More recently, it has been suggested that GPR56 also activates the cAMP/PKA pathway in β-cells (Dunér et al., 2016), although this signal transduction coupling has not been identified in other cells types.

In additional to neural regulation of β-cell function, blood vessels, which supply islets with oxygen and nutrients and distribute hormones secreted by the pancreas, also act as modulators of insulin secretion. During embryogenesis, endocrine cells lie in close proximity to blood vessels and the development of a properly vascularised islet is dependent on interactions between the islet cells and vascular endothelial cells (Lammert et al., 2003). In the early post natal phase of islet development, the characteristic rapid growth in islet mass has been associated with increased vascular density and a surge in the proliferation of vascular endothelial cells (Johansson et al., 2006). To further highlight the importance of the vascular bed in islet functions, abnormalities in islet perfusion have been observed in rodent models of diabetes mellitus (Iwase et al., 2002; Svensson et al., 2005).

Adhesion GPCRs are thought to be important in blood vessel formation. Thirteen members of this class of GPCRs, including GPR56, have been identified as being enriched in vascular

endothelium (Nolan et al., 2013), suggesting that they may play a role in endothelial cell functions. Notable among them is GPR124, which has been associated with embryonic death in endothelial-specific GPR124 null mice due to vascular malformations (Kuhnert et al., 2010). Adhesion GPCRs are important in cell migration, and the angiogenesis arrest seen in GPR124 KO mice was due to deficiency in the migratory capabilities of the developing endothelial cells. As GPR56 is highly expressed in islets, it is hypothesised that it may contribute to the development of islet vasculature, which may be important in appropriate regulation of glucose homeostasis.

In this chapter, the effect of GPR56 deletion on glucose homeostasis in mice was explored. The islet architecture, innervation and vascularisation in GPR56 KO mice and also in mice in which both GPR56 and one of its binding partners, transglutaminase 2 (TG2), had been deleted were also examined.

4.2 Aims

- Determine whether deletion of GPR56 has any effect on glucose homeostasis, insulin secretion and insulin content of mouse islets.
- Investigate whether GPR56 contributes to islet innervation and islet blood vessel development.

4.3 Methods

4.3.1 Mice

Mouse studies were performed during my research secondments to Dr Xianhua Piao's lab in the Division of Newborn Medicine, Boston and were carried out according to the guidelines of the Animal Use and Care Committee of Boston Children's Hospital. Adult male and female GPR56 WT and KO mice were bred and genotyped as described in Section 2.9.2.1. GPR56 strain was maintained by Het X Het breeding and WT littermates were used as controls. In some of the experiments, pancreases from GPR56/TG2 double KO mice and WT littermates were used.

4.3.2 Insulin secretion and insulin content quantification

Islets were isolated from GPR56 KO and WT mice (Section 2.2.1) and incubated in the presence of buffers supplemented with either 2mM or 20mM glucose for 1 h at 37^0C. For the dynamic insulin secretion experiments, groups of 40 islets were initially perifused in the presence of 2mM glucose for 1 h in a temperature-controlled perifusion chamber. Perifusates were collected every 2 min for the next 10 min in physiological salt solution containing 2mM glucose, with a further 20 min in physiological buffer containing 20mM glucose. Insulin secretion in the static incubation and perifusion experiments was quantified by radioimmunoassay. To measure insulin content, groups of 10 size-matched islets were incubated in 200µl of acidified ethanol at -20°C until insulin was quantified by radioimmunoassay.

4.3.3 Glucose tolerance test

Glucose tolerance was measured in mice that had been fasted overnight for 16 hours by the intraperitoneal administration of 2 g glucose/kg body weight. Plasma glucose levels were measured prior to glucose administration and at 15, 30, 60, 90 and 120 min post injection using a glucometer.

4.3.4 Immunohistochemistry

Freshly retrieved mouse pancreases were fixed in 4% paraformaldehyde overnight before being cryoprotected in OCT medium and frozen. Immunohistochemistry was carried out on 10µm sections with antibodies directed against GPR56, insulin, glucagon, TUJ1 (marker for neuronal

cells) or CD31 (endothelial cell marker) (Table 2-15). Each section was incubated with primary antibodies overnight after antigen retrieval was carried out in citrate buffer. For rat monoclonal CD31, antigen retrieval was not carried out since sections treated in citrate buffer prior to immunostaining were negative for CD31 signals, perhaps indicative of citrate-induced endothelial cell loss. Following incubation with fluorophore-coupled secondary antibodies, nuclei were stained with DAPI and images were acquired using a Nikon TE2000 or Nikon Eclipse Ti microscopes.

4.3.5 Histomorphometrical analysis

8-bit RGB photomicrographs of the immunostained pancreas sections, obtained from Nikon TE2000 or Nikon Eclipse Ti microscopes, were scored blindly before quantification. The total area of insulin staining, interpreted as islet area, was determined with Image J software. The total area of TUJ1 or CD31 staining within insulin+ islets was also quantified morphometrically in pancreas sections using Image J software and interpreted as islet nerve area and islet vascular area, respectively.

4.4 Results

4.4.1 Confirmation of GPR56 gene knockout

GPR56 KO mice were generated in Boston by targeted deletion of exons 2 and 3, producing a whole body knockout model. The genotypes of the mice were determined by PCR, carried out on genomic DNA extracted from the tails (Section 2.9.2). The primers were designed such that amplification of a 639bp product indicated WT mice. In the KO model, exons 2 and 3, which are 270bp long, were deleted, thus, amplification of a 369bp amplicon indicated KO mice, while in the heterozygous mice both 639bp and 369bp products were amplified (Figure 4-1 A). To confirm that the GPR56 gene was deleted in the pancreas, immunohistochemistry was carried out on 10μm fixed-frozen, adult mouse pancreas sections using a previously validated GPR56 antibody (Luo et al., 2011). Consistent with the data shown in Figure 3.3, GPR56 was detected in the pancreas of WT mice, where it colocalised with insulin produced by the β-cells (Figure 4-1 B, C & D). As expected, GPR56 was not detected in the KO pancreas sections (Figure 4-1 E, F & G), indicating that GPR56 protein was deleted in the pancreas by the knockout strategy.

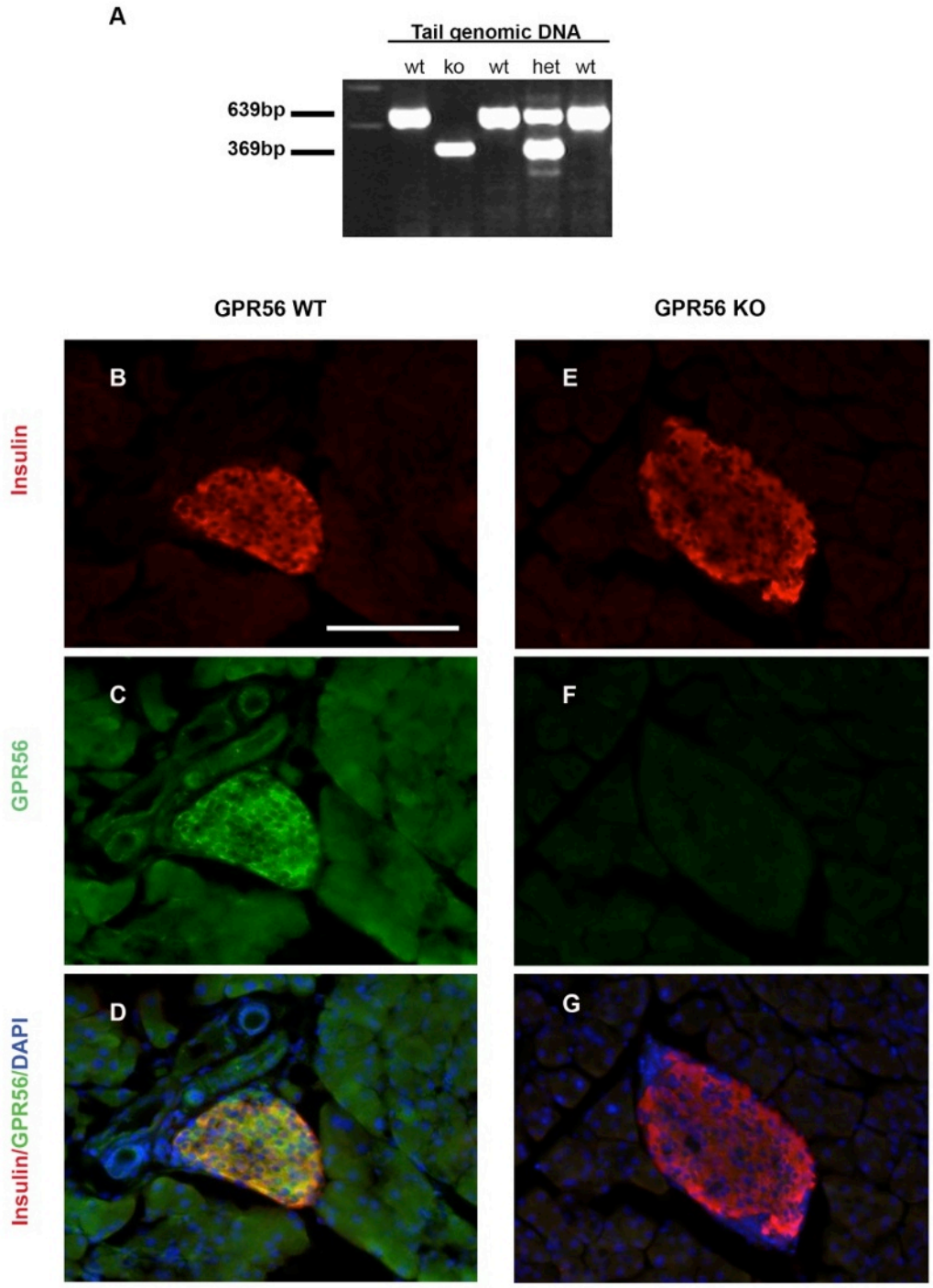

Figure 4-1 Confirmation of GPR56 gene knockout. A) Tail genomic DNA was subjected to PCR and resolved on a 1.5% agarose gel containing ethidium bromide. DNA was revealed under UV light. A 639bp product indicated WT mice, a 369bp product represented KO mice and the presence of both products is indicative of heterozygous mice. B – D) Representative images of pancreases from adult GPR56 WT mice showing the expression of GPR56 and its colocalisation with insulin. E – G) Representative images showing that GPR56 was not detected in pancreases from GPR56 KO mice. Scale bar = 50μm.

4.4.2 GPR56 KO islets have higher number of α-cells and less β-cells

To determine whether the decreased differentiation of endocrine progenitors observed following GPR56 deletion, as reported in Chapter 3, had any effect on the number of terminally differentiated islet cells, wax-embedded pancreas sections from P9 WT and GPR56 KO mice were immunostained for insulin and glucagon. The number of insulin$^+$ and glucagon$^+$ cells per islet was counted manually. There were no striking morphological differences in pancreas cytoarchitecture between GPR56 WT and KO mice (Figure 4-2A-D). However, GPR56 KO mice have less β-cells (% β-cells/islet; WT: 68.5±0.8, KO: 54.8±3.0, n=3 mice/genotype, $p<0.05$), but higher numbers of α-cells in KO islets (% α-cells/islet; WT: 17.7±0.9, KO: 33.7±2.8, n=3 mice/genotype, $p<0.01$) (Figure 4-2 E & F).

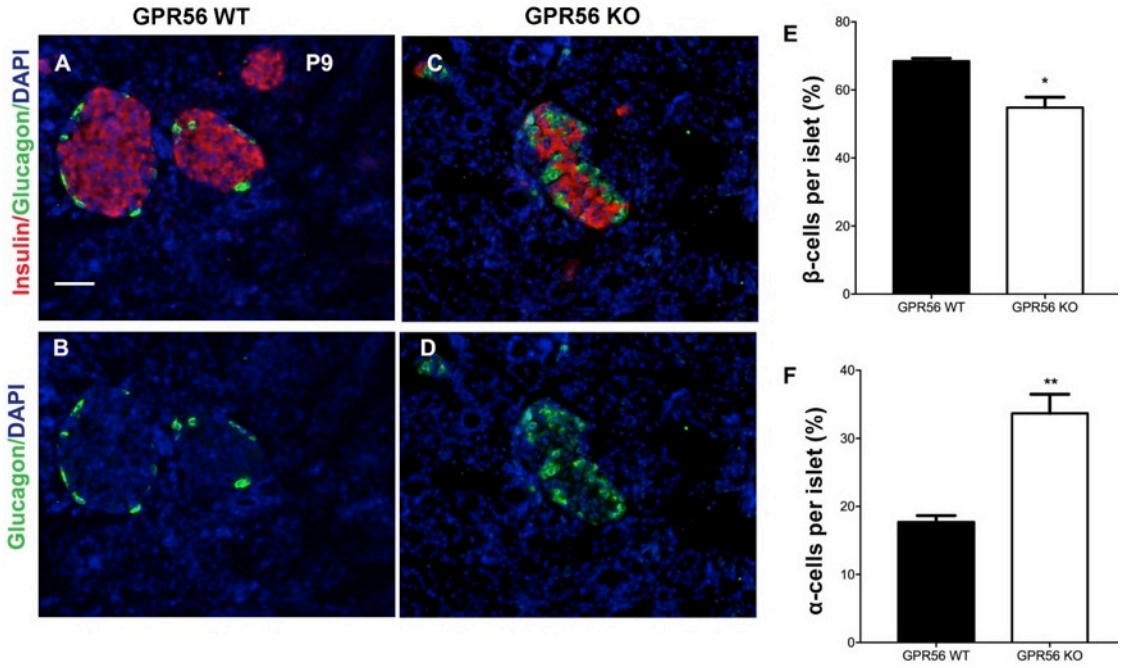

Figure 4-2 Effect of GPR56 deletion on the number of β- and α-cells per islet in P9 mice. Wax-embedded pancreas sections of A-B) GPR56 WT mice and C-D) GPR56 KO mice were immunoprobed for insulin and glucagon and the number of β-cells and α-cells were counted. Scale bar = 50μm E) Percentage insulin$^+$ β-cells per islet in GPR56 WT and KO pancreas were shown. Data are expressed as Mean + SEM, n=3 mice/genotype, *$p<0.05$, Student's t-test. F) The percentage of α-cells obtained from the number of glucagon$^+$ cells per islet in GPR56 WT and KO pancreas were shown. Data are expressed as Mean + SEM, n=3 mice/genotype, **$p<0.01$, Student's t-test.

4.4.3 GPR56 KO mice have normal body weight and fasting glucose levels

GPR56 KO and WT mice were maintained on a normal diet and measurement of body weight at 8 weeks indicated that both genotypes were the same weight. This demonstrates that GPR56 does not play a role in regulation of total body mass when mice were fed a standard diet (Figure 4-3 A). To determine whether there were alterations in glucose metabolism upon GPR56 deletion, plasma glucose levels were measured immediately before and after the mice were fasted overnight. Similar to the lack of differences in body weight, glucose levels of WT mice were not significantly different from those quantified in the KO mice during the fasting conditions (Figure 4-3 B).

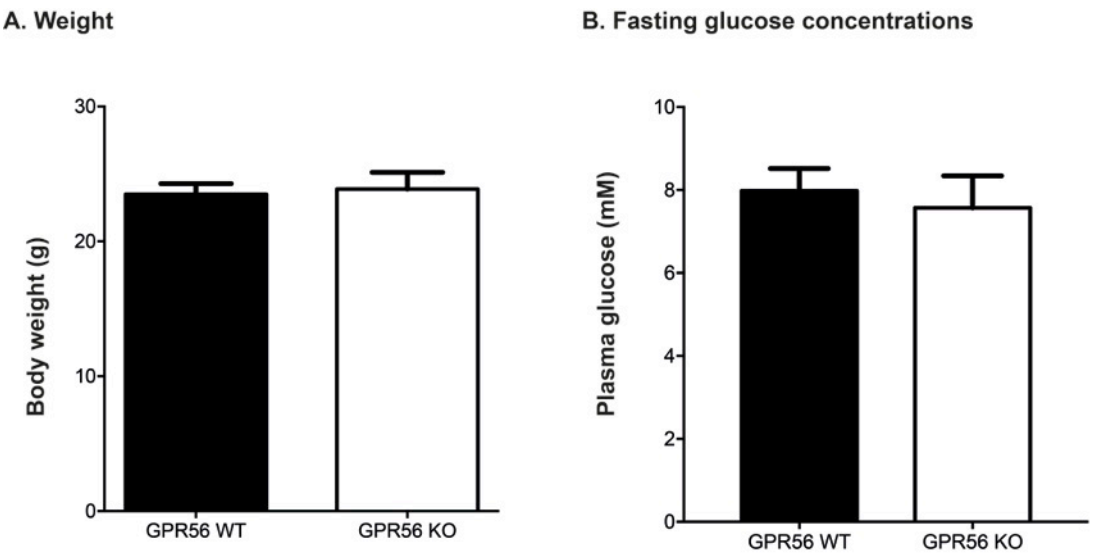

Figure 4-3 GPR56 KO mice have similar body weight and plasma glucose concentrations to WT mice. A) Total body weight of 8-week-old WT and KO mice. Data are represented as mean + SEM of 7 WT and 8 KO mice. B) Plasma glucose concentrations were measured after an overnight fast. The means + SEM from 6 animals/genotype are shown, $p>0.2$, unpaired Student's t-test.

4.4.4 GPR56 mice are mildly glucose intolerant

To further evaluate the role of GPR56 in glucose metabolism, male and female GPR56 WT and KO mice were injected IP with 2g/kg glucose, and plasma glucose concentrations were measured at 0, 15, 30, 60, 90 and 120 min post injection. In the male mice, there was a slight, but not statistically significant, increase in glucose concentration in the KO mice at all the time points measured after glucose administration (Figure 4-4 A), but there were no genotype-dependent differences when the area under the curve (AUC) for the entire 120 min was evaluated (Figure 4-4 B). The trend of modest glucose intolerance was also observed in female mice (Figure 4-4 C), and there was a sharp decline in the glucose concentration at 30 min post injection in both female WT and KO mice that was not seen in the males (Figure 4-4 C). In addition, at 30 min post glucose injection there was a statistically significant increase ($p<0.01$) in glucose concentration in the female KO mice, suggesting that there may be gender-specific differences in glucose handling when the GPR56 gene is deleted as this was not observed for male mice. However, as for the observations made with the male mice, AUC measurements indicated that there were no genotype-specific differences in glucose tolerance (Figure 4-4 D).

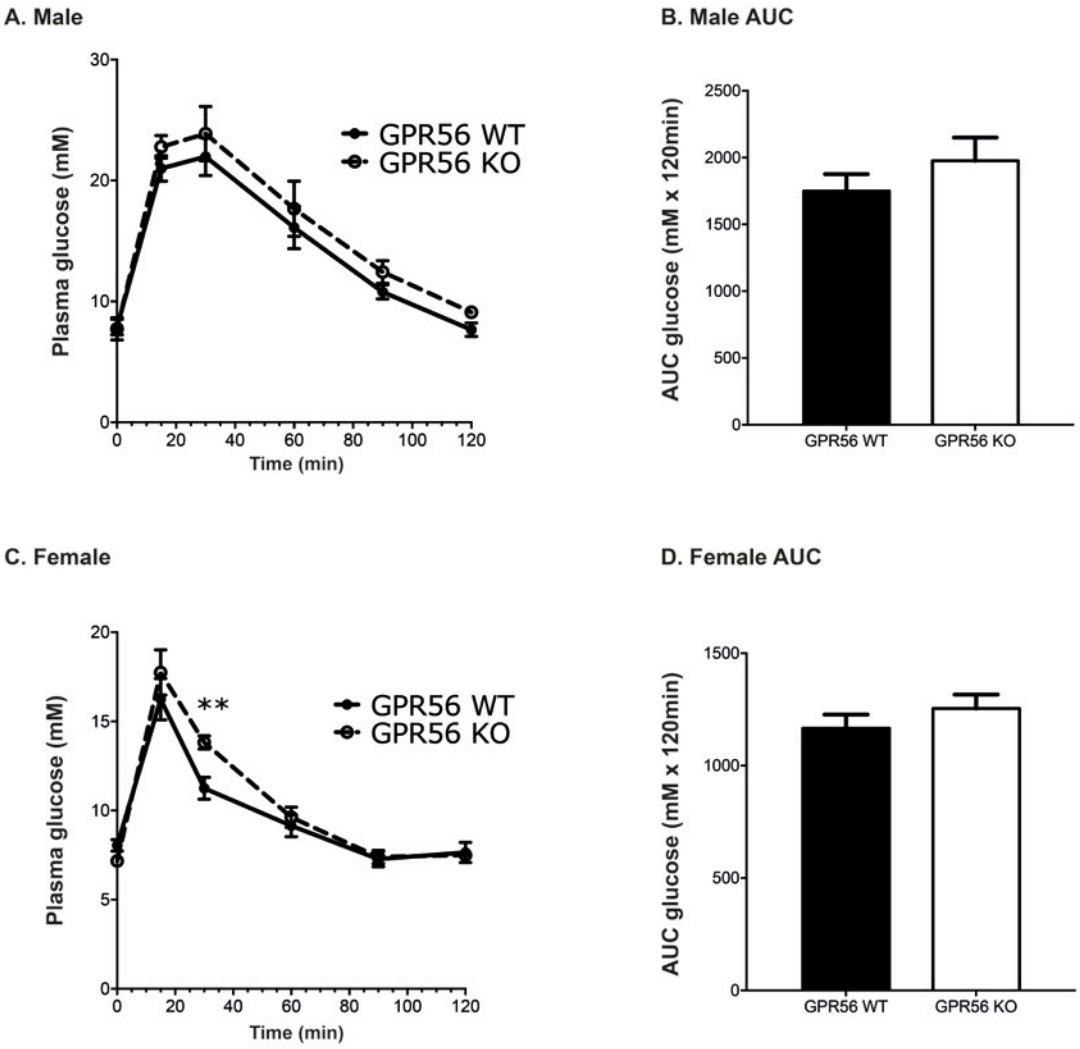

Figure 4-4 Glucose tolerance of male and female GPR56 KO mice. 2g/kg glucose was administered to overnight fasted (16h) mice at 8 weeks old. A) Glucose concentrations were measured at time 0, 15, 30, 60, 90 and 120 min post glucose injection in male mice and B) area under the curve (AUC) was determined. C) Plasma glucose of female mice was also determined at the indicated time points. D) AUC was calculated from the glucose tolerance curve for the female mice. Data are mean ± SEM, n=5 male mice and 4 female mice per genotype, **p<0.01, Two-way ANOVA with repeated measurements.

4.4.5 GPR56 KO islets respond appropriately to glucose

Islets isolated from age-matched GPR56 WT and KO mice were matched for size, incubated in medium supplemented with either 2mM or 20mM glucose for 1hr at 37^0C and insulin secretion was quantified by radioimmunoassay. As shown in Figure 4-5 A (dark bars), there was a 5-fold increase in insulin secretion when GPR56 WT islets were exposed to medium supplemented with 20mM glucose and a similar magnitude of glucose-induced insulin secretion was observed from islets isolated from GPR56 KO mice (Figure 4-5 A, white bars). Insulin content of isolated islets was determined by acidified ethanol extraction, which indicated that there was no significant difference in the amount of insulin per islet following GPR56 deletion (Figure 4-5 B).

To investigate the dynamics of insulin secretion following GPR56 deletion, groups of 40 islets per genotype were continuously perifused at a constant temperature of 37^0C, simulating normal physiological conditions. After perifusing the islets in medium containing 2mM glucose for 1h, perifusates were collected every 2 min for 10 min in medium containing 2mM glucose and the next 20 min in buffer supplemented with 20mM glucose. In medium containing 2mM glucose, insulin secretion from WT islets was between 2-5pg/islet/min, which was not significantly different from the KO islets. Both WT and KO islets responded similarly when challenged with buffer containing 20mM glucose, with peak insulin secretion at 6 - 8 min after exposure to high glucose. The initial rapid initiation of insulin secretion followed by a period of sustained release was not statistically different in both WT and KO islets (Figure 4-6 A – C).

A. Insulin secretion

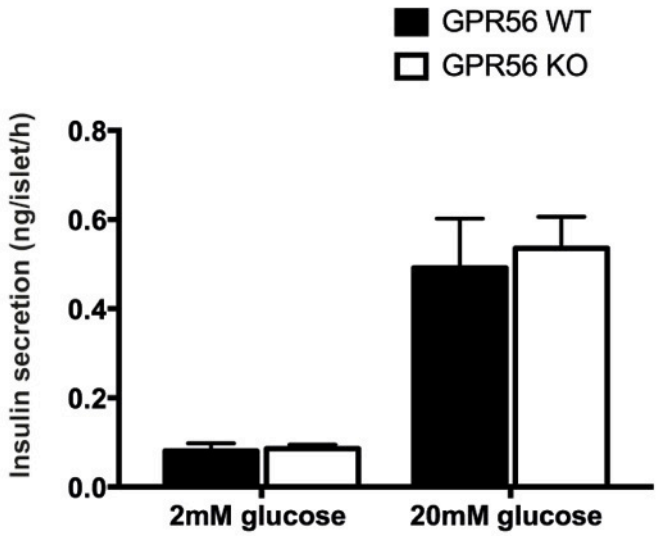

B. Insulin content

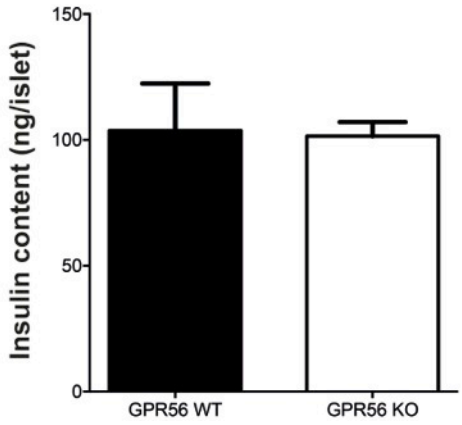

Figure 4-5 Islets isolated from GPR56 KO mice responded similarly to a glucose challenge and have similar insulin content as islets from WT mice. A) Isolated islets from GPR56 WT and KO mice were incubated in buffer supplemented with either 2mM or 20mM glucose for 1 h at 37^0C and insulin secretion was quantified by radioimmunoassay. Data are mean + SEM, n=8, representing three independent experiments. B) Islets were matched for size and incubated overnight in acidified ethanol before being briefly sonicated and insulin content was determined by radioimmunoassay. Data are mean + SEM, n=3 batches of 10 islets pooled from 5 mice/genotype, $p>0.2$, Student's t-test.

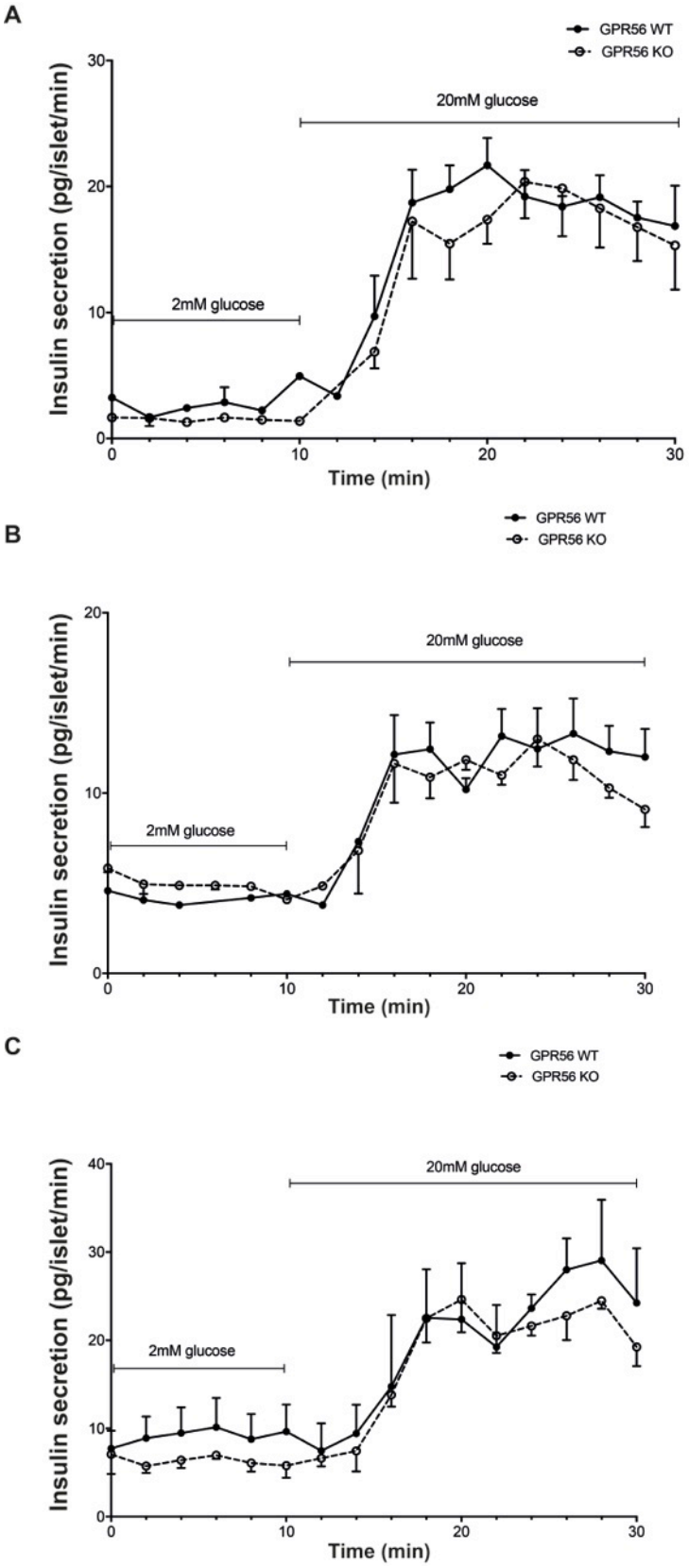

Figure 4-6 Insulin secretory kinetics of islets from GPR56 mice. A – C) Isolated islets were continuously perifused with buffer solution at 37°C in a temperature-controlled chamber. Data from three independent experiments show that GPR56 deletion has no significant effect (AUC, $p>0.2$) on dynamic glucose-induced

insulin secretion. Data are means + or – SEM, n=3-4 separate chambers, each containing 40 islets pooled from 5 animals/genotype.

4.4.6 GPR56 is not required for islet vascularisation

Islets are able to adapt their vascular networks to cope with changes in metabolic demand, the failure of which may lead to impaired glucose homeostasis (Dai et al., 2013). The requirement of GPR56 for appropriate islet vascularisation was investigated by immunohistochemical staining of pancreas sections from neonatal WT and GPR56 KO mice. Islet capillaries were identified by fluorescently staining for the vascular endothelial cell marker, CD31. Any fluorescently labelled endothelial cell or endothelial cell cluster, that was clearly distinct from adjacent cells, was counted as a single blood vessel, according to the method described by Weidner and colleagues (Weidner, 1995). In both WT and GPR56 KO pancreases, it was observed that islets have a richer supply of blood vessels than the surrounding exocrine tissues, but there were no differences in islet capillary density between the WT and KO mice (Figure 4-7).

To better understand the vascular phenotype of GPR56 deletion in islets, mice in which both GPR56 and tissue transglutaminase 2 had been deleted were employed. Transglutaminase 2 was identified as a binding partner of GPR56 and together they regulate angiogenesis and tumour growth in cancer cells (Xu et al., 2006; Xu and Hynes, 2007). Immunohistochemistry was carried out on 10μm sections obtained from GRP56 WT/ TG2 KO and GPR56 KO/TG2 KO mice at P10 using insulin and CD31 antibodies. TG2 was deleted in both mouse strains; therefore any effect on the islet vasculature will not be due to contributions from TG2 signalling. Representative images revealed that islets are more highly vascularised than the surrounding acinar cells (Figure 4-8 A). Vascular parameters measured using Image J software revealed that there was no significant impact of GPR56 and TG2 deletion on the islet capillary density, represented by the number of blood vessels per islet, or on the area occupied by the blood vessels in each islet (Figure 4-8 B & C).

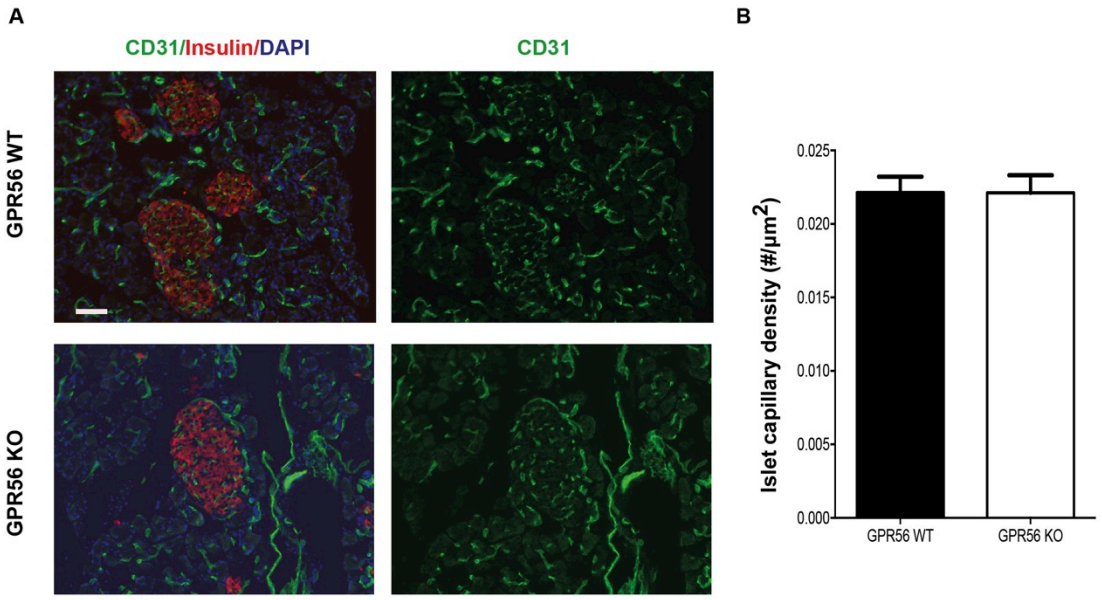

Figure 4-7 Representative fluorescent images of GPR56 WT and KO pancreases from P9 mice, showing the expression of insulin and CD31. Scale bar = 50µm. B) Islet capillary density was quantified by determining the number of CD31+ blood vessels within the insulin^{+} islet area in the WT and KO mice. Data are mean + SEM of n = 10 sections, p>0.2, Student's t-test.

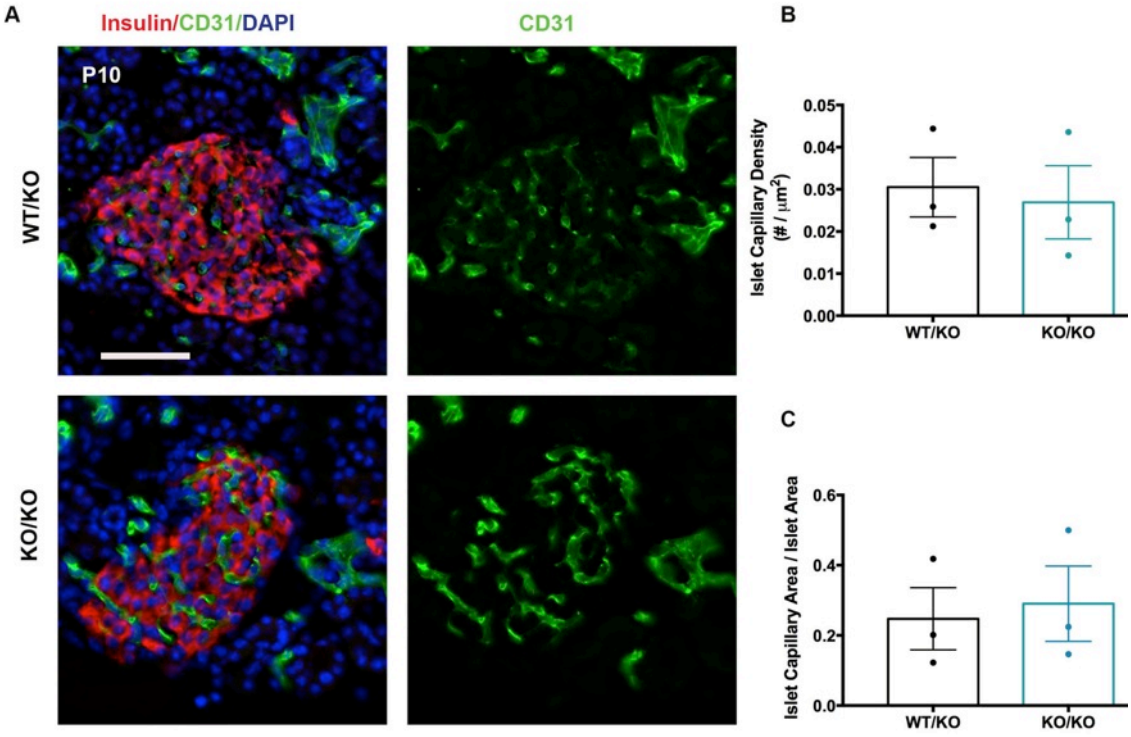

Figure 4-8 A) Representative fluorescent images of GPR56/TG2 WT/KO and KO/KO pancreases from P10 mice, showing the expression of insulin and CD31. B) Islet capillary density was quantified by determining the number of CD31^{+} blood vessels within the insulin^{+} islet area in the WT and KO mice. n = 3 mice per

genotype C) Quantification is shown for the area occupied by islet capillary vessels, as measured by the area of $CD31^+$ blood vessels per $insulin^+$ islet area. Data are represented as mean ± SEM, n = 3 mice per genotype, p>0.2, Student's t-test. Each dot represents a mouse with >30 islets/mouse counted. Scale bar = 50µm.

4.4.7 GPR56 is not required for islet innervation

To determine the effect of GPR56 on islet innervation, pancreases from GPR56 WT and GPR56 KO mice at E16 and P9 were immunostained for TUJ1, a neuron-specific structural protein present in axons. Neuronal axons were intensely fluorescent, confirming antibody specificity and tissue penetration (Figure 4-9 A & B). At E16 in GPR56 WT and GPR56 KO pancreases, TUJ1 positive nerve fibres were in close proximity to islets, with little or no staining in the exocrine cells (Figure 4-9 B & D). The pattern of innervation of islets in the pancreas sections from GPR56 KO mice was similar to that of the WT mice at both E16. Quantification of the total TUJ1 area in the pancreas revealed that there was no significant difference between GPR56 WT and GPR56 KO mice at either stage of development (Figure 4-9 E).

Islets were also strongly innervated in pancreases retrieved from both WT and GPR56 KO mice at P9. In the WT mice individual islets were surrounded by $TUJ1^+$ nerve endings and TUJ1 immunoreactivity was generally less prominent in the KO pancreas sections (Figure 4-10). However, analysis of multiple sections indicated that there was no significant difference in the percentage of TUJ1 positive area in the WT and KO pancreases (Figure 4-10). Few fine nerve fibres penetrated islets in both genotypes, but there was little evidence of colocalisation with $insulin^+$ cells. Similar to the observations made in pancreases obtained from P9 WT mice, peri-insular nerve endings appeared to be more pronounced around the islets in pancreas sections from P10 GPR56/TG2 WT/KO mice than in the KO/KO mice at P10 (Figure 4-11 A & B). The decrease in TUJ1 staining in pancreases from GPR56 null mice was not statistically significant (Figure 4-11 C), but the nerve fibre density in the KO/KO pancreases was increased by 34% (p=0.1).

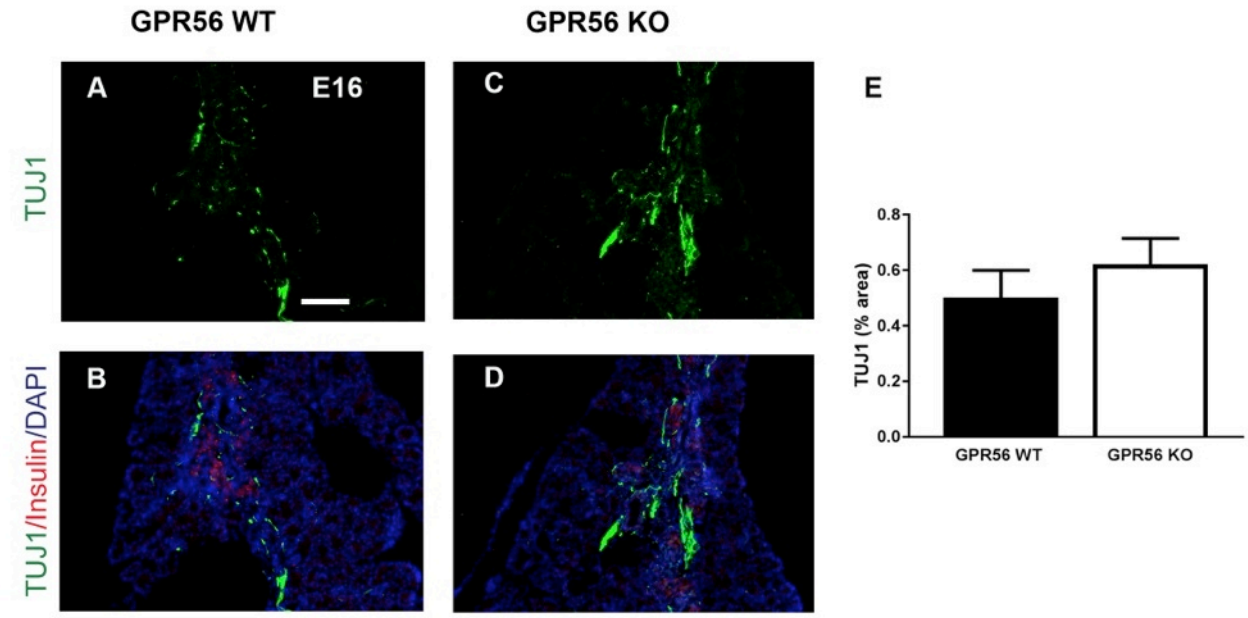

Figure 4-9 Detection of TUJ1 positive neurons in E16 pancreases. 10µm pancreas sections were immunoprobed for TUJ1 and insulin. A – B) Images show the expression of TUJ1 and insulin in a pancreas section from a WT mouse. C – D) Images show the expression of TUJ1 and insulin in GPR56 KO pancreases. E) Quantification of the area of $TUJ1^{+}$ neurons per field is shown. Data are mean + SEM of 10 sections from 1 mouse per genotype. Scale bar = 50µm.

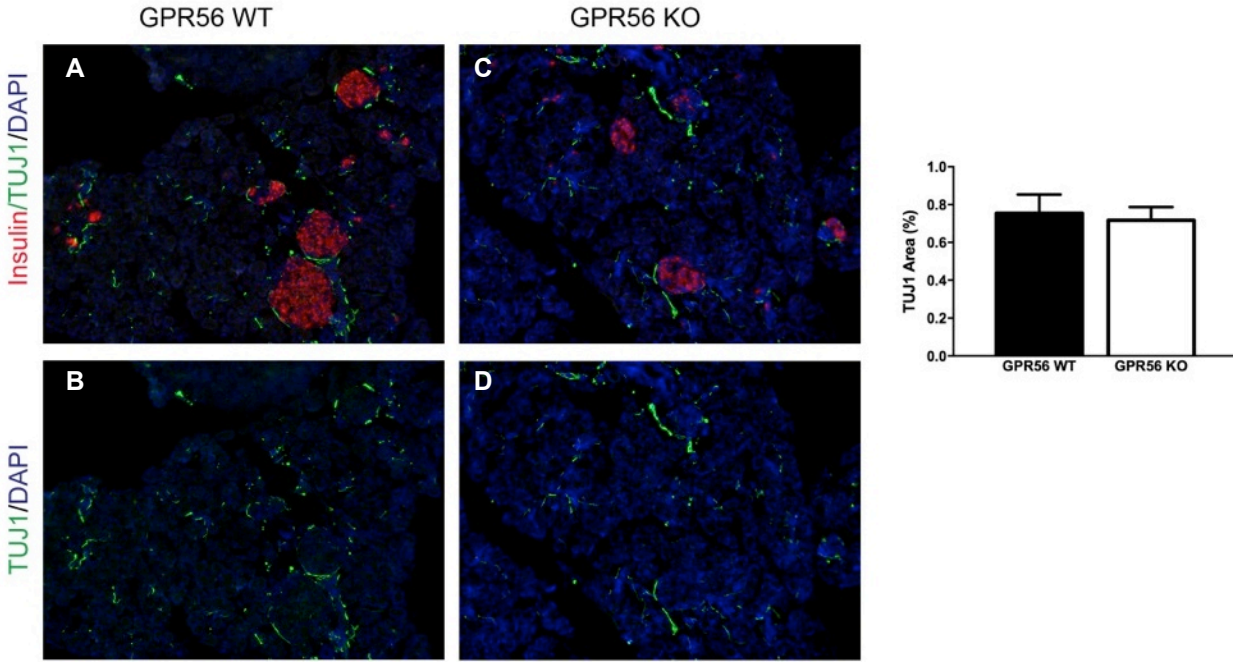

Figure 4-10 Representative images of GPR56 WT and KO pancreases showing expression of TUJ1 and insulin at P9. The graph shows quantification of $TUJ1^{+}$ neurons. There was no statistically significant

difference in the nerve area between the two genotypes (p>0.2, Student's t-test). Data are mean + SEM of n=3 mice per genotype, 10 sections per mouse.

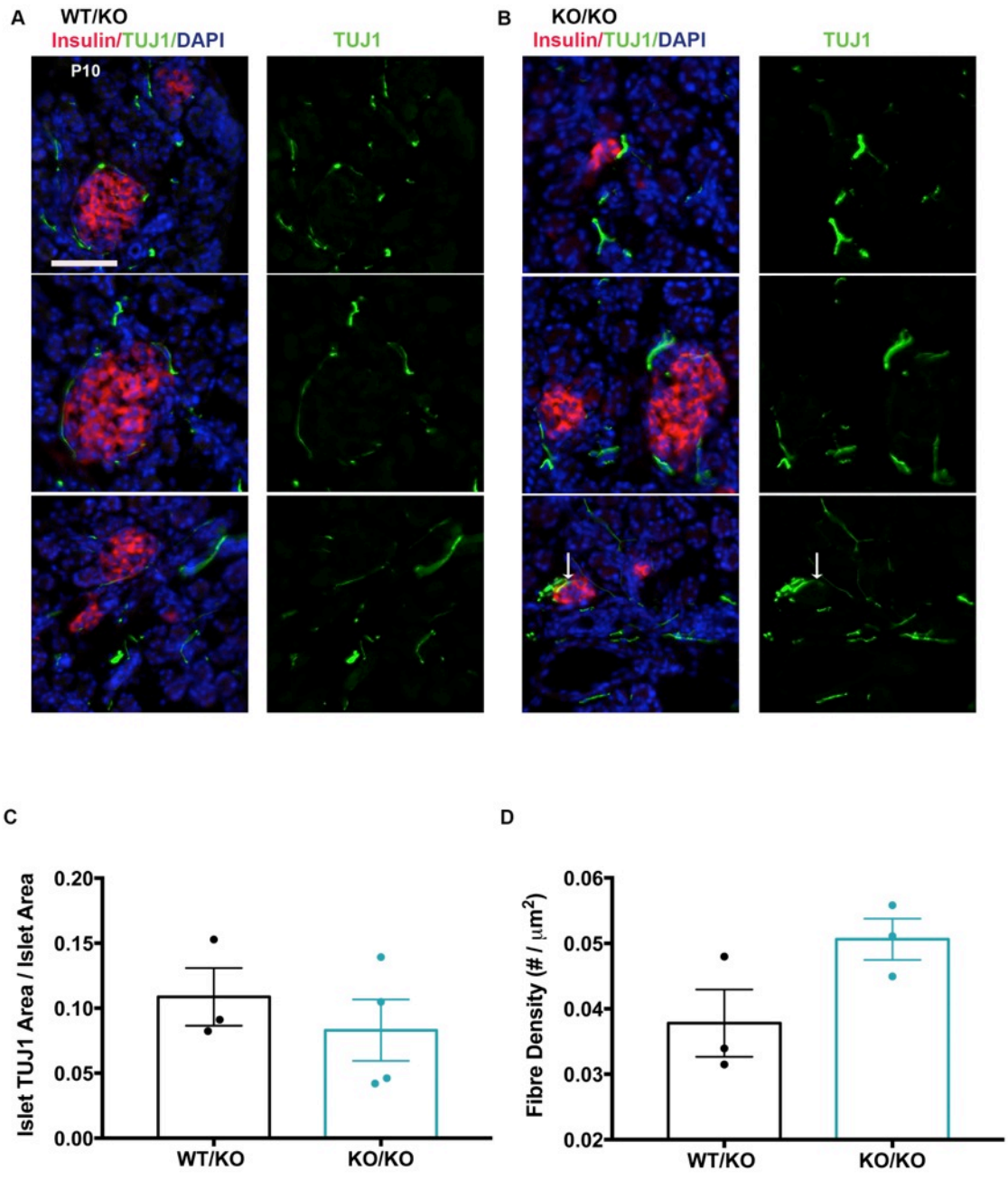

Figure 4-11 Representative fluorescent images of A) GPR56 WT/TG2 KO and B) GPR56 KO/TG2 KO pancreases at P10 showing the expression of insulin and TUJ1, a marker for nerve fibres. C) Quantification of the area occupied by the nerve fibre per islet area and D) nerve fibre densities in the WT/KO and KO/KO pancreases. Data are presented as mean ± S.E.M. Each dot represents a mouse, in which 6-10 sections were quantified, p>0.2, Student's t-test. Scale bar = 50μm.

4.4.8 GPR56 and peri-islet Schwann cells

Islets are surrounded by a peri-insular capsule that is made up of a thin layer of collagens, fibroblasts and peri-islet Schwann cells (Sunami et al., 2001; Tsui et al., 2008). The peri-islet Schwann cells (pSc), characterised by their proximity to neurons and the expression of glial markers such as glial fibrillary acidic protein (GFAP) and S100β, are among the first cells to be selectively destroyed in T1D associated autoimmunity (Winer et al., 2003). The functions of pSc in the pancreas are not yet known, but they may be similar to the physiological roles played by peripheral Schwann cells, which form tight mantle around tissues (Winer et al., 2003). To investigate whether deletion of GPR56 has any effect on the pSc, immunostaining was carried out on E16 pancreases for glial fibrillary acidic protein (GFAP). In both WT and KO pancreases, GFAP positive cells were seen mainly around islets or the endocrine trunk and there was less GFAP expression in the exocrine cells (Figure 4-12 A – D). Quantification of the area of $GFAP^+$ Schwann cells b Image J analysis indicated that there was no significant difference between genotypes (Figure 4-12 E).

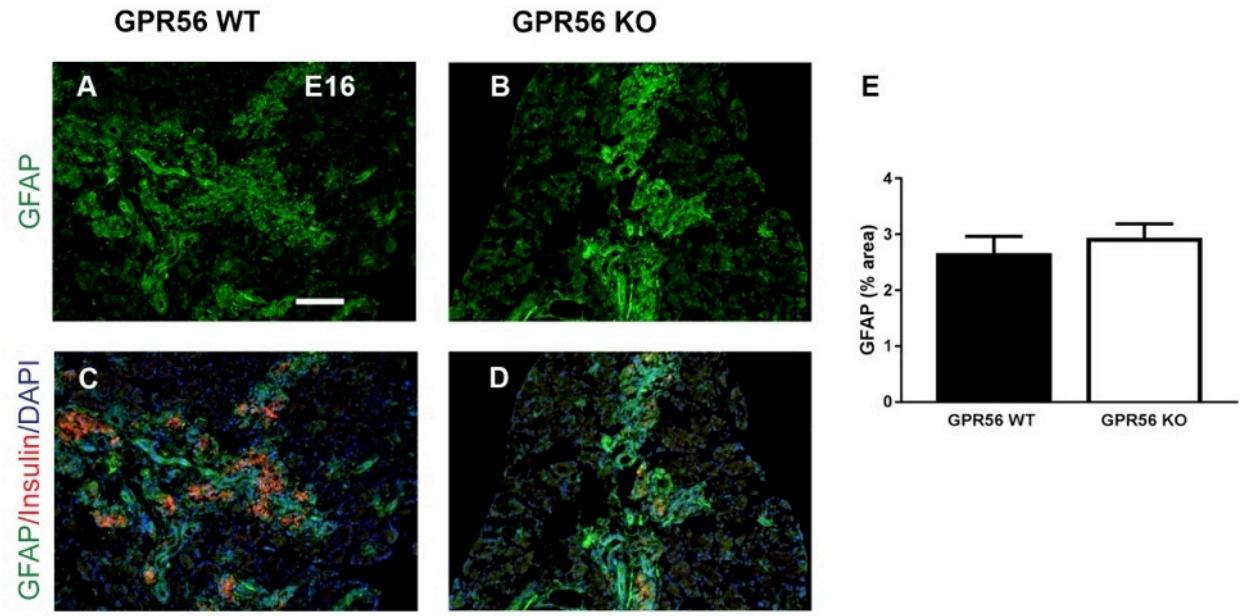

Figure 4-12 Expression of glial fibrillary acidic protein (GFAP) in GPR56 WT and KO pancreases. 10µm E16 mouse pancreas sections were immunoprobed for GFAP and insulin. A – C) Images show the expression of GFAP and insulin in GPR56WT pancreas. B– D) Images show the expression of GFAP and insulin in GPR56 KO pancreases. E) Quantification of the area of $GFAP^+$ peri-islet Schwann cells per field is shown. Data are mean + SEM of 10 sections from 1 mouse per genotype. Scale bar = 50µm.

4.5 Discussion

The data presented in this chapter demonstrate that deletion of GPR56 leads to less β-cells but higher numbers of α-cells in GPR56 KO islets. It was not possible to investigate the functional significance of the increased number of α-cells due to time constraints, but this is clearly an area of further research. For example, it is possible that there was dedifferentiation of β-cells to α-cells following GPR56 deletion, and this is something that could be investigated using lineage tracing. Under normal physiological conditions, GPR56 is not involved in whole body glucose homeostasis in adult mice, although a trend towards mild glucose intolerance was observed. The glucose excursion curve for the female mice showed a sharp decline at 30 min following glucose administration and there was a tendency for the GPR56 KO female mice towards glucose intolerance. This pattern was consistent with that reported for GLP-1 deficient female mice, where the excursion curve showed a sharp decline at 30 min and the female mice were more glucose intolerant than the males (Preitner et al., 2004). As glucose delivered by the intraperitoneal route does not pass through the GI tract, there was no contribution from the incretin effect or gastric emptying time to the glucose clearance pattern observed. In perifusion experiments, the classical biphasic pattern of insulin secretion was seen, where there is an initial rapid increase in insulin release followed by a sustained second phase. In T2D, first phase insulin secretion is almost completely abolished while the second phase is greatly reduced (Hosker et al., 1989). However, no defect was observed in GPR56 KO islets in these phases, indicating that islet GPR56 is not required for an appropriate insulin secretory response to increased glucose concentration. It was not possible to determine whether the mild glucose intolerance in the female mice was a result of reduced insulin secretion, because it was necessary to pool islets isolated from male and female mice to have sufficient quantities for the perifusion experiments. Nonetheless, there was no evidence of compromised insulin secretion in vitro, suggesting that the mild glucose intolerance is likely to be a consequence of reduced sensitivity of target tissues to insulin after GPR56 deletion.

Some mice in which GPCRs have been deleted do show impaired fuel homeostasis under conditions of metabolic stress. For example, under standard conditions GPR39 KO mice have normal phenotypes (Tremblay et al., 2007) but they exhibit metabolic abnormalities when stressed by high fat diet (Moechars et al., 2006; Tremblay et al., 2009). It is therefore possible

that different phenotypic characteristics may be observed if GPR56 KO mice are maintained under conditions of metabolic stress, such as high fat or high carbohydrate feeding. Under these conditions, β-cells will be forced to compensate for increased metabolic demand by increasing insulin output and islet mass, and the importance of GPR56 for these compensatory processes will be evident.

Interestingly, a recent study found that GPR56 mRNA was decreased in isolated islets from T2D patients and from db/db mice – a rodent model of obesity and T2D, and the authors speculated that this downregulation may have a causal link to dysfunctional β-cells in T2D (Dunér et al., 2016). The researchers also found a reduction in insulin content and a decreased ability of β-cells to respond to glucose when GPR56 expression was reduced in the INS1 insulin-secreting cell line. These findings are inconsistent with the data from GPR56 KO mice presented in this chapter. Thus, the data presented here demonstrate that there were no differences in the insulin content of islets isolated from KO and WT littermates and there were also no reductions in their insulin secretory response to glucose. However, it was found that GPR56 deletion resulted in a small reduction in pancreatic insulin content (WT: 117.1±18.4 ng insulin/mg protein, n=3; KO: 96.85, n=1). There was insufficient availability of pancreases from GPR56 KO mice to make any meaningful comparison, but given that the data in chapter 2 implicated GPR56 in islet development it is perhaps not surprising that there was reduced insulin content after its deletion. This may not have been evident when insulin content was quantified in isolated islets since size-matched islets were used for this, which would have masked any reductions in overall content due to the overall smaller size of islets in the GPR56 KO mice. In addition, several studies investigating glucose response profile of islets isolated from GPCR-null mice, such as GPR40, GPR119 and GLP-1R KO mice, found that GPCR deletion did not affect glucose-induced insulin secretion (Chu et al., 2007; Steneberg et al., 2005; Latour et al., 2007; Flamez et al., 1998). This is not surprising, as glucose initiates insulin secretion through its metabolism while GPCRs are targets for agonists that potentiate this secretory response. Consistent with this, islets isolated from GPCR null mice failed to show an appropriate potentiation of glucose-induced insulin secretion. It is not clear why Dunér and colleagues found that glucose-induced insulin release was decreased following GPR56

knockdown, but it may be because they used INS1 cells, which are less reliable and less representative than primary islets.

T2D is a complex disease that involves interaction between multiple genes and the environment. It is therefore instructive to note that single gene is directly important for glucose phosphorylation in β-cell, deletion does not usually result in overt diabetes. As islets express at least 293 GPCRs (Amisten et al., 2013), is it most likely that there is functional redundancy in case GPCRs are deleted, mutated or malfunctions. GPR56, for example, is on the same loci as genes encoding the adhesion GPCRs GPR114, GPR64 and GPR97 (Fredriksson et al., 2002; Peng et al., 2011) and GPR56/GPR97/GPR114 gene cluster has been postulated to possess functional redundancy in immune cells (Hamann et al., 2016). It is therefore possible that GPR114, GPR64 or GPR97 will compensate for the loss of function of GPR56, and in future studies it may be worthwhile quantifying the expression level of GPR114, GPR64 and GPR97 in islets from WT and GPR56 KO mice.

GPR56 mRNA has been reported to undergo alternative splicing. Alternative splicing can occur in the non-coding region upstream of the transcriptional start site of GPR56, and this is thought to regulate cerebral cortex patterning in human (Bae et al., 2014). Alternative splicing has also been reported in GPR56 coding regions, resulting in four variants named S1 to S4 (Kim et al., 2010). The targeting strategy for generating GPR56 KO mice used in this study deleted exons 2 and 3, which are the regions that coincide with S1 to S3 variants. S4 variant has its start codon in exon 4, which meant that variant 4 was preserved in the current model of GPR56 KO. Indeed, S4 was recently detected in the current model of GPR56 KO mice and its presence was associated with increased basal activities (Salzman et al., 2016). To date, no studies have investigated the expression of these variants in the pancreas and the extent to which they may affect β-cell function is unknown.

Islets require an abundant blood supply to allow them to rapidly sense changes in circulating glucose concentrations and distribute the insulin that they secrete. Islets are richly vascularised, and it is well established that blood vessel endothelial cells play crucial roles in maintaining homeostasis in the islet microenvironment. The development of the islet vasculature begins

during embryogenesis and requires the production of angiogenic factors such as vascular endothelial growth factor A (VEGF-A), which is critical for the recruitment of endothelial cells during islet vascularisation in the developing pancreas. The failure of this process leads to decreased islet mass and impaired glucose homeostasis (Reinert et al., 2013). Overexpression of GPR56 has been associated with increased expression of VEGF genes (Kim et al., 2010), suggesting that GPR56 may play a role in blood vessel formation. Although no study exists to support this notion in normal tissues, it has been established in cancerous cells that GPR56 can either promote or inhibit angiogenesis through VEGF signalling, depending on whether GPR56 is expressed in a cleaved or full length form (Yang et al., 2011). In some cancer types, particularly in melanoma, downregulation of GPR56 is necessary for metastasis and disease progression. It is therefore possible that a GPR56 deficient islet, like a tumour mass, would increase the production of angiogenic factors such as VEGF and increase its vascular supply. To investigate the role of GPR56 in development of the islet vasculature, the endothelial CD31 marker was used to quantify vascular density in GPR56 KO and WT pancreases. Surprisingly, there were no differences in islet vascular density and area in the absence of GPR56 suggesting that this receptor is not essential for the formation of new blood vessels.

The effect of GPR56 on angiogenesis in melanoma cells is potentiated by its interaction with transglutaminase 2, a cross-linking enzyme present in the ECM that inhibits tumour growth by restricting the formation of new blood vessels (Jones et al., 2006). It has been proposed that tumour growth and angiogenesis may be enhanced by degrading and internalising TG2 through the N-terminal domain of GPR56 (Yang et al., 2014). It was therefore hypothesised that if TG2 and GPR56 act together to inhibit angiogenesis, mice in which both genes have been deleted might be hypervascularised. A double KO mouse model of GPR56 and TG2 was used to investigate this hypothesis. The mice used for these studies were those in which GPR56 was expressed and TG2 was deleted (WT/KO) and those in which both GPR56 and TG2 were deleted (KO/KO). Ideally, comparison should also have been made with the pancreases from WT/WT mice, but they were not available. In addition, limited availability of mice for these studies meant that it was only possible to quantify islet vascular density in pancreases retrieved from P10 mice. It was found that there were no differences in the area occupied by islet vessels or in the vascular densities when both GPR56 and TG2 were deleted. . The lack of differences

in vascular density may not be surprising, as when islets adapt to metabolic demand during insulin resistance to increase oxygen supply, they do so not by generating new blood vessels but by dilatation of pre-existing blood vessels (Dai et al., 2013). It may therefore be worth measuring vessel diameter in future studies to determine whether this is altered following KO of GPR56 and TG2. Moreover, a compensatory mechanism may also be present to inhibit undue angiogenesis in normal tissues, in order to prevent tumour growth.

During embryogenesis, islet vascular networks formed from VEGF signalling provide scaffolds for nerve fibre development, thus indicating that VEGF indirectly controls islet innervation (Reinert et al., 2014). Since islet nerve fibres fine-tune insulin secretion through the release of neurotransmitters (Ahrén, 2000), the requirement of GPR56 in islet innervation was determined. Although there was no difference in the innervation between GPR56 WT and KO islets, there was a 34% increase in fibre density in GPR56/TG2 KO/KO islets, indicating that TG2 may also be a binding partner of GPR56 in islets. It will be interesting to investigate the effect of deleting both GPR56 and TG2 on glucose homeostasis in the future, as at the time of this study, adult GPR56/TG2 KO/KO mice were not available.

When comparing islet innervation and vascularisation, it could be observed that at P10 in GPR56/TG2 mice, there was a trend of increased fibre density in the double KO mice compared to the WT, while there was no trend in vascular density. This may be attributed to the different developmental age when innervation and vascularisation occur in mice. Islet vascularisation begins during the second phase of progenitor differentiation and is completed at birth while islet innervation starts during islet clustering around E15.5 and is not completed until during weaning at P21 (Reinert et al., 2014). When the quantifications were carried out at P10, nerve fibres are still developing whereas blood vessel formation has already been completed. The time at which innervation and vascularisation was investigated may therefore impact on the ability to detect any differences in the effect of GPR56 deletion, and ideally quantifications would have been carried out over a range of ages if the mice had been available.

Finally, analysis of nerve processes in islet function should also consider the contribution of peri-islet Schwann cells, as the network of nerve fibres in the pancreas is a combination of

axons and Schwann cells (Ushiki and Watanabe, 1997). Schwann cells provide vital trophic support for neurons as they branch into a meshwork upon reaching islet surfaces, indicating that they may be important in neuroendocrine regulation of islet function. In NOD mice, it has been reported that infiltration of cells within islets by reactive T cells was not possible without the peri-islet glial sheath being compromised or destroyed (Winer et al., 2003). From the embryo to adult life, adhesion GPCRs are necessary for the proper function and signalling of Schwann cells (Sigoillot et al., 2016). GPR56 is important for CNS myelination (Giera et al., 2015) but its role in the PNS is not yet documented. However, its close family member, GPR126, plays a crucial role in the normal functioning of Schwann cells in the PNS (Mogha et al., 2013). Since axons in the pancreas are mainly unmyelinated (Ushiki and Watanabe, 1997), GPR56 may have an indirect effect on peri-islet Schwann cells through other members of Group VIII adhesion GPCRs, possibly by interacting with GPR126. It was not possible to investigate this, as only one mouse per genotype was available for this work, which is too few to make any logical conclusion.

In conclusion, this chapter has provided insights in to the role of GPR56 in the pancreas under normal physiological conditions. Deletion of GPR56 has no effect on insulin secretion, islet innervation and vascularisation in 8-week-old mice. Further studies are needed to clarify whether GPR56 KO mice will behave differently with ageing or under increased metabolic stress such as high fat feeding. It is also worth investigating the metabolic phenotype of islet-specific GPR56 KO mice, since GPR56 is highly expressed in islets.

Chapter 5

Chapter 5 GPR56 regulates β-cell proliferation and islet mass

5.1 Introduction

Diabetes mellitus is characterised by loss of functional β-cells leading to decreased islet mass, with the resultant inability of sufficient insulin secretion to meet metabolic demands. In T1D, β-cells are destroyed by autoimmune antibodies while in T2D the inability of β-cells to adapt appropriately to increased metabolic demand primarily drives the progressive loss of β-cells (Kahn, 2001). In addition, loss of β-cells may be underpinned by genetic defects. Data from genome wide association studies have shown that inherited abnormalities in β-cell mass and/or functions are critical to the onset of T2D, as many risk variants identified impact either on β-cell renewal or insulin secretion (McCarthy and Hattersley, 2008; Voight et al., 2010).

Physiologically, β-cell mass is dependent on three main processes: replication of existing β-cells, increase in size of individual cells, and formation of new β-cells through differentiation or neogenesis. Of these processes, β-cell replication is the primary determinant of β-cell mass postnatally (Georgia and Bhushan, 2004). The ability of pre-existing β-cells to proliferate is vital to the maintenance of adult islet mass (Dor et al., 2004) and for sustaining glucose homeostasis in the presence of insulin resistance (Cerf, 2013).

In the past decades, research efforts have been geared towards understanding the physiological mechanisms regulating β-cell proliferation, with the intent of harnessing the information to increase islet mass in diabetes patients. Such efforts have led to the identification of the role played by gut hormones in maintaining islet neogenesis and β-cell proliferation. Thus, it was shown that chronic administration of exendin-4, an analogue of the gut hormone GLP-1, led to increased islet mass and cured rodent models of diabetes by activating a G-protein coupled receptor, GLP-1R (Xu et al., 1999; Tourrel et al., 2001; Ogawa et al., 2004). This breakthrough led to increased research interest in the role of islet GPCRs in regulating β-cell function and mass. As islets express many other GPCRs, some of which have no known functions, it is possible that some of them may have the appropriate characteristics for a next-generation type T2D therapy.

GPCRs are highly tractable drug targets. Currently, approximately 30-50% of all drugs in clinical use are directed at them (Cook, 2010). Indeed, novel T2D drugs must target the key dysfunctions associated with diabetes, one of which is reduced islet mass. Such drugs must prevent loss of β-cells by inhibiting cell death/de-differentiation, initiate the formation of new β-cells or have the capacity to stimulate β-cells to proliferate. Increasing evidence points to islet-expressed adhesion GPCRs as meeting at least some of these criteria. For instance, pancreas-specific deletion of the adhesion GPCRs CELSR2 and CELSR3 produced mice that were glucose intolerant, because the absence of these adhesion GPCRs resulted in fewer β-cells as a consequence of decreased β-cell replication (Cortijo et al., 2012). CD97, another adhesion GPCR, enhanced cell survival by inhibiting intrinsic and extrinsic apoptosis in cancer cells (Hsiao et al., 2015). In addition, brain angiogenesis inhibitor 1 (BAI1) is an engulfment adhesion receptor on phagocytes that identifies and traps apoptotic cells (Park et al., 2007). Overexpression of BAI1 prevents tumour growth by initiating apoptosis while loss of BAI1 turns gliomas to aggressive glioblastoma (Nishimori et al., 1997; Kang et al., 2006). Regulation of proliferation and apoptosis may be a conserved function of the adhesion GPCRs.

GPR56, the adhesion GPCR that is the subject of the experiments described in this thesis, has been implicated in many biological processes involving proliferation, apoptosis and organ mass. In the CNS, deletion of GPR56 resulted in fewer myelinated axons due to decreased proliferation of oligodendrocyte precursor cells (Giera et al., 2015). In leukaemia cells, and haematopoietic stem cells extracted from GPR56 KO mice, knockdown of GPR56 led to accumulation of apoptotic-related proteins such as p53 and cleaved caspase-3, due to DNA damage. The authors further concluded that GPR56 promotes cell survival by degrading p53 (Saito et al., 2013). In addition, forced expression of GPR56 led to myotube hypertrophy and GPR56 signalling is important for maintaining muscle mass in models of muscle hypertrophy (White et al., 2014). From the foregoing, and because of the abundant expression of GPR56 in β-cells, it was hypothesised that GPR56 may play a role in β-cell proliferation and mass. Using gain-of-function and loss-of-function approaches, the role of GPR56 in β-cell mass expansion as a consequence of β-cell proliferation and apoptosis was investigated.

5.2 Aims

- Determine the effect of GPR56 overexpression on β-cell proliferation and apoptosis.
- Determine whether deletion of GPR56 in vivo has any effect on β-cell proliferation and mass.

5.3 Methods

5.3.1 siRNA-mediated downregulation of GPR56 expression in mouse islets

Short interfering RNAs (siRNAs) employ the biological process of RNA interference, where the sequence of a protein-encoding gene is degraded by complementary RNA sequences, leading to directed silencing of gene expression and translation. Due to the three dimensional structure of islets, optimal delivery of siRNA to islets using the conventional delivery methods is challenging. Dharmacon Accell® siRNA technology, a self-deliverable RNAi method, that was used successfully to deliver siRNA into difficult-to-transfect leukaemia cells (Larsen et al., 2011), was therefore tested in islets to knock down GPR56 expression. Uptake of siRNA was first assessed by incubating islets in RPMI supplemented with 2% fetal calf serum containing fluorescently labelled non-targeting siRNA (1μM) and monitored under a fluorescent microscope for 24 or 48 h. The target sequence for the negative control siRNA was 5'-UGGUUUACAUGUCGACUAA-3'. In a separate tube, 200 mouse islets were incubated with 1μM Accell SMARTpool GPR56 siRNAs containing the following sequences: 5'-GUGUCAUCCACAGAGGUAG-3', 5'-CCACUAUGAUCAAUCUUCA-3', 5'-UCCUCAUCUUCCUGUGGUA-3' and 5'-CUCUUCAGCAUCAUAACUU-3' in RPMI for 24 or 48h before RNA was extracted and reversed transcribed. Expression of GPR56 was quantified by qPCR using the following GPR56 primers: forward primer 5'-TTGCAGCAGCTTAGCAGGTA-3' and reverse primer 5'-GATCCTCTAGACCGGCTGTG-3'.

5.3.2 Overexpression of GPR56 by transient transfection

Full-length GPR56 plasmid was a gift from Dr Xianhua Piao (Boston Children's Hospital) and was shipped to London on filter papers. Plasmid DNAs were retrieved, expanded in *E. coli* (section 2.4) and the identities were confirmed by sequencing and BLAST searches. $3x10^5$ MIN6 cells were seeded into 6-well plates and incubated overnight at 37^0C. Cells were

transiently transfected with 0 – 1200ng of full-length GPR56 plasmid for 24, 48 or 72 h using lipofectamine (Section 2.4.3), and the degree of transfection was determined by qPCR. In a parallel experiment, the efficiency of Lipofectamine and Viafect in delivering plasmids to MIN6 cells was determined by incubating MIN6 cells for 24-72h with 0 – 1200ng of a plasmid encoding eGFP in the presence of these transfection reagents.

5.3.3 In vitro measurement of β-cell proliferation following GPR56 overexpression

The effect of GPR56 overexpression on β-cell proliferation was determined by quantifying BrdU incorporation into replicating DNA using a colometric BrdU ELISA kit. MIN6 cells transfected with empty pcDNA3 vector or MIN6 cells that were transiently transfected with GPR56 plasmids were cultured overnight in DMEM containing 10% fetal bovine serum. The cells were subsequently serum-starved for 24 h before being labelled with 100μM BrdU for 4 hours in 96 well plates. Following fixation of the cells and addition of an anti-BrdU antibody, absorbance was read at 450nm as described in section 2.7.4.

5.3.4 In vitro measurement of β-cell apoptosis following GPR56 overexpression

Apoptosis was determined by measuring caspase 3/7 activities following transient overexpression of GPR56 in MIN6 cells. MIN6 cells transfected with empty pcDNA3 vector or MIN6 cells that were transiently transfected with GPR56 plasmids were cultured in medium containing 2% fetal bovine serum for 24 h with a further 20 h incubation in medium supplemented with a cytokine cocktail (1U/μl TNF-α, 0.05U/μl IL-1β and 1U/μl IFN-γ). Cells were incubated with Caspase 3/7 Glo working solution and caspase 3/7 activities were measured using a Veritas luminometer as described in section 2.7.2.

5.3.5 Static insulin secretion

Insulin secretion following GPR56 overexpression was determined by incubating 30,000 MIN6 cells transfected with scrambled vector or GPR56 plasmids in 96 well plates in medium supplemented with 2mM glucose for 1 hour at 37^0C. Insulin secretion was determined by radioimmunoassay.

5.3.6 In vivo BrdU delivery

Post-natal (P9) mice were given 50mg/kg BrdU intraperitoneally for 24 h prior to pancreas retrieval. To enable maximum labelling of replicating adult β-cells, age-matched WT and GPR56KO P56 mice were injected with 50mg/kg BrdU IP daily for 5 days.

5.3.7 Assessment of β-cell proliferation and islet mass in vivo

Pancreases were retrieved from WT and GPR56 KO mice that have received BrdU and either fixed-frozen or processed for paraffin embedding. Pancreases were cut at 5μm (fixed-frozen) or 10μm thick (paraffin-embedded) and sections that were more than 100μm apart were immunoprobed for BrdU, insulin and Ki67 as described in section 2.5.5. Images were taken with a Nikon fluorescent microscope and scored blindly before quantification of $BrdU^+$ β-cells and $Ki67^+$ cells were carried out using ImageJ software.

5.4 Results

5.4.1 Down regulation of GPR56 expression

The discovery that short interfering RNAs transiently downregulate genes of interest has led to the development of exogenous siRNAs as biological tools for identifying the function of particular genes. However, for efficient downregulation to be achieved, optimal delivery of functional siRNA to the target of interest is essential. Accell siRNA employs a novel, chemically modified non-viral delivery method that has been used successfully to silence genes in difficult-to-transfect cells such as primary leukemic cells (Larsen et al., 2011). The technology was tried on islets, which are also difficult to transfect, to investigate whether it is efficient in suppressing GPR56 expression. The method was validated by first evaluating the entry of scrambled siRNA into mouse islets. As shown in Figure 5-1 A and B, fluorescently labelled non-targeting siRNAs were detected in islet cells, with more cells fluorescing green after 48 h in culture (B) compared to when they were cultured for 24 h (A). This indicated that the Accell siRNAs were able to penetrate the islets and reach cells in the interior. To confirm whether the uptake seen with non-targeting siRNA could result in gene silencing when the siRNA was directed against GPR56, islets were incubated in a medium containing a mixture of GPR56 siRNAs and GPR56 mRNA downregulation was determined by qPCR. There was a significant reduction ($p<0.001$) in GPR56 mRNA expression when islets were incubated with Accell GPR56 siRNAs for 24 or 48 h compared to control. 1μM GPR56 siRNA induced a 31% knockdown when islets were cultured for 24 h, which was comparable to when islets were incubated for 48 h in the presence of 1μM GPR56 siRNA. Although there was a significant reduction in GPR56 expression following siRNA treatment, the 31% knockdown achieved was not sufficient to produce any functional effects on insulin secretion or β-cell proliferation. Other approaches to manipulate GPR56 expression in vitro, such as by transient overexpression and in vivo, by using GPR56 KO mice were employed to investigate the role of GPR56 in β-cell proliferation and other functions.

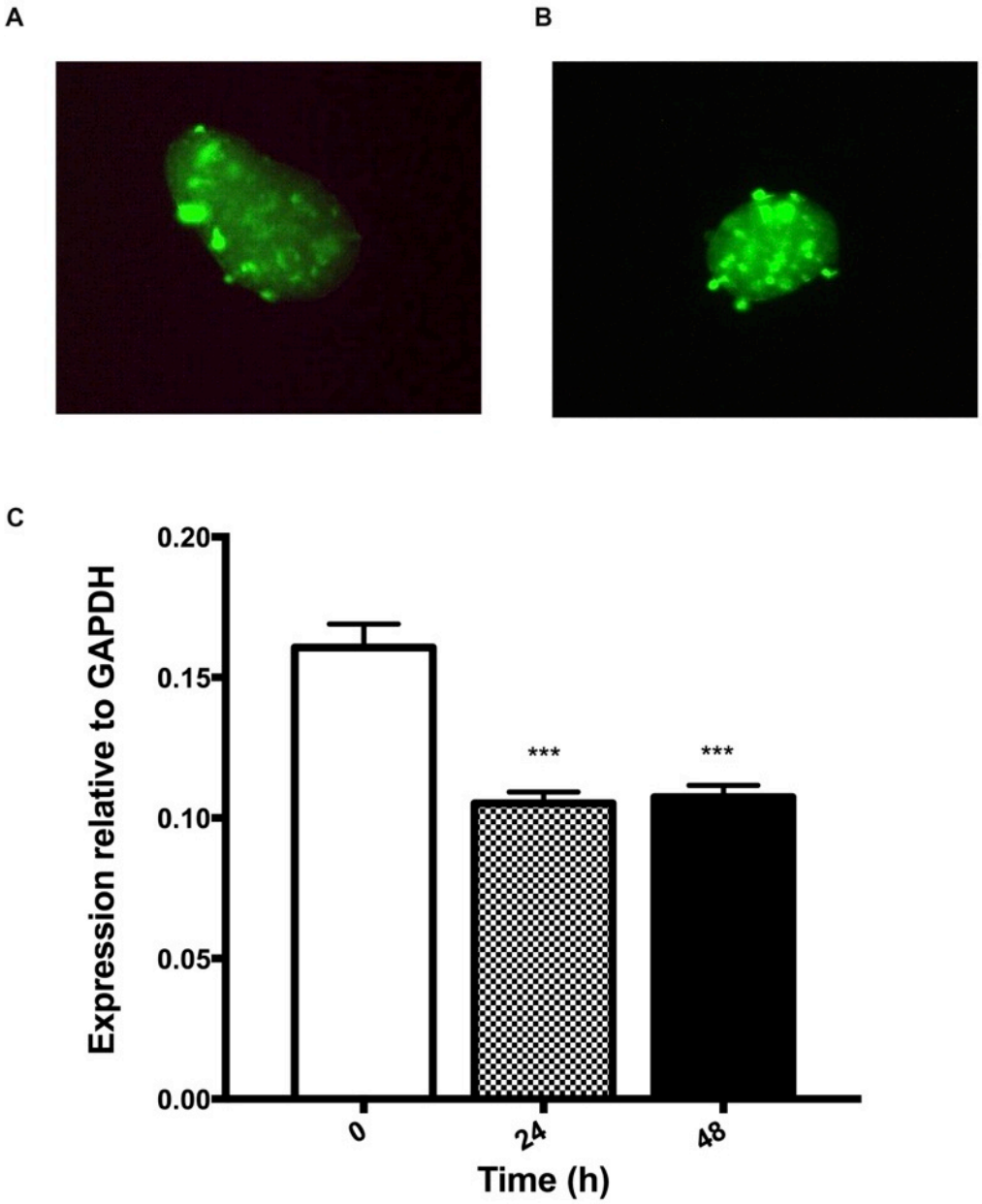

Figure 5-1 siRNA-mediated knockdown of GPR56 expression in mouse islets. A – B) To follow the uptake of Accell siRNA, islets were incubated with Accell green negative control siRNA and images were taken after A) 24 h and B) 48 h. C) Mouse islets (150 each) were incubated in medium containing 1µM Accell siRNA targeting GPR56 for 0, 24 and 48 h. RNAs were extracted, reversed transcribed and the expression of GPR56 relative to GAPDH was quantified by qPCR. Data are presented as mean + SEM, n=4, $p<0.001$, One-way ANOVA with Dunnett's post-hoc test.

5.4.2 Plasmid sequencing and BLAST search

As indicated above, siRNA knockdown of GPR56 in β-cells was inefficient, therefore overexpression of GPR56 in MIN6 β-cells was carried out to investigate whether this would result in a gain of function. To carry out overexpression studies, plasmids encoding full length GPR56 were obtained from Dr Xianhua Piao of Boston Children's Hospital. The plasmid DNA was extracted and sequenced. After translating the DNA sequence to protein, the identity of the sequence was confirmed by a protein Basic Local Alignment Search Tool (BLAST). Mouse GPR56 has 687 amino acids. The region amplified for sequencing covered the first 255 amino acids as shown in Figure 5-2. There was 100% similarity between the amino acids of GPR56 full-length plasmid (Query) and mouse GPR56 in the reference database (Sbjct), confirming the plasmid identity and that it encodes for the mouse GPR56 protein.

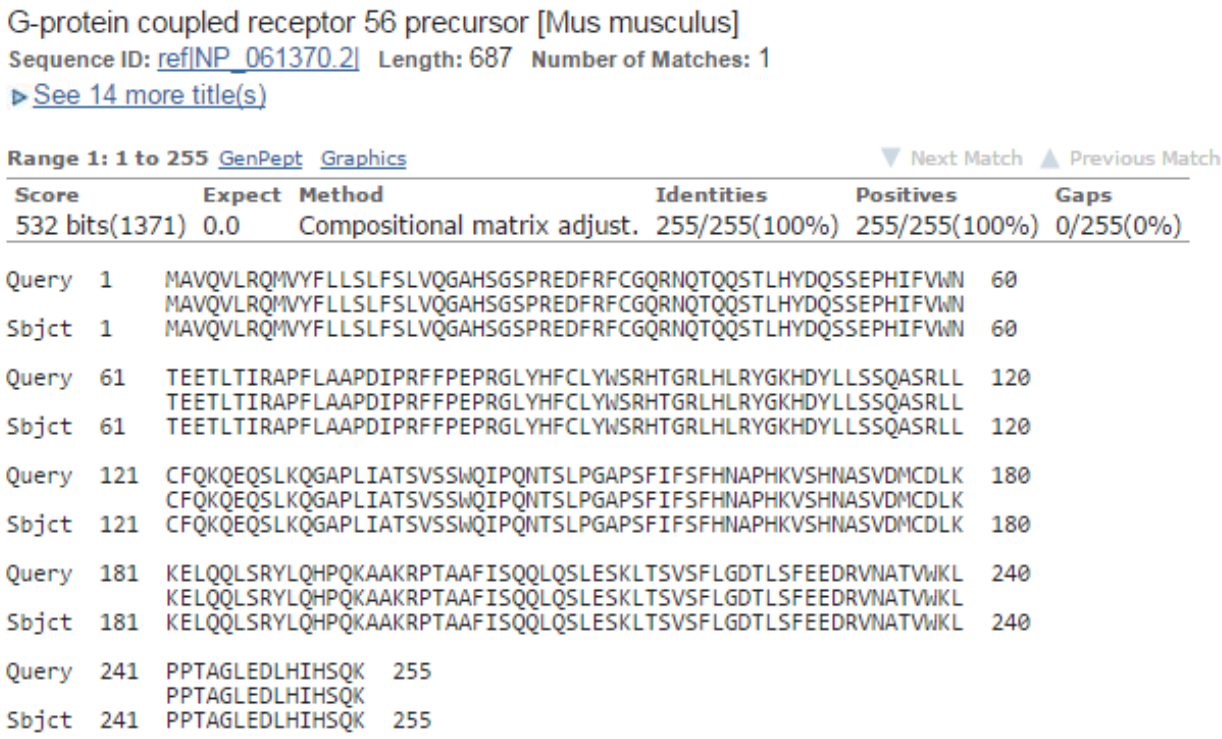
G-protein coupled receptor 56 precursor [Mus musculus]
Sequence ID: ref|NP_061370.2| Length: 687 Number of Matches: 1
See 14 more title(s)

Range 1: 1 to 255 GenPept Graphics Next Match Previous Match

Score	Expect	Method	Identities	Positives	Gaps
532 bits(1371)	0.0	Compositional matrix adjust.	255/255(100%)	255/255(100%)	0/255(0%)

```
Query  1    MAVQVLRQMVYFLLSLFSLVQGAHSGSPREDFRFCGQRNQTQQSTLHYDQSSEPHIFVWN  60
            MAVQVLRQMVYFLLSLFSLVQGAHSGSPREDFRFCGQRNQTQQSTLHYDQSSEPHIFVWN
Sbjct  1    MAVQVLRQMVYFLLSLFSLVQGAHSGSPREDFRFCGQRNQTQQSTLHYDQSSEPHIFVWN  60

Query  61   TEETLTIRAPFLAAPDIPRFFPEPRGLYHFCLYWSRHTGRLHLRYGKHDYLLSSQASRLL  120
            TEETLTIRAPFLAAPDIPRFFPEPRGLYHFCLYWSRHTGRLHLRYGKHDYLLSSQASRLL
Sbjct  61   TEETLTIRAPFLAAPDIPRFFPEPRGLYHFCLYWSRHTGRLHLRYGKHDYLLSSQASRLL  120

Query  121  CFQKQEQSLKQGAPLIATSVSSWQIPQNTSLPGAPSFIFSFHNAPHKVSHNASVDMCDLK  180
            CFQKQEQSLKQGAPLIATSVSSWQIPQNTSLPGAPSFIFSFHNAPHKVSHNASVDMCDLK
Sbjct  121  CFQKQEQSLKQGAPLIATSVSSWQIPQNTSLPGAPSFIFSFHNAPHKVSHNASVDMCDLK  180

Query  181  KELQQLSRYLQHPQKAAKRPTAAFISQQLQSLESKLTSVSFLGDTLSFEEDRVNATVWKL  240
            KELQQLSRYLQHPQKAAKRPTAAFISQQLQSLESKLTSVSFLGDTLSFEEDRVNATVWKL
Sbjct  181  KELQQLSRYLQHPQKAAKRPTAAFISQQLQSLESKLTSVSFLGDTLSFEEDRVNATVWKL  240

Query  241  PPTAGLEDLHIHSQK  255
            PPTAGLEDLHIHSQK
Sbjct  241  PPTAGLEDLHIHSQK  255
```

Figure 5-2 Sequencing of GPR56 encoded by plasmid DNA. GPR56 cDNA in pCMV-sport6 vector was expanded in E.coli and DNA was extracted for sequencing. Sequenced nucleotides were translated using ExPASy and protein identity was revealed by a BLAST search against the NCBI database. Sequencing was carried out by Source Bioscience Cambridge.

5.4.3 Assessment of transfection efficiency

Two commercial transfecting reagents, Lipofectamine and Viafect were available in our lab. To determine which of them yielded optimal transfection, they were used to deliver pcDNA3 plasmids encoding enhanced green fluorescent protein (eGFP) to MIN6 cells. Equal numbers of MIN6 cells were incubated for 48 h with 1.25μg of eGFP in the presence of Lipofectamine (1:15) or Viafect (1:6) and the number of 'green' cells were counted under a fluorescent microscope. Transfection efficiency, defined as the percentage of the total number of MIN6 cells expressing eGFP, was determined. There were fewer MIN6 cells fluorescing green when Viafect was used as the transfecting reagent compared to Lipofectamine (Figure 5-3 A). As shown in Figure 5-3 B, the transfection efficiency (TE) of Lipofectamine was about 26 times greater than Viafect (% TE; Lipofectamine: 78.0 ± 2.7; Viafect: 3.0 ± 1.0). Lipofectamine was therefore used for subsequent transient transfection of MIN6 cells.

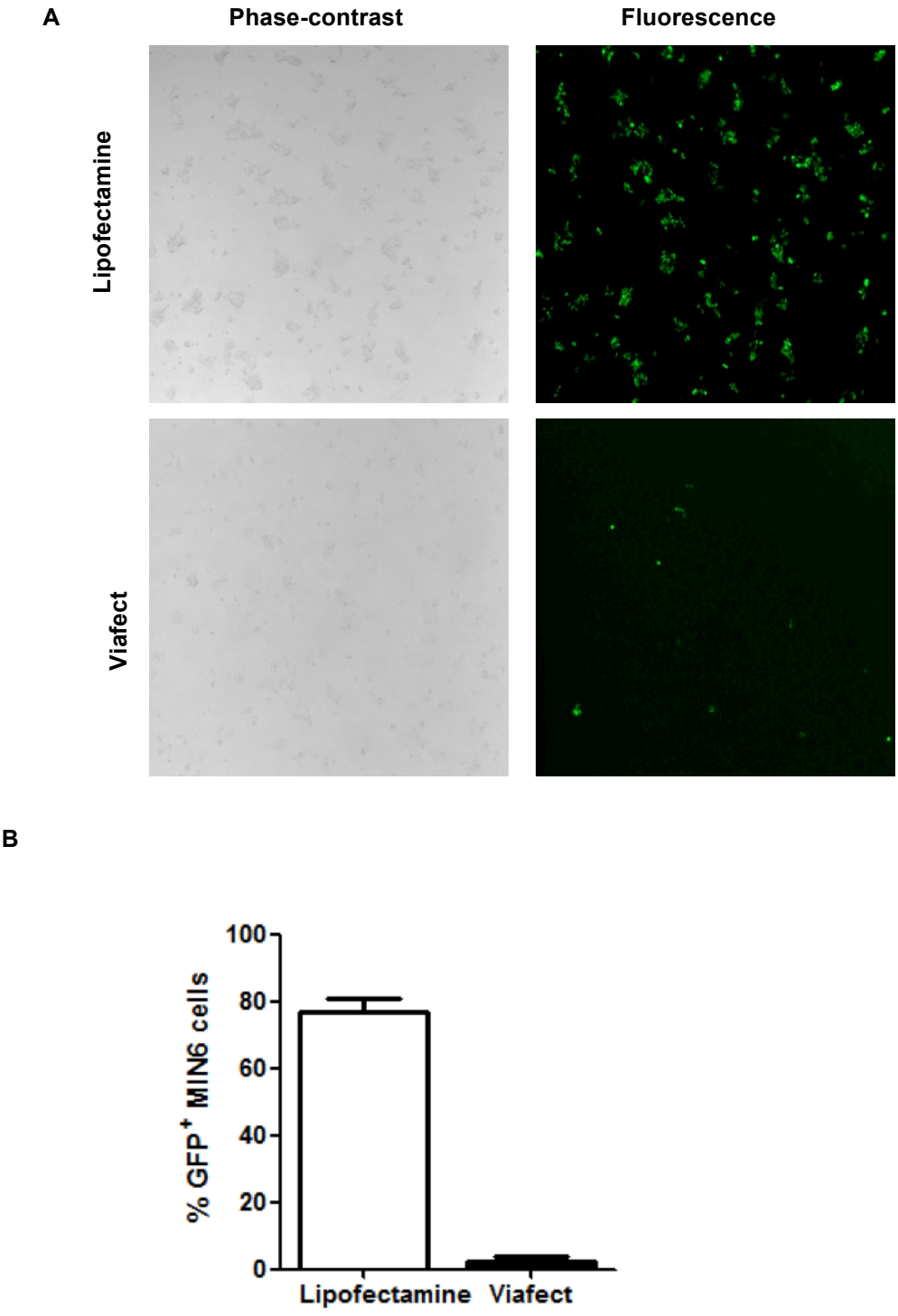

Figure 5-3 Comparing transfection efficiency of two transfecting reagents using an eGFP plasmid. A) eGFP was transfected into MIN6 cells using lipofectamine or viafect. After 48hours, the number of cells expressing eGFP was determined by fluorescence microscopy. B) The bar graph shows the percentage of MIN6 cells expressing eGFP with lipofectamine or viafect. Data are mean + SEM, n=3 fields each.

5.4.4 Overexpression of GPR56 plasmid in MIN6 cells

Having established that Lipofectamine was a better transfecting reagent than Viafect it was used to transfect MIN6 cells with a GPR56 plasmid. MIN6 cells were transfected with empty vector (basal) or vectors containing 12, 120 or 1200ng of GPR56 plasmid and cultured for 24 to 72 h. There was no change in GPR56 mRNA expression when MIN6 cells were transfected with 12ng GPR56 plasmid, even after the cells were cultured for 72 hours, indicating that it was a sub-optimal concentration (Figure 5-4 A). At 120ng, there was an increase in GPR56 mRNA expression at 48 and 72 h post-transfection (Basal: 0.057 ± 0.005; 48h: 0.224 ± 0.017; 72h: 0.442 ± 0.086), but these were not statistically significant elevations. At 1200ng of GPR56 plasmid, there was a significant increase in GPR56 mRNA expression by MIN6 cells after 24 h in culture ($p = 0.019$). The high GPR56 expression continued to increase at 48 and 72 h post transfection (24h: 0.858 ± 0.46, 48h: 1.413 ± 0.063, 72h: 1.694 ± 0.086). At 72 h with 1200ng plasmid, there was an approximately 20-fold increase in GPR56 mRNA expression compared to basal. Melt-curve analysis revealed a single peak curve (Figure 5-4 B) and agarose gel electrophoresis of the amplified product produced single DNA bands of the expected size of 96bp (Figure 5-4 C), indicating that there were no primer-dimer or nucleic acid contaminants. Western blot also revealed that the overexpressed GPR56 protein was of the predicted molecular weight of 70kDa (Figure 5-4 D). 1200ng GPR56 plasmid was therefore delivered to MIN6 cells for subsequent functional assays.

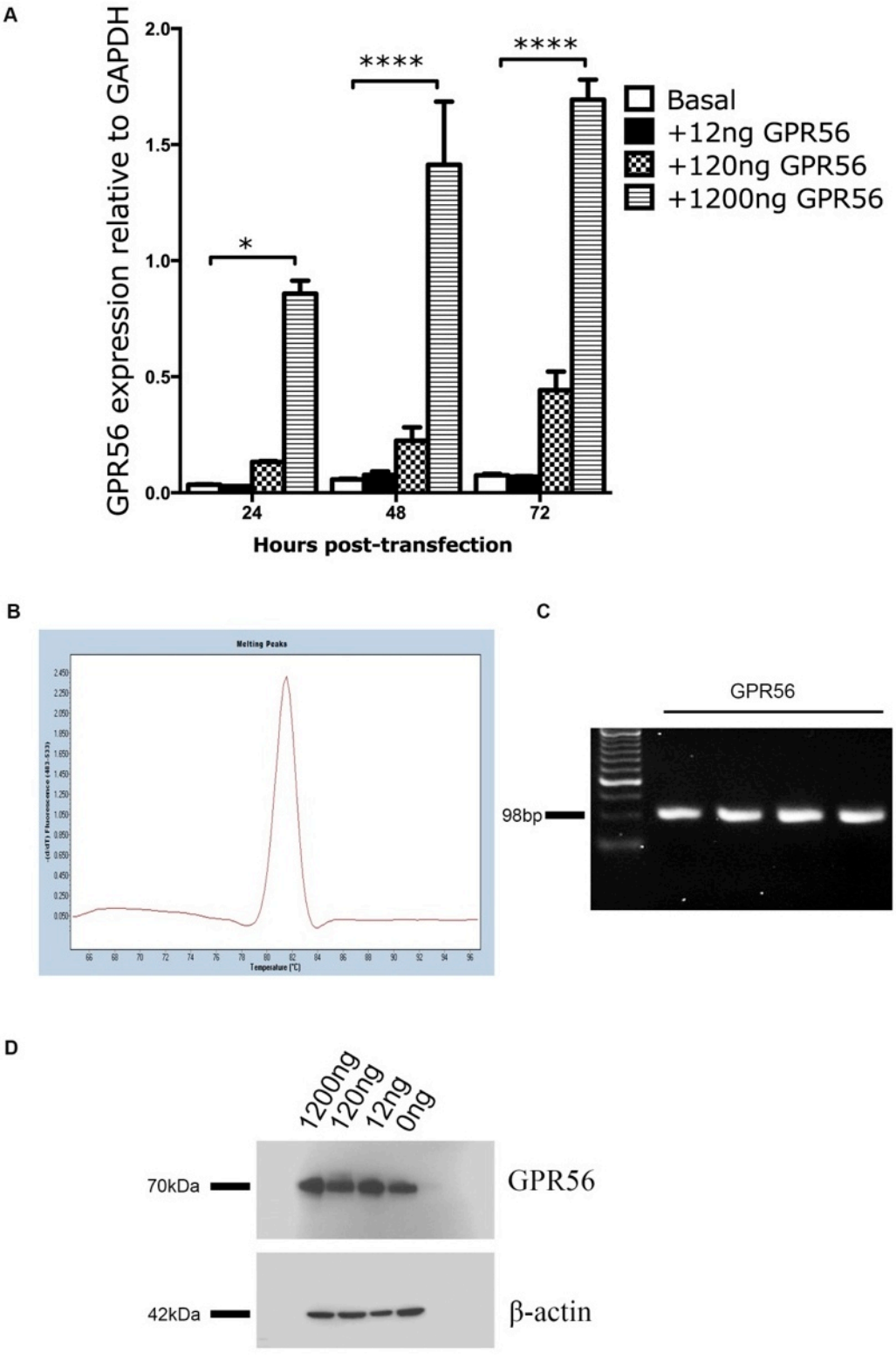

Figure 5-4 Evaluating GPR56 overexpression in MIN6 cells. A) Expression of GPR56 in MIN6 β-cells transfected with GPR56 plasmid is concentration-dependent. MIN6 cells were transiently transfected with different concentrations of GPR56 plasmid DNA using lipofectamine, and cultured for 24, 48 or 72 hours. cDNAs were prepared and expression of GPR56 mRNA was quantified by qPCR. Data are mean + SEM, n=3, *p<0.05, ****p<0.0001, two-way ANOVA with Tukey post-host test. B) Melt curve analysis following

qPCR showed a single band of GPR56 indicating that there was no primer dimer or other nucleic acid contaminations. B) Products of qPCR were subjected to agarose gel electrophoresis in the presence of ethidium bromide and DNA bands were revealed by UV light. The image shows single bands of GPR56 amplicons at the appropriate product size of 98bp. C) Western blot image following GPR56 overexpression 24h post incubation. β-actin was used as a loading control.

5.4.5 Effect of GPR56 overexpression on β-cell proliferation, insulin secretion and apoptosis

MIN6 β-cell proliferation, insulin secretion and apoptosis were evaluated following transient overexpression of 1200ng GPR56 plasmid. After 72 h culture in the presence of empty vector or the GPR56 plasmid, the cells were labelled with BrdU to measure DNA replication. MIN6 β-cells that were transfected with the GPR56 plasmid had a significantly higher number of cells with BrdU incorporated into their DNA compared to cells that were transfected with empty vector ($p=0.04$) (Figure 5-5 A). Overexpression of GPR56 had no effect on basal insulin secretion at 2mM glucose, suggesting that the secretory mechanisms of the β-cells were not disrupted (Figure 5-5 B). The number of β-cells undergoing basal apoptosis was significantly reduced following up-regulation of GPR56 ($p=0.01$), and while there was a trend towards protection against cytokine-induced apoptosis this was not statistically significant (Figure 5-5 C & D).

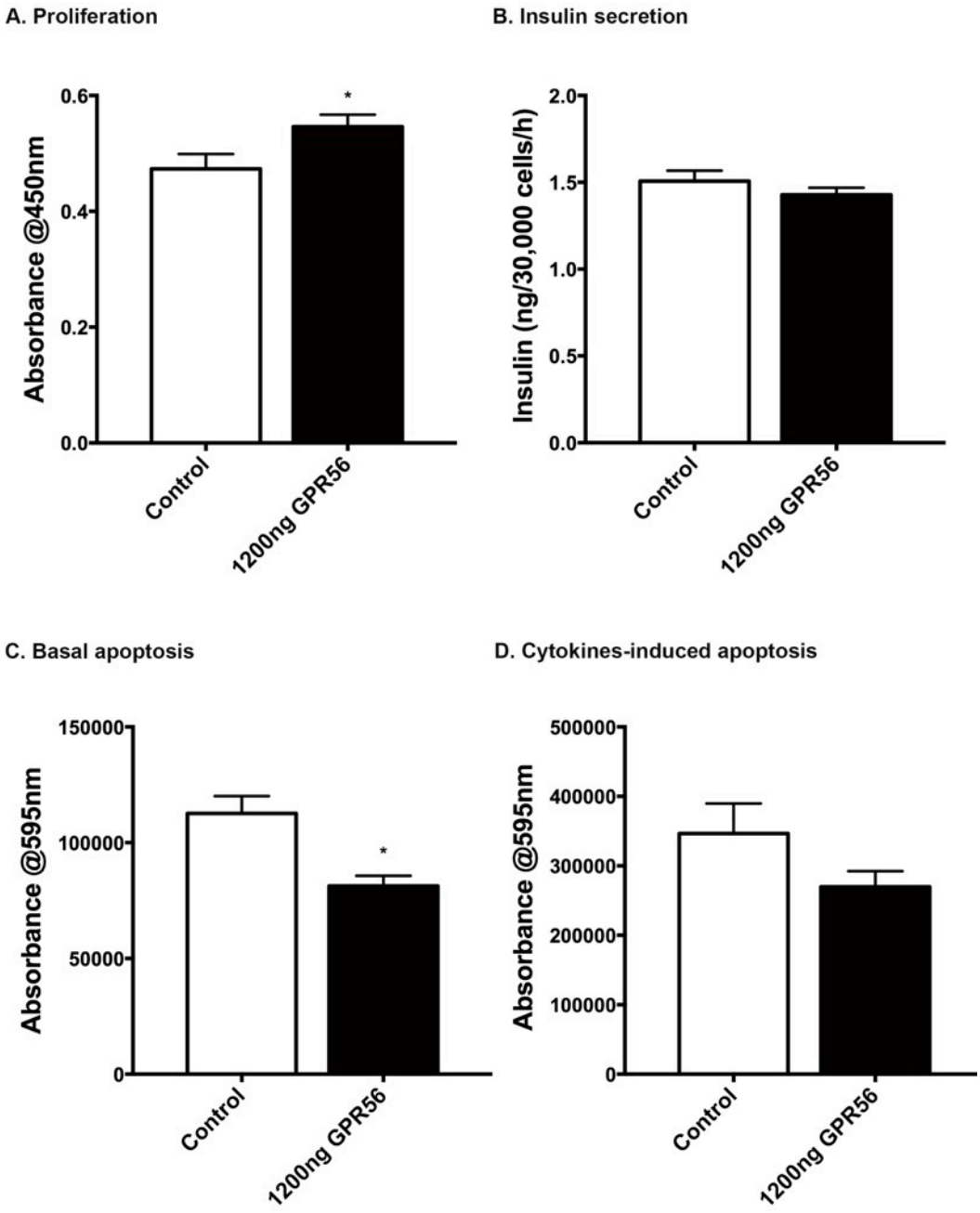

Figure 5-5 Effect of GPR56 overexpression on β-cell proliferation, basal insulin secretion and apoptosis. MIN6 cells were transfected with empty vector (control) or 1200ng of full length GPR56 plasmid and cultured for 72 h. At 72 h, functional studies were carried out to determine the effect of overexpressing GPR56 on A) MIN6 cell proliferation using a BrdU ELISA, n=8, B) insulin secretion, n=8, C) basal apoptosis and D) cytokine-induced apoptosis by measuring caspase 3/7 activities, n=4. Data are mean + SEM, *$p<0.05$, Student's t-test.

5.4.6 Effect of GPR56 deletion on β-cell proliferation in vivo

To investigate the effect of GPR56 on β-cell proliferation in vivo, age-matched WT and GPR56KO mice were injected intraperitoneally with BrdU. Replicating β-cells were counted at two time points: post natal day 9 (P9) and P56. P9 was chosen to coincide with the period of a surge in β-cell proliferation that normally occurs between the 4^{th} and 10^{th} neonatal days in rodents (Kaung, 1994) while P56 represented young adult mice. BrdU delivery to the P9 mice was given as a single IP injection on that day, followed by culling of the mice twenty four hours later, while for adult mice BrdU was given daily for 5 days (P56-P61) to ensure maximal labelling of replicating β-cells. The number of BrdU-labelled β-cells was determined by immunostaining for insulin and BrdU.

At P9, the number of replicating β-cells was significantly higher in the WT mice compared to the GPR56 KO littermates ($p<0.001$) (Figure 5-6 B). Since this decreased proliferation in the GPR56 KO neonatal mice could have resulted from β-cells exiting the cell cycle and being in the quiescent G_0 phase (Teta et al., 2005), a cell cycle exit assay was conducted to determine whether the decreased β-cell proliferation in the KO mice was due to premature cell-cycle exit of the β-cells. This was carried out by dual staining for BrdU and Ki67 (Figure 5-6 A, lower panel). Ki67 is a proliferative marker that labels cells in all of the cell cycle phases except the resting phase G_0. BrdU is incorporated into cells at S-phase during DNA replication and will not be detected in the preceding G_1 phase. However, it will be detected at G_1 in daughter cells that are re-entering the cell cycle since BrdU is passed on to daughter cells after mitosis (Kee et al., 2002). Cells that are positive for both BrdU and Ki67 are therefore cells that are actively cycling and replicating while cells that are $BrdU^+/Ki67^-$ are no longer in the cell cycle. Co-labelled $BrdU^+/Ki67^+$ cells from ten pancreas sections that were >100 μm apart were counted. It can be seen from Figure 5-6 C that significantly fewer numbers of pancreatic $BrdU^+/Ki67^+$ cells ($p<0.05$, n=3 mice per genotype) were seen in P9 GPR56 KO mice compared to their littermate controls, suggesting that the decreased proliferation in the KO mice is partly due to the cells exiting the cell cycle prematurely.

In P56 adult mice, a similar trend was observed. The number of $BrdU^+$/ β-cells was considerably lower ($p=0.005$) in the KO pancreases compared to those from WT mice (Figure 5-7 A & B).

Moreover, the rate of β-cell replication in P56 WT mice was twelve-fold lower than in P9 WT mice ($BrdU^+$/ β-cells; P9 WT: 13.3 ± 5.5, P56 WT: 1.1 ± 0.3), consistent with published data that β-cell replication progressively declines with age (Teta et al., 2005; Finegood et al., 1995).

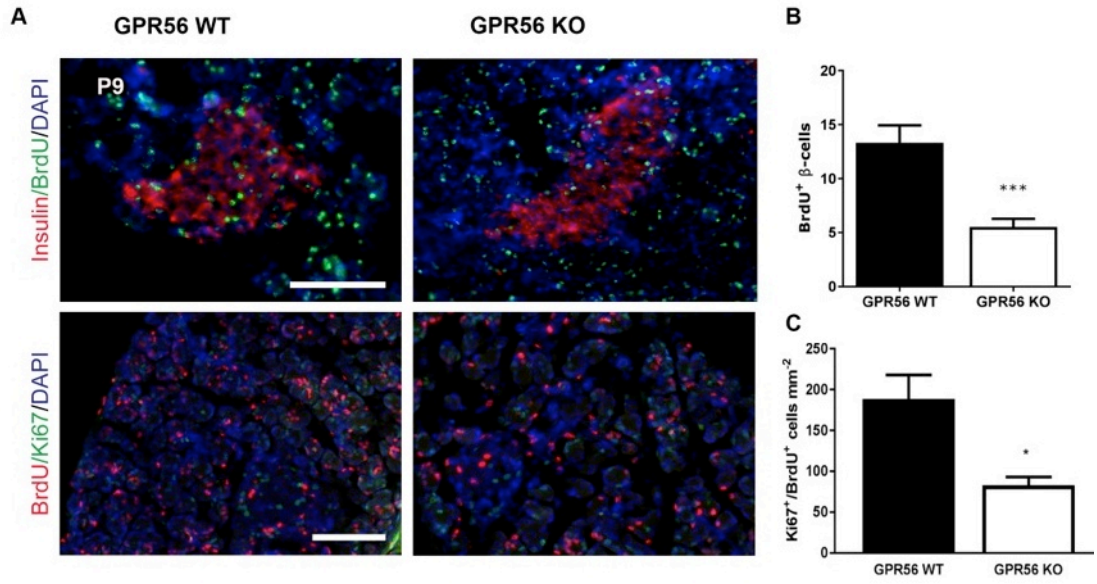

Figure 5-6 Effect of GPR56 deletion on β-cell proliferation in P9 mice. Postnatal day 9 mice were given BrdU IP and pancreases were retrieved 24 hours later, fixed and embedded in paraffin. A) 5μm sections were immunostained for BrdU, insulin and Ki67. Scale bar = 100 μm. B) ***p<0.001, n = 37 islets per genotype from 10 consecutive sections, Mann-Whitney test C) *p<0.05, n=3 mice per genotype, unpaired t-test.

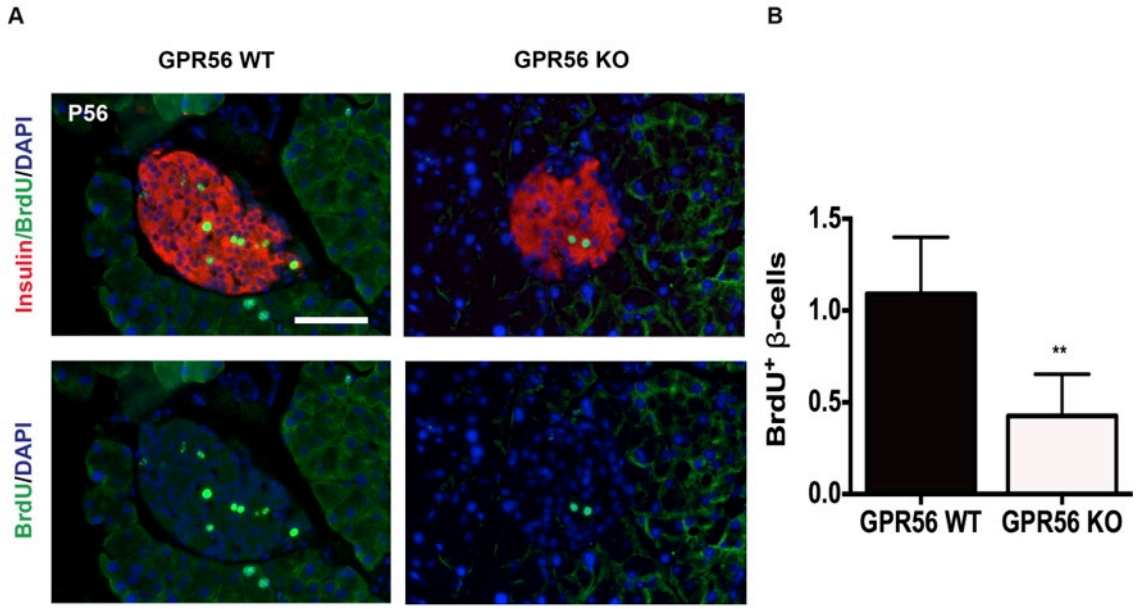

Figure 5-7 Effect of GPR56 deletion on β-cell proliferation in P56 adult mice. 8 week old GPR56 WT and KO mice were given BrdU IP daily for 5 days before pancreases were removed, fixed and embedded in paraffin. A) Pancreas sections were immunoprobed for insulin and BrdU. Scale bar = 50 μm. B) Data are presented as Mean + SEM, **p=0.005, n=33 islets from WT mice and 47 islets from KO mice, Mann Whitney test.

5.4.7 Effect of GPR56 deletion on islet mass

Postnatal islet mass is primarily driven by duplication of pre-existing β-cells (Dor et al., 2004). To investigate the extent to which the effect of GPR56 deletion on β-cell proliferation affects islet mass, the area occupied by insulin-positive β-cells was measured in pancreases retrieved from WT and GPR56KO mice (Figure 5-8 A). Islet size was determined at the same developmental stages of P9 and P56, where β-cell proliferation had been quantified. In P9 mice, GPR56 deletion resulted in islets being significantly smaller ($p<0.01$) compared to the littermate controls (Figure 5-8 B). There was also a small, non-significant reduction in islet size in the adult KO mice compared to the WT mice (Figure 5-8 C). Quantification of islet size distribution revealed that in P9 mice the majority of the islets were not bigger than 10×10^3 μm^2 while in P56 mice most of the islets were less than or equal to 18×10^3 μm^2 in size. (Figure 5-9 A & B). GPR56 deletion was associated with increased numbers of islets of less than 2×10^3 μm^2, in both P9 and P56 KO mice. Although the data in Figure 5-9 were from n = 1 mouse per

genotype, and so the chances of coincidence may not be ruled out, it is interesting to note that no islets were found within the size range of 10 x 10^3 μm^2 and 18 x 10^3 μm^2 in both P9 and P56 KO mice. In the WT mice, 40% of islets were found within this size range in P56 mice, compared to 13% in P9 mice. Thus, from the pattern of the graphs in Figure 5-9 A & B, it appears that there is a relationship between cells that are less than 2 x 10^3 μm^2 and cells in the 10 – 18 x 10^3 μm^2 size group. In P9 mice, about 50% of the β-cells were within the > 2 x10^3 μm^2 size group and 8% were in the 10 – 18 x 10^3 μm^2 range, but this trend was reversed in the P56 mice.

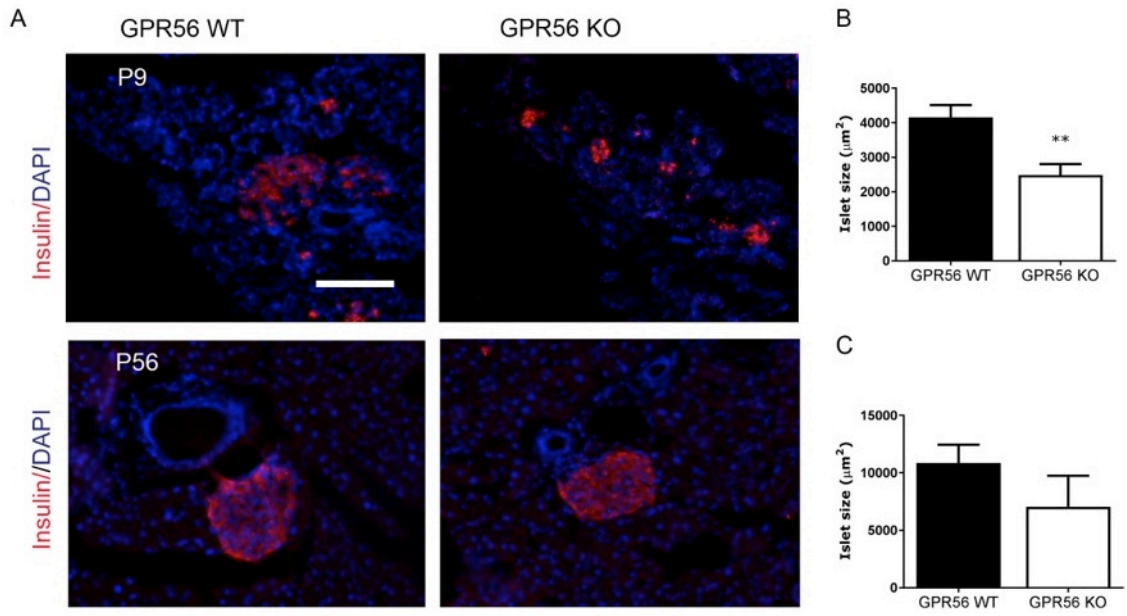

Figure 5-8 Islet sizes of P9 and P56 GPR56 WT and KO mice. Wax-embedded mouse pancreas sections were immunostained for insulin and the islet area was measured. B) Islet sizes of P9 WT and KO mice were significantly different. Data are mean+ SEM, **p<0.01. C) There was no difference in islet size at P56. Scale bar = 50μm.

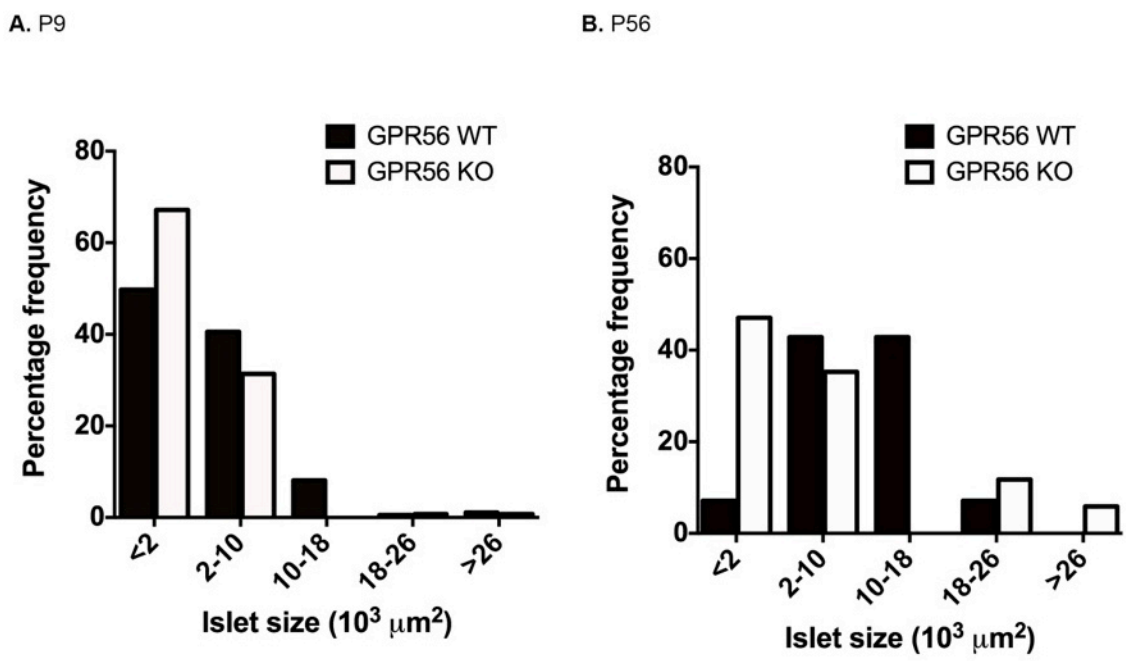

Figure 5-9 Size distribution of islets from P9 and P56 mice. Islet size was determined by measuring the area occupied by insulin positive β-cells and the percentage frequency of β-cells in the indicated size ranges in A) P9 and B) P56 mice was plotted. Data were obtained from 10 pancreas sections from a P9 mouse (185 islets) and a P56 mouse (134 islets).

5.5 Discussion

The experiments carried out in this chapter demonstrate that GPR56 plays a role in regulating β-cell proliferation and islet mass. In the gain of function study in which GPR56 was overexpressed and constitutively activated in β-cells, its functional activity was investigated independently of agonists. Transient overexpression of GPR56 in MIN6 cells led to increased β-cell proliferation and decreased apoptosis. These observations were consistent with data from GPR56 KO mice, indicating that deletion of GPR56 in vivo resulted in decreased islet mass as a consequence of decreased β-cell proliferation. In addition, a higher number of replicating β-cells exit the cell cycle prematurely in the KO islets compared to WT controls.

Attempts to knock down islet GPR56 using siRNAs produced variable and unsatisfactory results, most likely as a result of poor accessibility of the siRNAs to the core of intact islets. The function of GPR56 in β-cells was therefore investigated using a receptor overexpression strategy. As expected, increasing the concentration of GPR56 plasmid delivered to β-cells produced a corresponding increase in GPR56 mRNA expression. The increased GPR56 expression translated to enhanced β-cell survival and proliferation without any changes in basal insulin secretion.

G-protein coupled receptors (GPCR) are the largest and most studied cell surface receptors in the human genome. They consist of seven transmembrane helices with N- and C-terminal domains at both ends. Binding of an agonist to the N-terminal domain leads to receptor activation and subsequent downstream signalling. However, some GPCRs have been found to be minimally active in the absence of an agonist (Lefkowitz et al., 1993), and this activity is termed basal or constitutive activity. Such basal activity can be increased to a point where downstream signalling can be detected either by introducing a mutation to the receptor or by overexpressing the wild-type strain. For β_2-adrenoceptors, introducing a mutation to the C-terminal segment of the third intracellular loop or overexpression of the wild-type receptor led to a marked increase in cAMP generation in the absence of an agonist (Samama et al., 1993).

The constitutive activity of GPCRs arises from equilibrium between their active and inactive conformations. Although receptor overexpression does not alter this equilibrium, when GPCRs

are overexpressed, the number of receptors in both active and inactive forms is increased, and once a certain threshold is reached, downstream signalling of the active receptors will be detected (Hamann et al., 2015). The concept of constitutive signalling has been investigated in adhesion GPCRs and it is now known that the majority of adhesion GPCRs are functionally activated when their wild-type receptors are overexpressed. Using this approach, direct evidence for adhesion GPCR coupling to G protein subunits has been uncovered. For example, overexpression of GPR133 caused an increase in cAMP signalling, providing the first evidence that it is G_s coupled (Bohnekamp and Schöneberg, 2011). Coupling to other G-protein subunits such as G_q, G_i and $G_{12/13}$ have been demonstrated for several other adhesion GPCRs such as GPR126, GPR97, BAI1, GPR110 and GPR114 by overexpressing their wild-type strain (Gupte et al., 2012).

To study the effect of GPR56 deletion on β-cell replication and islet mass in vivo, newly formed β-cells and islet sizes were examined using pancreases retrieved from GPR56KO mice at P9 and P56. Shortly before birth, at E18, there is a dramatic increase in β-cell neogenesis and proliferation leading to increased islet mass. The islet mass enlargement in rodents continues after birth as a result of a rapid increase in β-cell replication: from P10, the rate of replication progressively declines until weaning at P28, where it remains fairly constant until adulthood (Kaung, 1994). As described in Chapter 3, a progressive increase in GPR56 expression was observed in islets between E18 and P9. As this period of increased GPR56 expression occurred when β-cell proliferation is at its peak, the absence of GPR56 may explain the decreased capacity of β-cells to proliferate at P9 in GPR56KO mice.

Furthermore, the surge in perinatal β-cell proliferation reported in rodents between the 4^{th} and 10^{th} days after birth is associated with increased expression of cyclin D2. Cyclin D2 is a proliferative gene that partners with cyclin dependent kinases (CDKs) to initiate cell cycle progression in β-cells (Cozar-Castellano, Fiaschi-Taesch, et al., 2006). Cyclin D2 KO mice have reduced β-cell replicative capacity with a resultant decrease in islet mass and they are glucose intolerant (Georgia and Bhushan, 2004). It has been reported that at P10, β-cells in islets of CDK-4 null mice showed about 60% reduction in their rate of proliferation (Martín et al., 2003). Although time constraints meant that it was not possible to measure the expression of cyclin D2

and CDKs in GPR56 KO islets, there has been a previous report of reduced CDK-2 protein in oligodendrocyte progenitor cells isolated from GPR56KO mouse brain (Giera et al., 2015), indicating that cell cycle regulators may play a part in the decreased replication of β-cells observed in the GPR56 KO islets. The decreased number of replicating and cycling $BrdU^+/Ki67^+$ cells observed in GPR56KO pancreas further supports this.

Other cell cycle proteins that may account for the decreased number of $BrdU^+/Ki67^+$ cells seen in GPR56KO pancreas include E2F and nuclear factor of activated T cells (NFAT). Forced expression of GPR56 in HEK293T cells considerably induced the expression of E2F and NFAT (Kim et al., 2010), supporting a role for GPR56 signalling in influencing cell cycle progression. As replicating cells pass through the S phase of the cell cycle, their DNA contents are duplicated. The duplication process is under the control of a myriad of genes such as those encoding for ribosomal enzymes and enzymes for DNA synthesis, that can either slow down or increase cell progression through the S phase. The DNA replication genes are themselves under the control of E2F proteins (Cozar-Castellano et al., 2006a). Six members of the E2F protein family have been detected in murine islets (Cozar-Castellano et al., 2006b). NFAT and its upstream effector, calcineurin, also play critical role in postnatal β-cell proliferation, and β-cell-specific loss of calcineurin/NFAT led to a significant decrease in β-cell proliferation in postnatal mice (Heit et al., 2006). Additional studies are required to confirm which cell cycle transcription factors are involved in the regulation of β-cell proliferation by GPR56 and their relative contributions.

Although β-cell replication is the primary determinant of islet size postnatally (Georgia and Bhushan, 2004), elements of β-cell neogenesis have been described to take place shortly before weaning at P28, and this contribute to adult islet mass (Scaglia et al., 1997). The observation that islets in pancreases from P56 GPR56KO mice were not smaller than those from age-matched WT mice, while there was a significant reduction in size at P9 in the GPR56 KO mice, suggests that other processes in addition to β-cell replication may contribute to adult islet mass. The first postnatal month is associated with many changes in the developing pancreas including a wave of increased apoptosis observed between P13 and P17. However, despite increased apoptosis and decreased proliferation, β-cell mass in rat was stable between

P2 and P20, suggesting that neogenesis is important for maintaining a constant β-cell mass (Scaglia et al., 1997). It was also reported that β-cell mass more than doubled between P2 and P5 but the cross-sectional area remained unchanged, indicating that increased β-cell number rather than size contributed to the increased mass (Bouwens et al., 1994). A sharp increase in β-cell mass was observed after P21 and based on islet mass at P31, data from mathematical modelling and duct-specific lineage tracing suggested that neogesis contributed between 30% to 50% of β-cell mass at the end of the first postnatal month (Finegood et al., 1995; Bonner-Weir et al., 2010). It is likely that GPR56 does not contribute to β-cell neogenesis and further studies using markers of ductal cell differentiation is required to confirm this.

The heterogeneity of islet cells, comprising, α, β, δ and PP cells, is well established (Steiner et al., 2010; Stanger and Hebrok, 2013). However, the heterogeneity is not limited to islet cell identity alone but it is now apparent that islets are made up of unique populations that are distinguishable based on size and function. This idea was first conceived by Bonner-Weir and colleagues, who classified islets into small and large based on their diameter (Bonner-Weir and Like, 1980), but the functional implication of this classification was not appreciated until recently. In addition, β-cells can be subdivided based on their ability to divide into proliferation-competent β-cells, expressing Fltp, a WNT/planar cell polarity effector gene and mature, proliferation-incompetent β-cells, lacking Fltp gene (Bader et al., 2016). The pancreases of GPR56KO mice contain considerably more small islets (>2000μm^2) than those from WT mice. In adult (P56) GPR56 KO mice, about 47% of all islets were less than 2000μm^2 in size compared to about 7% in this size range in pancreases from GPR56WT mice. Small islets (both in situ and isolated) are reported to contain more insulin granules/area, have higher insulin content and they secrete more insulin upon glucose challenge than large islets in rats (Huang et al., 2011) and humans (Farhat et al., 2013). Small islets also yield superior islet graft outcomes than large islets in transplantation studies (Li et al., 2014; Lehmann et al., 2007). The high number of small islets in GPR56KO mouse pancreas may partly explain why GPR56KO mice were not glucose intolerant, as they will compensate by secreting more of their insulin content.

The extent to which reduced β-cell mass contributes to T2D is an ongoing debate. It is not yet clear what residual islet mass is required to maintain normal glucose homeostasis. A substantial

decrease of up to 60% in islet mass has been reported in pancreases obtained from people with T2D (Butler et al., 2003), but removal of 50% of the pancreas mass from patients with pancreatitis had little effect on glucose tolerance (Menge et al., 2008). Also, when half of the pancreas mass was removed from healthy donors only one-fifth of the patients developed impaired glucose tolerance (Kendall et al., 1990), indicating that a decrease in islet mass alone is not sufficient to cause T2D. Indeed, β-cell function rather than β-cell number may play a more crucial role in the onset of T2D, as when islets from T2D patients were normalised to insulin content, they still secreted less insulin compared to islets from healthy subjects (Ashcroft and Rorsman, 2012). The role of β-cell function is further supported by the reversal of diabetes following administration of GLP-1 analogues or bariatric surgery in patients with long standing T2D with reduced β-cell mass (Steven et al., 2015).

In summary, the data presented in this chapter indicate that islet GPR56 plays an important role in fine-tuning β-cell proliferation and apoptosis, especially in the neonatal period, and suggest that this receptor may be a potential therapeutic target for optimising functional islet mass in T2D.

Chapter 6

Chapter 6 The role of collagen III in islet functions

6.1 Introduction

The extracellular matrix (ECM) is a specialised structure of glycoproteins that, in addition to providing structural support and anchorage sites for cells, serves to mediate signal transductions from the immediate environment of cells to their intracellular environment. The signalling interaction between islets and ECM is complex and interdependent, and is key in maintaining normal islet physiology especially cell survival, adhesion and insulin secretion. Islets are surrounded by a capsule of ECM known as the peri-insular basement membrane (BM), and this is among the first structures to be compromised in T1D (Korpos et al., 2013). Following islet isolation, the peri-insular BM is lost and this can lead to increased islet apoptosis (Rosenberg et al., 1999). Within each islet are deposits of ECM produced by endothelial cells of the blood vessels, forming the peri-vasular BM (Otonkoski et al., 2008). The islet BM is a dynamic complex of proteins that is continually modified throughout life and it is composed primarily of laminin and collagens (Deijnen et al., 1994). As nearly all islet β-cell are in contact with the BM (Peiris et al., 2014), components of the BM can directly influence β-cell function. Collagen IV, for instance, promotes adhesion, migration and insulin secretion of human β-cells (Kaido et al., 2004).

The potential of islet-matrix interactions to enhance islet survival and β-cell function has considerable translational impact on islet transplantation, which is increasingly becoming a popular treatment option for T1D. However, the current clinical procedure is associated with a high rate of early graft failure, especially during the first few weeks after transplantation (Saudek et al., 2010), thereby necessitating further grafts until euglycaemia is restored. In addition to immuno-rejection, one of the main reasons for graft failure is the uncontrolled and almost complete enzymatic digestion of the peri-islet matrix during the isolation process (Wang and Rosenberg, 1999). This is supported by the observation that transplantation of impure islets, such as those still attached to acinar or matrix tissues, has superior outcomes compared to the use of pure islet preparations possibly due to the trophic effect of the cell matrix on islet mass (Metrakos et al., 1993; Kerr-Conte et al., 1996). Although the lost ECM layer is replaced in vitro

after several days in culture, the new matricellular proteins are of different compositions to those in vivo and the effect of matrix variability on graft failure is not yet known (Londono et al., 2016). In addition, loss of ECM leads to disruption of islet microvasculature, causing increased islet cell death in vitro as a result of reduced oxygen supply (Irving-Rodgers et al., 2014). Strategies that improve islet survival, such as incubating them on ECM derived from fibroblasts or tumour cells, have been reported (Jalili et al., 2011; Tsuchiya et al., 2015), but they do not effectively translate to improved clinical outcomes, possibly as a result of ECM variability and uncertainty in their compositions.

Increased knowledge of individual ECM components, as well as the composition of the final transplant preparations is necessary to ensure that appropriate trophic support is supplied. Although the effect of complex matrices and the commonest members of the basement membrane on β-cell survival, proliferation and insulin secretion are well documented (Stendahl et al., 2009; Daoud et al., 2010; Weber et al., 2008; Wang and Rosenberg, 1999), the role of collagen III in islet function is not yet clear. It was reported in Chapter 3 that collagen III was not localised to the β cells but was found within the peri-islet capsule and islet blood vessels, supporting a previous report that collagens, including collagen III, are produced by the vascular endothelial cells (Nikolova et al., 2006). Collagen III is a ligand for GPR56 in the developing brain where it couples to $G_{\alpha 12/13}$ to elicit RhoA signalling (Iguchi et al., 2008; Luo et al., 2011). Since nearly all β cells are in contact with vascular endothelial cells and peri-vascular BM (Bonner-Weir, 1988; Peiris et al., 2014), and given the proximity of collagen III to the β cells, it was hypothesised that a paracrine activation of GPR56 by collagen III is likely, and GPR56-collagen III interactions may be physiologically relevant in islet functions.

6.2 Aims

The aims of this chapter were to:

- Determine whether GPR56 is necessary for β-cell adhesion.
- Investigate the effect of exogenous collagen III on β-cell adhesion, proliferation and survival.

- Determine whether incubation of islets with collagen III potentiates glucose-induced insulin secretion and whether this is via activation of GPR56 using islets isolated from GPR56KO mice.
- Define the mechanisms by which collagen III induces insulin secretion.

6.3 Methods

6.3.1 Quantification of GPR56 mRNA expression in MIN6 pseudoislets

Pseudoislets were formed by culturing 150,000 MIN6 β-cells in uncharged 9cm petri dishes for 7 days in DMEM, supplemented with 10% fetal bovine serum. In parallel, 150,000 MIN6 β-cells were grown as adherent monolayers for 7 days. Total RNAs were extracted from pseudoislets and adherent MIN6 β-cells, and reversed transcribed to cDNAs. GPR56 expression in the pseudoislets and adherent MIN6 β-cells was quantified by qPCR as described in Section 2.3.5.

6.3.2 Adhesion assay

MIN6 β-cells of approximately 80% confluency were maintained in FBS-free DMEM for 8 h prior to the adhesion assay. To determine the number of cells required for adhesion assay, MIN6 β-cells were seeded into a 96-well plate at densities ranging from 10,000 to 100,000 cells and allowed to adhere for 90 min at 37^0C. Unattached cells were washed off and adherent cells were fixed and quantified by a colorimetric assay of crystal violet binding to DNA as described in Section 2.7.1. The assay was then repeated using 96-well plates pre-coated with collagens I, III and IV.

6.3.3 Apoptosis and proliferation assays

Groups of 20,000 MIN6 β-cells per well were cultured in media containing 2% FBS in the presence or absence of 100nM collagen III for 48 h, with subsequent 20h incubation in the presence or absence of a cytokine cocktail (1U/μl TNF-α, 0.05U/μl IL-1β and 1U/μl IFN-γ). Apoptosis was determined by measuring caspase 3/7 activities as described in Section 2.7.2. Proliferation of β-cells *in vitro* was determined by BrdU incorporation using a colorimetric BrdU ELISA kit as described in Section 2.7.4. Groups of 20,000 MIN6 β-cells were incubated in the

presence or absence of 100nM collagen III for 48 h before being labelled with 100μM BrdU for 4h at 37^0C. For the proliferation assay, cells cultured in 10% FBS served as positive control.

6.3.4 Single cell calcium microfluorimetry

MIN6 β-cells were seeded at a density of 100,000 cells on acid-ethanol washed coverslips and incubated overnight at 37^0C in DMEM supplemented with 10% FBS. The cells were incubated with 5μM of the calcium fluorophore Fura-2AM for 30 min before being perifused with physiological solution containing 2mM or 20mM glucose in the presence or absence of collagen III or IV. Some experiments were carried out in the presence of 1mM EGTA to remove extracellular calcium from the buffer. Cells were alternatively exposed to light at 340nm and 380nm and emitted light was filtered at 510nm to determine changes in $[Ca^{2+}]i$ (Section 2.8.1).

6.3.5 Islet isolation

For insulin secretion experiments, islets were isolated from ICR mice, GPR56KO mice and age-matched GPR56WT mice using collagenase digestion of the pancreas (Bowe et al., 2013). Islets were cultured overnight in RPMI medium supplemented with 10% NCS and 100U/ml penicillin/0.1mg/ml streptomycin prior to use.

6.3.6 Static insulin secretion

To determine the acute effect of collagen III on insulin secretion, islets isolated from male ICR mice were incubated in physiological solution containing 2mM or 20mM glucose in the presence or absence of 100nM collagen III for 1 hour and insulin secretion was determined by radioimmunoassay. In parallel experiments to assess the chronic effect of collagen III on insulin secretion, islets were cultured on dishes coated with 100nM collagen III for 48 h before being retrieved and exposed to buffer supplemented with either 2mM or 20mM glucose for 1 hour. Insulin secretion was determined by radioimmunoassay.

6.3.7 Dynamic insulin secretion

To determine whether collagen III acts via GPR56 to increase insulin secretion, the dynamic secretory profile of islets isolated from GPR56KO mice and from their WT littermates to 2mM and 20mM glucose in the presence or absence of 100nM collagen III was determined.

Perifusate was collected every 2 min and insulin secretion was quantified by radioimmunoassay.

6.3.8 Statistical analysis

Statistical analysis was determined either with Student's t-test or ANOVA, as appropriate. Data are represented as mean ± SEM. $p<0.05$ was considered significant.

6.4 Results

6.4.1 Expression of GPR56 mRNA in MIN6 pseudoislets

Adhesion receptors and ECM components provide cell-cell cohesion and are necessary for maintaining structural configuration of tissues (Nagata et al., 2001). Since islets are three-dimensional organs of tightly packed cells, it is possible that adhesion GPCRs play a role in the adhesiveness of these cells. It was hypothesised that the expression of GPR56, being an adhesion receptor, will be higher in a model of β-cell aggregates known as pseudoislets compared to MIN6 β-cell monolayers. Pseudoislets are spherical 'islet-like' clusters that are formed when MIN6 β-cells are cultured on uncharged surfaces or on petri dishes coated with gelatin (Figure 6-1 B). Pseudoislets are known to have increased expression of adhesion receptors such as E-cadherin (Hauge-Evans et al., 1999). Using quantitative PCR, the expression of GPR56 mRNA in pseudoislets was found to be about 125% higher than in MIN6 β-cells (Figure 6-1 C). However, the difference was not statistically significant when the means of three independent experiments were averaged ($p=0.2$). In future studies, deletion or knockdown of GPR56 in MIN6 β-cells is required to confirm whether it is necessary for β-cells to form pseudoislets.

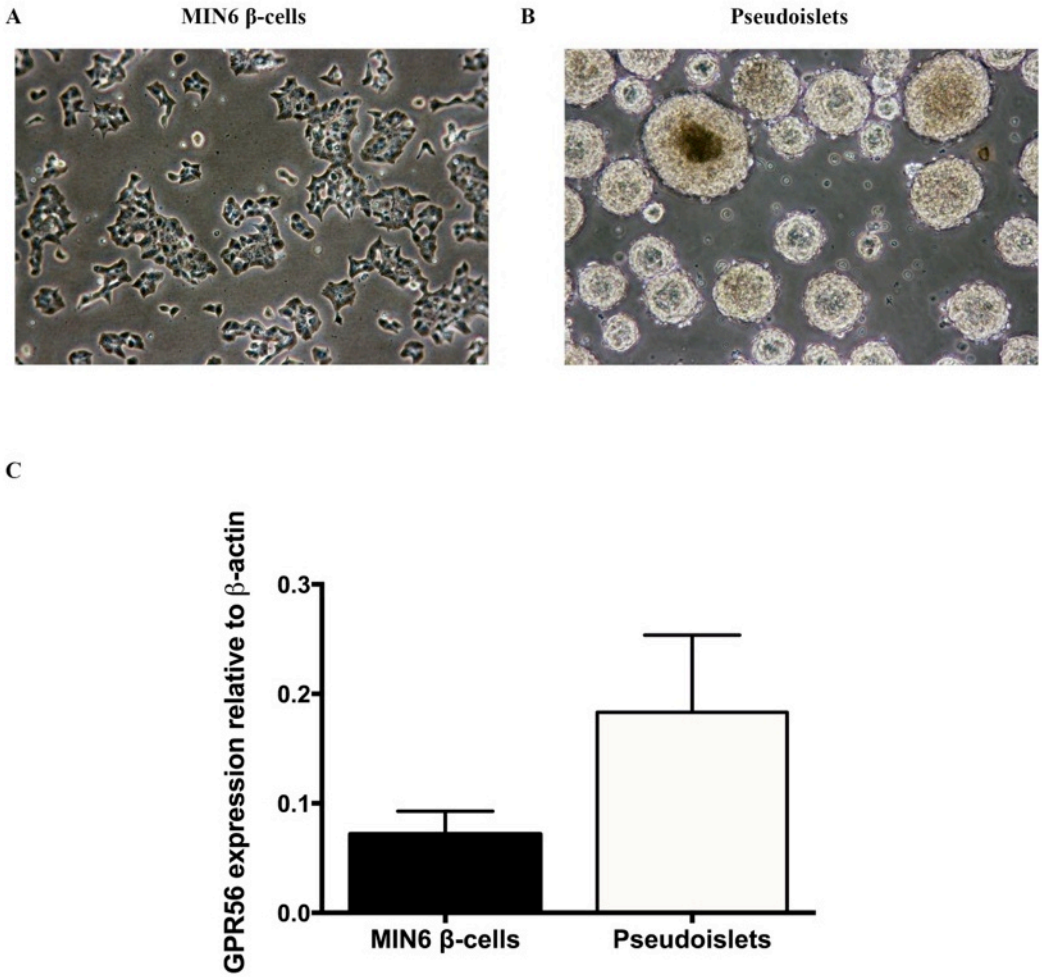

Figure 6-1 Expression of GPR56 mRNA in MIN6 pseudoislets. A) Equal numbers of MIN6 β-cells were grown as adherent monolayers or B) on uncharged petri dishes to form pseudoislets after 7 days in culture. RNAs were extracted and reversed transcribed into cDNAs. Expression of GPR56 was quantified by qPCR. C) Bar graph shows the expression of GPR56 mRNA in MIN6 β-cells and pseudoislets relative to β-actin. Data are presented as Mean + SEM, n=3 independent experiments, p=0.2, Student's t-test.

6.4.2 Validation of the β-cell adhesion assay

Given that GPR56 is an adhesion receptor activated by collagen III (Luo et al., 2011), it was investigated whether collagens increased the adhesiveness of β-cells. To do this, a crystal violet-based adhesion assay was first validated by determining the minimum density of MIN6 β-cells required to yield optimum adhesion. Non-adherent cells were washed off while adherent β-cells were quantified by a colorimetric method. As shown in Figure 6-2, there was a gradual increase in the absorbance of cells retaining the dye as the cell density increased. At a density of 30,000 cells, the absorbance of adherent cells was significantly higher ($p<0.05$) than at 10,000 cells. However, at cell densities above 30,000, there was no corresponding increase in

cell adhesion as measured by changes in absorbance, suggesting that 30,000 cells is the optimum cell density to achieve adequate MIN6 β-cell adhesion in a 96-well plate.

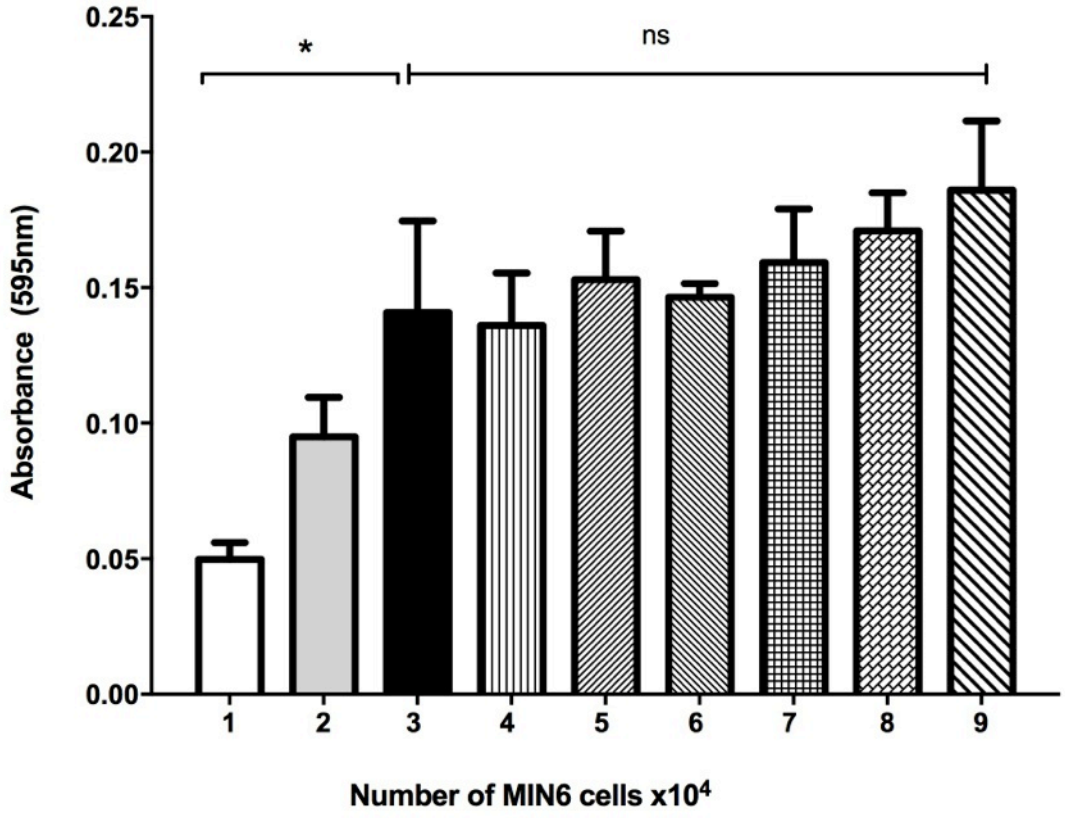

Figure 6-2 Determining the lowest density of MIN6 cells with optimum adhesion. Serum-starved MIN6 cells were seeded at densities ranging from 1 x10^4 to 9 x10^4 cells on 96-well plates and incubated for 90 min. Non-adherent cells were washed off while adherent MIN6 β-cells were fixed and quantified by a colorimetric assay involving crystal violet binding to DNA where absorbance was quantified at 595nm. Data are mean + SEM, n=5, *p<0.05, ns = not significant, One-Way ANOVA with Tukey's multiple comparisons test.

6.4.3 Effects of collagens on β-cell adhesion

Having validated that 30,000 cells is the optimum cell density for the MIN6 β-cell adhesion assay, the effect of collagens on β-cell adhesion was investigated. Collagens, being structural components of the ECM, may play a role in the three dimensional architecture of islets by enabling β-cells to adhere to themselves and other cell types in vivo. To test this hypothesis in

vitro, MIN6 β-cells were seeded at a density of 30,000 cells on petri dishes pre-coated with 100nM collagens I, III and IV. Collagens I and III did not have any effect on β-cell adhesion ($p>0.2$) at 100nM. However, collagen IV produced a statistically significant increase in β-cell adhesion ($p<0.01$) as measured by increased absorbance at 595nm as a result of crystal violet binding to DNA of adhered cells compared to the BSA control (Figure 6-3). This may highlight one of the differences between the three collagen subtypes: collagens I and III belong to the same class of fibre-forming collagens while collagen IV is a structural collagen of the basement membrane.

In addition, when mouse islets were cultured on dishes coated with collagen III or IV for 72 h in serum-free media and observed via light microscopy, differences in islet morphology were evident (Figure 6-4). Islets cultured on uncharged petri dishes were intact but loosely attached cells were visible (Figure 6-4 A). Islets cultured on 100nM collagen III had the best morphology with few loose cells and no cell spreading (Figure 6-4 B). However, islets cultured on 100nM collagen IV exhibited cell recruitment to collagen IV although the overall islet integrity was not compromised (Figure 6-4 C). Cell recruitment was more pronounced at 200nM collagen IV (Figure 6-4 D) and at this higher concentration islets were strongly attached to the dishes and were difficult to remove.

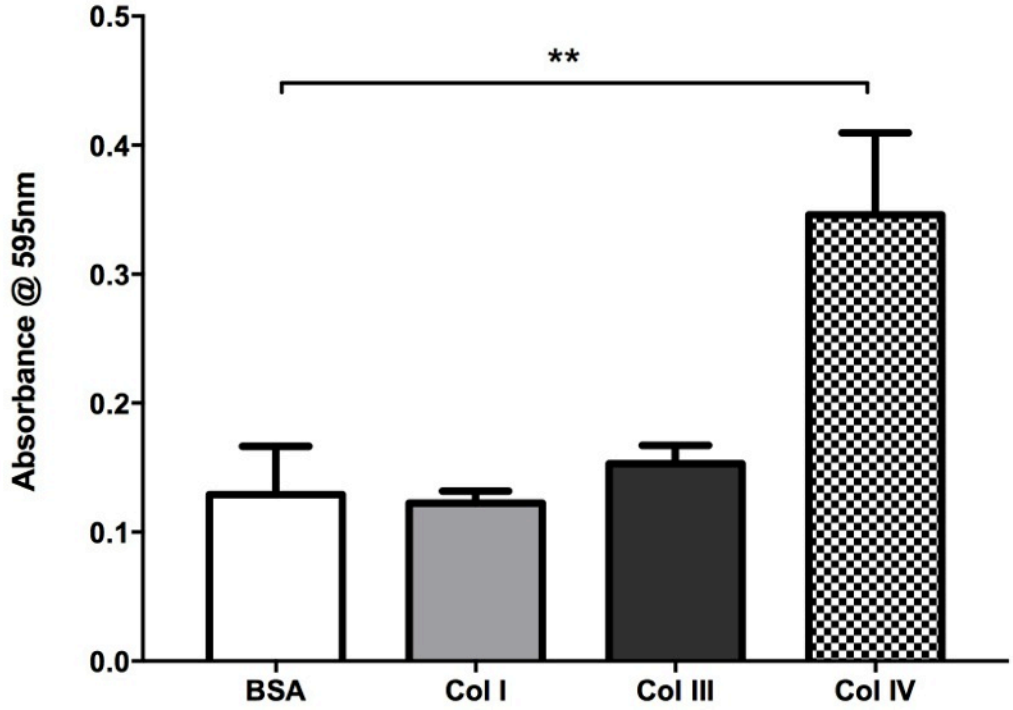

Figure 6-3 Adhesion of MIN6 β-cells to ECM components. Serum-starved MIN6 β-cells were seeded onto 96-well plates coated with 100nM collagens I, III, IV, or 0.5% BSA at a density of 30,000 cells/well and allowed to adhere for 90 min. Non-adherent cells were washed off. Adherent MIN6 β-cells were fixed and quantified by a colorimetric assay involving crystal violet binding to DNA. Data are mean + SEM, n=3 independent experiments, **p<0.01, One-way ANOVA with Dunnett's multiple comparisons test.

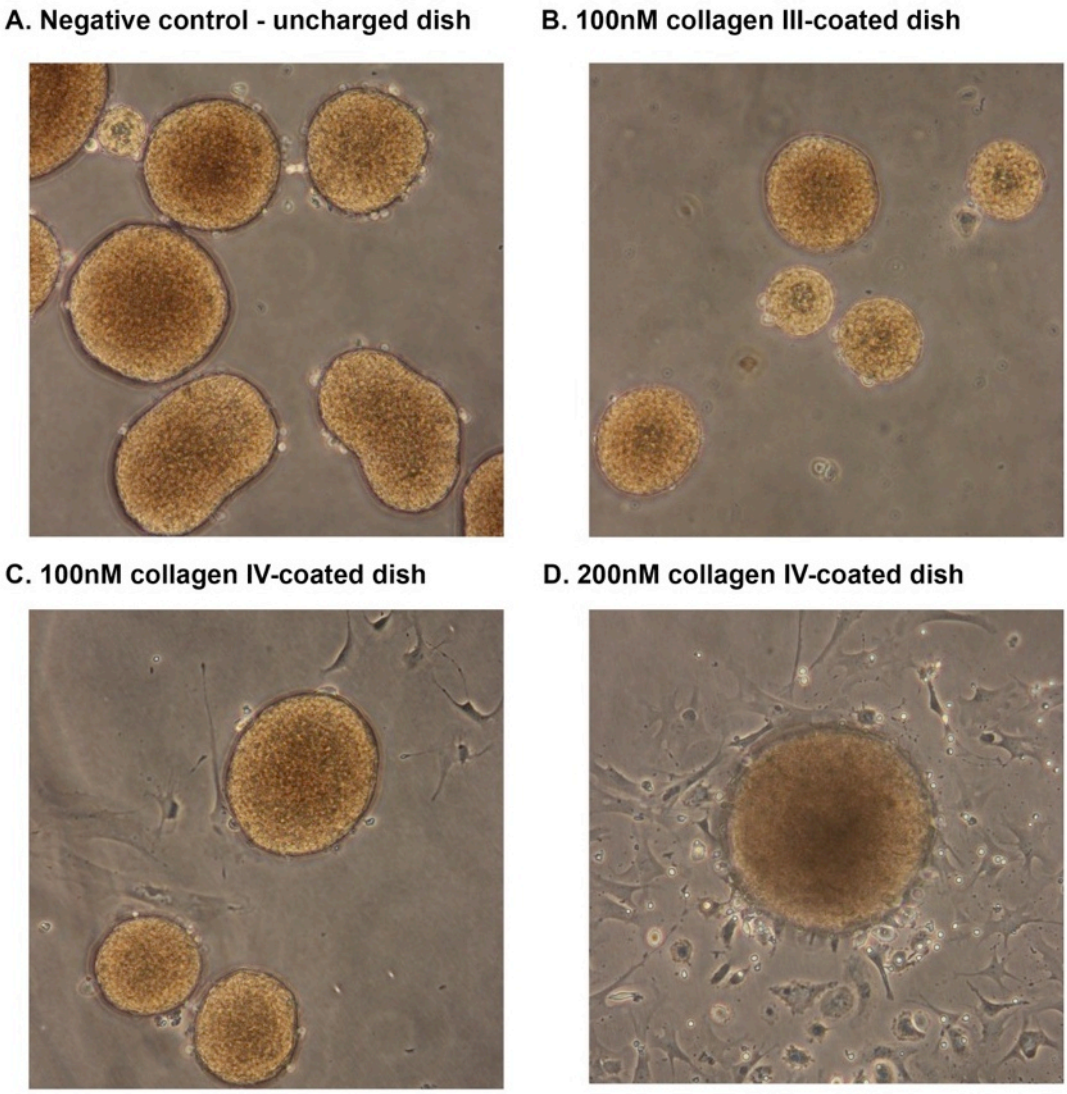

Figure 6-4: Phase contrast images of islets cultured in serum-free media for 72h on A) uncharged petri dishes B) uncharged petri dishes coated with 100nM collagen III C) uncharged petri dishes coated with 100nM collagen IV and D) uncharged petri dishes coated with 200nM collagen IV. All images were taken at 10X.

6.4.4 Effect of collagen III on β-cell apoptosis

Increased β-cell apoptosis is central to the progression of both T1D and T2D and it is one of the main drivers of decreased islet mass (Butler et al., 2003; Cernea and Dobreanu, 2013). Factors that promote cell survival are therefore beneficial for improved β-cell function in people with diabetes. To investigate whether collagen III had any effect on β-cell apoptosis, MIN6 β-cells were exposed to collagen III for 48 h, a time-course selected to ensure uniformity with the proliferation and chronic insulin secretion assays in this chapter. As shown in Figure 6-5, collagen III produced a modest decrease in basal apoptosis ($p>0.2$). However, when apoptosis was induced by a cocktail of cytokines in the continued presence of collagen III, there was a significant decrease in β-cell apoptosis ($p<0.01$), suggesting that collagen III may protect β-cells from environmental insults.

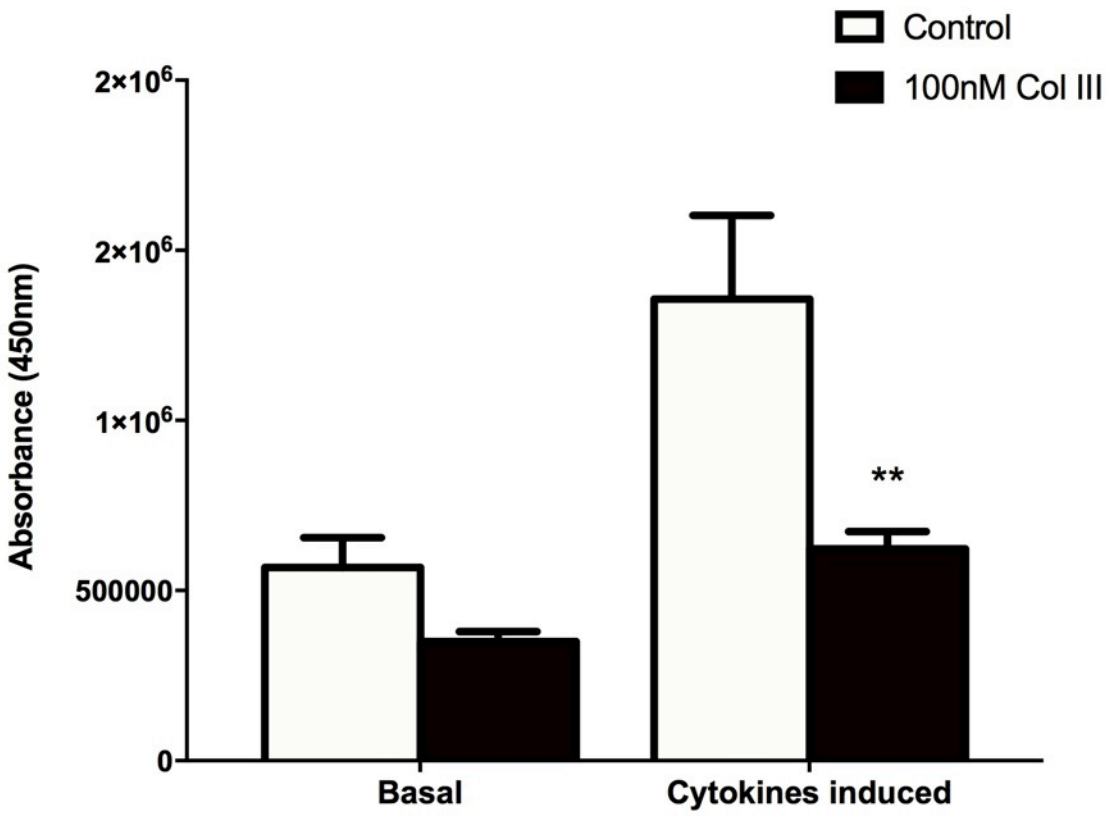

Figure 6-5 Effect of collagen III on β-cell apoptosis. Groups of 20,000 MIN6 β-cells were cultured in media for 48 h in the presence or absence of collagen III. They were subsequently incubated for a further 20 h in the presence or absence of cytokines before caspase 3/7 activities were measured by a luminescence based method. Data are presented as mean + SEM, n=5, **p<0.01, Two-Way ANOVA with Bonferroni's post-hoc test.

6.4.5 Effect of collagen III on β-cell proliferation

Having demonstrated in Chapter 5 that loss of GPR56 led to decreased β-cell proliferation in postnatal mice, it was investigated whether collagen III, a GPR56 agonist, had any effect on β-cell proliferation. MIN6 β-cells were serum-starved and cultured in media in the presence or absence of 100nM collagen III for 48 h. MIN6 β-cells cultured in the presence of 10% FBS served as a positive control. Replicating β-cells were labelled for 4 h with 100μM BrdU and quantified by a colorimetric ELISA method. 100nM collagen III had no effect on β-cell proliferation (Figure 6-6) whereas 10% FBS produced a significantly increased β-cell proliferation ($p<0.01$), as expected.

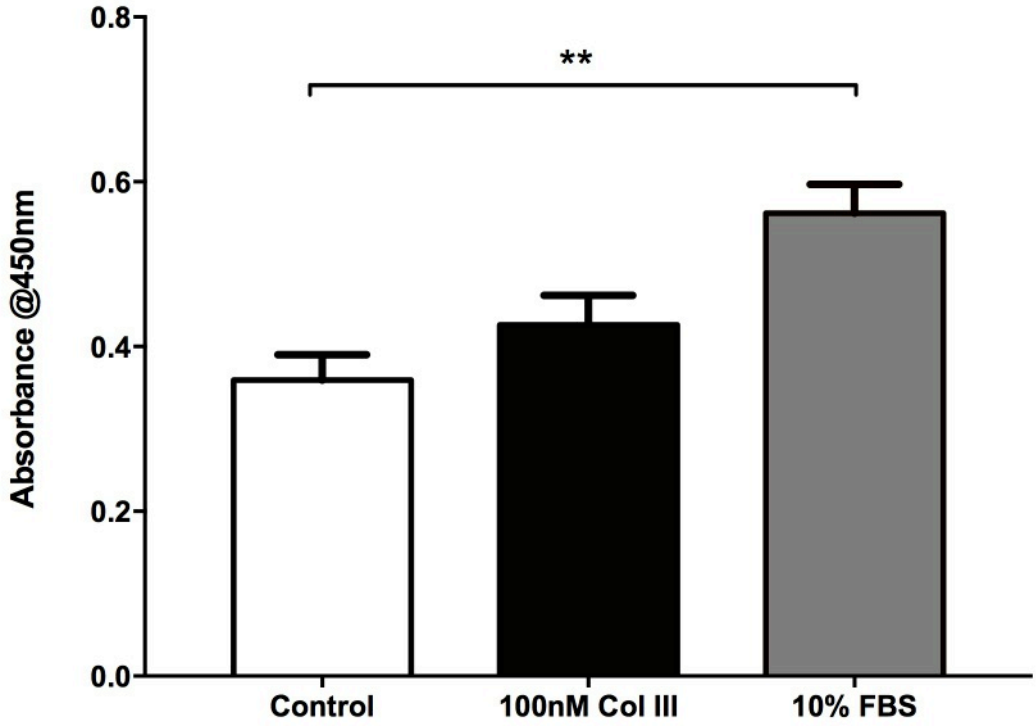

Figure 6-6 Effect of collagen III on β-cell proliferation. MIN6 cells were cultured in media containing 2% FBS in the presence or absence of collagen III for 48 h before being labelled with BrdU for 4 h. Cells grown in media containing 10% FBS served as a positive control. Proliferating cells labelled with BrdU were determined with a BrdU ELISA. Data are presented as Mean + SEM, n=4 independent experiments, **p<0.01, One-Way ANOVA with Bonferroni's post-hoc test.

6.4.6 Effect of collagens III and IV on intracellular calcium levels

It is well known that elevation of cytosolic calcium is critical for insulin release. To investigate whether collagen III had any effect on β-cell calcium levels, calcium microfluorimetry experiments were carried on MIN6 β-cells exposed to 1nM, 10nM, 100nM and 1μM of collagen III, and real-time changes in cytosolic calcium concentration ($[Ca^{2+}]i$) were measured (Figure 6-7). At 1nM collagen III, there was no change in $[Ca^{2+}]i$. However, collagen III produced reversible increases in cytosolic calcium at 10nM, 100nM and 1μM. The effect of collagen III on $[Ca^{2+}]i$ was not concentration-dependent as there was no difference in the basal to peak responses when 10, 100 and 1μM of collagen III were administered ($p>0.2$). Subsequent exposure of MIN6 β-cells to ATP produced a rapid and short-lived increase in cytosolic calcium while tolbutamide produced a more robust and sustained increase as expected. The ability of ATP and tolbutamide to elevate $[Ca^{2+}]i$ after the cells had been exposed to varying concentrations of collagen III indicated that the cells were viable and collagen III was not toxic to them. Since collagen III activates GPR56 at 84nM in neuronal cells (Luo et al., 2011), subsequent experiments were carried out with 100nM collagen III. Collagen IV also caused an increase in cytosolic calcium in MIN6 β-cells at 100nM (Figure 6-8).

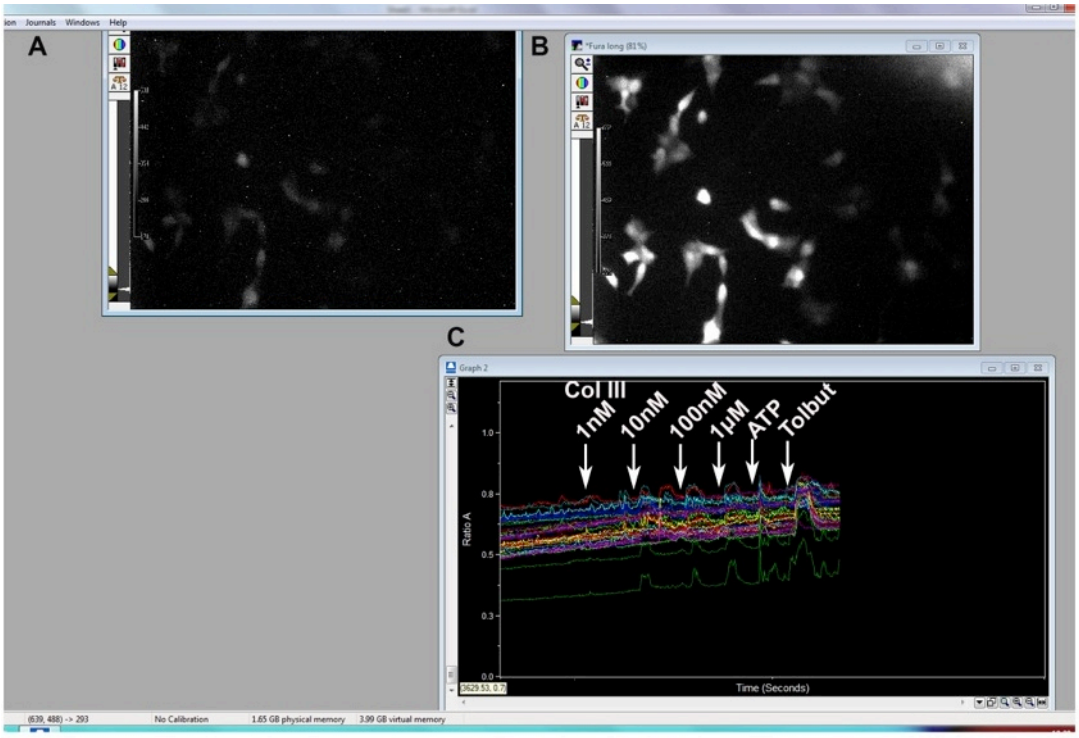

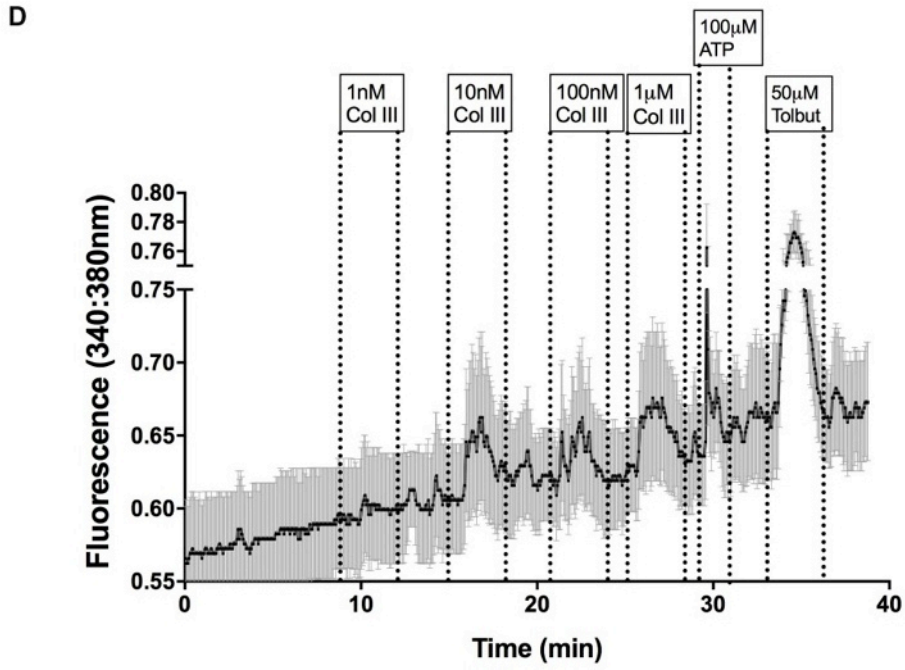

Figure 6-7: Concentration-dependent effects of collagen III on cytosolic calcium levels in MIN6 β-cells. MIN6 cells were loaded with Fura-2 and perifused with physiological solutions supplemented with different concentrations of collagen III at the indicated time points. A) & B) Screenshots of fura-2-loaded MIN6 β-cells at two fluorescence wavelengths, fura-short and fura-long respectively. C) A screenshot of the calcium imaging software showing the response of individual MIN6 β-cells to the various test agents. D). Mean fluorescence ratio of the cells was plotted against time. ATP and tolbutamide were used as positive

controls to check the viability of MIN6 cells at the end of the experiment. Changes in intracellular calcium were expressed as 340/380nm ratiometric data. Data are expressed as mean ± SEM, n=3 cells.

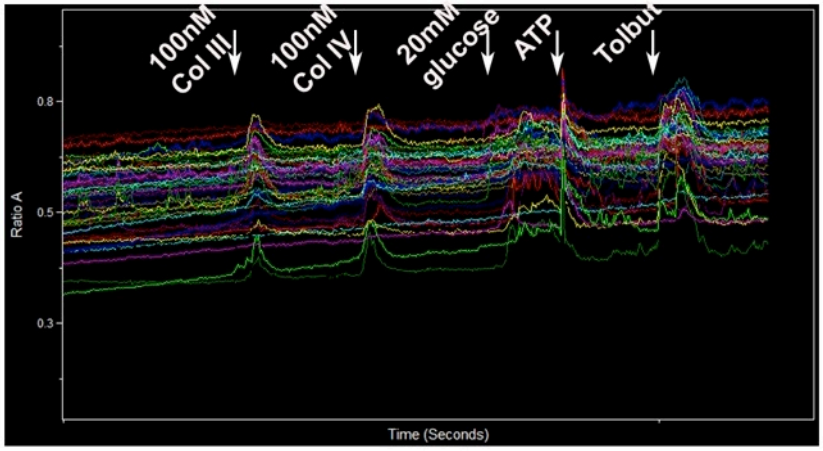

Figure 6-8: Effect of collagens III and IV on $[Ca^{2+}]i$ in MIN6 β-cells. MIN6 β-cells were loaded with Fura-2 and perifused with physiological buffers containing 100nM collagen III, 100nM collagen IV, 100μM ATP and 50μM tolbutamide at the indicated time points. ATP and tolbutamide were used as positive controls to check the viability of the MIN6 cells. Changes in intracellular calcium are expressed as 340/380nm ratiometric data. n=31 cells.

6.4.7 Effects of collagens on preproinsulin gene expression

Since the primary function of the β-cells is to secrete insulin, the effect of collagens on preproinsulin gene expression was investigated. MIN6 β-cells were incubated with 100nM collagens I, III and IV for 7 days while equal numbers of MIN6 β-cells in culture in the absence of collagens served as a control. Since MIN6 β-cells were derived from mouse, expression of the Ins1 gene was evaluated since it is a rodent-specific retrogene, derived from the partially processed mRNA of Ins2 (Shiao et al., 2008). Quantification of Ins1 showed that irrespective of the collagen subtypes used, there was a significant increase in insulin gene expression (Figure 6-9).

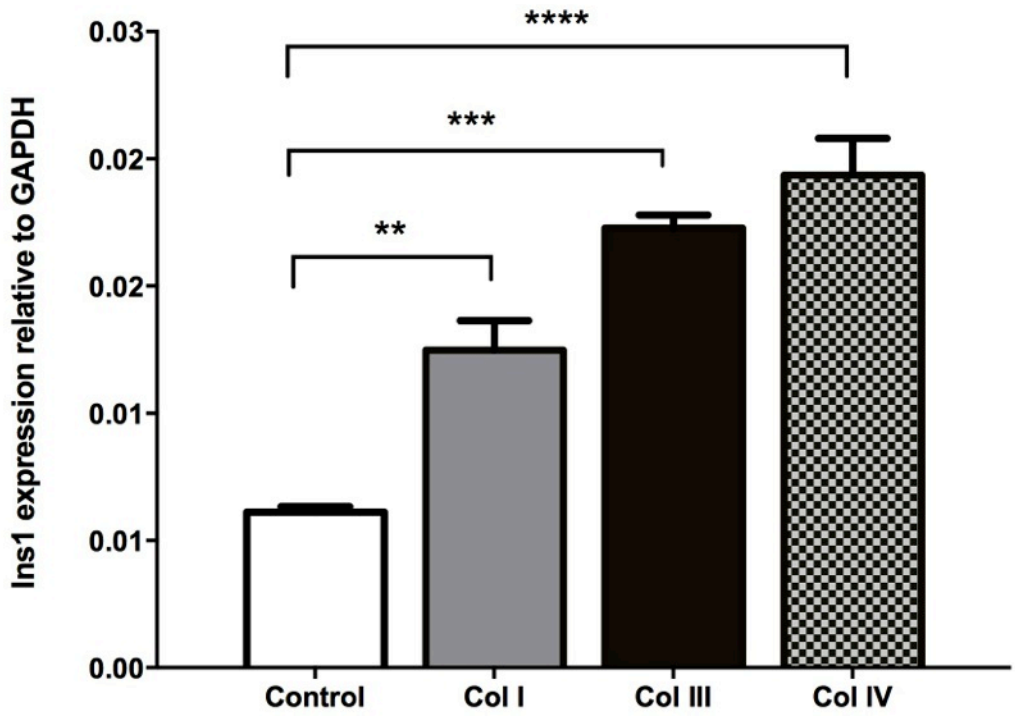

Figure 6-9 Effect of ECM components on insulin gene expression. MIN6 cells were cultured on dishes coated with 100nM of collagens I, III, or IV for 7 days. On day 7, RNAs were extracted from each sample and reverse-transcribed. Quantitative RT-PCR was carried out using the Pfaffl method of relative quantification. Results represent the mean change in Ins1 gene expression relative to GAPDH + SEM, n=3, **p<0.01, ***p<0.001, ****p<0.0001 compared to basal insulin expression, One-Way ANOVA with Bonferroni's post-hoc test.

6.4.8 Acute effect of collagen III on insulin secretion

To investigate the effect of collagen III on insulin secretion, isolated mouse islets were incubated in physiological solution containing 2mM or 20mM glucose in the presence or absence of 100nM collagen III at 37^0C. After 1 h incubation, the tubes containing islets were placed on ice to inhibit further insulin release. Quantification of insulin secretion from the supernatant showed that collagen III had no effect on basal insulin secretion at 2mM glucose (Figure 6-10). The islets responded appropriately to 20mM glucose with a 5 fold increase over basal insulin secretion and 100nM collagen III substantially potentiated glucose-induced insulin secretion ($p<0.05$).

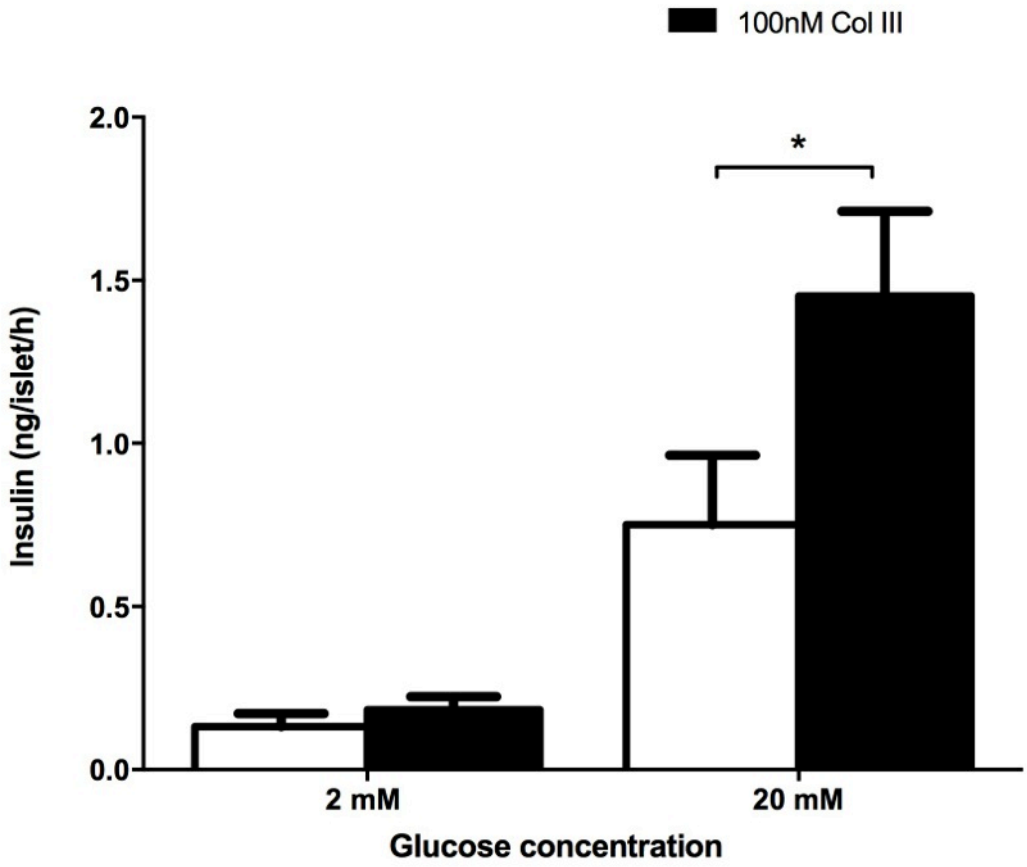

Figure 6-10 Acute effect of collagen III on insulin secretion from mouse islets. Insulin secretion was determined by radioimmunoassay. Data are presented as Mean + SEM, *p<0.05, n = 3 independent experiments, Two-way ANOVA with Bonferroni's post-hoc test.

6.4.9 Chronic effect of collagen III on insulin secretion

Although β-cells interact directly with ECM in both mouse and human islets, mechanisms exist to prevent continuous activation of ECM receptors such as through the remodelling of ECM to either expose or hide ECM recognition sites. Since components of the ECM are in close proximity to the β-cells, the long-term effect of collagen III on insulin secretion was therefore investigated in vitro and it was also determined whether chronic incubation of islets with collagen III had any effect on insulin content. Islets were incubated on collagen III coated dishes or dishes coated with vehicle for 48 h, after which islets were retrieved and challenged with glucose. At 2mM glucose, there was no change in insulin secretion in islets pre-exposed to collagen III (Figure 6-11 A), similar to what was observed when islets were acutely challenged with collagen III at a sub-stimulatory glucose concentration. There was also a significant

potentiation of glucose-induced insulin secretion in islets previously incubated with collagen III to a similar extent to that observed in the acute collagen III exposure experiment (Figure 6-11 A). To determine whether the increased insulin secretion was as a result of changes in insulin content, islets were lysed in acidified ethanol to extract insulin. As shown in Figure 6-11 B, there was no change in insulin content of islets that were pre-treated for 48 h with collagen III at 2mM and 20mM glucose, suggesting that the increased secretion was as a result of increased release of pre-existing stored insulin rather than synthesis of new insulin.

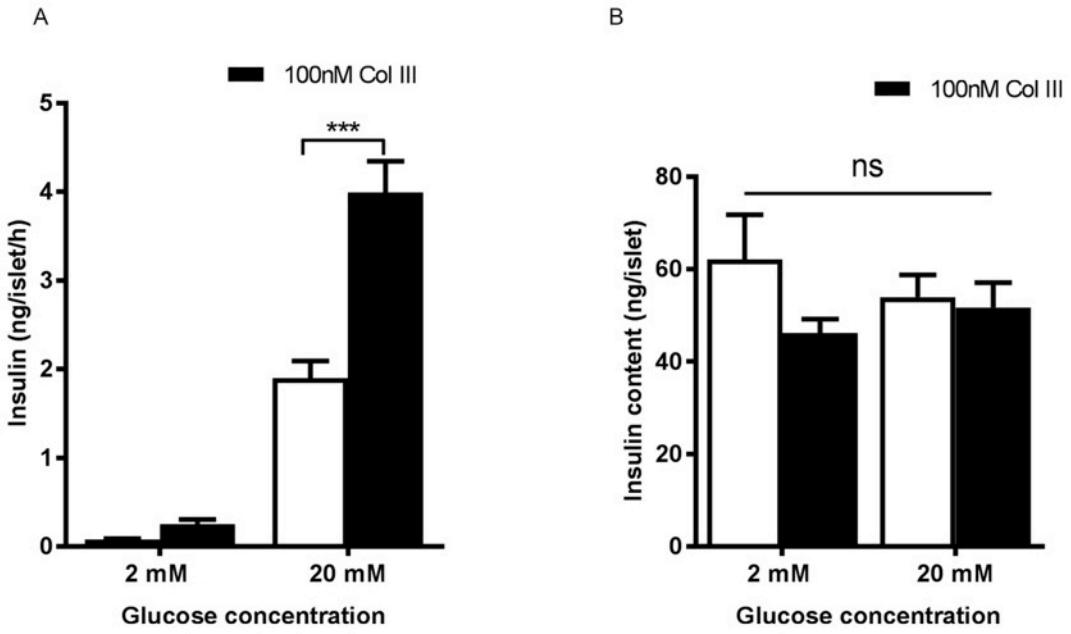

Figure 6-11 Chronic effect of collagen III on insulin secretion. A) Isolated islets were cultured on vehicle or collagen III-coated dishes for 48 h after which they were retrieved and challenged with 2mM or 20mM glucose for 1 h. Insulin secretion was quantified by radioimmunoassay. B) Groups of 10 islets from the treatment groups in A) were lysed in acidified ethanol to extract their insulin. Insulin content was determined by radioimmunoassay and normalised per islet. Data are presented as Mean + SEM, n=6-8 replicates from 5 mice and representative of two independent experiments, ***p<0.001, ns = not significant, Two-Way ANOVA with Bonferroni's post-hoc test.

6.4.10 Collagen III-induced insulin secretion depends on extracellular calcium influx

Calcium-induced exocytosis of insulin granules is the primary determinant of insulin secretion (Rorsman and Renström, 2003). There are two sources of intracellular Ca^{2+} in β-cells: influx of calcium ions through voltage-dependent calcium channels following membrane depolarisation, which is the main route of Ca^{2+} entry and, secondly, mobilisation of Ca^{2+} ions from the endoplasmic reticulum store (Jones and Persaud, 2010). To test whether collagen III can augment the glucose-induced increase in cytosolic calcium, Fura-2 loaded MIN6 β-cells were perifused with physiological buffers supplemented with 20mM glucose, with or without 100nM collagen III. As shown in Figure 6-12 A (upper line), exposure of β-cells to 20mM glucose elicited an increase in $[Ca^{2+}]i$ followed by an additional ~50% increase in basal to peak ratio in the presence of collagen III (Figure 6-12 C). The increase in cytosolic Ca^{2+} concentration was reversible upon withdrawal of collagen III. Collagen III is therefore able to augment glucose-induced $[Ca^{2+}]i$ concentration and the cells also responded appropriately to ATP and tolbutamide indicating that they were still viable.

To investigate the source of the cytosolic Ca^{2+}, the experimental protocol was repeated by perifusing MIN6 β-cells with calcium-free physiological solution supplemented with 1mM EGTA, to chelate any available calcium in the buffer. In the absence of extracellular calcium, 20mM glucose, collagen III and tolbutamide were unable to increase cytosolic Ca^{2+}, indicating that influx of extracellular calcium is the primary source of elevated $[Ca^{2+}]i$ with these agonists. ATP, on the other hand, caused an increase in cytosolic Ca^{2+} in the absence of extracellular calcium, indicating that it mobilises Ca^{2+} from internal stores consistent with its action as a purinergic receptor agonist (Figure 6-12 A: lower line). However, the magnitude of the peak was considerably lower compared to the presence of calcium, indicating that calcium-induced calcium release from the ER store is likely to play a role in ATP action.

Using a temperature-controlled perifusion system, it was next investigated whether collagen III-induced calcium influx is required for its stimulatory effects on insulin secretion, and whether removal of calcium had any effect on collagen III-induced insulin secretion. Isolated mouse islets were perifused with physiological buffer containing 2mM or 20mM glucose with or without extracellular calcium. In the presence of calcium, 20mM glucose induced an approximately 2

fold increase in insulin secretion. In the absence of calcium, insulin secretion was completely abolished, indicating that extracellular calcium is necessary for glucose-induced insulin secretion (Figure 6-13 A: t_{14} – t_{34} min). The increase in $[Ca^{2+}]i$ concentration caused by collagen III, as shown in Figure 6-12 A: upper line, corresponded to potentiation of glucose-induced insulin secretion in isolated islets (Figure 6-13 A: upper line). In the absence of extracellular calcium, collagen III was still able to stimulate insulin secretion albeit at a statistically lower AUC (Figure 6-13 C). Although collagen III could not increase $[Ca^{2+}]i$ in calcium-free media as shown in Figure 6-12 A: lower line, it is possible that the peak was too small to be detected, since collagen III was able to cause an increase in insulin secretion in the absence of calcium influx. Alternatively, it is possible that the elevation in $[Ca^{2+}]i$ in response to collagen III is not required for its stimulatory effects on insulin release.

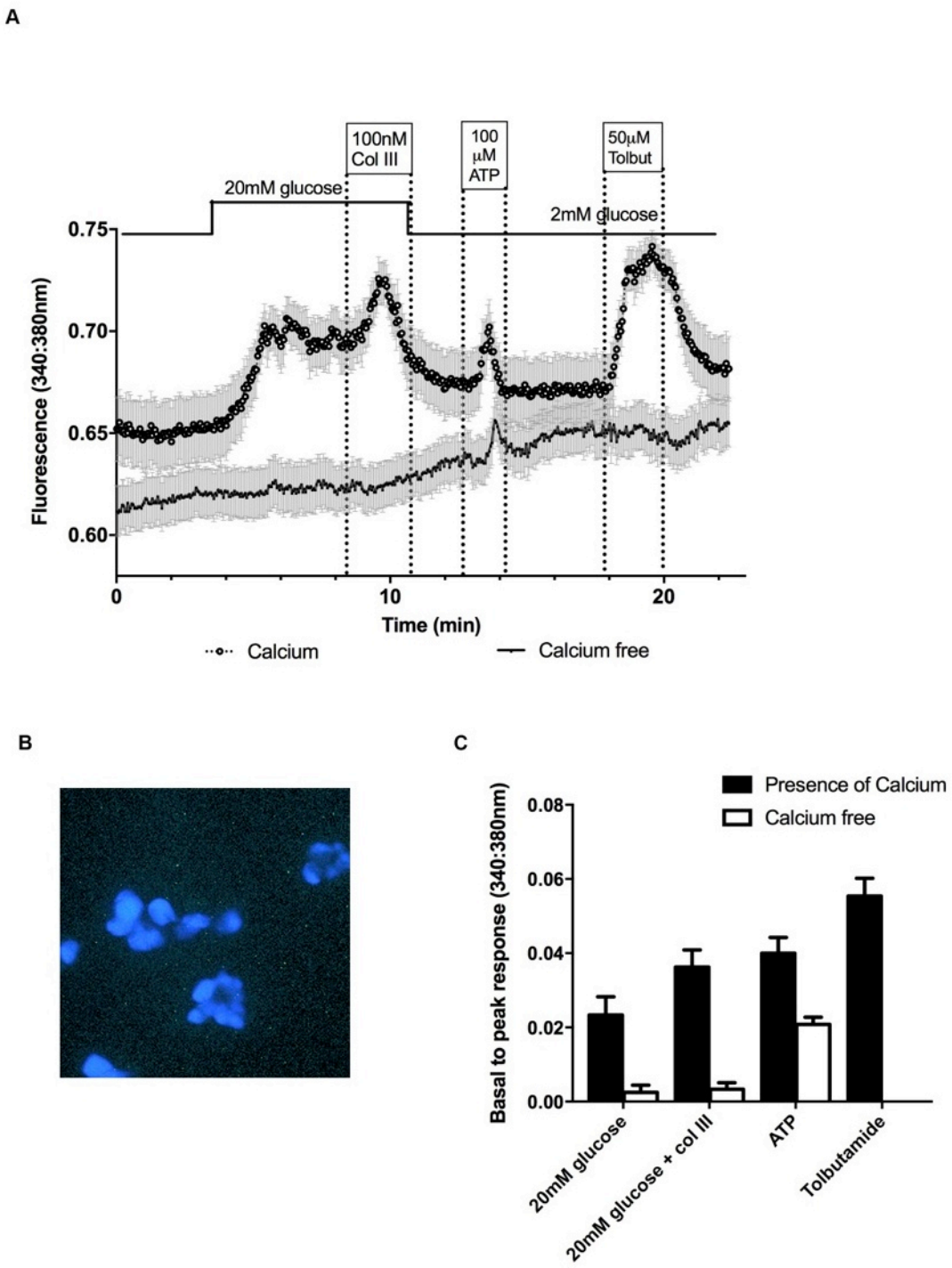

Figure 6-12: Effect of collagen III on $[Ca^{2+}]i$ in the presence or absence of extracellular calcium. A) MIN6 β-cells were loaded with Fura-2 and perifused with either calcium-free physiological buffers or buffers containing 2mM calcium, and supplemented with agonists as shown. ATP and tolbutamide were used as positive controls to check the viability of the MIN6 cells. Changes in intracellular calcium are expressed as 340/380nm ratiometric data. Data are presented as mean ± SEM, n=19 cells, representative of three separate experiments. B) Image shows fluorescent MIN6 β-cells loaded with Fura-2. C) Graph shows peak amplitude responses of MIN6 β-cells to the agonists in the presence or absence of extracellular calcium. Data are presented as mean + SEM, n=24 cells.

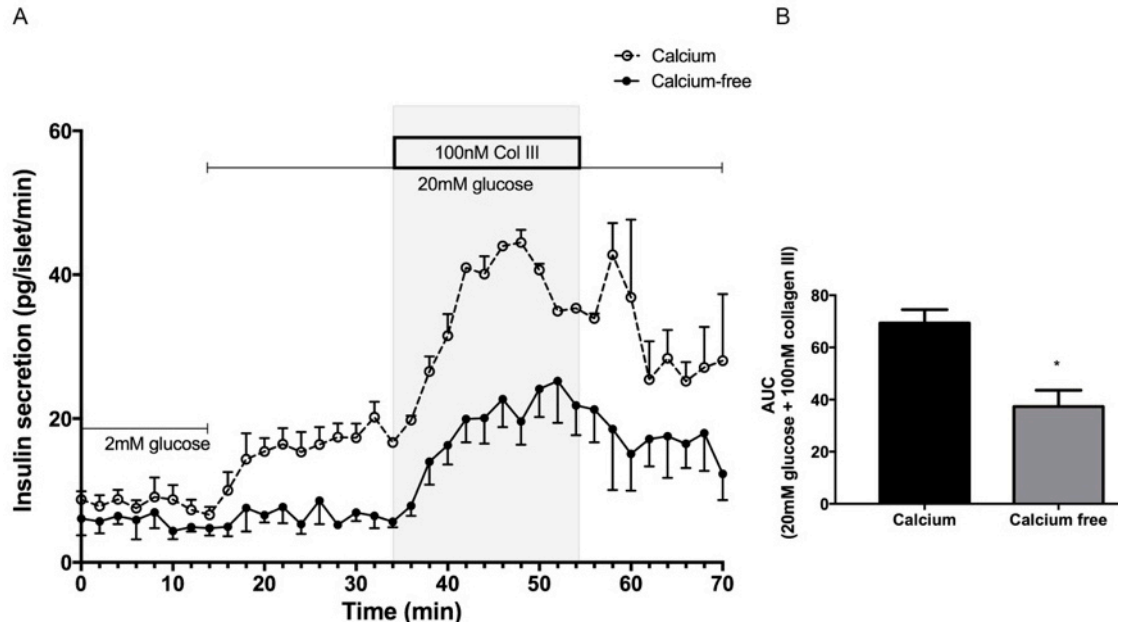

Figure 6-13: Effect of collagen III on insulin secretion in the presence or absence of extracellular calcium. Isolated mouse islets were perifused with physiological buffers supplemented with 100nM collagen III and 20mM glucose in the presence or absence of extracellular calcium. Islets were initially perifused with media containing 2mM glucose. Insulin secretion was quantified by radioimmunoassay. B) Area under the curve for collagen III-induced insulin secretion between time t34 and t54 min in the presence or absence of extracellular calcium. Data are presented as mean + SEM, n=4, *p<0.05, Student's t-test.

6.4.11 Collagen III increases insulin output via GPR56 activation

Having established that collagen III potentiates glucose-stimulated insulin secretion, it was investigated whether it does this by activating GPR56 since collagen III is a ligand of GPR56 in the developing brain (Luo et al., 2011). Dynamic insulin secretion of islets isolated from GPR56KO and GPR56WT mice were determined using the physiologically relevant temperature-controlled perifusion system. In the presence of collagen III at 2mM glucose, there was no change in insulin secretion in either WT or KO islets; further confirming the result of the static insulin secretion experiments shown in Figure 6-10 that collagen III has no effect on basal insulin secretion. Exposure of the islets to a physiological solution containing 20mM glucose produced a robust increase in insulin secretion, characterised by the classical short-lived first phase and the sustained second phase of insulin secretion (Figure 6-14). There was no difference in the response of GPR56KO and GPR56WT islets to 20mM glucose (secretion at 60 min, pg/islet: WT: 21.7 ± 2.7, KO: 17.4 ± 1.9, n=4, p>0.2), indicating that deletion of GPR56 has

no effect on the capacity of β-cells to secrete insulin at stimulatory glucose concentration. When GPR56WT islets (closed circles) were exposed to 100nM collagen III in buffer containing 20mM glucose, there was potentiation of insulin secretion and this effect was fully reversible when collagen III was removed. This augmentation of insulin secretion was not observed when GPR56KO islets were exposed to 100nM collagen III in a physiological solution containing 20mM glucose (open circles). This indicates that the potentiation of glucose-stimulated insulin secretion in the presence of 100nM collagen III was via activation of GPR56 and that collagen III is an agonist of GPR56 in mouse islets.

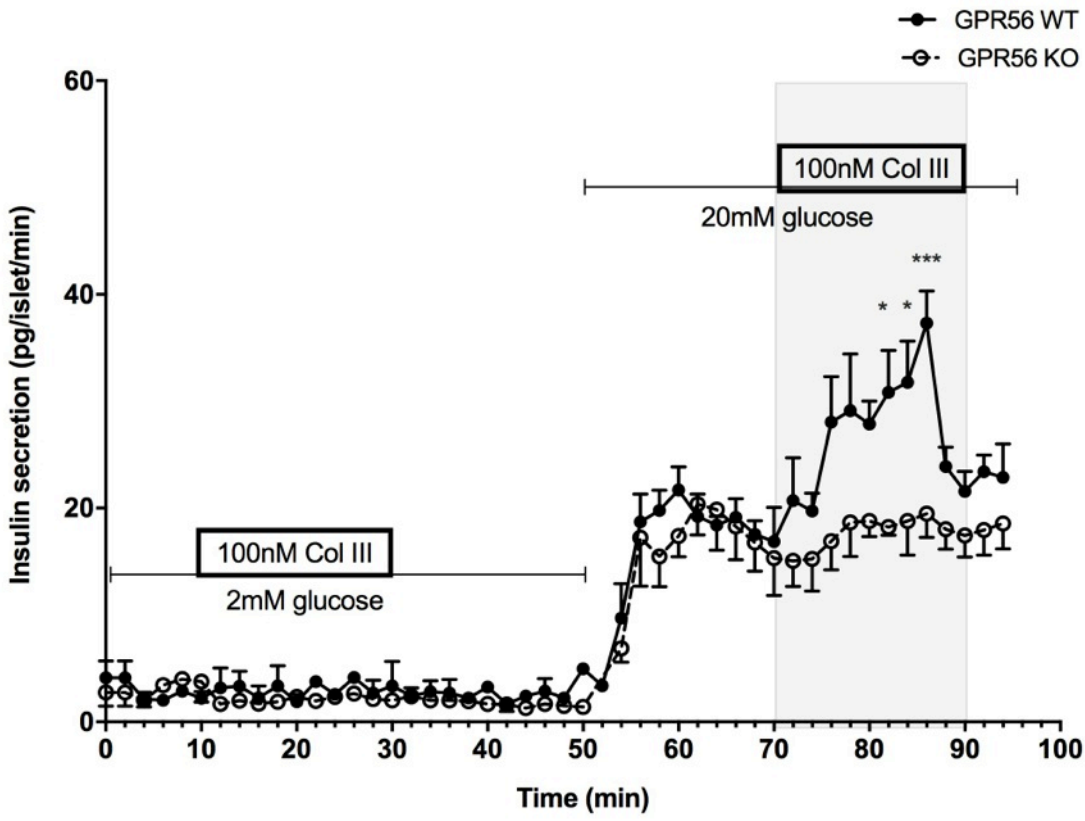

Figure 6-14 Collagen III potentiates glucose-induced insulin secretion via GPR56 activation. Islets isolated from GPR56 KO and WT mice were perifused with 2mM or 20mM glucose in the presence of 100nM collagen III at the indicated time points. Samples were collected every 2 min and insulin secretion was determined by radioimmunoassay. Data are presented as Mean + SEM, n=4 replicates of 40 islets each isolated from 5 mice per genotype and representative of three independent experiments, *p<0.05, ***p<0.001, Two-way ANOVA with Bonferonni's post-hoc test.

6.4.12 Effect of collagen III on islet RhoA activation

To investigate whether collagen III activation of GPR56 in islets signalled via the $G_{12/13}$ pathway, activated downstream RhoA was measured. Groups of 400 islets were incubated in a physiological solution containing 20mM glucose in the presence or absence of 100nM collagen III for 10 min and activated RhoA was measured by immunoblotting as described in Section 2.8.2. Exposure of islets to 20mM glucose and collagen III indicated the presence of total RhoA, but active RhoA could not be detected after a pull-down assay (Figure 6-15). Although the experiment was repeated with 600 islets, it was still not possible to detect active RhoA. It is therefore likely that the protein content in the samples was too low for active RhoA to be detected, since it has previously been reported that 20mM glucose activated RhoA in MIN6 β-cells (Liu et al., 2016).

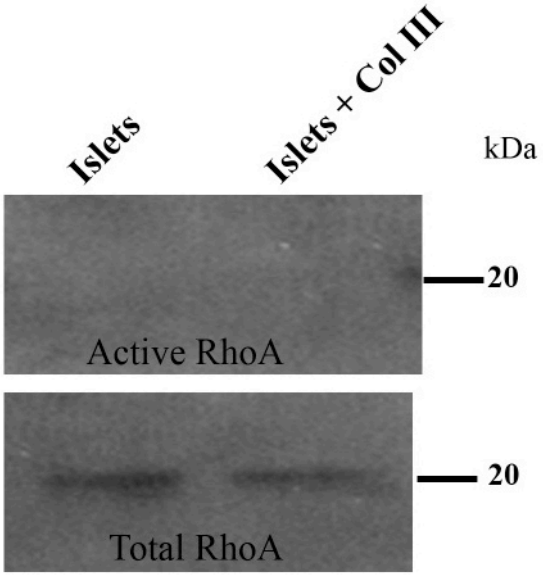

Figure 6-15 Effect of collagen III on RhoA activation in mouse islets. Groups of 400 islets were incubated in a physiological solution containing 20mM glucose in the presence or absence of 100nM collagen III for 10 min. Cells were lysed and incubated with 30µg rhotekin-RBD affinity beads to pull down active RhoA before being fractionated by SDS-PAGE. Active and total RhoA were determined by Western blotting.

6.5 Discussion

Novel data on the role of collagen III in islet functions have been presented in this chapter. Collagen III, a component of the peri-islet and peri-vascular basement membrane, promoted β-cell survival, increased cytosolic calcium concentration and insulin gene expression, and potentiated glucose-stimulated insulin secretion. The integrin superfamily has five collagen receptors (White et al., 2004), so most earlier studies on the effect of collagens on islet functions have largely focused on collagen-integrin interactions (Krishnamurthy et al., 2008; Wang et al., 1999; Wang and Rosenberg, 1999; Kaido et al., 2004). Here, it was demonstrated that collagen III acts via the adhesion GPCR GPR56 to potentiate glucose-stimulated insulin secretion in mouse islets. Evidence was also provided on the role of GPR56 and other islet ECM components on β-cell adhesion.

The cellular organisation and the three dimensional structure of tissues are regulated by cells adhering to their neighbours and/or to the ECM (Heino, 2007; Liu et al., 1997; Rozario and DeSimone, 2010). Cell adhesion is important for the correct movement of progenitor cells during brain development and in ensuring that cells are situated in their proper locations (Jeong et al., 2012). With the unique 3D architecture of islets, and the peri-insular basement membrane partially encasing each islet, cell adhesion may play crucial roles in islet organogenesis, and this may be achieved through the individual ECM proteins. Indeed, ECM proteins control branching of the developing pancreas by modulating adhesiveness of the early progenitor cells (Shih et al., 2016). The effect of collagens on β cell adhesion was therefore investigated and it was found that only collagen IV promoted adhesion of MIN6 β-cells out of the three collagen sub-types investigated. It was not possible to determine whether this is due to activation of GPR56 but this should be investigated in future studies.

Considering that GPR56 has sticky motifs in its N-terminal and can form homo- or heterodimers (Langenhan et al., 2013), it was hypothesised that it could play a part in the adherent nature of β cells. To investigate the role of GPR56 in β-cell adhesion, GPR56 expression in MIN6 β-cells grown as monolayers, was compared with its expression in MIN6 islet-like clusters known as pseudoislets. The ability of β-cells to aggregate and form pseudoislets provides a useful tool to study β-cell interactions in a three dimensional model. Pseudoislets are spherical islet-like cell

clusters formed when MIN6 β-cells are grown in suspension and they are largely comparable in function to primary islets (Persaud et al., 2010; Hauge-Evans et al., 1999). An increase in GPR56 expression in pseudoislets indicated that GPR56 might improve the capacity of β-cells to adhere to each other, but since the expression was not statistically significant, other adhesion molecules such as E-cadherin may play more important roles in pseudoislet formation. However, experiments involving knockdown or deletion of GPR56 are necessary to confirm whether GPR56 is required for pseudoislet formation. GPR56 may also prevent β-cell migration, enabling them to cluster together, as brain studies have shown that activation of GPR56 prevents migration of developing neurons (Li et al., 2008), which is an important step in the normal formation of the cerebral cortex (Jeong et al., 2012). Mutations that prevent the expression of GPR56 in the brain lead to over-migration of neurons resulting in a rare disorder known as bilateral frontoparietal polymicrogyra (Piao et al., 2004). Cancer studies have also indicated that GPR56 prevents cell migration by inhibiting metastasis (Xu and Hynes, 2007). Taken together, GPR56 may play a role in islet development ensuring β-cell compactness and contributing to the 3D nature of islets. Further studies are required to determine whether GPR56 plays any role in islet structural arrangement.

Collagens I and III belong to the same class of fibrillar collagen and they have been implicated in maintaining elasticity and distensibility of tissues (Leitinger and Hohenester, 2007). Loss of collagens I and III in vivo causes skin blistering and aortic rupture (Liu et al., 1997). Collagen IV, on the other hand, is a structural collagen important for maintaining cohesiveness. The difference in functions of collagen III and IV was highlighted by the increased adhesion of MIN6 β-cells observed with collagen IV treatment but not with collagen III. The ability of collagens to cause tissues to adhere or to distend is likely a physical property and not necessarily due to downstream genomic activation. Another difference observed between collagen III and IV is their effect on mouse islet morphology. Islets cultured on collagen III had good integrity with few loosely attached cells while those cultured on collagen IV exhibited cell spreading and they were difficult to retrieve after few days in culture. Collagen III may therefore have beneficial effects on islets maintained in culture prior to transplantation. Indeed, collagen III preserved β-cells by suppressing cytokine-induced apoptosis. This is in agreement with a recent report, which showed that collagen III at the higher concentration of 2μM reduced glucose-induced

caspase 3 activities. The ability of collagen III to reduce apoptosis was lost once GPR56 was down-regulated (Dunér et al., 2016), indicating that it signals via this receptor in β-cells, consistent with the data shown in this thesis using islets for GPR56 KO mice.

GPR56 is both Gq and $G_{12/13}$ coupled (Little et al., 2004; Iguchi et al., 2008); pathways that are associated with elevation of intracellular calcium. The effect of collagen III on β-cell $[Ca^{2+}]i$ was therefore investigated and elevations in intracellular calcium were observed at 10nM, 100nM and 1μM collagen III with calcium profiles similar to those obtained with tolbutamide. Tolbutamide is a sulphonylurea that closes K_{ATP} channels and the subsequent depolarisation of the cell membrane leads to calcium influx through voltage-gated calcium channels. It cannot elevate $[Ca^{2+}]i$ without calcium influx as shown by the complete loss of its effects on calcium when extracellular calcium was removed from the physiological buffer. Removal of extracellular calcium when MIN6 β-cells were exposed to collagen III led to a complete loss of response, suggesting that the increase in $[Ca^{2+}]i$ requires calcium.

Although the effect of collagen III to increase $[Ca^{2+}]i$ was lost when MIN6 β-cells were perifused with calcium-free media, collagen III was able to significantly potentiate glucose-stimulated insulin release in the absence of extracellular calcium, suggesting that collagen III can promote insulin secretion independently from its effects to promote calcium influx. However, the amount of insulin released in response to collagen III was lower than when islets were perifused with physiological solution containing 2mM calcium. These data suggest that collagen III may be acting via a different cascade to promote insulin release in the absence of calcium influx. One possibility is the activation of protein kinases PKA and PKC. Activation of PLC from Gq stimulation produces simultaneous increase in IP_3 and DAG. While IP_3 causes Ca^{2+} release from the internal store, DAG activates PKC, which in turn regulates insulin secretion by modulating cell excitability, calcium influx and it can directly enhance non-calcium mediated exocytosis (Hille et al., 1999). In addition, collagen III can activate PKA through the Gs/cAMP pathway to increase insulin secretion (Dunér et al., 2016)

Acute exposure of islets to 100nM collagen III potentiated glucose-stimulated insulin secretion in a static incubation assay and chronic pre-exposure of islets to collagen III also led to increase

insulin secretion when islets were retrieved and challenged with 20mM glucose. In both cases, there was no increase in basal insulin secretion indicating that collagen III functions to regulate the magnitude of insulin exocytosis in response to a physiological response. The most logical reason for the increase in insulin secretion when islets pre-cultured on collagen III-coated plates were exposed to high glucose is a direct increase in insulin exocytosis, since there was no increase in insulin content. This is similar to the effect of exogenous administration of the phospholipid PIP_2 on β-cells, which causes increased insulin secretion as a result of priming and increased insulin granule docking (Tomas et al., 2010). PIP_2 is hydrolysed to the second messengers IP_3 and DAG after Gq mediated activation of PLC and its level is modulated by ECM (Takenawa and Itoh, 2001). Although there was no increase in insulin content after 48 h exposure to collagen III, incubation of β-cells on collagen III-coated dishes for 7 days led to increased preproinsulin gene expression. It is therefore likely that collagen III has a time-dependent effect on insulin synthesis.

To determine whether collagen III acted via GPR56 to increase insulin release, dynamic perifusion of isolated islets from GPR56KO mice and their WT littermates was used. Molecules such as serotonin, amylin, and nucleotides that can activate GPCRs are known to be co-secreted with insulin upon a glucose challenge (Fehmann et al., 1990; Sassmann et al., 2010). In static secretion experiments, these substances can have a paracrine effect on the β-cells, thus a perifusion system that prevents accumulation of secreted substances is preferred. Using a temperature-controlled perifusion system, it was demonstrated that collagen III reversibly potentiated glucose-stimulated insulin secretion in a GPR56-dependent manner. The mechanisms downstream of GPR56 that mediate collagen III-induced insulin secretion are not yet clear but they may include Ca^{2+} signalling and interplay between Gq/PIP2 (Little et al., 2004), $G_{12/13}$/RhoA (Iguchi et al., 2008; Kanda et al., 2006) and more recently the Gs/PKA pathway has been implicated (Dunér et al., 2016). The effect of collagen III on insulin secretion may also be linked to remodelling of actin cytoskeleton via RhoA signalling. The effect of collagen III was investigated on RhoA pathway, but activated RhoA was not detected. Further studies are therefore required to elucidate the downstream signalling of GPR56.

In summary, this chapter demonstrated the beneficial effects of collagen III on β-cell function in terms of improving cell survival and insulin secretion. It also established that collagen III acts by activating GPR56 to potentiate glucose-stimulated insulin secretion. Taken together, these data provided insights into the role played by the ECM protein collagen III and GPR56 in regulating islet functions, which may be useful in optimising islet function prior to transplantation in T1D patients, or in targeting GPR56 for new therapies for T2D. Since collagen products are commercially available and are generally well tolerated during clinical trials (Borumand and Sibilla, 2014), it may be worth investigating whether people consuming collagen supplements have improved metabolic functions, especially as ingestion of collagen peptides derived from fish has been shown to reduce fasting blood glucose and Hb1Ac in randomised Chinese patients with T2D (Zhu et al., 2010). However, ingested collagens would have been digested in the GI tract, so any beneficial effects that they may have on glucose homeostasis would not be as a consequence of activation of β-cell GPR56.

Chapter 7

Chapter 7 General Discussion

With the current trend of globalisation, physical inactivity, increasing obesity and people living longer, T2D will continue to pose considerable health challenges for the foreseeable future. Indeed, it is projected that by 2040, diabetes will affect more than 0.6 billion people, which translates to one in every ten adults having diabetes if urgent actions are not taken. The situation is particularly gloomy for developing countries, where two-thirds of the people living with diabetes are undiagnosed and 80% of deaths arising from diabetes-related complications occur in this region alone (International Diabetes Federation, 2015). Diabetes is also likely to impact detrimentally on the economies of many nations: its cost to the UK is currently at 10% of the NHS budget, translating to over £1.5m every hour (Kanavos et al., 2012), while the USA spends 20% of its health care budget on diabetes (American Diabetes Association, 2013). To put the cost into perspective, the estimated annual global expenditure associated with diabetes is equal to the gross domestic product (GDP) of Switzerland and twice the GDP of South Africa (da Rocha Fernandes et al., 2016; International Monetary Fund, 2016). The real cost to society is likely to be even higher than estimated, as the figures quoted above excluded care provided by family members of patients, pain and suffering, and the costs associated with undiagnosed diabetes and pre-diabetes.

Moreover, another issue of considerable concern is that some of the currently available drugs for T2D are failing or are associated with serious side effects. For instance, one of the most recent therapies for T2D, Byetta, targets GLP-1 receptors on β-cells to stimulate insulin secretion, and studies in mice suggest that it also increases β-cell mass (Chon and Gautier, 2016). However, Byetta has been associated with pancreatitis and kidney dysfunction in some individuals (Elashoff et al., 2011; Butler et al., 2013; Monami et al., 2017) so there is a need for development of novel therapies with minimal side-effects. G-protein coupled receptors (GPCRs) play important roles in modern medicine, and they are the targets of approximately 50% of all prescription drugs (Cook, 2010). Interestingly, many pharmaceutical companies are investing heavily in developing new T2D therapies that act via GPCRs (Filmore, 2004; Nguyen et al., 2011). In our lab, we have shown that human islets express nearly 300 GPCRs, the majority of which are of unknown function and which may have the appropriate characteristics for next

generation T2D therapy. This led us to focus on GPR56, which we have shown to be the most abundant GPCR in human islets (Amisten et al., 2013).

As described previously, GPR56 is a member of the adhesion GPCRs and it is one of the few GPCRs to be associated with a human disease. Germline mutation in GPR56 causes bilateral frontoparietal polymicrogyra (BFPP), a deformity of the cerebral cortex, which presents as seizure, mental retardation and developmental difficulties in children (Chiang et al., 2011; Luo et al., 2011; Fujii et al., 2013; Piao et al., 2004). GPR56 has a wide tissue distribution and is involved in cell migration, organ development, cell adhesion, muscle hypertrophy, proliferation and inhibition of apoptosis (Shashidhar et al., 2005; White et al., 2014; Ke et al., 2007; Saito et al., 2013; Iguchi et al., 2008; Chen et al., 2010; Giera et al., 2015). The expression and function of GPR56 was therefore investigated from the embryonic stage of pancreas development to adulthood, with a focus on β-cell adhesion, proliferation and apoptosis.

7.1 GPR56 and embryonic pancreas development

GPR56, being a developmental gene, is critical for the proper formation of the cerebellum as it allows the developing neurons to adhere to the extracellular matrix of the pial basement membrane. Ectopia and numerous small gyri are characteristic features of the cerebral cortex of BFPP patients, and they arise as a result of mutations in GPR56 (Singer et al., 2013; Parrini et al., 2009; Piao et al., 2004). Moreover, loss of GPR56 during embryogenesis leads to decreased male fertility and hypomyelination of the CNS as a result of defective development of oligodendrocyte precursor cells (Chen et al., 2010; Bahi-Buisson et al., 2010; Giera et al., 2015). Since GPR56 mRNA is robustly expressed in $NGN3^+$ endocrine progenitors in the pancreas (Gu et al., 2004), it was hypothesised that GPR56 may play a role in islet development. The expression of GPR56 was therefore investigated in developing mouse pancreas at E11 to P9.

Pancreas development involves a carefully orchestrated series of molecular activities that transform the single epithelium of the primitive foregut into two morphologically distinct structures: exocrine and endocrine segments of the mature pancreas. At post-conception day 9 to 9.5 (E9 to E9.5, where 0.5 is the afternoon from where the vaginal plug was observed), the

pancreas is specified in mice by condensation of the mesenchyme. This is followed by evagination, proliferation and branching morphogenesis to form dorsal and ventral buds (Stanger and Hebrok, 2013; Jørgensen et al., 2007). As a result of gut rotation and elongation, the dorsal and ventral buds come into contact and fuse to form a single entity at around E12 to E13. This stage, known as the primary transition, is characterised by extensive proliferation of multipotent progenitor cells (MPCs) and it coincided with high GPR56 expression by pancreatic progenitors, as reported in Chapter 3. At this stage, GPR56 was strongly expressed by cells expressing PDX1, which is a marker for uncommitted MPCs (Gittes, 2009; Marty-Santos and Cleaver, 2016). As the pancreas develops, up to E18, GPR56 expression was progressively downregulated. GPR56 may act during the primary transition to keep undifferentiated cells in a proliferative state, thereby maintaining a pool of progenitor cells. This role is supported by the observations that GPR56 expression was downregulated during the secondary transition from E14 to E18, when MPCs differentiate to the various pancreatic cell types. This is similar to what was observed in the brain, where GPR56 was strongly expressed in oligodendrocyte precursor cells (OPCs) but its expression gradually decreased as the OPCs matured into myelinating oligodendrocytes (Giera et al., 2015).

In addition, the results from chapter 3 indicated that in the developing mouse pancreas GPR56 was also co-localised with $SOX9^+$ and $NGN3^+$ cells, markers for ductal cells and endocrine progenitors respectively (Gu et al., 2002; Seymour, 2014). However, there were $NGN3^+$ cells that were negative for GPR56, indicating that some terminally differentiated endocrine cells will not express GPR56. Among the major endocrine cell types, GPR56 was only expressed by the β-cells. At E16, there was an increased number of $NGN3^+$ progenitors in pancreases from GPR56 KO mice, suggesting reduced differentiation, but there was no difference in the number of proliferating progenitor cells between GPR56 WT and KO mice at E16. This implies that islet development involves a tight regulation of endocrine precursor cell proliferation and differentiation, and that progenitor cells cannot be differentiating and proliferating at the same time. There were no striking morphological differences between the embryonic pancreases of GPR56 KO and WT mice, suggesting that GPR56 is not an instructive signal in islet development or that other genes are playing a compensatory role for its deletion. Further

studies using lineage tracing and β-cell specific deletion of GPR56 are required to confirm the role of GPR56 at key stages of embryonic islet development.

7.2 The role of GPR56 in developing post-natal pancreas

As described in Chapter 3, GPR56 expression was upregulated three days prior to birth, at E18, and maintained at a high level until P9, the latest time point when GPR56 expression was studied. This phase of increased GPR56 expression coincided with the period of increased β-cell replication. Since the rate of replication declines progressively from P10 until weaning at P28, where it remains fairly constant until adulthood (Kaung, 1994), the requirement of GPR56 for β-cell proliferation, β-cell number and mass was investigated at P9. Deletion of GPR56 in vivo resulted in decreased islet size at P9 as a result of decreased β-cell proliferation. The number of cells proliferating and still in the cell cycle was significantly lower at P9, leading to less β-cells but higher numbers of α-cells in GPR56 KO islets. It was not possible to investigate the functional significance of the increased number of α-cells due to time constraints, but this is clearly an area of further research. For example, it is possible that there was dedifferentiation of β-cells to α-cells following GPR56 deletion, and this is something that could be investigated using lineage tracing. Interestingly, there was no difference in islet area between GPR56 KO and WT mice at P56, although there was a higher proportion of small islets of less than 2×10^3 μm^2 in P56 KO pancreases.

The observation that islets in pancreases from P56 GPR56 KO mice were not smaller than those from age-matched WT mice, while there was a significant reduction in size at P9 in the GPR56 KO mice, suggests that other processes in addition to β-cell replication may contribute to adult islet mass. The first postnatal month is associated with many changes in the developing pancreas, including a wave of increased apoptosis observed between P13 and P17 (Figure 7-1). However, it has been reported that β-cell mass in rats was stable between P2 and P20 despite increased apoptosis and decreased proliferation, suggesting that neogenesis is important for maintaining a constant β-cell mass (Scaglia et al., 1997). It was also reported that β-cell mass was more than doubled between P2 and P5 but the cross-sectional area remained unchanged, indicating that increased β-cell number rather than size contributed to the increased mass (Bouwens et al., 1994). Data from mathematical modelling and duct-specific lineage

tracing suggested that neogenesis contributed between 30% to 50% of β-cell mass at the end of the first postnatal month (Finegood et al., 1995; Bonner-Weir et al., 2010). It is therefore likely that neogenesis enables GPR56 KO islets to catch up in size with their WT counterparts at adulthood or that GPR56 is not required for the formation of new β-cells postnatally. The extent to which GPR56 contributes to postnatal β-cell neogenesis warrants further studies using markers of ductal cell differentiation or genetic lineage tracing.

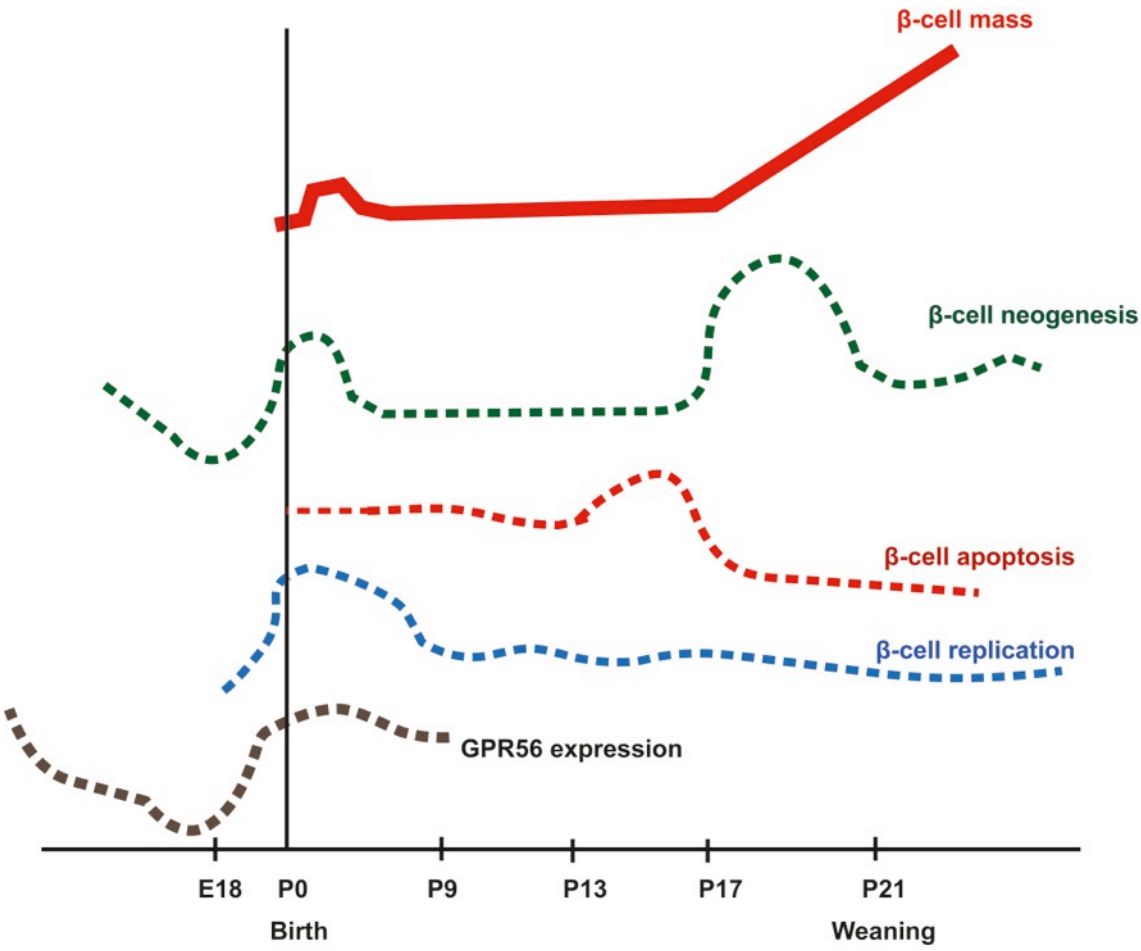

Figure 7-1: A schematic representing the various factors contributing to β-cell mass postnatally (not drawn to scale). β-cell replication is at its peak in the first week of birth and accounts for about 50%-70% of islet mass at the first postnatal month. GPR56 is strongly expressed between E18 and P9, coinciding with the phase of increased β-cell replication and minimal neogenesis. A wave of apoptosis between P13 and P17 precedes a period of substantial neogenesis, which overall accounts for 30% to 50% of β-cell mass at P31. Data on β-cell replication, apoptosis, neogenesis and β-cell mass were adapted from (Bonner-Weir et al., 2016; Scaglia et al., 1997).

7.3 Functions of GPR56 in mature islets

To date, the majority of studies on the beneficial effects of ECM on β-cell survival and function have focused on the roles of integrins (Kaido et al., 2004; White et al., 2004; Weber et al., 2008; Shih et al., 2016; Jiang and Harrison, 2002). However, the sheer complexity of ECM interactions with the many variants of integrin heterodimers has made it difficult to translate the understanding of β-cell-ECM interaction into novel therapeutic targets. It is therefore necessary to identify other, more tractable, targets through which the effect of ECM on β-cell function may be manipulated. A recent report using siRNA-mediated silencing of gene expression suggests that GPR56 could be one of the mechanisms through which ECM may influence β-cell function (Dunér et al., 2016). Using GPR56 KO mice, this thesis confirmed that GPR56 is a β-cell sensor for ECM-mediated effects on islet function.

Collagen III, the primary agonist of GPR56, was identified within the peri-islet and peri-vascular basement membranes of mature mouse and human islets, as described in Chapter 3. However, collagen III mRNA was not detected in MIN6 β-cells and this was supported by IHC, indicating that β-cells do not lay down collagen III but this ECM protein is produced by fibroblasts and endothelial cells of islet blood vessels. Studying the requirement of collagen III on islet function in vivo was not possible as collagen III deletion in mice results in perinatal lethality, with only 5% of mutant mice surviving beyond P2 (Liu et al., 1997). The effect of collagen III on islet function was therefore studied in vitro using isolated mouse islets as described in Chapter 6. 100nM Collagen III increased intracellular calcium in Fura-2 loaded β-cells and protected β-cells

against cytokine-induced apoptosis, but it had no effect on β-cell adhesion. Acute and chronic exposure of islets to 100nM collagen III potentiated glucose-stimulated insulin secretion in static incubation assays. In both cases, there was no increase in basal insulin secretion indicating that collagen III functions to regulate the magnitude of insulin exocytosis in response to nutrients. The most logical reason for the increase in insulin secretion, when islets pre-cultured on collagen III-coated plates were exposed to high glucose, is a direct increase in insulin exocytosis, since there was no increase in insulin content. In addition, the perifusion data in Chapter 6 demonstrate that GPR56 is not required for appropriate insulin secretion in response to increased glucose concentration, but that it is essential for collagen III-induced potentiation of insulin secretion. The mechanisms by which collagen III activates GPR56 in β-cells to augment insulin release are not yet known but they may include Ca^{2+} signalling and interplay between Gq/PIP_2 (Figure 7-2) (Little et al., 2004), $G_{12/13}$/RhoA (Iguchi et al., 2008; Kanda et al., 2006), and, more recently, the Gs/PKA pathway has been suggested (Dunér et al., 2016).

Chapter 4 showed that GPR56 is not involved in whole body glucose homeostasis in adult mice fed on a normal chow diet, although a trend towards mild glucose intolerance was observed. The glucose excursion curve for the female mice showed a sharp decline at 30 minutes following glucose administration and there was a tendency for the GPR56 KO female mice towards glucose intolerance. Nonetheless, there was no evidence of compromised insulin secretion in vitro, suggesting that the mild glucose intolerance is likely to be a consequence of reduced sensitivity of target tissues to insulin after GPR56 deletion. Furthermore, deletion of GPR56 had no effect on islet innervation and vascularisation. Further studies are needed to clarify whether GPR56 KO mice will behave differently with ageing or under increased metabolic stress such as occurs with high fat feeding.

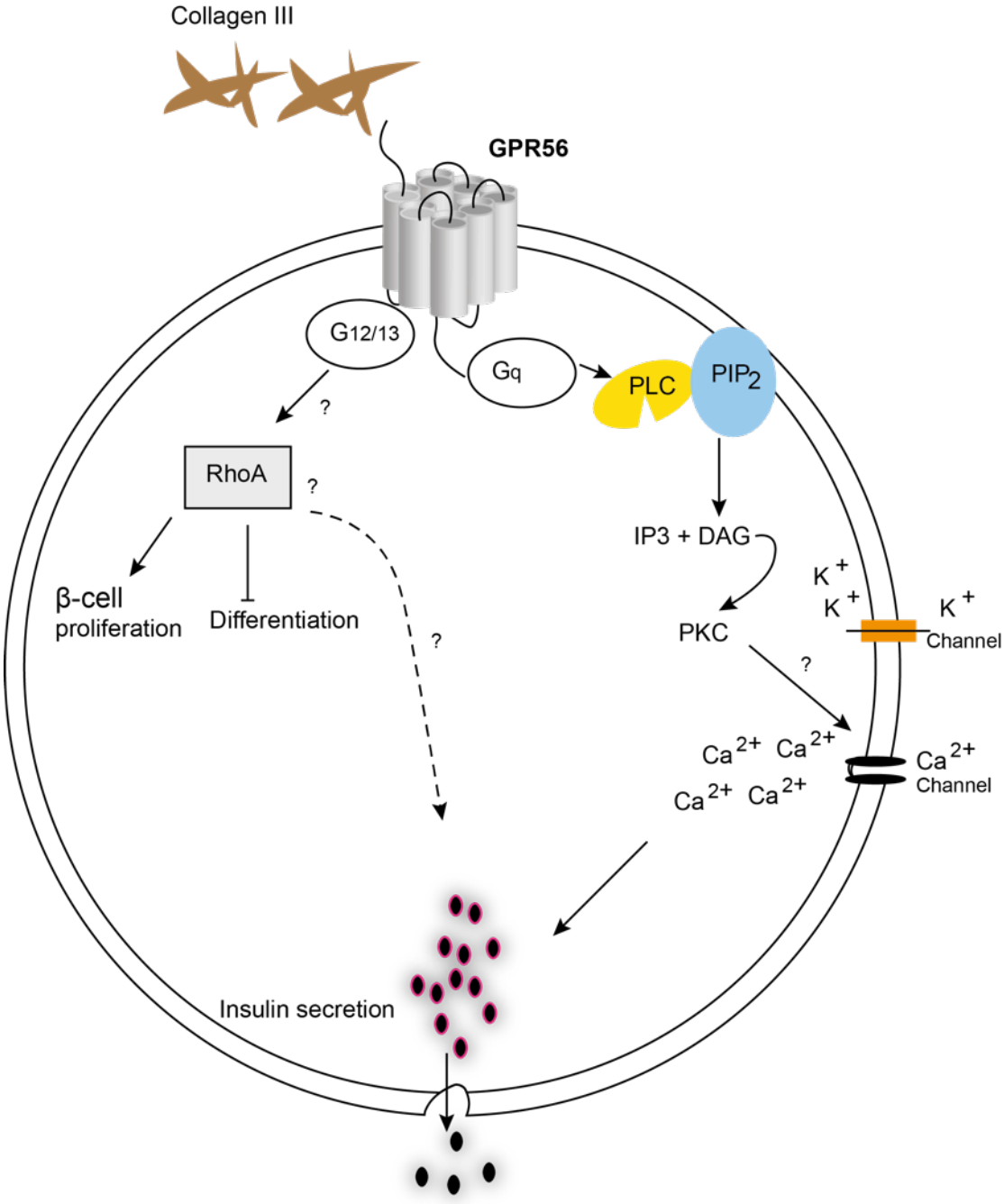

Figure 7-2: Schematic summary of the signalling pathways downstream of GPR56 in the regulation of β-cell function. Collagen III activates GPR56 to stimulate insulin secretion, possibly through elevations in cytosolic calcium via PKC phosphorylation of voltage-dependent calcium channels. The increased intracellular calcium stimulates insulin exocytosis. GPR56 also promotes β-cell proliferation and inhibits differentiation perhaps via the $G_{12/13}$/RhoA pathway in islet development, but further experiments are required to confirm this.

7.4 Future studies

7.4.1 Perspectives on future translational potential

The experiments described in this thesis have established that GPR56/agonist interaction in β-cells might have translational potential for T1D and T2D. It is possible that maintenance of islets with collagen III may improve transplantation outcomes for T1D since islet integrity and survival were improved when mouse islets were incubated with collagen III for 48 h. In addition, pre-exposure of islets to collagen III before they were challenged with glucose led to potentiation of glucose-stimulated insulin secretion. However, future work should first determine whether the protective effect of collagen III on mouse islets and its ability to stimulate insulin secretion can be demonstrated in human islets, since species differences exist in the response of GPCRs to agonists (Amisten et al., 2017). The requirement of GPR56 for the improved insulin secretion observed after 48 h exposure of mouse islets to collagen III should also be investigated by using islets isolated from GPR56 KO mice and appropriate controls from WT mice.

GPR56 may also be a novel target for T2D therapy. Reduction in islet mass is a hallmark feature of T2D and two separate reports have indicated that GPR56 expression is reduced in islets obtained from T2D donors (Taneera et al., 2012; Dunér et al., 2016). The size distribution of islets from GPR56 KO mice indicated a higher proportion of small islets as a result of decreased β-cell proliferation, as evidenced by the number of replicating $BrdU^+$ β-cells in GPR56 KO and WT pancreases. This suggests that GPR56 may be a promising target for improving functional β-cell mass in T2D. It may be worth investigating whether activation of GPR56 offers a therapeutic target for maintaining functional β-cell mass by using mice with β-cell-specific deletion of GPR56, under metabolic stress. In this condition, the requirement for GPR56 in the islet adaptive response to stress imposed by high fat feeding would be determined. It is conceivable that mice with β-cell-specific GPR56 deletion will be unable to compensate appropriately to increased metabolic demand. It may also be worth investigating the mechanisms by which collagen III stimulates insulin secretion. Moreover, a GPR56-specific agonist, TYFAVLM, is now available commercially, and it activates GPR56 with an EC50 of 35μM (Stoveken et al., 2015). It will be interesting to know whether TYFAVLM replicates the effects of collagen III in islets, and whether these effects are lost following GPR56 deletion.

7.4.2 GPR56 may be involved in the crosstalk between β-cells and intra-islet endothelial cells.

As mentioned earlier, islets of Langerhans are highly vascularised, with a blood vessel density five times higher than exocrine cells and they make use of about 15% of the total pancreas blood supply, despite contributing only 2% to the pancreas mass (Zanone et al., 2008). The interaction between islet endocrine cells and this large vascular bed has been of great interest recently. Thus, it has been suggested that there is crosstalk between the endocrine cells and the vascular endothelial cells. This crosstalk regulates ECM protein production, angiogenesis and insulin secretion (Cao and Wang, 2014). ECM is an important islet component as the peri-islet basement membrane has been shown to serve as a protective mantle against inflammatory leucocytes (Korpos et al., 2013). As islet β-cells do not produce ECM, they rely on communication with the vascular endothelial cells to produce this important component (Figure 7-3). On the other hand, the endothelial cells depend on vascular endothelial growth factor (VEGF) secreted from the β-cells for angiogenesis and vascularisation (Nikolova et al., 2007). Since VEGF attracts endothelial cells to the β-cells and lays a network of blood capillaries near the β-cells, any factor that distorts the balance between ECM production and angiogenesis may therefore cause pathologic features in islets.

It has been reported that a progressive deposition of collagen I and III occurs at the islet-exocrine cell interface and within the islets of the Zucker rat obese model of T2D as inflammation and fibrosis progresses (Jones et al., 2013). Evidence from cancer studies and idiopathic lung fibrosis, where the microenvironment is characterised by excessive deposition of ECM, suggest that GPR56 may play a role in T2D by modulating fibrosis and ECM composition. In those disease conditions, expression of GPR56 was downregulated and over-expression of GPR56 in a mouse model of lung fibrosis was able to rescue the phenotype (Yang et al., 2011; Yang et al., 2014). It may therefore be worth investigating the expression level of GPR56 in an obese mouse model of T2D since it might be expected that low levels of GPR56 expression may contribute to islet fibrosis. The mechanism by which GPR56 may regulate ECM production is hypothesised to be secondary to VEGF production via a PKCα signalling pathway (Figure 7-3), since it has been reported that VEGF production in melanoma cells is regulated by GPR56 and PKCα (Yang et al., 2011).

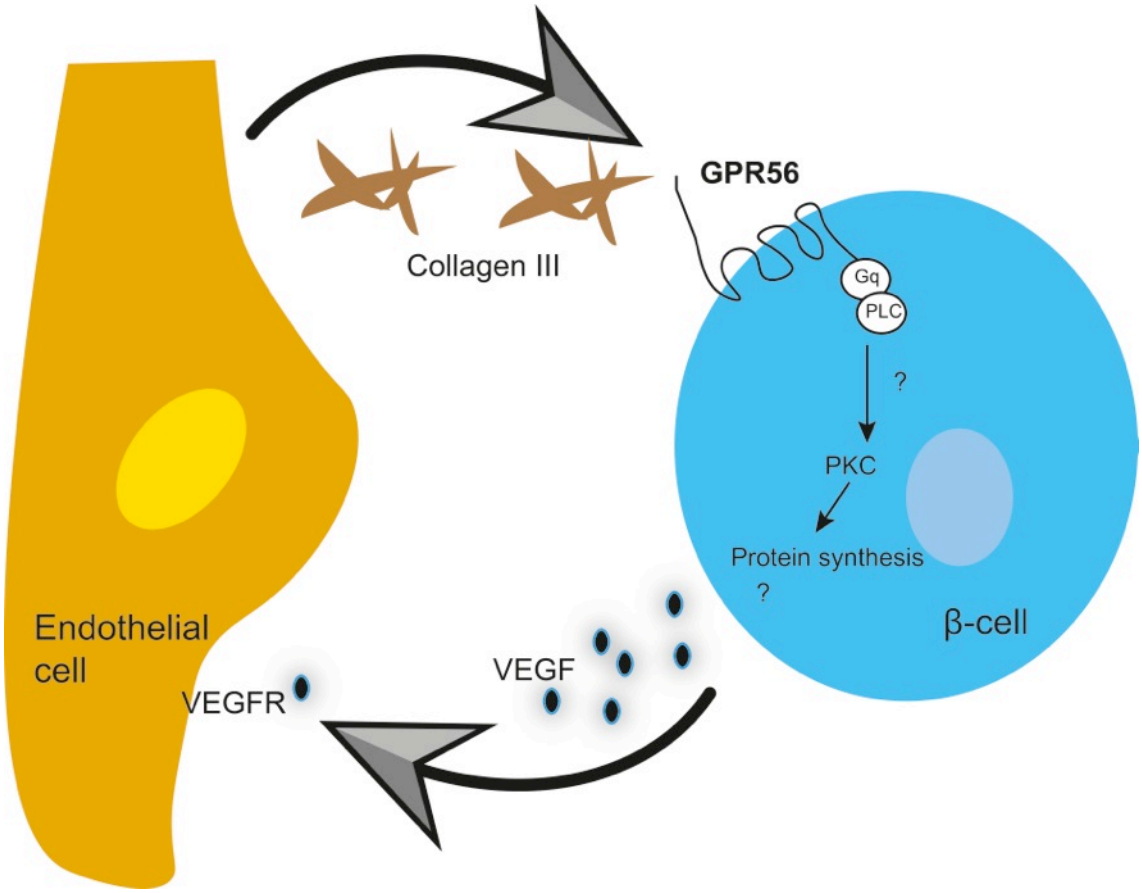

Figure 7-3: Proposed crosstalk between islet β-cells and vascular endothelial cells. Endothelial cells are known to produce the islet basement membrane that contains collagen III, laminins, etc. The secreted factors stimulate β-cells to produce VEGF, which in turn induces endothelial cell-mediated vascularisation. This may be mediated via GPR56: Activation of GPR56 leads to VEGF production, which attracts endothelial cells to β-cells and causes new blood vessel formation and secretion of collagen III. The interaction of collagen III and GPR56 may also improve insulin secretion and help islet survival.

References:

Ahrén, B. (2000). Autonomic regulation of islet hormone secretion--implications for health and disease. *Diabetologia*, *43*(4), 393–410.

Ahrén, B. (2009). Islet G protein-coupled receptors as potential targets for treatment of type 2 diabetes. *Nature Reviews Drug Discovery*, *8*(5), 369–85.

American Diabetes Association. (2011). Standards of Medical Care in Diabetes--2012. *Diabetes Care*, *35*(Supplement 1), S11–S63.

American Diabetes Association. (2013). Economic Costs of Diabetes in the U.S. in 2012. *Diabetes Care*, *36*(4).

American Diabetes Association. (2014). Diagnosis and Classification of Diabetes Mellitus. *Diabetes Care*, *383*(1), 69–82.

Amisten, S., Atanes, P., Hawkes, R., Ruz-Maldonado, I., Liu, B., Parandeh, F., Zhao, M., Huang, G.C & Persaud, S. J. (2017). A comparative analysis of human and mouse islet G-protein coupled receptor expression. *Scientific Reports*, *7*, 46600.

Amisten, S., Neville, M., Hawkes, R., Persaud, S. J., Karpe, F., & Salehi, A. (2015). An atlas of G-protein coupled receptor expression and function in human subcutaneous adipose tissue. *Pharmacology & Therapeutics*, *146*, 61–93.

Amisten, S., Salehi, A., Rorsman, P., Jones, P. M., & Persaud, S. J. (2013). An atlas and functional analysis of G-protein coupled receptors in human islets of Langerhans. *Pharmacology & Therapeutics*, *139*(3), 359–91.

Araç, D., Boucard, A. a, Bolliger, M. F., Nguyen, J., Soltis, S. M., Südhof, T. C., & Brunger, A. T. (2012). A novel evolutionarily conserved domain of cell-adhesion GPCRs mediates autoproteolysis. *The EMBO Journal*, *31*(6), 1364–78.

Ashcroft, F. M., Harrison, D. E., & Ashcroft, S. J. H. (1984). Glucose induces closure of single potassium channels in isolated rat pancreatic β-cells. *Nature*, *312*(5993), 446–448.

Ashcroft, F. M., & Rorsman, P. (2012). Diabetes Mellitus and the β Cell: The Last Ten Years. *Cell*, *148*(6), 1160–1171.

Bader, E., Migliorini, A., Gegg, M., Moruzzi, N., Gerdes, J., Roscioni, S. S., Bakhti, M., Brandi, E., Irmier, M., Beckers, J, Aichler, M., Feuchtinger, A., Leitzinger, C., Zischka, H, Wang-Sattler, R., Jastroch, M., Tschop, M., Machicao, F., Staiger, H., Haring, HU., Chmelova, H., Chouinard, J.A., Oskolkov, N., Korsgren, O., Speier, O & Lickert, H. (2016).

Identification of proliferative and mature β-cells in the islets of Langerhans. *Nature*, *535*(7612), 430–4.

Bae, B.-I., Tietjen, I., Atabay, K. D., Evrony, G. D., Johnson, M. B., Asare, E., Wang, P.P., Murayama, A.Y., Im, K., Lisgo, S.N., Overman, L., Sestan, N., Chang, B.S., Barkovich, A.J., Grant, P.E., Topcu, M., Politsky, J., Okano, H., Piao, X & Walsh, C. a. (2014). Evolutionarily dynamic alternative splicing of GPR56 regulates regional cerebral cortical patterning. *Science (New York, N.Y.)*, *343*(6172), 764–8.

Bahi-Buisson, N., Poirier, K., Boddaert, N., Fallet-Bianco, C., Specchio, N., Bertini, E., Caglayan, O., Lascelles, K., Elie, C., Rambaud, J., Baulac, M., An, I., Dias, P., des Portes, V., Moutard, M.L., Soufflet, C., El Maleh, M., Beldjord, C., Villard, L & Chelly, J. (2010). GPR56-related bilateral frontoparietal polymicrogyria: further evidence for an overlap with the cobblestone complex. *Brain : A Journal of Neurology*, *133*(11), 3194–209.

Banères, J.-L., Popot, J.-L., & Mouillac, B. (2011). New advances in production and functional folding of G-protein-coupled receptors. *Trends in Biotechnology*, *29*(7), 314–22.

Benninger, R. K. P., Head, W. S., Zhang, M., Satin, L. S., & Piston, D. W. (2011). Gap junctions and other mechanisms of cell-cell communication regulate basal insulin secretion in the pancreatic islet. *The Journal of Physiology*, *589*(Pt 22), 5453–66.

Bernassola, F., Federici, M., Corazzari, M., Terrinoni, A., Hribal, M. L., De Laurenzi, V., Ranalli, M., Massa, O., Sesti, G., McLean, W.H., Citro, G., Barbetti, F & Melino, G. (2002). Role of transglutaminase 2 in glucose tolerance: knockout mice studies and a putative mutation in a MODY patient. *FASEB Journal : Official Publication of the Federation of American Societies for Experimental Biology*, *16*(11), 1371–8.

Bishay, R. H., & Greenfield, J. R. (2016). A review of maturity onset diabetes of the young (MODY) and challenges in the management of glucokinase-MODY. *The Medical Journal of Australia*, *205*(10), 480–485.

Bjarnadóttir, T. K., Fredriksson, R., Höglund, P. J., Gloriam, D. E., Lagerström, M. C., & Schiöth, H. B. (2004). The human and mouse repertoire of the adhesion family of G-protein-coupled receptors. *Genomics*, *84*(1), 23–33.

Bohnekamp, J., & Schöneberg, T. (2011). Cell adhesion receptor GPR133 couples to G s protein. *Journal of Biological Chemistry*, *286*(49), 41912–41916.

Bonner-Weir, S. (1988). Morphological evidence for pancreatic polarity of β-cell within islets of

Langerhans. *Diabetes*, *37*(5), 616–621.

Bonner-Weir, S., Aguayo-Mazzucato, C., & Weir, G. C. (2016). Dynamic development of the pancreas from birth to adulthood. *Upsala Journal of Medical Sciences*, *121*(2), 155–8.

Bonner-Weir, S., Li, W. C., Ouziel-Yahalom, L., Guo, L., Weir, G. C., & Sharma, A. (2010). β-cell growth and regeneration: Replication is only part of the story. *Diabetes*, *59*(10), 2340–2348.

Bonner-Weir, S., & Like, A. A. (1980). A dual population of islets of Langerhans in bovine pancreas. *Cell and Tissue Research*, *206*(1), 157–70.

Bonnevie-Nielsen, V., Skovgaard, L. T., & Lernmark, Å. (1983). β-Cell Function Relative to Islet Volume and Hormone Content in the Isolated Perfused Mouse Pancreas*. *Endocrinology*, *112*(3), 1049–1056.

Borden, P., Houtz, J., Leach, S. D., & Kuruvilla, R. (2013). Sympathetic innervation during development is necessary for pancreatic islet architecture and functional maturation. *Cell Reports*, *4*(2), 287–301.

Borumand, M., & Sibilla, S. (2014). Daily consumption of the collagen supplement Pure Gold Collagen reduces visible signs of aging. *Clinical Interventions in Aging*, *9*, 1747–1758.

Bouwens, L., Wang, R. N., De Blay, E., Pipeleers, D. G., & Klöppel, G. (1994). Cytokeratins as markers of ductal cell differentiation and islet neogenesis in the neonatal rat pancreas. *Diabetes*, *43*(11), 1279–83.

Bowe, J. E., Chander, A., Liu, B., Persaud, S. J., & Jones, P. M. (2013). The permissive effects of glucose on receptor-operated potentiation of insulin secretion from mouse islets: A role for ERK1/2 activation and cytoskeletal remodelling. *Diabetologia*, *56*(4), 783–791.

Braun, M. (2014). The somatostatin receptor in human pancreatic β-cells. *Vitamins and Hormones*, *95*, 165–193.

Brissova, M., Shostak, A., Fligner, C. L., Revetta, F. L., Washington, M. K., Powers, A. C., & Hull, R. L. (2015). Human Islets Have Fewer Blood Vessels than Mouse Islets and the Density of Islet Vascular Structures Is Increased in Type 2 Diabetes. *The Journal of Histochemistry and Cytochemistry : Official Journal of the Histochemistry Society*, *63*(8), 637–645.

Bungay, P. J., Owen, R. a, Coutts, I. C., & Griffin, M. (1986). A role for transglutaminase in glucose-stimulated insulin release from the pancreatic beta-cell. *The Biochemical Journal*,

235(1), 269–78.

Burant, C. F. (2013). Activation of GPR40 as a Therapeutic Target for the Treatment of Type 2 Diabetes. *Diabetes Care*, *36*(Supplement 2).

Butler, A. E., Janson, J., Bonner-Weir, S., Ritzel, R., Rizza, R. A., & Butler, P. C. (2003). Beta-cell deficit and increased beta-Cell apoptosis in humans with type 2 diabetes. *Diabetes*, *52*(January), 102–10.

Cabrera, O., Berman, D. M., Kenyon, N. S., Ricordi, C., Berggren, P.-O., & Caicedo, A. (2006). The unique cytoarchitecture of human pancreatic islets has implications for islet cell function. *Proceedings of the National Academy of Sciences of the United States of America*, *103*(7), 2334–9.

Cerf, M. E. (2013). Beta cell dysfunction and insulin resistance. *Frontiers in Endocrinology*, *4*, 37.

Cernea, S., & Dobreanu, M. (2013). Diabetes and beta cell function: From mechanisms to evaluation and clinical implications. *Biochemia Medica*. Croatian Society for Medical Biochemistry and Laboratory Medicine.

Chen, G., Yang, L., Begum, S., & Xu, L. (2010). GPR56 is essential for testis development and male fertility in mice. *Developmental Dynamics an Official Publication of the American Association of Anatomists*, *239*, 3358–3367.

Chiang, N.-Y., Chang, G.-W., Huang, Y.-S., Peng, Y.-M., Hsiao, C.-C., & Kuo, M.-L. (2016). Heparin interacts with adhesion-GPCR GPR56 / ADGRG1 , reduces receptor shedding , and promotes cell adhesion and motility. *Journal of Cell Science*, *1*, 1–39.

Chiang, N.-Y., Hsiao, C.-C., Huang, Y.-S., Chen, H.-Y., Hsieh, I.-J., Chang, G.-W., & Lin, H.-H. (2011). Disease-associated GPR56 mutations cause bilateral frontoparietal polymicrogyria via multiple mechanisms. *The Journal of Biological Chemistry*, *286*(16), 14215–25.

Chu, Z. L., Jones, R. M., He, H., Carroll, C., Gutierrez, V., Lucman, A., Moloney, M., Gao, H., Mondala, H., Bagnol, D., Unett, D., Liang, Y., Demarest, K., Semple, G., Behan, D.P & Leonard, J. (2007). A role for β-cell-expressed G protein-coupled receptor 119 in glycemic control by enhancing glucose-dependent insulin release. *Endocrinology*, *148*(6), 2601–2609.

Cortijo, C., Gouzi, M., Tissir, F., & Grapin-Botton, A. (2012). Planar Cell Polarity Controls Pancreatic Beta Cell Differentiation and Glucose Homeostasis. *Cell Reports*, *2*(6), 1593–

1606.

Cozar-Castellano, I., Fiaschi-Taesch, N., Bigatel, T. A., Takane, K. K., Garcia-Ocaña, A., Vasavada, R., & Stewart, A. F. (2006). Molecular control of cell cycle progression in the pancreatic β-cell. *Endocrine Reviews*, 27(4), 356-370.

Cozar-Castellano, I., Weinstock, M., Haught, M., Velazquez-Garcia, S., Sipula, D., & Stewart, A. F. (2006). Evaluation of β-cell replication in mice transgenic for hepatocyte growth factor and placental lactogen: comprehensive characterization of the G1/S regulatory proteins reveals unique involvement of p21cip. *Diabetes*, *55*(1), 70–77.

da Rocha Fernandes, J., Ogurtsova, K., Linnenkamp, U., Guariguata, L., Seuring, T., Zhang, P., Cavan, D & Makaroff, L. E. (2016). IDF Diabetes Atlas estimates of 2014 global health expenditures on diabetes. *Diabetes Research and Clinical Practice*, *117*, 48–54.

Dahan, T., Ziv, O., Horwitz, E., Zemmour, H., Lavi, J., Swisa, A., Leibowitz, G., Ashcroft, F.M., In't Veld, P., Glaser, B & Dor, Y. (2016). Pancreatic beta cells express the fetal islet hormone gastrin in rodent and human diabetes. *Diabetes*, *66*(2), 1–33.

Dahl, U., Sjødin, A., & Semb, H. (1996). Cadherins regulate aggregation of pancreatic beta-cells in vivo. *Development (Cambridge, England)*, *122*(9), 2895–2902.

Dai, C., Brissova, M., Reinert, R. B., Nyman, L., Liu, E. H., Thompson, C., Shostak, A., Shiota, M., Takahashi, T & Powers, A. C. (2013). Pancreatic islet vasculature adapts to insulin resistance through dilation and not angiogenesis. *Diabetes*, *62*(12), 4144–4153.

Daoud, J., Petropavlovskaia, M., Rosenberg, L., & Tabrizian, M. (2010). The effect of extracellular matrix components on the preservation of human islet function in vitro. *Biomaterials*, *31*(7), 1676–82.

DeFronzo, R. A. (2009). From the Triumvirate to the Ominous Octet: A New Paradigm for the Treatment of Type 2 Diabetes Mellitus. *Diabetes Care*, *58*(4), 773–795.

Deijnen, J. H. M. Van, Snylichem, P. T. R. Van, Wolters, G. H. J., & Schilfgaarde, R. Van. (1994). Cell & Tissue Distribution of collagens type I , type III and type V in the pancreas of rat , dog , pig and man. *Cell & Tissue Research*, *277*, 115–121.

Della Chiesa, M., Falco, M., Parolini, S., Bellora, F., Petretto, A., Romeo, E., Balsamo, M., Gambarotti, M., Scordamaglia, F., Tabellini, G., Facchetti, F., Vermi, W., Bottino, C., Moretta, A & Vitale, M. (2010). GPR56 as a novel marker identifying the CD56dull CD16+ NK cell subset both in blood stream and in inflamed peripheral tissues. *International*

Immunology, *22*(2), 91–100.

Demberg, L. M., Rothemund, S., Schöneberg, T., & Liebscher, I. (2015). Identification of the tethered peptide agonist of the adhesion G protein-coupled receptor GPR64/ADGRG2. *Biochemical and Biophysical Research Communications*, *464*(3), 743–7.

Do, O. H., & Thorn, P. (2015). Insulin secretion from beta cells within intact islets: Location matters. *Clinical and Experimental Pharmacology and Physiology*, *42*(4), 406–414.

Dong, P. D. S., Provost, E., Leach, S. D., & Stainier, D. Y. R. (2008). Graded levels of Ptf1a differentially regulate endocrine and exocrine fates in the developing pancreas. *Genes & Development*, *22*(11), 1445–50.

Dor, Y., Brown, J., Martinez, O. I., & Melton, D. A. (2004). Adult pancreatic β-cells are formed by self-duplication rather than stem-cell differentiation. *Nature*, *429*(6987), 41–46.

Doyle, M. E., & Egan, J. M. (2007). Mechanisms of action of glucagon-like peptide 1 in the pancreas. *Pharmacology & Therapeutics*, *113*(3), 546–93.

Dunér, P., Al-Amily, I. M., Soni, A., Asplund, O., Safi, F., Storm, P., Groop, L., Amisten, S & Salehi, A. (2016). Adhesion G-protein coupled receptor G1 (ADGRG1/GPR56) and pancreatic β-cell function. *The Journal of Clinical Endocrinology & Metabolism*, 101(120), 4637-4645.

Farhat, B., Almelkar, A., Ramachandran, K., Williams, S. J., Huang, H. H., Zamierowski, D., Novikova, L & Stehno-Bittel, L. (2013). Small human islets comprised of more β-cells with higher insulin content than large islets. *Islets*, *5*(2), 87–94.

Fehmann, H. C., Weber, V., Giike, R., Giike, B., & Arnold, R. (1990). Cosecretion of amylin and insulin from isolated rat pancreas, *262*(2), 279–281.

Filmore, D. (2004). It's a GPCR world. *J. Modern D. Discov.*, *7*(11), 24–27.

Finegood, D. T., Scaglia, L., & Bonner-Weir, S. (1995). Dynamics of beta-cell mass in the growing rat pancreas. Estimation with a simple mathematical model. *Diabetes*, *44*(3), 249–56.

Flamez D, Van Breuseghem A, Scrocchi LA, Quartier E, P. D., & Drucker DJ, S. F. (1998). Mouse pancreatic_-cells exhibit preserved glucose competence after disruption of the glucagon-like peptide 1 receptor gene. *Diabetes*, *47*(April), 646–652.

Fredriksson, R., Lagerström, M. C., Höglund, P. J., & Schiöth, H. B. (2002). Novel human G protein-coupled receptors with long N-terminals containing GPS domains and Ser/Thr-rich

regions. *FEBS Letters*, *531*(3), 407–14.

Fredriksson, R., Lagerström, M. C., Lundin, L.-G., & Schiöth, H. B. (2003). The G-protein-coupled receptors in the human genome form five main families. Phylogenetic analysis, paralogon groups, and fingerprints. *Molecular Pharmacology*, *63*(6), 1256–72.

Fredriksson, R., & Schiöth, H. B. (2005). The repertoire of G-protein-coupled receptors in fully sequenced genomes. *Molecular Pharmacology*, *67*(5), 1414–25.

Fuchsberger, C., Flannick, J., Teslovich, T. M., Mahajan, A., Agarwala, V., Gaulton, K. J., … McCarthy, M. I. (2016). The genetic architecture of type 2 diabetes. *Nature*, *536*(7614), 41–7.

Fujii, Y., Ishikawa, N., Kobayashi, Y., Kobayashi, M., & Kato, M. (2014). Compound heterozygosity in GPR56 with bilateral frontoparietal polymicrogyria. *Brain & Development*. 36(6), 528-531

Gao, Q., & Chess, A. (1999). Identification of candidate Drosophila olfactory receptors from genomic DNA sequence. *Genomics*, *60*(1), 31–9.

Gembal, M., Gilon, P., & Henquin, J. C. (1992). Evidence that glucose can control insulin release independently from its action on ATP-sensitive K+ channels in mouse B cells. *The Journal of Clinical Investigation*, *89*(4), 1288–95.

Georgia, S. & Bhushan, A. (2004). Beta cell replication is the primary mechanism for maintaining postnatal beta cell mass. *The Journal of Clinical Investigation*, *114*(7), 963–8.

Gether, U. (2000). Uncovering molecular mechanisms involved in activation of G protein-coupled receptors. *Endocrine Reviews*, 21(1), 90-113.

Giera, S., Deng, Y., Luo, R., Ackerman, S. D., Mogha, A., Monk, K. R., Ying, Y., Jeong, S.J., Makinodan, M., Bialas, A.R., Chang, B.S., Stevens, B., Corfas, G & Piao, X. (2015). The adhesion G protein-coupled receptor GPR56 is a cell-autonomous regulator of oligodendrocyte development. *Nature Communications*, *6*, 6121.

Gittes, G. K. (2009). Developmental biology of the pancreas: A comprehensive review. *Developmental Biology*, *326*(1), 4–35.

Gromada, J., Høy, M., Buschard, K., Salehi, A., & Rorsman, P. (2001). Somatostatin inhibits exocytosis in rat pancreatic alpha-cells by G(i2)-dependent activation of calcineurin and depriming of secretory granules. *The Journal of Physiology*, *535*(Pt 2), 519–32.

Gu, G., Dubauskaite, J., & Melton, D. A. (2002). Direct evidence for the pancreatic lineage:

NGN3+ cells are islet progenitors and are distinct from duct progenitors. *Development*, *129*, 2447–2457.

Gu, G., Dubauskaite, J., & Melton, D. A. (2002). Direct evidence for the pancreatic lineage: NGN3+ cells are islet progenitors and are distinct from duct progenitors. *Development (Cambridge, England)*, *129*(10), 2447–57.

Gu, G., Wells, J. M., Dombkowski, D., Preffer, F., Aronow, B., & Melton, D. a. (2004). Global expression analysis of gene regulatory pathways during endocrine pancreatic development. *Development (Cambridge, England)*, *131*(1), 165–179.

Guo, X., Li, H., Xu, H., Woo, S., Dong, H., Lu, F., Lange, A.J & Wu, C. (2012). Glycolysis in the control of blood glucose homeostasis. *Acta Pharmaceutica Sinica B*, *2*(4), 358–367.

Gupte, J., Swaminath, G., Danao, J., Tian, H., Li, Y., & Wu, X. (2012). Signaling property study of adhesion G-protein-coupled receptors. *FEBS Letters*, *586*(8), 1214–1219.

Haitina, T., Olsson, F., Stephansson, O., Alsiö, J., Roman, E., Ebendal, T., Schioth, H.B & Fredriksson, R. (2008). Expression profile of the entire family of Adhesion G protein-coupled receptors in mouse and rat. *BMC Neuroscience*, *9*, 43.

Hamann, J., Aust, G., Arac, D., Engel, F. B., Formstone, C., Fredriksson, R., … Schioth, H. B. (2015). International Union of Basic and Clinical Pharmacology. XCIV. Adhesion G Protein-Coupled Receptors. *Pharmacological Reviews*, *67*(2), 338–367.

Hamann, J., Hsiao, C. C., Lee, C. S., Ravichandran, K. S., & Lin, H. H. (2016). Adhesion GPCRs as modulators of immune cell function. In *Handbook of Experimental Pharmacology* (Vol. 234, pp. 329–350). Springer International Publishing.

Handelsman, Y., Mechanick, J. I., Blonde, L., Grunberger, G., Bloomgarden, Z. T., Bray, G. A., … Wyne, K. L. (2011). American Association of Clinical Endocrinologists Medical Guidelines for clinical practice for developing a diabetes mellitus comprehensive care plan: executive summary. *Endocr Pract*, *17*(2), 287–302.

Hauge-Evans, A. C., Squires, P. E., Persaud, S. J., & Jones, P. M. (1999). Pancreatic beta-cell-to-beta-cell interactions are required for integrated responses to nutrient stimuli: Enhanced Ca2+ and insulin secretory responses of MIN6 pseudoislets. *Diabetes*, *48*(7), 1402–1408.

Heino, J. (2007). The collagen family members as cell adhesion proteins. *BioEssays*, 29(10), 1001-1010.

Heit, J. J., Apelqvist, Å. A., Gu, X., Winslow, M. M., Neilson, J. R., Crabtree, G. R., & Kim, S. K.

(2006). Calcineurin/NFAT signalling regulates pancreatic β-cell growth and function. *Nature*, *443*(7109), 345–349.

Henquin, J. C. (2000). Triggering and amplifying pathways of regulation of insulin secretion by glucose. *Diabetes*. 49(11), 1751-60.

Hille, B., Billiard, J., Babcock, D. F., Nguyen, T., & Koh, D. S. (1999). Stimulation of exocytosis without a calcium signal. *Journal of Physiology*, *520*(1), 23–31.

Hodge, R. J., Lin, J., Vasist Johnson, L. S., Gould, E. P., Bowers, G. D., & Nunez, D. J. (2013). Safety, pharmacokinetics, and pharmacodynamic effects of a selective TGR5 Agonist, SB-756050, in Type 2 Diabetes. *Clinical Pharmacology in Drug Development*, *2*(3), 213–222.

Hosker, J. P., Rudenski, A. S., Burnett, M. A., Matthews, D. R., & Turner, R. C. (1989). Similar reduction of first- and second-phase B-cell responses at three different glucose levels in type II diabetes and the effect of gliclazide therapy. *Metabolism*, *38*(8), 767–772.

Hsiao, C.-C., Keysselt, K., Chen, H.-Y., Sittig, D., Hamann, J., Lin, H.-H., & Aust, G. (2015). The Adhesion GPCR CD97 / ADGRE5 inhibits apoptosis. *The International Journal of Biochemistry & Cell Biology*, *65*, 197–208.

Huang, H. H., Novikova, L., Williams, S. J., Smirnova, I. V, & Stehno-Bittel, L. (2011). Low insulin content of large islet population is present in situ and in isolated islets. *Islets*, *3*(1), 6–13.

Huang, Y., Fan, J., Yang, J., & Zhu, G.-Z. (2008). Characterization of GPR56 protein and its suppressed expression in human pancreatic cancer cells. *Molecular and Cellular Biochemistry*, *308*, 133–139.

Iguchi, T., Sakata, K., Yoshizaki, K., Tago, K., Mizuno, N., & Itoh, H. (2008). Orphan G protein-coupled receptor GPR56 regulates neural progenitor cell migration via a G alpha 12/13 and Rho pathway. *The Journal of Biological Chemistry*, *283*, 14469–14478.

Iismaa, S. E., Aplin, M., Holman, S., Yiu, T. W., Jackson, K., Burchfield, J. G., Mitchell, C.J., O'Reilly, L., Davenport, A., Cantley, J., Schmitz-Peiffer, C., Biden, T.J., Cooney, G.J & Graham, R. M. (2013). Glucose homeostasis in mice is transglutaminase 2 independent. *PloS One*, *8*(5),

International Diabetes Federation. (2015). *IDF Diabetes Atlas* (7th ed.). Brussels, Belgium.

International Monetary Fund. (2016). *World Economic Outlook. Subdued demands: Symptoms and remedies*. Washington.

Irving-Rodgers, H. F., Choong, F. J., Hummitzsch, K., Parish, C. R., Rodgers, R. J., & Simeonovic, C. J. (2014). Pancreatic Islet basement membrane loss and remodeling after mouse islet isolation and transplantation: Impact for allograft rejection. *Cell Transplantation*, *23*(1), 59–72.

Ismail-Beigi, F. (2012). Glycemic Management of Type 2 Diabetes Mellitus. *New England Journal of Medicine,* 366, 1319-1327.

Iwase, M., Uchizono, Y., Tashiro, K., Goto, D., & Iida, M. (2002). Islet hyperperfusion during prediabetic phase in OLETF rats, a model of type 2 diabetes. *Diabetes*, *51*(8), 2530–2535.

Jalili, R. B., Moeen Rezakhanlou, A., Hosseini-Tabatabaei, A., Ao, Z., Warnock, G. L., & Ghahary, A. (2011). Fibroblast populated collagen matrix promotes islet survival and reduces the number of islets required for diabetes reversal. *Journal of Cellular Physiology*, *226*(7), 1813–1819.

Jensen, J., Heller, R. S., Funder-Nielsen, T., Pedersen, E. E., Lindsell, C., Weinmaster, G., Madsen, O.D & Serup, P. (2000). Independent development of pancreatic alpha- and beta-cells from neurogenin3-expressing precursors: a role for the notch pathway in repression of premature differentiation. *Diabetes*, *49*(2), 163-176.

Jiang, F.-X., & Harrison, L. C. (2002). Extracellular signals and pancreatic beta-cell development: a brief review. *Molecular Medicine (Cambridge, Mass.)*, *8*(12), 763–70.

Jin, G., Sakatani, K., Wang, H., Jin, Y., Dubeykovskiy, A., Worthley, D. L., Tailor, Y & Wang, T. C. (2017). The G-protein coupled receptor 56, expressed in colonic stem and cancer cells, binds progastrin to promote proliferation and carcinogenesis. *Oncotarget*, 1–14.

Jin, Z., Tietjen, I., Bu, L., Liu-Yesucevitz, L., Gaur, SK., Walsh, CA., & Piao, X (2007). Disease-associated mutations affect GPR56 protein trafficking and cell surface expression. *Human Molecular Genetics. 16*(16), 1972–1985.

Johansson, M., Andersson, A., Carlsson, P. O., & Jansson, L. (2006). Perinatal development of the pancreatic islet microvasculature in rats. *Journal of Anatomy*, *208*(2), 191–196.

Jones, P. M., & Persaud, S. J. (2010). Islet Function and Insulin Secretion. In R. Holt, C. Cockram, A. Flyvbjerg, & B. Goldstein (Eds.), *Textbook of Diabetes* (4th ed., pp. 85–103). Oxford, UK: Wiley-Blackwell.

Jones, R. A., Kotsakis, P., Johnson, T. S., Chau, D. Y. S., Ali, S., Melino, G., & Griffin, M. (2006). Matrix changes induced by transglutaminase 2 lead to inhibition of angiogenesis

and tumor growth. *Cell Death & Differentiation*, *13*(9), 1442–1453.

Jørgensen, M. C., Ahnfelt-Rønne, J., Hald, J., Madsen, O. D., Serup, P., & Hecksher-Sørensen, J. (2007). An illustrated review of early pancreas development in the mouse. *Endocrine Reviews*, *28*(6), 685–705.

Kahn, S. E. (2001). The Importance of β-Cell Failure in the Development and Progression of Type 2 Diabetes. *The Journal of Clinical Endocrinology & Metabolism*, *86*(9), 4047–4058.

Kahn, S. E., Cooper, M. E., & Del Prato, S. (2014). Pathophysiology and treatment of type 2 diabetes: perspectives on the past, present, and future. *Lancet*, *383*(9922), 1068–83.

Kaido, T., Yebra, M., Cirulli, V., & Montgomery, A. M. (2004). Regulation of human beta-cell adhesion, motility, and insulin secretion by collagen IV and its receptor alpha1beta1. *The Journal of Biological Chemistry*, *279*(51), 53762–9.

Kanavos, P., Aardweg, S. Van Den, & Schurer, W. (2012). Diabetes Expenditure, Burden of Disease and Management in 5 EU Countries. *LSE Health*, (January), 1–113.

Kanda, T., Wakino, S., Homma, K., Yoshioka, K., Tatematsu, S., Hasegawa, K., Takamatu, I., Sugano, N., Hayashi, K & Saruta, T. (2006). Rho-kinase as a molecular target for insulin resistance and hypertension. *FASEB Journal , 20*(1), 169–71.

Kang, X., Xiao, X., Harata, M., Bai, Y., Nakazaki, Y., Soda, Y., Kurita, R., Tanaka, T., Komine, F., Izawa, K., Kunisaki, R., Setoyama, M., Nishimori, H., Natsume, A., Sunamura, M., Lozonshi, L Tani, K. (2006). Antiangiogenic activity of BAI1 in vivo: implications for gene therapy of human glioblastomas. *Cancer Gene Therapy*, *13*(4), 385–392.

Kathiresan, S., Melander, O., Guiducci, C., Surti, A., Burtt, N. P., Rieder, M. J., … Orho-Melander, M. (2008). Six new loci associated with blood low-density lipoprotein cholesterol, high-density lipoprotein cholesterol or triglycerides in humans. *Nature Genetics*, *40*(2), 189–197.

Kaung, H. L. (1994). Growth dynamics of pancreatic islet cell populations during fetal and neonatal development of the rat. *Developmental Dynamics : An Official Publication of the American Association of Anatomists*, *200*(2), 163–175.

Kawai, K., Ipp, E., Orci, L., Perrelet, A., & Unger, R. H. (1982). Circulating somatostatin acts on the islets of Langerhans by way of a somatostatin-poor compartment. *Science (New York, N.Y.)*, *218*(4571), 477–478.

Ke, N., Sundaram, R., Liu, G., Chionis, J., Fan, W., Rogers, C., … Li, Q.-X. (2007). Orphan G

protein-coupled receptor GPR56 plays a role in cell transformation and tumorigenesis involving the cell adhesion pathway. *Molecular Cancer Therapeutics*, *6*, 1840–1850.

Kee, N., Sivalingam, S., Boonstra, R., & Wojtowicz, J. M. (2002). The utility of Ki-67 and BrdU as proliferative markers of adult neurogenesis. *Journal of Neuroscience Methods*, *115*(1), 97–105.

Kendall, D. M., Sutherland, D. E. R., Najarian, J. S., Goetz, F. C., & Robertson, R. P. (1990). Effects of hemipancreatectomy on insuline secretion and glucose tolerance in healthy humans. *New England Journal of Medicine*, *322*(13), 898–903.

Kerr-Conte, J., Pattou, F., Lecomte-Houcke, M., Xia, Y., Boilly, B., Proye, C., & Lefebvre, J. (1996). Ductal cyst formation in collagen-embedded adult human islet preparations: A means to the reproduction of nesidioblastosis in vitro. *Diabetes*, *45*(8), 1108–1114.

Kim, A., Miller, K., Jo, J., Kilimnik, G., Wojcik, P., & Hara, M. (2009). Islet architecture: A comparative study. *Islets*, *1*(2), 129–136.

Kim, J., Han, J., Park, C., Shin, KJ., Ahn C., Seong, JY & Hwang, JI (2010). Splicing variants of the orphan G-protein-coupled receptor GPR56 regulate the activity of transcription factors associated with tumorigenesis. *Journal of Cancer of cancer research and clinical oncology 136*, 47–53.

Kishore, A., Purcell, R. H., Nassiri-Toosi, Z., & Hall, R. A. (2016). Stalk-dependent and Stalk-independent Signaling by the Adhesion G Protein-coupled Receptors GPR56 (ADGRG1) and BAI1 (ADGRB1). *The Journal of Biological Chemistry*, *291*(7), 3385–94.

Koirala, S., Jin, Z., Piao, X., & Corfas, G. (2009). GPR56-regulated granule cell adhesion is essential for rostral cerebellar development. *The Journal of Neuroscience*, *29*(23), 7439–7449.

Kolakowski, L. F. (1994). GCRDb: a G-protein-coupled receptor database. *Receptors & Channels*, *2*(1), 1–7.

Korpos, É., Kadri, N., Kappelhoff, R., Wegner, J., Overall, C. M., Weber, E., Holmberg, D., Cardell, S & Sorokin, L. (2013). The peri-islet basement membrane, a barrier to infiltrating leukocytes in type 1 diabetes in mouse and human. *Diabetes*, *62*(2), 531–42.

Krishnamurthy, M., Li, J., Al-Masri, M., & Wang, R. (2008). Expression and function of alphabeta1 integrins in pancretic beta (INS-1) cells. *Journal of Cell Communication and Signaling*, *2*(3–4), 67–79.

Kuhnert, F., Mancuso, M. R., Shamloo, A., Wang, H.-T., Choksi, V., Florek, M., Su, H., Fruttiger, M., William, L.Y., Heilshorn, S.C & Kuo, C. J. (2010). Essential regulation of CNS angiogenesis by the orphan G protein-coupled receptor GPR124. *Science*, *330*(6006), 985–9.

Lammert, E., Gu, G., McLaughlin, M., Brown, D., Brekken, R., Murtaugh, L. C., Gerber, H., Ferrara, N & Melton, D. A. (2003). Role of VEGF-A in vascularization of pancreatic islets. *Current Biology*, *13*(12), 1070–1074.

Langenhan, T., Aust, G., & Hamann, J. (2013). Sticky signaling--adhesion class G protein-coupled receptors take the stage. *Science Signaling*, *6*(276),

Langenhan, T., Piao, X., & Monk, K. R. (2016). Adhesion G protein-coupled receptors in nervous system development and disease. *Nature Reviews Neuroscience*, *17*(9), 550–561.

Larsen, H. Ø., Roug, A. S., Nielsen, K., Søndergaard, C. S., & Hokland, P. (2011). Nonviral transfection of leukemic primary cells and cells lines by siRNA-a direct comparison between Nucleofection and Accell delivery. *Experimental Hematology*, *39*(11), 1081–1089.

Larsson, L. I., Rehfeld, J. F., Sundler, F., & Hakanson, R. (1976). Pancreatic gastrin in foetal and neonatal rats. *Nature*, *262*(5569), 609–610.

Latour, M. G., Alquier, T., Oseid, E., Tremblay, C., Jetton, T. L., Luo, J., Lin, D.C.H & Poitout, V. (2007). GPR40 is necessary but not sufficient for fatty acid stimulation of insulin secretion in vivo. *Diabetes*, *56*(4), 1087–1094.

Lefkowitz, R. J., Cotecchia, S., Samama, P., & Costa, T. (1993). Constitutive activity of receptors coupled to guanine nucleotide regulatory proteins. *Trends in Pharmacological Sciences*. 14(8), 303-307.

Lehmann, R., Zuellig, R. A., Kugelmeier, P., Baenninger, P. B., Moritz, W., Perren, A., Clavien, P., Weber, M & Spinas, G. A. (2007). Superiority of small islets in human islet transplantation. *Diabetes*, *56*(3), 594–603.

Leitinger, B., & Hohenester, E. (2007). Mammalian collagen receptors. *Matrix Biology*. 26(3), 146-155.

Leslie, R. D. G., Kolb, H., Schloot, N. C., Buzzetti, R., Mauricio, D., De Leiva, A., Yderstraede, K., Sarti, C., Thivolet, C., Hadden, D., Hunter, S., Schernthaner, G., Scherbaum, W., Williams, R & Pozzilli, P. (2008). Diabetes classification: Grey zones, sound and smoke:

Action LADA 1. *Diabetes/Metabolism Research and Reviews*. 24(7), 511-519.

Leslie, R. D., Palmer, J., Schloot, N. C., & Lernmark, A. (2016). Diabetes at the crossroads: relevance of disease classification to pathophysiology and treatment. *Diabetologia*. 59(1), 13-20.

Li, D. S., Yuan, Y. H., Tu, H. J., Liang, Q. L., & Dai, L. J. (2009). A protocol for islet isolation from mouse pancreas. *Nat Protoc*, *4*(11), 1649–1652.

Li, S., Jin, Z., Koirala, S., Bu, L., Xu, L., Hynes, R. O., … Piao, X. (2008). GPR56 Regulates Pial Basement Membrane Integrity and Cortical Lamination. *Journal of Neuroscience*, *28*(22), 5817–5826.

Li, W., Zhao, R., Liu, J., Tian, M., Lu, Y., He, T., Cheng, M., Liang, K., Li, X., Wang, X., Sun, Y & Chen, L. (2014). Small islets transplantation superiority to large ones: Implications from islet microcirculation and revascularization. *Journal of Diabetes Research*, *2014*, 192093.

Liebscher, I., Schön, J., Petersen, S. C., Fischer, L., Auerbach, N., Demberg, L. M., Mogha, A., Coster, M., Simon, K., Rothemund, S., Monk, K.R & Schöneberg, T. (2014). A tethered agonist within the ectodomain activates the adhesion G protein-coupled receptors GPR126 and GPR133. *Cell Reports*, *9*(6), 2018–26.

Little, K. D., Hemler, M. E., & Stipp, C. S. (2004). Dynamic regulation of a GPCR-tetraspanin-G protein complex on intact cells: central role of CD81 in facilitating GPR56-Galpha q/11 association. *Molecular Biology of the Cell*, *15*(5), 2375–87.

Liu, B., Song, S., Maldonado, I. R., Pingitore, A., Huang, G. C., Baker, D., Jones, P.M & Persaud, S. J. (2016). GPR55-dependent stimulation of insulin secretion from isolated mouse and human islets of Langerhans. *Diabetes, Obesity & Metabolism*, *18*(12), 1263–1273.

Liu, M., Parker, R., Darby, K., & Eyre, H. (1999). GPR56, a novel secretin-like human G-protein-coupled receptor gene. *Genomics*, *305*(1999), 296–305.

Liu, M., Wright, J., Guo, H., Xiong, Y., & Arvan, P. (2014). Proinsulin entry and transit through the endoplasmic reticulum in pancreatic beta cells. *Vitamins and Hormones*, *95*, 35–62.

Liu, X., Wu, H., Byrne, M., Krane, S., & Jaenisch, R. (1997). Type III collagen is crucial for collagen I fibrillogenesis and for normal cardiovascular development. *Proceedings of the National Academy of Sciences of the United States of America*, *94*(5), 1852–6.

Lorand, L., & Graham, R. M. (2003). Transglutaminases: crosslinking enzymes with pleiotropic

functions. *Nature Reviews. Molecular Cell Biology*, *4*(2), 140–56.

Luo, R., Jeong, S.-J., Jin, Z., Strokes, N., Li, S., & Piao, X. (2011). G protein-coupled receptor 56 and collagen III, a receptor-ligand pair, regulates cortical development and lamination. *Proceedings of the National Academy of Sciences of the United States of America*, *108*, 12925–12930.

Luo, R., Jeong, S.-J., Yang, A., Wen, M., Saslowsky, D. E., Lencer, W. I., Arac, D & Piao, X. (2014). Mechanism for Adhesion G Protein-Coupled Receptor GPR56-Mediated RhoA Activation Induced By Collagen III Stimulation. *PloS One*, *9*(6), e100043.

Luo, R., Yang, H. M., Jin, Z., Halley, D. J. J. J., Chang, B. S., MacPherson, L., Brueton, L & Piao, X. (2011). A novel GPR56 mutation causes bilateral frontoparietal polymicrogyria. *Pediatric Neurology*, *45*(1), 49–53.

MacCracken, J., Hoel, D., & Jovanovis, L. (1997). From ants to analogues. Puzzles and promises in diabetes management. *Postgraduate Medicine*, *101*(5), 138–140.

Martín, J., Hunt, S. L., Dubus, P., Sotillo, R., Néhmé-Pélluard, F., Magnuson, M. A., … Barbacid, M. (2003). Genetic rescue of Cdk4 null mice restores pancreatic β-cell proliferation but not homeostatic cell number. *Oncogene*, *22*(34), 5261–9.

Marty-Santos, L., & Cleaver, O. (2016). Pdx1 regulates pancreas tubulogenesis and E-cadherin expression. *Development (Cambridge, England)*, *143*(1), 101–12.

McCarthy, M. I., & Hattersley, A. T. (2008). Learning from molecular genetics: Novel insights arising from the definition of genes for monogenic and type 2 diabetes. *Diabetes*. 57(11), 2889-98.

Menge, B. A., Tannapfel, A., Belyaev, O., Drescher, R., Müller, C., Uhl, W., Schmidt, W.E & Meier, J. J. (2008). Partial pancreatectomy in adult humans does not provoke β-cell regeneration. *Diabetes*, *57*(1), 142–149.

Metrakos, P., Yuan, S., Agapitos, D., & Rosenberg, L. (1993). Intercellular communication and maintenance of islet cell mass--implications for islet transplantation. *Surgery*, *114*(2), 423–428.

Moechars, D., Depoortere, I., Moreaux, B., de Smet, B., Goris, I., Hoskens, L., … Coulie, B. (2006). Altered Gastrointestinal and Metabolic Function in the GPR39-Obestatin Receptor-Knockout Mouse. *Gastroenterology*, *131*(4), 1131–1141.

Mogha, A., Benesh, A. E., Patra, C., Engel, F. B., Schöneberg, T., Liebscher, I., & Monk, K. R.

(2013). Gpr126 functions in Schwann cells to control differentiation and myelination via G-protein activation. *The Journal of Neuroscience*, *33*(46), 17976–85.

Moltchanova, E. V., Schreier, N., Lammi, N., & Karvonen, M. (2009). Seasonal variation of diagnosis of Type 1 diabetes mellitus in children worldwide. *Diabetic Medicine*, *26*(7), 673–678.

Mombaerts, P. (2004). Genes and ligands for odorant, vomeronasal and taste receptors. *Nature Reviews Neuroscience*. 5(4), 263-278.

Monami, M., Nardini, C., & Mannucci, E. (2014). Efficacy and safety of sodium glucose co-transport-2 inhibitors in type 2 diabetes: a meta-analysis of randomized clinical trials. *Diabetes, Obesity & Metabolism*, *16*(5), 457–66.

Mueckler, M., & Thorens, B. (2013). The SLC2 (GLUT) family of membrane transporters. *Molecular Aspects of Medicine*, *34*(2–3), 121–38.

Nagata, N., Gu, Y., Hori, H., Balamurugan, A. N., Touma, M., Kawakami, Y., Wang, W., Baba, TT., Satake, A., Nozawa, M., Tabata, Y & Inoue, K. (2001). Evaluation of insulin secretion of isolated rat islets cultured in extracellular matrix. In *Cell Transplantation*, 10, 447–451.

Narayan, K. M. V., Ali, M. K., & Koplan, J. P. (2010). Global Noncommunicable Diseases — Where Worlds Meet. *New England Journal of Medicine*, *363*(13), 1196–1198.

Negre-Salvayre, A., Salvayre, R., Augé, N., Pamplona, R., & Portero-Otín, M. (2009). Hyperglycemia and Glycation in Diabetic Complications. *Antioxidants & Redox Signaling*, *11*(12), 3071–3109.

Nguyen, Q. T., Thomas, K. T., Lyons, K. B., Nguyen, L. D., & Plodkowski, R. A. (2011). Current therapies and emerging drugs in the pipeline for type 2 diabetes. *American Health and Drug Benefits*, 4(5), 303-311.

Nie, T., Hui, X., Gao, X., Li, K., Lin, W., Xiang, X., Ding, M., Kuang, Y., Xu, A., Fei, J., Wang, Z & Wu, D. (2012). Adipose tissue deletion of Gpr116 impairs insulin sensitivity through modulation of adipose function. *FEBS Letters*, *586*(20), 3618–3625.

Nijmeijer, S., Vischer, H., & Leurs, R. (2016). Adhesion GPCRs in immunology. *Biochemical Pharmacology*, *114*, 88–102.

Nishimori, H., Shiratsuchi, T., Urano, T., Kimura, Y., Kiyono, K., Tatsumi, K., Yoshida, S., Ono, M., Kuwano, M., Nakamura, Y & Tokino, T. (1997). A novel brain-specific p53-target gene, BAI1, containing thrombospondin type 1 repeats inhibits experimental angiogenesis.

Oncogene, *15*(18), 2145–2150.

Nolan, D., Ginsberg, M., Israely, E., Palikuqi, B., Poulos, M. G., James, D., Ding, BS., Schachterle, W., Liu, Y., … Rafii, S. (2013). Molecular Signatures of Tissue-Specific Microvascular Endothelial Cell Heterogeneity in Organ Maintenance and Regeneration. *Developmental Cell*, *26*(2), 204–219.

Notkins, A. L & Lernmark, A. (2001). Autoimmune type 1 diabetes: resolved and unresolved issues. *The Journal of Clinical Investigation*, *108*(9), 1247–52.

Ogawa, N., List, J. F., Habener, J. F., & Maki, T. (2004). Cure of overt diabetes in NOD mice by transient treatment with anti-lymphocyte serum and exendin-4. *Diabetes*, *53*(7), 1700–1705.

Oh, D. Y., & Olefsky, J. M. (2016). G protein-coupled receptors as targets for anti-diabetic therapeutics. *Nature Reviews Drug Discovery*, *15*(3), 161–172.

Osundiji, M. A., Lam, D. D., Shaw, J., Yueh, C.-Y., Markkula, S. P., Hurst, P., Colliva, C., Roda, A., Heisler, LK & Evans, M. L. (2012). Brain glucose sensors play a significant role in the regulation of pancreatic glucose-stimulated insulin secretion. *Diabetes*, *61*(2), 321–8.

Otonkoski, T., Banerjee, M., Korsgren, O., Thornell, L.-E., & Virtanen, I. (2008). Unique basement membrane structure of human pancreatic islets: implications for β-cell growth and differentiation. *Diabetes, Obesity and Metabolism*, *10*, 119–127.

Ottensmeyer, F. P., Beniac, D. R., Luo, R. Z., & Yip, C. C. (2000). Mechanism of transmembrane signaling: Insulin binding and the insulin receptor. *Biochemistry*. 39(40), 12103-12.

Owens, D. R., Matfin, G., & Monnier, L. (2014). Basal insulin analogues in the management of diabetes mellitus: What progress have we made? *Diabetes/Metabolism Research and Reviews*, *30*(2), 104–119.

Paavola, K. J., Stephenson, J. R., Ritter, S. L., Alter, S. P., & Hall, R. a. (2011). The N terminus of the adhesion G protein-coupled receptor GPR56 controls receptor signaling activity. *The Journal of Biological Chemistry*, *286*(33), 28914–21.

Park, D., Tosello-Trampont, A.-C., Elliott, M. R., Lu, M., Haney, L. B., Ma, Z., … Ravichandran, K. S. (2007). BAI1 is an engulfment receptor for apoptotic cells upstream of the ELMO/Dock180/Rac module. *Nature*, *450*(7168), 430–434.

Parrini, E., Ferrari, A. R., Dorn, T., Walsh, C. A., & Guerrini, R. (2009). Bilateral frontoparietal

polymicrogyria, Lennox-Gastaut syndrome, and GPR56 gene mutations. *Epilepsia*, *50*(6), 1344–1353.

Parton, L. E., Ye, C. P., Coppari, R., Enriori, P. J., Choi, B., Zhang, C.-Y., Xu, C., Vianna, C.R., Balthasar, N., Lee, C.E., Elmquist, J.K., Cowley, M.A & Lowell, B. B. (2007). Glucose sensing by POMC neurons regulates glucose homeostasis and is impaired in obesity. *Nature*, *449*(7159), 228–232.

Peiris, H., Bonder, C. S., Coates, P. T. H., Keating, D. J., & Jessup, C. F. (2014). The β-cell/EC axis: how do islet cells talk to each other? *Diabetes*, *63*(1), 3–11.

Peng, Y.-M., Van De Garde, M. D. B., Cheng, K.-F., Baars, P. A., Remmerswaal, E. B. M., Van Lier, R. A. W., … Hamann, J. (2011). Specific expression of GPR56 by human cytotoxic lymphocytes. *Journal of Leukocyte Biology*, *90*, 735–40.

Persaud, S. J., Arden, C., Bergsten, P., Bone, A. J., Brown, J., Dunmore, S., Harrison, M., Hauge-Evans, A.C., Kelly, C., King, A., Maffucci, T., Marriott, C.E., McClenaghan, N., Morgan, N.E., Reers, C., Russel, M.A., Turner, M.D., Willoughby, E., Younis, M.Y.G, Zhi, Z.L & Jones, P. M. (2010). Pseudoislets as primary islet replacements for research: Report on a symposium at King's College London, London UK. *Islets*, 2(4)236-239.

Persaud, S. J., & Jones, P. M. (2003). Metabolic Changes in Diabetes: A Summary. In P. J. Watkins, S. A. Amiel, S. L. Howell, & E. Turner (Eds.), *Diabetes and its Management* (Sixth, pp. 33–37). Oxford, UK: Blackwell Publishing Ltd.

Pfaffl, M. W. (2001). A new mathematical model for relative quantification in real-time RT-PCR. *Nucleic Acids Research*, *29*(9), e45.

Piao, X., Hill, R. S., Bodell, A., Chang, B. S., Basel-Vanagaite, L., Straussberg, R., Dobyns, W.B., Qasrawi, B., Winter, R.M., Innes, A.M, Volt, T., Ross, M.E, Michaud, J.L, Descarie, J, Barkovich, A.J & Walsh, C. a. (2004). G protein-coupled receptor-dependent development of human frontal cortex. *Science*, *303*(5666), 2033–6.

Polonsky, K. S. (2012). The Past 200 Years in Diabetes The Role of the Pancreas and the Discovery of Insulin. *The New England Journal of Medicine, 1436714*(4), 1332–40.

Porzio, O., Massa, O., Cunsolo, V., Colombo, C., Malaponti, M., Bertuzzi, F., … Barbetti, F. (2007). Missense mutations in the TGM2 gene encoding transglutaminase 2 are found in patients with early-onset type 2 diabetes. *Human Mutation*, *28*(11), 1150.

Preitner, F., Ibberson, M., Franklin, I., Binnert, C., Pende, M., Gjinovci, A., Hanaotia, T.,

Drucker, D.J., Wolheim, C., Burcelin, R & Thorens, B. (2004). Gluco-incretins control insulin secretion at multiple levels as revealed in mice lacking GLP-1 and GIP receptors. *Journal of Clinical Investigation*, *113*(4), 635–645.

Regard, J., Sato, I. T., & Coughlin, S. R. (2008). Anatomical Profiling of G Protein-Coupled Receptor Expression. *Cell*, *135*(3), 561–571.

Reimann, F., & Gribble, F. M. (2016). G protein-coupled receptors as new therapeutic targets for type 2 diabetes. *Diabetologia*, 59(2), 229-233.

Reinert, R. B., Brissova, M., Shostak, A., Pan, F. C., Poffenberger, G., Cai, Q., Hundemer, G.L., Kant, J., Thompson, C.S., Dai, C., McGuinness, O.C & Powers, A. C. (2013). Vascular Endothelial Growth Factor-A and Islet Vascularization Are Necessary in Developing, but Not Adult, Pancreatic Islets. *Diabetes*, *62*(12), 4154-4164.

Reinert, R. B., Cai, Q., Hong, J.-Y., Plank, J. L., Aamodt, K., Prasad, N., Aramandla, R., Dai, C., Levy, S.E., Pozzi, A., Labosky, P.A., Wright, C.V.E., Brissova, M & Powers, A. C. (2014). Vascular endothelial growth factor coordinates islet innervation via vascular scaffolding. *Development (Cambridge, England)*, *141*(7), 1480–91.

Ritter, K., Buning, C., Halland, N., Pöverlein, C., & Schwink, L. (2016). G Protein-Coupled Receptor 119 (GPR119) Agonists for the Treatment of Diabetes: Recent Progress and Prevailing Challenges. *Journal of Medicinal Chemistry*, 59(8), 3579-92.

Rodriguez-Diaz, R., Abdulreda, M. H., Formoso, A. L., Gans, I., Ricordi, C., Berggren, P. O., & Caicedo, A. (2011). Innervation patterns of autonomic axons in the human endocrine pancreas. *Cell Metabolism*, *14*(1), 45–54.

Rodriguez-Diaz, R., Dando, R., Jacques-Silva, M. C., Fachado, A., Molina, J., Abdulreda, M. H., Ricordi, C., Roper, S.D., Berggren, P-O & Caicedo, A. (2011). Alpha cells secrete acetylcholine as a non-neuronal paracrine signal priming beta cell function in humans. *Nature Medicine*, *17*(7), 888–892.

Rolandsson, O., & Palmer, J. P. (2010,). Latent autoimmune diabetes in adults (LADA) is dead: Long live autoimmune diabetes! *Diabetologia*, 53(7), 1250-1253.

Rooman, I., Lardon, J., & Bouwens, L. (2002). Gastrin stimulates beta-cell neogenesis and increases islet mass from transdifferentiated but not from normal exocrine pancreas tissue. *Diabetes*, *51*(3), 686–690.

Rorsman, P., & Renström, E. (2003). Insulin granule dynamics in pancreatic beta cells.

Diabetologia, 46(8), 1029-1045.

Rosenberg, L., Wang, R., Paraskevas, S., & Maysinger, D. (1999). Structural and functional changes resulting from islet isolation lead to islet cell death. *Surgery*, *126*, 393–398.

Rozario, T., & DeSimone, D. W. (2010). The extracellular matrix in development and morphogenesis: A dynamic view. *Developmental Biology*, 341(1), 126-140.

Ryall, C. L., Viloria, K., Lhaf, F., Walker, A. J., King, A., Jones, P., Mackintosh, D., McNiece, R., Kocher, H., Flodstrom-Tullberg, M., Edling, C & Hill, N. J. (2014). Novel role for matricellular proteins in the regulation of islet ??cell survival: The effect of SPARC on survival, proliferation, and signaling. *Journal of Biological Chemistry*, *289*(44), 30614–30624.

Saisawat, P., Kohl, S., Hilger, A. C., Hwang, D.-Y., Yung Gee, H., Dworschak, G. C., … Hildebrandt, F. (2014). Whole-exome resequencing reveals recessive mutations in TRAP1 in individuals with CAKUT and VACTERL association. *Kidney International*, *85*(6), 1310–7.

Saito, M., Fujii, K., Mori, Y., & Marumo, K. (2006). Role of collagen enzymatic and glycation induced cross-links as a determinant of bone quality in spontaneously diabetic WBN/Kob rats. *Osteoporosis International*, *17*(10), 1514–1523.

Saito, Y., Kaneda, K., Suekane, a, Ichihara, E., Nakahata, S., Yamakawa, N., Nagai, K., Mizuno, N., Miura, I., Itoh, M & Morishita, K. (2013). Maintenance of the hematopoietic stem cell pool in bone marrow niches by EVI1-regulated GPR56. *Leukemia*, *27*(8), 1637–49.

Salzman, G. S., Ackerman, S. D., Ding, C., Koide, A., Leon, K., Luo, R., Stoveken, H.M., Fernandez, C.G., Tall, G.G., Piao, X., Monk, K.R., Koide, S & Araç, D. (2016). Structural Basis for Regulation of GPR56/ADGRG1 by Its Alternatively Spliced Extracellular Domains. *Neuron*, *91*(6), 1292–1304.

Samama, P., Cotecchia, S., Costa, T., & Lefkowitz, R. J. (1993). A mutation-induced activated state of the beta 2-adrenergic receptor. Extending the ternary complex model. *The Journal of Biological Chemistry*, *268*(7), 4625–4636.

Sanlioglu, A. D., Altunbas, H. A., Balci, M. K., Griffith, T. S., & Sanlioglu, S. (2013). Clinical utility of insulin and insulin analogs. *Islets*, 5(2), 67-78.

Sassmann, A., Gier, B., Gröne, H., Drews, G., Offermanns, S., & Wettschureck, N. (2010). The G q / G 11 -mediated signaling pathway is critical for autocrine potentiation of insulin

secretion in mice. *The Journal of Clinical Investigation*, *120*(6), 2184–2193.

Sato, Y., & Henquin, J. (2014). The K + - ATP Channel–Independent Pathway of Regulation of Insulin Secretion by Glucose In Search of the Underlying Mechanism. *Diabetes*, *47*(19), 1713–1722.

Saudek, F., Jirák, D., Girman, P., Herynek, V., Dezortová, M., Kříž, J., Peregrin, J., Berkova, Z., Zacharovova, K & Hájek, M. (2010). Magnetic Resonance Imaging of Pancreatic Islets Transplanted Into the Liver in Humans. *Transplantation*, *90*(12), 1602–1606.

Scaglia, L., Cahil, C., Finegood, D., & Bonner-Weir, S. (1997). Apoptosis Participates in the Remodelling of the Endocrine Pancreas. *Endocrinology*, *138*(4), 1736–1741.

Seymour, P. A. (2014). Sox9: a master regulator of the pancreatic program. *The Review of Diabetic Studies*, *11*(1), 51–83.

Shashidhar, S., Lorente, G., Nagavarapu, U., Nelson, A., Kuo, J., Cummins, J., Nikolich, K., Urfer, R., & Foehr, E. D. (2005). GPR56 is a GPCR that is overexpressed in gliomas and functions in tumor cell adhesion, 24(10), 1673–1682.

Shiao, M. S., Liao, B. Y., Long, M., & Yu, H. T. (2008). Adaptive evolution of the insulin two-gene system in mouse. *Genetics*, *178*(3), 1683–1691.

Shih, H. P., Panlasigui, D., Cirulli, V., & Sander, M. (2016). ECM Signaling Regulates Collective Cellular Dynamics to Control Pancreas Branching Morphogenesis. *Cell Reports*, *14*(2), 169–179.

Shih, H. P., Wang, A., & Sander, M. (2013). Pancreas Organogenesis: From Lineage Determination to Morphogenesis. *Annual Review of Cell and Developmental Biology*, *29*(1), 81–105.

Shimizu, T., Nathan, D. M., Buse, J. B., Davidson, M. B., Ferrannini, E., Holman, R. R., Sherwin, R & Zinman, B. (2012). Medical management of hyperglycemia in type 2 diabetes: a consensus algorithm for the initiation and adjustment of therapy: a consensus statement of the American Diabetes Association and the European Association for the Study of Diabetes. *Nihon Rinsho*, *70 Suppl 3*(1), 591–601.

Sigoillot, S. M., Monk, K. R., Piao, X., Selimi, F., & Harty, B. L. (2016). Adhesion GPCRs as Novel Actors in Neural and Glial Cell Functions: From Synaptogenesis to Myelination (pp. 275–298). Springer International Publishing.

Simon-Areces, J., Membrive, G., Garcia-Fernandez, C., Garcia-Segura, L. M., & Arevalo, M.-A.

(2010). Neurogenin 3 cellular and subcellular localization in the developing and adult hippocampus. *The Journal of Comparative Neurology*, *518*(10), 1814–1824.

Simon, M., Strathmann, M., & Gautam, N. (1991). Diversity of G proteins in signal transduction. *Science*, *543*(1971).

Simundza, J., & Cowin, P. (2013). Adhesion G-Protein-Coupled Receptors: Elusive Hybrids Come of Age. *Cell Communication & Adhesion*, 1–13.

Singer, K., Luo, R., Jeong, S.-J. S., & Piao, X. (2013). GPR56 and the Developing Cerebral Cortex: Cells, Matrix, and Neuronal Migration. *Molecular Neurobiology*, *47*(1), 186–196.

Singh, V. P., Bali, A., Singh, N., & Jaggi, A. S. (2014). Advanced glycation end products and diabetic complications. *Korean Journal of Physiology & Pharmacology ,* 18(1), 1-14

Solaimani Kartalaei, P., Yamada-Inagawa, T., Vink, C. S., de Pater, E., van der Linden, R., Marks-Bluth, J., … Dzierzak, E. (2015). Whole-transcriptome analysis of endothelial to hematopoietic stem cell transition reveals a requirement for Gpr56 in HSC generation. *Journal of Experimental Medicine*, *212*(1), 93.

Stanger, B. Z., & Hebrok, M. (2013). Control of cell identity in pancreas development and regeneration. *Gastroenterology*, *144*(6), 1170–1179.

Steiner, D. J., Kim, A., Miller, K., & Hara, M. (2010). Pancreatic islet plasticity: Interspecies comparison of islet architecture and composition. *Islets*, 2(3), 135-145.

Stendahl, J. C., Kaufman, D. B., & Stupp, S. I. (2009). Extracellular matrix in pancreatic islets: Relevance to scaffold design and transplantation. *Cell Transplantation*, *18*(1), 1–12.

Steneberg, P., Rubins, N., Bartoov-Shifman, R., Walker, M. D., & Edlund, H. (2005). The FFA receptor GPR40 links hyperinsulinemia, hepatic steatosis, and impaired glucose homeostasis in mouse. *Cell Metabolism*, *1*(4), 245–258.

Stephenson, J. R., Paavola, K. J., Schaefer, S. A., Kaur, B., Van Meir, E. G., & Hall, R. A. (2013). Brain-specific angiogenesis inhibitor-1 signaling, regulation, and enrichment in the postsynaptic density. *Journal of Biological Chemistry*, *288*(31), 22248–22256.

Steven, S., Carey, P. E., Small, P. K., & Taylor, R. (2015). Reversal of Type 2 diabetes after bariatric surgery is determined by the degree of achieved weight loss in both short- and long-duration diabetes. *Diabetic Medicine*, *32*(1), 47–53.

Stoveken, H. M., Bahr, L. L., Anders, M. W., Wojtovich, A. P., Smrcka, A. V, & Tall, G. G. (2017). Dihydromunduletone is a Small-Molecule Selective Adhesion G Protein-Coupled

Receptor Antagonist. *Molecular Pharmacology, 90*(3), 214-224.

Stoveken, H. M., Hajduczok, A. G., Xu, L., & Tall, G. G. (2015). Adhesion G protein-coupled receptors are activated by exposure of a cryptic tethered agonist. *Proceedings of the National Academy of Sciences of the United States of America*, *112*(19), 6194–9.

Strathmann, M. P., & Simon, M. I. (1991). G alpha 12 and G alpha 13 subunits define a fourth class of G protein alpha subunits. *Proceedings of the National Academy of Sciences of the United States of America*, *88*(13), 5582–6.

Straub, S. G., & Sharp, G. W. G. (2002). Glucose-stimulated signaling pathways in biphasic insulin secretion. *Diabetes/Metabolism Research and Reviews*, 18(6), 451-463.

Sunami, E., Kanazawa, H., Hashizume, H., Takeda, M., Hatakeyama, K., & Ushiki, T. (2001). Morphological characteristics of Schwann cells in the islets of Langerhans of the murine pancreas. *Arch.Histol.Cytol.*, *64*, 191–201.

Suzuki, N., Hajicek, N., & Kozasa, T. (2009). Regulation and physiological functions of G12/13-mediated signaling pathways. *NeuroSignals*, 17(1), 55-70.

Svensson, A. M., Östenson, C. G., Bodin, B., & Jansson, L. (2005). Lack of compensatory increase in islet blood flow and islet mass in GK rats following 60% partial pancreatectomy. *Journal of Endocrinology*, *184*(2), 319–327.

Takenawa, T., & Itoh, T. (2001). Phosphoinositides, key molecules for regulation of actin cytoskeletal organization and membrane traffic from the plasma membrane. *Biochimica et Biophysica Acta (BBA) - Molecular and Cell Biology of Lipids*, *1533*(3), 190–206.

Taneera, J., Lang, S., Sharma, A., Fadista, J., Zhou, Y., Ahlqvist, E., Jonsson, A., Lyssenko, V., Vikman, P., Hansson, O., Parikh, H, Korsgren, O., Soni, A., Krus, U., Zhang, E., Jing, X-J., Esguerra, J.L.S., Wolheim, C.B., Salehi, A & Groop, L. (2012). A systems genetics approach identifies genes and pathways for type 2 diabetes in human islets. *Cell Metabolism*, *16*(1), 122–134.

Terskikh, A., Easterday, M., Li, L., Hood, L., Kornblum, H., Geschwind, D., & Weissman, I. (2001). From hematopoiesis to neuropoiesis: evidence of overlapping genetic programs. *Proc Natl Acad Sci U S A*, *98*(14), 7934–7939.

Teta, M., Long, S. Y., Wartschow, L. M., Rankin, M. M., & Kushner, J. A. (2005). Very slow turnover of beta-cells in aged adult mice. *Diabetes*, *54*(September), 2557–2567.

Tomas, A., Yermen, B., Regazzi, R., Pessin, J. E., & Halban, P. A. (2010). Regulation of insulin

secretion by phosphatidylinositol-4,5-bisphosphate. *Traffic (Copenhagen, Denmark)*, *11*(1), 123–37.

Tourrel, C., Bailbé, D., Meile, M. J., Kergoat, M., & Portha, B. (2001). Glucagon-Like Peptide-1 and Exendin-4 Stimulate β-Cell Neogenesis in Streptozotocin-Treated Newborn Rats Resulting in Persistently Improved Glucose Homeostasis at Adult Age. *Diabetes*, *50*(7), 1562–1570.

Tremblay, F., Perreault, M., Klaman, L. D., Tobin, J. F., Smith, E., & Gimeno, R. E. (2007). Normal food intake and body weight in mice lacking the G protein-coupled receptor GPR39. *Endocrinology*, *148*(2), 501–506.

Tremblay, F., Richard, A.-M. T., Will, S., Syed, J., Stedman, N., Perreault, M., & Gimeno, R. E. (2009). Disruption of G Protein-Coupled Receptor 39 Impairs Insulin Secretion *in Vivo*. *Endocrinology*, *150*(6), 2586–2595.

Tritarelli, A., Oricchio, E., Ciciarello, M., Mangiacasale, R., Palena, A., Lavia, P., … Cundari, E. (2004). p53 Localization at Centrosomes during Mitosis and Postmitotic Checkpoint Are ATM-dependent and Require Serine 15 Phosphorylation. *Molecular Biology of the Cell*, *15*(April), 3751–3737.

Tsuchiya, H., Sakata, N., Yoshimatsu, G., Fukase, M., Aoki, T., Ishida, M., Katayose, Y., Egawa, S & Unno, M. (2015). Extracellular matrix and growth factors improve the efficacy of intramuscular islet transplantation. *PLoS ONE*, *10*(10), e0140910.

Tsui, H., Winer, S., Chan, Y., Truong, D., Tang, L., Yantha, J., Paltser, G & Dosch, H. M. (2008). Islet glia, neurons, and β cells: The neuroimmune interface in the pathogenesis of type 1 diabetes. In *Annals of the New York Academy of Sciences*, 1150, 32–42.

Tuomi, T., Santoro, N., Caprio, S., Cai, M., Weng, J., & Groop, L. (2014). The many faces of diabetes: a disease with increasing heterogeneity. *Lancet*, *383*(9922), 1084–94.

Uhlen, M., Fagerberg, L., Hallstrom, B. M., Lindskog, C., Oksvold, P., Mardinoglu, A., … Ponten, F. (2015). Proteomics. Tissue-based map of the human proteome. *Science, 347*(6220), 1260419.

Ushiki, T., & Watanabe, S. (1997). Distribution and ultrastructure of the autonomic nerves in the mouse pancreas. *Microscopy Research and Technique*, *37*(5–6), 399–406.

Vallon, V., & Thomson, S. C. (2017). Targeting renal glucose reabsorption to treat hyperglycaemia: the pleiotropic effects of SGLT2 inhibition. *Diabetologia*, 60(2), 215-225.

Virtanen, I., Banerjee, M., Palgi, J., Korsgren, O., Lukinius, a, Thornell, L.-E., Kikkawa, Y., Sekiguchi, K., Hukkanen, M., Konttinen, Y.T & Otonkoski, T. (2008). Blood vessels of human islets of Langerhans are surrounded by a double basement membrane. *Diabetologia*, *51*(7), 1181–91.

Voight, B. F., Scott, L. J., Steinthorsdottir, V., Morris, A. P., Dina, C., Welch, R. P., … GIANT Consortium. (2010). Twelve type 2 diabetes susceptibility loci identified through large-scale association analysis. *Nature Genetics*, *42*(7), 579–89.

Wang, R. N., Paraskevas, S., & Rosenberg, L. (1999). Characterization of Integrin Expression in Islets Isolated from Hamster, Canine, Porcine, and Human Pancreas. *Journal of Histochemistry & Cytochemistry*, *47*(4), 499–506.

Wang, R. N., & Rosenberg, L. (1999). Maintenance of beta-cell function and survival following islet isolation requires re-establishment of the islet-matrix relationship. *The Journal of Endocrinology*, *163*(2), 181–90.

Ward, Y., Lake, R., Yin, J. J., Heger, C. D., Raffeld, M., Goldsmith, P. K., Merino, M & Kelly, K. (2011). LPA receptor heterodimerizes with CD97 to amplify LPA-initiated RHO-dependent signaling and invasion in prostate cancer cells. *Cancer Research*, *71*(23), 7301–7311.

Weber, L. M., Hayda, K. N., & Anseth, K. S. (2008). Cell-matrix interactions improve beta-cell survival and insulin secretion in three-dimensional culture. *Tissue Engineering. Part A*, *14*(12), 1959–68.

Weidner, N. (1995). Current pathologic methods for measuring intratumoral microvessel density within breast carcinoma and other solid tumors. *Breast Cancer Research and Treatment*, 36(2), 169-180.

White, D. J., Puranen, S., Johnson, M. S., & Heino, J. (2004). The collagen receptor subfamily of the integrins. *International Journal of Biochemistry and Cell Biology*, 36(8), 1405-1410.

White, J. P., Wrann, C. D., Rao, R. R., Nair, S. K., Jedrychowski, M. P., You, J.-S., … Spiegelman, B. M. (2014). G protein-coupled receptor 56 regulates mechanical overload-induced muscle hypertrophy. *Proceedings of the National Academy of Sciences of the United States of America*, *111*(44), 15756–61.

Wilde, C., Fischer, L., Lede, V., Kirchberger, J., Rothemund, S., Schöneberg, T., & Liebscher, I. (2016). The constitutive activity of the adhesion GPCR GPR114/ADGRG5 is mediated by its tethered agonist. *FASEB Journal*, *30*(2), 666–673.

Winer, S., Tsui, H., Lau, A., Song, A., Li, X., Cheung, R. K., Sampson, A., Afifiyan, F., Elford, A., Jackowski, G., Becker, D.J., Santamaria, P., Ohashi, P & Dosch, H.-M. (2003). Autoimmune islet destruction in spontaneous type 1 diabetes is not beta-cell exclusive. *Nature Medicine*, *9*(2), 198–205.

Xu, G., Stoffers, D. A., Habener, J. F., & Bonner-We, S. (1999). Exendin-4 Stimulates Both β-Cell Replication and Neogenesis, Resulting in Increased β-Cell Mass and Improved Glucose Tolerance in Diabetic Rats. *Diabetes*, *48*(12), 2270–2276.

Xu, L., Begum, S., Hearn, J. D., & Hynes, R. O. (2006). GPR56 , an atypical G protein-coupled receptor , binds tissue transglutaminase , TG2 , and inhibits melanoma tumor growth and metastasis. *Proceedings of the National Academy of Sciences of the United States of America*, *103*(24), 9023–9028.

Xu, L., & Hynes, R. (2007). GPR56 and TG2: Possible roles in suppression of tumor growth by the microenvironment. *Cell Cycle*, *6*(2), 160–165.

Yang, L., Chen, G., Mohanty, S., & Scott, G. (2011). GPR56 regulates VEGF production and angiogenesis during melanoma progression. *Cancer Research*, *71*(16), 5558–5568.

Yang, L., Chen, G., Mohanty, S., Scott, G., Fazal, F., Rahman, A., Begum, S., Hynes, R.O & Xu, L. (2011). GPR56 Regulates VEGF Production and Angiogenesis during Melanoma Progression. *Cancer Research*, *71*, 5558–5568.

Yang, L., Friedland, S., Corson, N., & Xu, L. (2014). GPR56 inhibits melanoma growth by internalizing and degrading its ligand TG2. *Cancer Research*, *74*(4), 1022–1031.

Zhu, C. F., Li, G. Z., Peng, H. B., Zhang, F., Chen, Y., & Li, Y. (2010). Therapeutic effects of marine collagen peptides on Chinese patients with type 2 diabetes mellitus and primary hypertension. *The American Journal of the Medical Sciences*, 340(5), 360-366.

Conference abstracts:

Olaniru E.O, Pingitore A, Giera S, Piao X, Jones P.M and Persaud S.J (2017): Characterising the function of the adhesion receptor GPR56 in islets. *Diabetic Medicine* 34(S1): 27-28

Olaniru E.O, Giera S, Piao X, Jones P.M and Persaud S.J (2016): GPR56 plays a role in regulating islet mass and beta cell proliferation. *Diabetic Medicine* 33(S1): 20-22

Olaniru E.O, Jones P.M and Persaud S.J (2015): Collagen receptors GPR56 and GPR126 are expressed in islets and regulate insulin secretion. *Diabetic Medicine* 32(S1): 48

Olaniru E.O, Jones P.M and Persaud S.J (2014): Expression of GPR56 and collagen III in islets: a role in modulating insulin secretion. *Diabetologia* 57(S1): S173